REPORT DOCUMENTATION PAGE

Form Approved OMB No. 0704-0188

1. REPORT DATE *(DD-MM-YYYY)*	2. REPORT TYPE	3. DATES COVERED *(From – To)*
21-09-2010	Final Report	01-Sep-07 - 01-Sep-10

4. TITLE AND SUBTITLE

NON-SELF-MAINTAINED DISCHARGE APPLICATION FOR FUEL ACTIVATION

5a. CONTRACT NUMBER
ISTC Registration No: 3775p

5b. GRANT NUMBER

5c. PROGRAM ELEMENT NUMBER

6. AUTHOR(S)

Dr. Sergy Vladimirovich Denisiuk

5d. PROJECT NUMBER

5d. TASK NUMBER

5e. WORK UNIT NUMBER

7. PERFORMING ORGANIZATION NAME(S) AND ADDRESS(ES)

FSUE MRTI RAS
132 Warschavskoe shosse
Moscow 117519
Russia

8. PERFORMING ORGANIZATION REPORT NUMBER

N/A

9. SPONSORING/MONITORING AGENCY NAME(S) AND ADDRESS(ES)

EOARD
Unit 4515 BOX 14
APO AE 09421

10. SPONSOR/MONITOR'S ACRONYM(S)

11. SPONSOR/MONITOR'S REPORT NUMBER(S)
ISTC 07-7010

12. DISTRIBUTION/AVAILABILITY STATEMENT

Approved for public release; distribution is unlimited.

13. SUPPLEMENTARY NOTES

14. ABSTRACT

This report results from a contract tasking FSUE MRTI RAS as follows: Nowadays application of electrons created by electron beams and accelerated in external electric field for preliminary ionization and activation of flammable mixtures in high-speed flows is poorly investigated scientific direction. In pioneering experimental works it was shown that combustion completeness improves in combined impact of electron beam and electric field on weakly supersonic flow of propane-air mixture, but mechanisms of processes in the plasma left unclear. Non-homogeneous distributions of main plasma and flow parameters and high gas temperature in the set up have lead to difficulties of theoretical analysis, but it was shown that created plasma represents a composition of highly ionized, electronically and vibrationally excited molecules and active atoms. Presence of active atoms leads to decrease of ignition times by 2-6 times with respect to power put into the mixture. Basing on experience of these works one can assert that preliminary ionization and excitation of flammable mixture molecules accelerates combustion processes in high-speed flows. At that the application of combined method requires clarification of reaction accelerating mechanisms and aerodynamics impact on combustion processes in non-equilibrium conditions.

Main task of this project is: modification of model flammable mixture with the aim of combustion process efficiency improvement: decrease of combustion time, i.e. increase of flame propagation velocity; combustion intensification of lean mixtures. For investigation of electron-beam plasma impact on combustion of propane-air mixture in the high-speed flow we suppose to undertake experimental investigations with a help of electron beam set up.

Model flammable mixture comes to the excitation chamber from the external source. The electron beam in this chamber irradiates it. Electric field is applied to this chamber. This field can change parameters of non-self-maintained discharge realized in the excitation chamber. The excited flammable mixture flow is ignited by electrical spark in the combustion chamber either a) at the outlet of the excitation chamber, or b) at the inlet to the excitation chamber, and then comes to the diagnostic chamber where sensors are situated and measurements of main characteristics of high-speed flow take place. Measurements of spatial distributions of gas temperature and pressure in these two cases will allow to obtain a value of a thrust, so some engineering level information can be gained by looking at the variation in the combustion efficiency vs. electron flux and electric field strength. The following advantages of the proposed scheme are: known parameters of electron fluxes generated by the electron beam in the given geometry; capability of electron beam parameters control; capability of external electric field values control; capability of uniform plasma creation; capability of different plasma instabilities development elimination. Clarification of flammable mixture preliminary ionization and excitation impact on combustion processes by the electron beam in external electric field and without it will allow to determine an area of combined impact appropriate for propane-air combustion efficiency increase in the high-speed flow

15. SUBJECT TERMS

EOARD, Propulsion, Engines And Fuels, Combustion and Ignition

16. SECURITY CLASSIFICATION OF:			**17. LIMITATION OF ABSTRACT**	**18, NUMBER OF PAGES**	**19a. NAME OF RESPONSIBLE PERSON**
a. REPORT	**b. ABSTRACT**	**c. THIS PAGE**			Stephanie Masoni, Maj, USAF
UNCLAS	UNCLAS	UNCLAS	UL	138	**19b. TELEPHONE NUMBER** *(Include area code)* +44 (0)1895 616420

Standard Form 298 (Rev. 8/98)
Prescribed by ANSI Std. Z39-18

< Project ISTC # 3775p>

< Non- self -maintained discharge application for fuel activation >

Final Technical Report on the Project

On fulfillment of works in the period
from 01 September 2007 till 31 August 2010.

<Federal state unitary enterprise "Moscow radio-technical institute RAS" >
<Address: 117519, Russia, Moscow, Washavskoe shosse, 132>

Project manager	**< Denisyuk Sergei Vladimirovich >, Ph.D.**	
Director	**<Makarov Boris Aleksandrovich>, Ph.D.**	

Project title:	Non- self -maintained discharge application for fuel activation
Starting date on Project works fulfillment on the:	1 September2007.
Project duration:	36 months

Project manager: Denisiuk Sergei Vladimirovich

Telephone number: +7 495 315-24-97

Fax.: +7 495 314-1053

E-mail address: svdenisiuk@gmail.com

Head institute: 1. Federal State Unitary Enterprise "Moscow Radiotechnical Institute of the Russian Academy of Sciences"
Warshavskoe shosse 132, 117519, Moscow, Russia +7 495 314-31-11
mrti@mrtiran.ru

CONTENT

1. Short Description of the Work Plan: Project goal, expected results, technical approach

1.1. Project Goal

The goal of the Project consists in clarification of preliminary ionization and excitation of molecules possibility at impact by an electron beam in external electric field and without it, determination of combined impact boundaries useful for increase of propane-air mixture combustion efficiency in a high-speed flow.

Main goal of this project is: modification of model flammable mixture with the aim of combustion process efficiency improvement: Decrease of combustion time, i.e. increase of flame propagation velocity; Combustion intensification of lean mixtures.

1.1. Expected results

Proposed project is related to the fundamental investigations.

The following results will be achieved within the framework of the project in the experimental and theoretical investigations:

1. Existing set up will be modernized for undertaking of investigations on electron-beam plasma and external electric field excitation influence on propane-air mixtures combustion in conditions of subsonic flow.
2. Sensors for measurements of propane-air high-speed flow characteristics before and after irradiation by the electron flux with and without external electric field will be developed and experimentally tested.
3. Flame temperature will be measured and optical detection of combustion area will be made for propane-air mixture combustion parameters evaluation.
4. Qualitative evaluation of flammable mixture preliminary ionization and excitation (realized with a help of the electron flux) influence on combustion with be made.
5. Special device for regulation of propane concentration in propane-air mixture will be developed.
6. Evaluation of lean mixture combustion efficiency under irradiation by electron beam will be made.
7. Physical model of processes in non-self-maintained discharge and in subsonic flow of the flammable mixture in known experimental conditions will be developed.
8. Numerical model of processes in non-self-maintained discharge and in subsonic flow of the flammable mixture in known experimental conditions will be made; comparison of experimental and theoretical results will be made for determination of optimal excitation modes.

9. Formulation of recommendations on application of propane-air mixture irradiation by the electron beam in external electric field for combustion efficiency increase in the subsonic flow.

1.2. Technical approach

The basic experiments were carried out on existing in MRTI installations at carrying out of concrete experiments of installation modernized and supplemented with necessary elements. They will be in detail described in corresponding sections of the present Report.

Main theoretical works have been carried out by highly experienced team of theoreticians and computer simulation specialists, which tasks were connected with creation of theoretical models, their computer code embodiment, support at undertaking of experiments and analysis of the experimental results.

1.3. Tasks

Task 1. Modernization of existing set up for undertaking of investigations on electron-beam plasma and external electric field excitation influence of propane-air mixtures without a flow.
Task 2 . Modernization of existing set up for undertaking of investigations on electron-beam plasma and external electric field excitation influence on propane-air mixtures influence on propane-air mixtures combustion in conditions of subsonic flow.
Task 3. Developed and experimental test of sensors for measurements of propane-air mixture characteristics before and after irradiation by the electron flux with and without external electric field.
Task 4 . Developed and experimental test of sensors for measurements of propane-air mixture high-speed flow characteristics before and after irradiation by the electron flux with and without external electric field.
Task 5. Experimental investigations on qualitative evaluation of flammable mixture preliminary excitation with respect to the combustion process.
Task 6. Experimental investigations on qualitative evaluation of lean flammable mixture preliminary excitation with respect to the combustion process.
Task 7. Development of physical model of processes in non-self-maintained discharge in propane-air mixture without a flow.
Task 8. Development of physical model of processes in non-self-maintained discharge in propane-air mixture in subsonic air flow.
Task 9. Development of numerical model of processes in non-self-maintained discharge in propane -air mixture.
Task 10. Development of numerical gasdynamic model of processes in non-self-maintained discharge in subsonic flammable mixture flow.
Task 11. Analysis of obtained experimental results. Comparison of experimental and numerical results. Formulation of recommendations for modification of present and formulation of new experiments.
Task 12. Preparation of interim and final reports. Formulation of recommendations on application of propane-air mixture irradiation by the electron beam in external electric field for combustion efficiency increase in the subsonic flow

2. Investigation methods, experiments, theory, etc.

Investigation methods, experiments, theory, etc. are described below in the text of the Report.

Chapter 1.(Tasks 1,2,3 and 4 of the Project) Creation of experimental installation and preparation of the research equipment.

Under the Project it was supposed to investigate an influence of a beam of accelerated electrons and electric field on processes of propane-air burning mixture in the air stream. It was the zero order work, because for carrying out of experimental researches it was necessary to create the complex installation providing all the spectrum of prospective measurements.

The block the scheme of the given installation is represented in Fig. 1

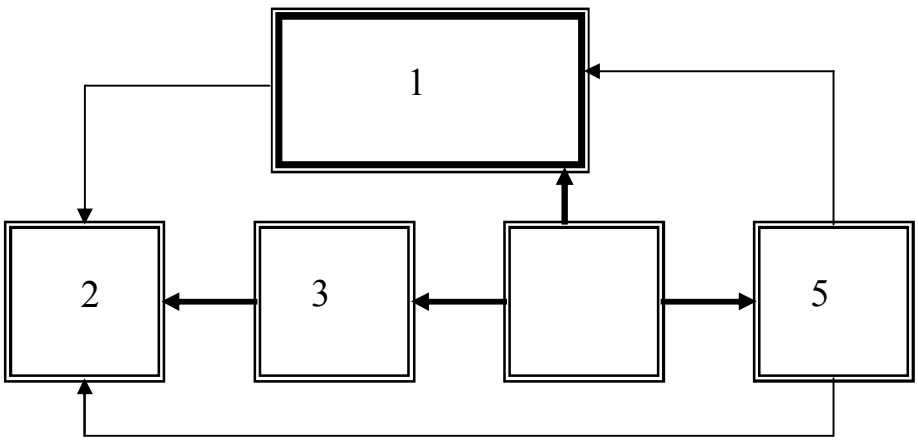

Fig. 1. The block - scheme of complex installation.

1 Modernized electron accelerator EOL - 400 M.
2 Experimental chamber.
3 Device of experiments.
4 Control system of installation
5 The diagnostic complex.

At the moment of the beginning of works under the Project majority of the blocks of our complex installation was either completely absent, or required to be created and modernized. So the initial stage was devoted to these works.

1.1 **Modernization of the electronic accelerator EOL-400M**

For obtaining of an electronic stream during works under the project the industrial accelerator of electrons EOL-400M has been used. The accelerator was for a long time at the preservation and for its switching on and getting of stable operational characteristics the necessary cycle of regenerative works has been carried out.

It is necessary to notice, that use of the given accelerator in experiments under the project is not defined by special requirements to an electron beam obtained in this type of installations, and based on definite device presence, but it was defined by presence of this device in working order. Creation of a new accelerator is quite a complex and the mainly an expensive problem. However, at necessity and sufficient financing any other electron accelerator can be created and used in experiments.

As a result of works for researches under the project the accelerator EOL-400M has been restored, the short description and the basic characteristics are represented in the given part of the report. The photo of the accelerator EOL-400M used in works under the Project is represented in Fig. 2.

Fig. .2 A photo of the industrial accelerator EOL-400M

The installation EOL -400 M represents the high-voltage electronic accelerator of direct action with a constant electron stream during an operating time.

The accelerator function scheme is represented in Fig.3.

The industrial electronic accelerator EOL-400M consists of (see Fig.3):

- A high-voltage accelerating tube (1);
- An injector of electrons with the thermo emission heated cathode (2);
- The high-voltage rectifier (3);
- A high-voltage connecting cable (4);
- Systems of scanning of the accelerated beam (5);
- Systems of a vacuum pump out (6);
- Vacuum windows for the beam release into the atmosphere at work of the accelerator (7) and (8)
- Systems of engineering support (9);
- Control and diagnostics systems (10).

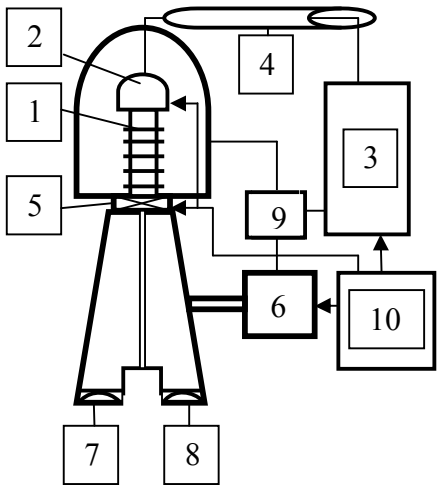

Fig.3 ***functioning scheme of the accelerator***

The high-voltage rectifier (3) provides presence of a continuous high voltage of negative polarity on an injector of electrons (2) and on the high-voltage end of the accelerating tube (1). The high-voltage rectifier and the accelerator elements are connected between themselves by a high-voltage connecting cable (4). The system of the vacuum pump out (6) provides necessary exhaustion in the field of injection and acceleration of the electronic beam. The given type of the accelerator assumes presence of two vacuum windows (7) and (8), necessary for leading of the beam accelerated electrons into the atmosphere for the technological purposes. The system of engineering support (9) allows to stably function to all auxiliary systems of the accelerator. The electron injector (2) is supplied by the thermo - emission cathode, allowing to generate an electron stream of the set value, depending on a cathode temperature. The electron-optical system of the injector and of the accelerating tube form at the outlet windows of the accelerator a beam of 1-2 cm in diameter. The system of scanning of the accelerated electron beam (5) allows to move the received the electron stream up and down of the outlet vacuum window with the chosen frequency depending on the put technological problem. Also the scanning system allowed to move the electron beam from a window to a window. The control and diagnostics system (10) allows to measure all necessary parameters of

the accelerator and to ensure functioning of the accelerator according to the chosen algorithm of work. In detail principles of such type accelerators work is described in reference [1].

As a result of all carried out works the source of the electron beam on the basis of the industrial accelerator EOL-400M with energy E=300÷320 keV and a current I = 0.1÷4 mA is obtained.

The given installation assumes leading of the continuous accelerated electron stream of 1÷2 cm in diameter 1÷2 cm in turn through two foil windows. The outlet accelerator windows have a length of 100 cm and a width of 5 cm, a thickness of used foils is 100 microns. The electron flux by means of a scanning system uniformly moves over all the surface of windows, as in the longitudinal and transversal directions. Frequency of the beam transition from a window to a window is of 50 Hz, frequency of longitudinal scan is of 300 Hz, frequency of a transversal scan is 5 kHz.

The given parameters of the scanning system allow to lead into the atmosphere a continuous beam of the maximum power for this type of the accelerator. In our case can be lead the beam with a current density up to 60 $\mu A/cm^2$.

For researches under the project the parameters of the scanning system of the electron flux in existing installation have been changed in a way to provide the greatest possible density of a beam current lead into the atmosphere in sizes smaller than the area of the outlet window. It is necessary for widening of the experiment possibilities.

In the modernized system of scanning the following sequence of switching on of the scanning coils has been used. A beam with the maximum parameters for the restored accelerator (E=300÷320 keV, I = 0,1÷4 mA), it is continuously lead into the atmosphere through one of the windows, thus the longitudinal and the transversal scan is kept in the same values, as for the unchanged system of scanning. The amplitude of a beam deviation in a longitudinal direction is of 100 cm and in the transversal one is 5 cm. The frequency of scanning of a beam both in the longitudinal, and in the transversal cross-section directions corresponds to the unmodernized system. At the certain moment of time the beam is moved to another window under which the experimental chamber is placed.

The amplitude of a current in magnetic coils of the longitudinal and the transversal scan of the beam at this window changes in way to to provide the electron beam passage with the greatest possible density of a current through a minimum possible area of an outlet foil. A frequency of scanning of the beam both in the longitudinal and in the transversal directions at that remains the same. In our case for a beam leading into the experimental chamber the amplitude of a deviation in the longitudinal direction has been chosen from 15 to 50 cm and of 3 cm in the transversal one. The density of the lead beam thus is 30 $\mu m/cm^2$. Some difference from the greatest possible value of the lead beam current density for the given type of accelerators is defined by a technological degree of safety. Time of stay of the beam at one or another window was determined at adjustment of experiments under the project. In detail time characteristics are described below.

At present it is necessary to mark only that in the changed system of scanning the beam can be moved to one of the outlet windows for any time interval.

The form of current pulses in magnetic coils of the scanning system is represented in Fig. 4.

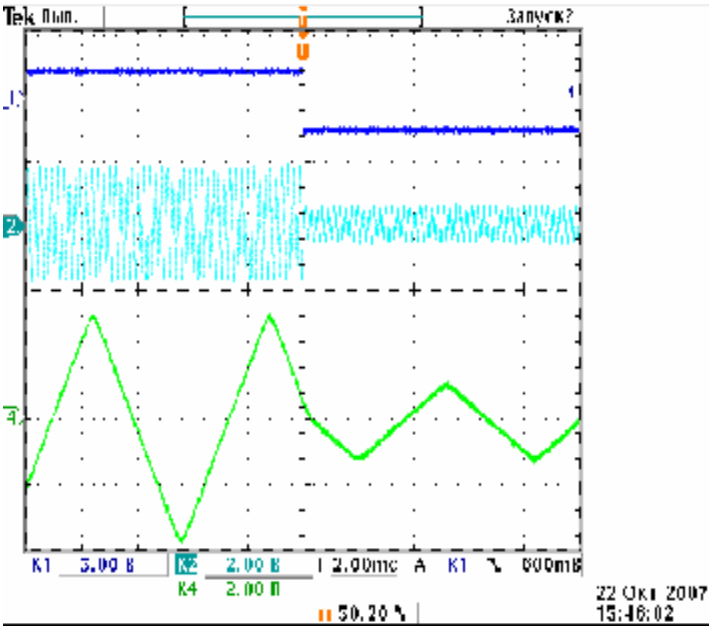

Fig.4 ***The form of currents in magnetic coils of the scanning systems***.
1- a current in the coil of transfer of a beam from one window to another window.
2 - a current in the coil of the transversal scan of a beam.
3 - a current in the coil of the longitudinal scan of a beam.
The left half of the waveforms - a current in magnetic coils of the scanning system at the full beam scanning over the outlet window.

The right half - a current in the coils at the beam lead during the experimental works.

Further we have to mark, that a beam of electrons, with the obtained parameters, will propagate in the atmosphere at a distance no greater than 56.7 cm before full slowing-down in air. In the presence of an additional foil this distance will be even smaller. Therefore the experimental chamber should be located as it is possible closer to the outlet foil window of the accelerator. In our case the distance of the chamber from the foil was no greater than 5 cm.

Also, at development of the experimental chamber, that fact was considered, that the distance between the outlet windows is no more greater than 25 cm, and each outlet foil of the accelerator is compulsorily cooled by an air stream. For gathering of the electron beam lead into the atmosphere and not used in experiments the special collector in the form of a massive aluminum plate has been made. This collector was settled down at a distance of 3 cm from the corresponding outlet vacuum window of the accelerator.

The system of the accelerator diagnostics allowed to measure all necessary parameter with sufficient degree of accuracy (an error of measurements is no greater than 10 %).

At this stage it was possible to consider that the electron accelerator modernization has been finished and for experimental researches the necessary source of the accelerated electron beam is created.

1.2 Creation of the experimental chamber

Investigations on influence of the accelerated electron stream and electric field on a burning processes of propane-air mixture was supposed to undertake in the experimental chamber specially developed for these purposes.

At creation of the experimental chamber limitations on the sizes and an arrangement of basic elements of the device were accounted for.

These limitations are connected with use of the available source of accelerated electrons and necessity of a correct arrangement of the elements, allowing to create in the chamber a required value of an electric field.

The distance between the outlet windows of the accelerator was no greater than 25cm, as is was told above. This fact brings limitations on the transversal sizes of the experimental chamber because the experimental volume should be located strictly under one of the outlet accelerator windows, and the beam lead into the atmosphere from another window should not influence a course of experiments.

Also it has been accounted for that each the outlet accelerator window is compulsorily cooled by the air stream that can affect results of experiments.

During works under the project, for creation of the electric field, it was supposed to use a high-voltage source with a voltage up to 10 kV.

From these reasons the constructive sizes of isolation gaps of the experimental chamber should provide a value of a field strength on a surface no greater than 7 kV/cm.

Considering the limitations set forth above, the experimental chamber used further in all experiments under the project wasdeveloped and made.

A drawing of the experimental chamber for researches under the project is represented in the Fig. 5.

The experimental chamber is a volume with a cross-section section of 30x50мм ² and length 500 mm; from sides it is limited by two transparent glass plates (1,2) of 25 mm thickness, necessary for ensuring of visual supervision over the processes occurring during experiments. The top metal plates (3,4) and the foil located between them (5) allow the accelerated electrons to get into the experimental volume. A thickness of aluminum plates is of 3 mm, and a thickness of a foil of aluminum is 50 microns. The size of the plates is 120x500 mm^2. The cut in the plates, for a foil placing is located strictly over an axis of the experimental volume, and has the size 20x470 mm^2. The foil presence is necessary for limitations of external factors influence on experiments. In the course of experiments to these plates and a foil high voltage of U=7-10 kV can be applied.

The bottom metal plate (6) is aimed for gathering of accelerated electrons, passed through the experimental volume, and also on it the device of of a fuel delivery (7), the device of ignition (8), the flame temperature measurement sensor (13) are located.

The thickness of a plate is of 3 mm and the sizes are 120x550 mm. The plate is isolated from the grounding in order that there was a measurement possibility of the current characteristics.

End faces of the experimental volume through the isolation spacers (9,10) are closed by an entrance (11) and the exit (12) flanges. The sizes of the isolation spacers are 30x80x120 mm^3. All elements of the experimental chamber are connected between themselves densely as possible to provide an absence of environment influence on results of researches. The air line is attached to an entrance flange (11) experimental chambers from the fan providing a stream of air for undertaking of investigations .

The exit flange (12) is connected with the device of bending of burning products from the experimental volume into a ventilating system of the accelerating installation.

As a result of the carried out works the experimental chamber which photo is represented in Fig. 6 has been developed, designed and manufactured.

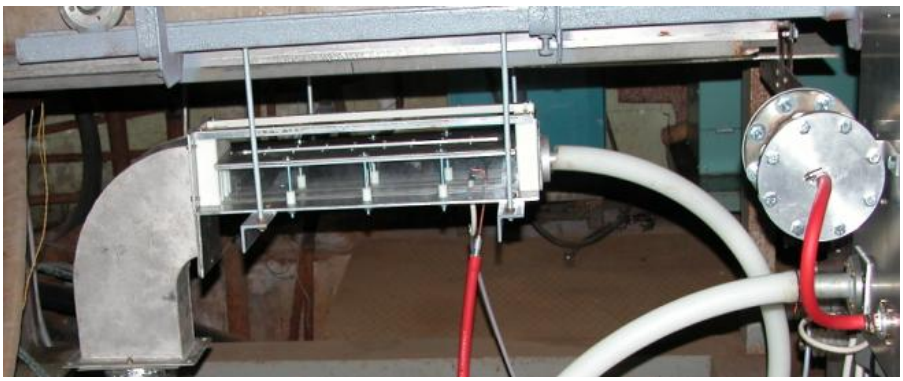

Fig.6 A photo of the experimental chamber .

The experimental chamber is created under the following algorithm of carrying out of experimental researches.

During the initial moment of the experiment from the entrance flange (11) the air stream of the required value is created, then through the device of fuel delivery (7) in the chamber a gas moves and by means of the ignition system (8) the obtained gas-air mixture is ignited. At any moment before the gas mixture ignition or, or after, presence of electric field in the chamber and presence of a accelerated electron beam can be provided.

Transparent walls of the experimental volume allow to carry out visual observation the processes taking place in the chamber. Temperature sensor (6) located on a plate (13) allows to carry out measurements of flame thermal characteristics in the conditions of the experiment.

At the given stage, it is possible to consider, that the experimental chamber is ready for carrying out of experimental researches.

1.3 Creation of experiments ensuring systems

By experiment conditions the electron beam from the accelerator should influence an area of propane-air mixture burning in the experimental chamber in the presence of the external electric field and in the presence of the directed air stream.

For insurance of these requirements during a course of works the device of experiments insurance is created.

Into a composition of the given device equipment enter: a system of a gas delivery, the device of a gas mixture preparation , the high-voltage discharge device for ignition of a gas mixture, the high-voltage source of constant voltage providing functioning of the discharge device, a high-voltage source of constant voltage for an electric field creation in the chamber and an air line with the fan for insurance of an air stream.

1.3.1 An air line with the fan for insurance of an air stream

Fig.7 A photo of a air flow velocity measurer ATT-1000

At the initial stage of works under the Project as a source, providing an air stream in the experimental chamber, the fan of the vacuum pump cooling was used. The fan exit was connected with an entrance flange of the experimental chamber by a plastic hose of 40 mm in diameter of 40 mm. The speed of an air stream created in the chamber was regulated by change of a feeding voltage of the fan. For measurement of an air stream speed an anemometer-adapter ATT-1000 is used. The device photo is represented in Fig. 7.

The given device allows to make measurements of an air stream speed in a range from 0.8 to 25 m/s that is quite sufficient at the given stage of researches. The measurements carried out in the experimental installation, have shown, that, at an existing configuration of air lines and the chosen type of an air supercharger, the speed of an air stream in the experimental chamber can be change from 1 to 5 m/s.

At such type of the device providing an air stream in the chamber, the certain cycle of experiments has been carried out.

For carrying out of experiments in which the air stream with greater speed in the chamber was necessary , a modernization of a source insuring an air flow has been carried out.

As modernization of the given system a replacement of the fan providing an air stream with a speed no greater than 5 m/s, by more perfect installation collected on base of impeller W/28/31 and a regulator of turns EF-ESC60A, BEC is made. The photo of basic elements of the new air system is represented in Fig. 8.

Fig.8. A photography of basic elements of the new air system.

The new air system allowed to change speed of an air stream in the experimental chamber over a wide range, namely from 1 to 25 km/s. It is necessary to notice, that a speed of a gas stream in the chamber, at use of the modernized system, it was regulated with high accuracy by means of electronics.

At the given stage of researches quality of the air stream in the chamber was not estimated, and it was impossible to define if the stream in the chamber was laminar or turbulent.

1.3.2. High voltage source of the constant voltage for creation of an electric field in the chamber

High voltage source of the high voltage in the chosen configuration of the is the industrial source IVN-10 with adjustable outlet voltage from 0 to 10 kV. A moment of a source switching on and duration of its work is set by the installation control system.

The source is connected with the top plates of the experimental chamber (3,4) and the foil located between them (5) (see Fig. 5) by means of the isolated high-voltage cable.

At the source switching on, at plates and a foil appears a voltage of positive polarity of 10 kV value.

As the distance between the top plates (3,4) and the bottom plate (6) of the experimental chamber is 5 cm it is possible to consider , that at switching on of the high-voltage source then in the experimental volume there will be realized an electric field with the strength from 0 to 2 kV/cm

1.3.3. The high-voltage discharge device for ignition of a gas mixture. The high-voltage source of constant voltage providing a functioning of the discharge device

For ignition of propane-air mixture is used the high-voltage discharge device.

This device is the two-electrode discharger connected with the high-voltage storing capacitor. The charging of the storing capacitor is insured by a high-voltage source of the constant voltage.

As the high-voltage and earthed electrode of the discharger the tungsten wire in of 0.8 mm in diameter is used.

Both electrodes are fastened to the isolated cylinder. A distance between electrodes over a surface of an insulator is 5 mm, and a distance from the electrodes over an insulator to the earthed plate (6) of the experimental chamber is 10 mm. Out of the insulator limits inside the chamber the electrodes of the discharger are moved forward for 15 mm.

In the top part of the electrodes moved forward in the chamber the spark gap is generated in which the distance between the electrodes is reduced to 0.7 mm. The discharger drawing is represented in Fig. 9.

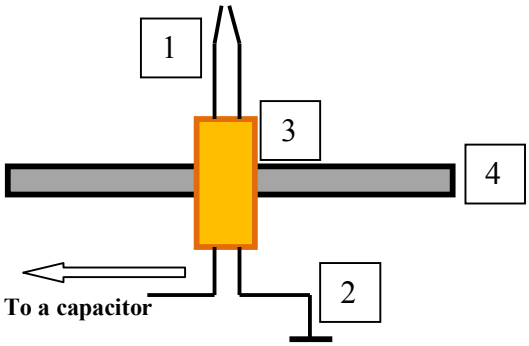

Fig. 9. A picture of the discharger of the gaseous mixture ignition system.

1- A high voltage electrode of the discharger;
2- Grounded electrode;
3- Isolation cylinder;
4- A plate (6) of the experimental chamber (Fig. 5 of Section 1.2)

The storing capacitor of the ignition system, is connected with a high-voltage electrode of the discharger. The capacitor is charged from the industrial high-voltage source UVN-20 to a voltage at which a breakdown of an inter electrode gap of the discharger takes place. Plasma appearing at the breakdown initiates ignition of the gas mixture. Level of energy of the initiating discharge can be regulated by means of the storing capacity variation or of a level of the voltage of its charging. . In the majority of experiments a level of energy of the initiating discharge was 100÷200 mJ. Duration of a discharge pulse was no greater than 20 μs. The length of a spark in the discharger was no greater than 1 mm. The industrial high-voltage source UVN-20 allows to charge the storing capacitor to a voltage of 20 kV.

1.3.4. A system of the gas delivery and a device for a gas mixture preparation

The system of a gas delivery consists of a gas balloon with a reducer, a manometer, a receiver, the pulse gas valve with the electric drive, connecting gas hoses. The system scheme is represented in Fig.10. A gas from a balloon by means of a reducer moves into a receiver and is given up to pressure required according to experiment conditions. Pressure is measured in a receiver by the manometer connected with it. At opening of the pulse gas valve the portion of gas necessary for experiments moves into the system of preparation of a gas mixture. The moment of opening of the gas valve and time of its staying in an open condition is set by the control system of installation and is defined by the experiment conditions.

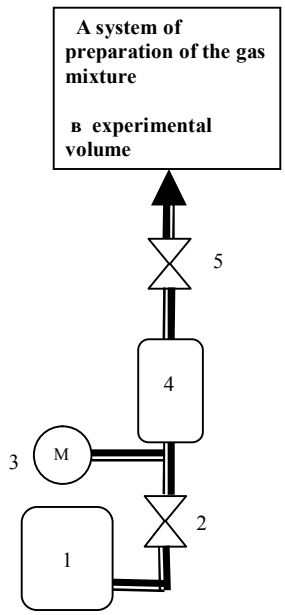

1 A balloon with a gas
2 Reducer
3 Manometer
4 Receiver
5 Pulsed valve

Fig.10 A scheme of the gas delivery system

A gas from a balloon by means of a reducer moves into a receiver and is delivered up to pressure required by the experimental conditions. Pressure is measured in a receiver by the manometer connected with it. At opening of the pulse gas valve the portion of gas necessary for experiments moves into the system of preparation of a gas mixture. The moment of opening of the gas valve and time of its staying in an open condition is set by the control system of the installation and is defined by experiment conditions.

As is known, a stable burning the propane -air mixture takes place at a weight ratio of a propane portion and a portion of air as 1:16. The device of preparation of a gas mixture is applied to insure these conditions. The device is the brass cylinder with internal diameter of 8 mm and length of 70 mm. A thickness of a wall of the cylinder is of 1 mm. At the distance of 10 mm from one of edges the cylinder is connected with a copper tube in diameter of 4 mm in diameter. In the top part of the tube located in the cylinder, there is a hole of 0.7 mm in diameter for leak in of a gas. The hole is oriented in a side of the longer part of the cylinder.

The bottom part of the tube is connected with a gas hose of the gas delivering system. The device is placed in an initial part of the experimental chamber, and is oriented by a short part of the cylinder towards an entrance flange of the chamber. The gas arriving from the gas delivery system propagates over the internal area of the cylinder mainly to a side of the longer part, due to the orientation of the entrance hole. In process of the propagation the gas mixes up with air in a proportion necessary for burning, and arrives at the area of ignition of a gas mixture. The device picture is represented in Fig. 11.

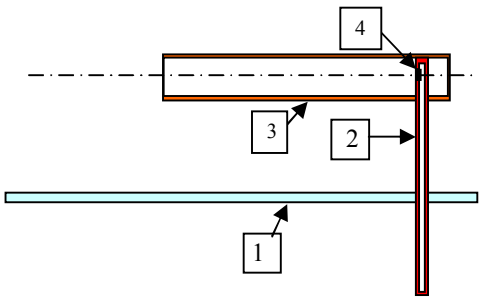

Fig.11. The device of preparation of the gas mixture.

For estimation of sizes of the gas mixture preparation system with some definite level of accuracy one can use empirical formulas represented in the book [2 . Loitsyanskyi L.G. “ Mechanics of Liquids and gases” , Nauka, Moscow. 1970].

$$M_{out} = \sqrt{[(p_0/p_{out})^{1/8,69} - 1]/0.65} \quad (1.1)$$

Where M_{out} is Mach number at propane outflow through the hole, P_0 gas pressure at the inlet into the hole, P_{out} - gas pressure at the gas outlet from the hole. In our case M_{out} = 0.13.

$$V_{out} = V_{sound} M_{out}$$

Where V_{out} – is propane velocity at the outlet from the hole. V_{sound}. Is a sound velocity for propane (V_{sound} = 250 m/s). For our case $V_{вout}$ = 32.5 m/s.

$$m = \rho_{out} \cdot V_{out} \cdot S_{out}, \text{ [g/s]}$$

m- is weight gas flow rate at propane leak out through the hole
$\rho_{out} = \rho_0 = 1.23 \cdot 10^{-3}$ g/cm^3· - propane density at the outlet from the hole.

S_{out} - the hole cross section area.
For our case m = 0,73 · 10^{-2} g/s.

Using the formula (1.1) for a calculation of the weight flow rate of a gas one can estimate the weight flow rate of air passed through a hole of a given cross section. For our case $M_{air} = 1{,}094 \cdot 10^{-1}$ g/s.

Thus, in the system of preparation of the gas mixture, at a speed of the air stream of V =3 km/s the propane-air mixture is created in a weight ratio of a portion of propane and a portion of air as 1:15.

It is obvious, that being based on the represented formulas it is possible to conclude, that at preservation of a portion of the gas which has got to the system of mixing, and at increase in speed of air flow through this system it is possible to regulate a percentage ratio of propane portion and a portion of air in the mixture. At increase in speed of an air stream by five times it is possible to obtain a mixture in weight proportions 1: 45. In the course of experimental works such a method of change of weight proportions of the propane-air mixture has been successfully used.

1.3.5 Arrangement of elements of systems of support of experiments

It is obvious that the spark discharger of the ignition system should be placed in direct proximity from the exit of a gas mixture from the preparation system to provide an ignition of the propane-air mixture in the set place of the experimental volume. During the researches in the experimental chamber the length of a flame at burning of prepared the propane-air mixture should be sufficient for convenience of carrying out of visual observation and measurements of temperature characteristics.

The arrangement of the system of the experiments insurance some elements in the experimental chamber is of great importance for performance of this condition.

It is obvious that for realization of the maximum length of a flame, the device of the gas mixture preparation should be in the beginning area of the experimental chamber, and the ignition device should be located as closely as possible to the outlet cut of the brass cylinder of the gas mixture preparation system.

In Fig. 12 the arrangement of elements of the experiments insurance system of experiments is represented in the experimental chamber.

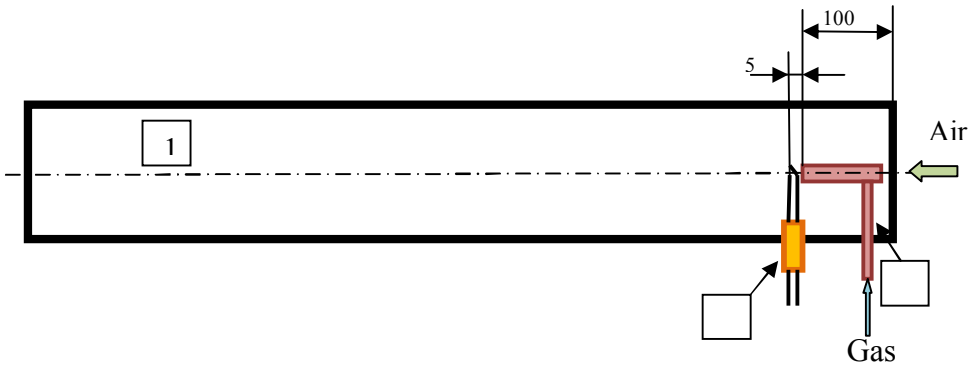

Fig.12. Experiments insuring system elements placing in the experimental chamber.

The outlet end of the brass cylinder of the gas mixture preparation system (3) is located at a distance of 100 mm from a the outlet cut of the experimental volume, and at the distance of 5 mm from it the spark gap of the discharger of the ignition system (2) is located.
The cylinder of the gas mixture preparation system is placed over the center of the experimental chamber (1). The cylinder axis is at a distance of 25 mm from the bottom plate of the chamber and at a distance of 15 mm from the glass plates of the chamber.

Thus 400 mm of the internal volume of the experimental chamber are aimed for carrying out of researches and placing of the diagnostic equipment.

4.1.Creation of the installation control system

The control system of EOL-400M restored at a stage of the accelerator modernization , provides obtaining of necessary parameters of an electronic beam arriving in the experimental chamber.

The control system of the complex installation allows to synchronize a switching of all the systems and devices of the installation for insurance of the experimental requirements.

The given system is created on the basis of a logic module LOGO! of the company SIEMENS which photo is represented in Fig. 13.

Fig. 13 The logic module of the LOGO! фирмы SIEMENSof the company SIEMENS

An electric scheme of the complex installation control system is represented in Fig. 14.

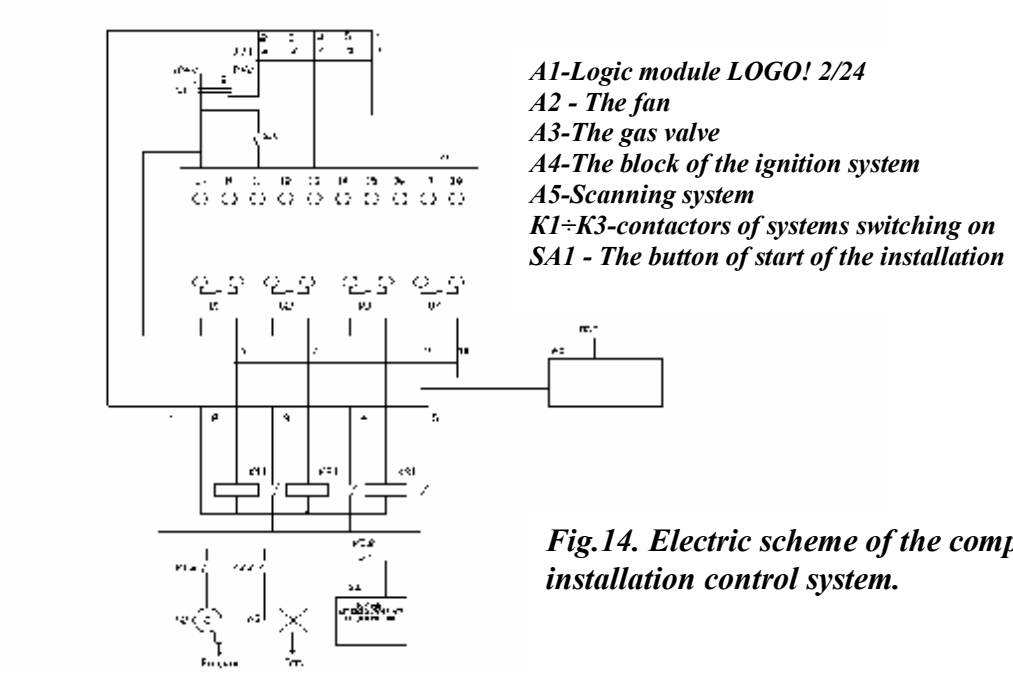

A1-Logic module LOGO! 2/24
A2 - The fan
A3-The gas valve
A4-The block of the ignition system
A5-Scanning system
K1÷K3-contactors of systems switching on
SA1 - The button of start of the installation

Fig.14. Electric scheme of the complex installation control system.

For carrying out of researches on influence of an electron beam and electric field on combustion processes of the propane - air mixture the following sequence of switching on of the equipment of the complex installation has been accepted.

1. The electron accelerator EOL-400M was switched on. By means of the modernized system of scanning the flux of the accelerated electrons was lead into the atmosphere through a vacuum window under which the collector was placed. (It is necessary to notice, that the given stage of switching on of the complex installation was autonomous and was controlled by the control system of the accelerator)
2. The fan providing an air stream through the experimental chamber was switched on at the initial moment of time.
3. At the same moment was switched on a source of the high voltage IVN-10 and an electric field was created in the experimental chamber.
4. Further by means of the modernized scanning system of the electron beam it was moved to a vacuum window under which the experimental chamber was located.
5. At a following stage the valve for propane leak in was opened.
6. Then the power supply of the ignition system of the gas mixture was switched on.
7. At the following step the power supply of the gas mixture ignition system was switched off, and were consequently switched off all earlier switched on systems in the sequence of return sequence of the switching on. (The accelerator was switched off only after a special command of the operator).

Actions 2÷7 were carried out automatically by pressing of the start button (SA1) of the complex installation control system. Duration of a time interval between the switching on and shut down of each of the systems was also insured by the control system of the complex installation.

The time diagram of the switching on sequence of the complex installation equipment is represented in Fig. 15.

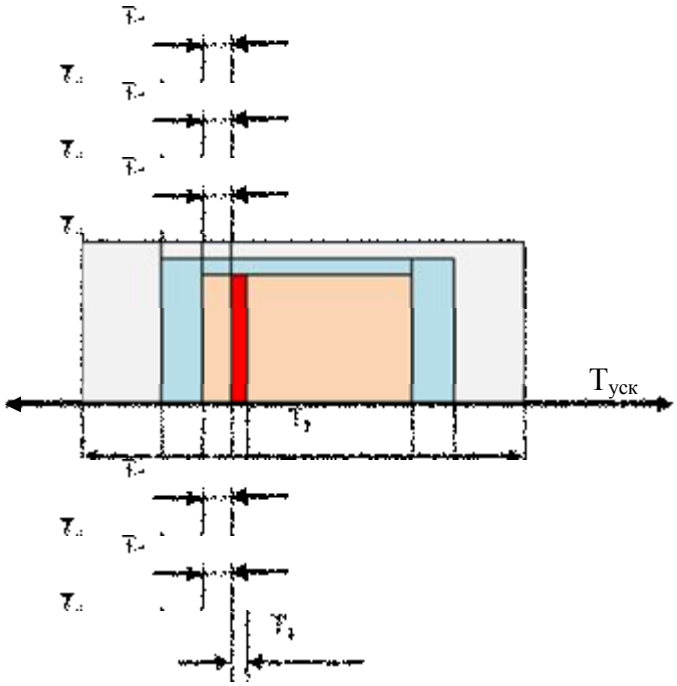

Fig.15 Time diagram of the switching on sequence of the complex installation equipment.

In the given picture the time sequence of switching on of the complex installation equipment during carrying out of experimental researches is represented.
T_{acc} - Switching on and off of the electron accelerator is carried out by means of the modernized EOL-400M control system.

Duration of work of the given device is defined by the operator serving the accelerator, as agreed with the experimenter.

T_1 - Duration of switching on of the fan defining presence of air stream in the experimental chamber, and the source IVN-10 providing presence of an electric field in the chamber.

For all carried out experiments $T_1 = 8$ seconds

(In the experiments with absence of the electric field the feeding of the source IVN-10 was not realized).

T_2 - Duration of accelerated electron beam presence in the experimental chamber.

For carried out experiments $T_2 = 4$ seconds.

(In experiments with absence of the electron beam the accelerator was not switch on).

T_3 - Time at which the valve forpropane leak in to the chamber is opened.

For carried out experiments $T_3 = 1.5$ seconds

Actions 2÷7 were carried out automatically by pressing of the button of start (SA1) of the complex installation control systems. Duration of a time interval between switching on and off of each of the systems was also provided by the control system of the complex installation.

The time diagram of the switching on sequence of the equipment of the complex installation is represented in Fig. 15.

(In experiments with absence of the propane stream the electric feeding to the valve was not given).

T_4-Duration of switching on of the feeding source of the ignition system of the gas mixture. For the carried out experiments $T_3 = 0.07$ seconds

(In experiments with absence of the propane stream the electric feeding to the high-voltage source of the ignition system was not given).
T_5 - Time of a switching delay of an accelerated electron flux, after occurrence of the air stream and the electric field in the chamber. For carried out experiments $T_5 = 2$ seconds.
T_6 - Time of a switching delay of the valve of the gas leak in after the electron flux occurrence in the chamber. For carried out experiments $T_6 = 1.5$ seconds.
T_7 - Time of a switching delay of the power supply of the ignition of the gas mixture system after the occurrence of a gas stream in the chamber. For the carried experiments $T_7 = 0,5$ seconds
The time characteristics represented here are obtained on the basis of adjustment experiments which will be described below.
The time diagram of the complex installation equipment switching on sequence is represented in Fig. 15.

1.5. Creation of the diagnostic complex

Into the diagnostic complex enter: the device of measurement of the electronic flux basic characteristics, a set of plates for measurement of currents in the experimental chamber, sensors for gas flame temperature measurements and the system of visual observation the processes occurring in the experimental chamber in the course of researches.

1.5.1. **Measurement of the basic characteristics of the electron beam**

Parametres of the electron beam at the outlet window of the accelerator are measured by the diagnostic aids of industrial accelerator EOL-400M. At the accelerator switching on a value of energy of the beam accelerated electrons and a total current are determined. At carrying out of researches under the project the beam with the energy of 300÷320 keV was used. The total current of the beam was changed from 0.1 to 4 mA depending on experiment requirements.

1.5.2 **Measurement of currents in the experimental chamber**

For carrying out of measurements of the currents flowing in the experimental chamber in the course of researches, the set of the plates which are constructive elements of the experimental chamber is applied. The scheme of this set is represented in Fig. 16.

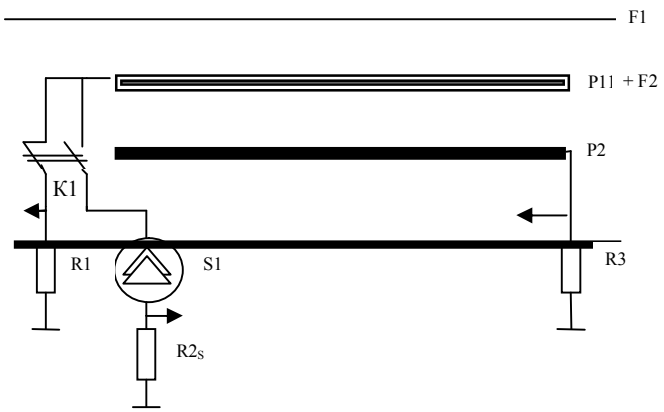

Fig.16 A scheme of the set of the plates for measuring of currents in the experimental chamber.

S1- High-voltage.
F1- Outlet foil of the accelerator -400M. (A width of the foil is 100 μm. Material - titanium).
P1 – upper plates 3.4) of the experimental chamber (see Fig. 5 , Chapter 1.2).
F2 – A foil Φ (5) of the experimental chamber, being between the plates (3,4) (see. Fig.5 Chapter 1.2). (A thickness of the foil - 50 μm. Material – aluminum).
P2 – a lower plate (6) of the experimental chamber. (see.Fig.5, Chapter. 1.2).

By a signal from the plate P1 and the foil F2 it was possible to measure a current of the electron beam, got to this plate - a current appearing in the chamber at burning the propane -air mixture in the presence of the electric field.

By a signal from the plate P2 it was possible to measure: - a bunch current of the electron beam, got to this plate - a current appearing in the chamber at burning the propane -air mixture in the presence of the electric field.

By the experimental conditions the constant high voltage can be applied to the plate P2 and the foil F2 up to 10 kV. For insuring of a possibility of
current measurements from this plate the key K1 is foreseen which, at switching-off of the high-voltage source, switches a current-measuring circuit of the given plate in accordance with the scheme represented in Fig.16.

1.5.3. Temperature measurement.

In the course of experiments is supposed to measure a temperature of the propane-air mixture which is inflammated at its ignition by the spark of the high-voltage discharger.

As the temperature sensor the hromel-alumel thermocouple (THA) has been used. This type of thermocouples allows with a sufficient accuracy to measure a joint temperature in limits of 500÷1300 C.
On the basis of this thermocouple the temperature sensor which appearance is represented in Fig. 17 is developed.

Fig.17 A photo of the temperature sensor

The temperature sensor represents a copper tube of 6 mm in diameter with a carving on an external surface for fastening possibility in the experimental chamber. Directly in this tube the thermocouple is placed. The place of the thermocouple joint is lead out of the limit of the copper tube for 5-7 mm. Temperature measurements are carried out by the value of a voltage signal on the cold end of the thermocouple, compared with data represented in the reference [3]. Accuracy of measurements are not above 10 ÷ 15 %.

The typical form of a signal from the temperature sensor is represented in Fig.18.

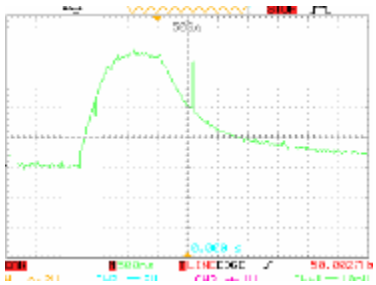

Fig.18. A typical signal form from the temperature sensor.

At carrying out of researches this sensor in various places of the experimental chamber is located, and by signals from them we determine the temperature of a gas flame. In our case for an arrangement of the temperature sensor in the plate (6) of the experimental chambers (see Fig. 5 of Chapter 1.2) the holes over the center of the narrow side of the plate and in regular intervals over the length of the wide side have been drilled. During researches under the project in these holes the temperature sensor was located so that the joint of the thermocouple was placed at a distance of 10 mm from the plate (6) of the experimental chamber.

Analyzing the typical form of a signal from the temperature sensor, it is possible to make the conclusion, that time during which the signal from the sensor comes to the constant value is no greater than 1 second. This value was considered further as a constant of time for the given sensor.

1.5.4. **System of a visual observation of the processes in the experimental chamber**

Since the experiments on influence of an electron flux on burning processes of the propane - air mixture fuel are carried out in the conditions of higher radiation then direct visual observations are impossible. Admissible level of the ionizing radiation is of 10 ÷ 20 mkR/hour. At the EOL-400M accelerator work this level of radiation increases by hundreds times, therefore accelerators of such type always are placed in the special protected premises. For carrying out of visual observation in the conditions of our experiment the system based on application of the IP-camera and the computer is created..

IP- camera location at the undertaking of experimental investigations is shown in Fig.19. The given system allows to write down, reproduce and process results of visual observation of the processes occurring in the experimental chamber in the conditions of higher radiation.

Fig.19 ***IP- camera location at the undertaking of experimental investigations***

Chapter 2. Results of the experimental investigations (Tasks 1, 2, 3, 4, 5 and 6 of the Project)

During works under the project we have created the complex installation at which use all spectrum of the planned experiments on research of an influence of a flux of the accelerated electrons and the electric field on processes of propane-air mixture burning has been carried out.

2.1 Preliminary experiments. (Tasks 1,2,3 and 4 of the Project)

A series of preliminary experiments was aimed for determination of working ability of the complex installation equipment in real conditions and selection of optimum time characteristics of the control system.

It was necessary to provide appearance of a stable flame at burning of the propane-air mixture, formed in the experimental volume.

It was necessary to adjust the system of the electron beam scanning system of scanning in a way to insure getting of the greatest possible part of the electron flax into the experimental volume. We had to measure a relative value of the electronic beam current which has gotten to the volume.

We had to define a working capacity of the temperature sensor in real conditions of the experiment.

2.1.1 Experiments on insurance of stable ignition and burning of the propane-air mixture

For occurrence and stable burning the propane - air gas mixture in the experimental chamber created by us, was supposed to ignite by means of the spark discharge in specially selected gas volume in the presence of necessary volume of air.

The experiment was carried out in the following sequence. From a balloon with the gas (1) through a reducer (2) the gas moved to a receiver (3). By means of a manometer (4) pressure of gas was measured in a receiver. (All listed devices are a part of the system of the gas deliver of the complex installation and are in detail are described in Chapter 1 section 1.3.4 of the present report (see Fig. 10). Simultaneously with it the fan of air stream insurance in the experimental chamber (see Chapter.1, 1.3.1) was switched on.

At the stage of preliminary experiments the fan from the vacuum pump was used.

At the following stage the gas valve (5) of the gas delivery system was opened and the power supply of the storing capacitor of the igniting system (Chapter.1, 1.3.3) was switched on.

A selection of gas pressure values in the receiver (3) of the gas delivery system (Fig. 10), speed of the air stream in the experimental chamber and a level of charging of the storing capacity of the device of the the ignition, providing stable conditions of ignition and burning of the propane- air mixture was the experiment purpose.

During carrying out of the given experiment the accelerator EOL-400M providing presence of the beam of the accelerated electrons, and the high-voltage source IVN-10 providing presence of the electric field in the experimental chamber was not switched on.

It is necessary to remind, that the speed of the air stream in the experimental chamber is in strict correspondence with the speed of the fan rotation which in turn depends on a voltage of the power supply of the latter.

At a stage of creation of complex installation A dependence of the air stream speed in the experimental chamber on a feeding voltage of the fan has been found at application of the air stream measuring instrument ATT-1000.

Stability of ignition and burning of the obtained propane-air mixture was determined at the analysis of visual observations.

In Fig. 20 the most typical photos of the burning process of the propane - air mixture are represented under various conditions of the experiment..

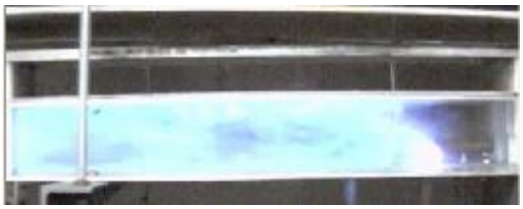

***Fig. 20a**. A photo of the propane-air mixture burning process in the experimental chamber at the air stream speed smaller than 0.5 m/s and pressure of gas in the receiver p=1.1 atm..*

***Fig. 20b**. A photo of the propane-air mixture burning process in the experimental chamber at the air stream speed 3 m/s and pressure of gas in the receiver p> 2 atm..*

***Fig. 20c**. A photo of the propane-air mixture burning process in the experimental chamber at the air stream speed 3 m/s and pressure of gas in the receiver p=1.1 atm.*

Analyzing the obtained images and results of visual observation, it is possible to make the following conclusions.

1. At the air stream speed smaller less than 0.5 m/s occurs sharp ignition of the propane-air mixture in all the volume of the experimental chamber only during the initial moment of gas delivery. Ignition occurs at gas pressure in the receiver of p=1.1 atm that is the minimum value of pressure which it is possible to measure by the applied manometer. (The pressure increase in a receiver was not carried out because of explosion danger of the obtained mixture). On the basis of this follows that the speed of the air stream in the experimental chamber should be greater than 0.5 m/s.

2. At the air stream speed in the chamber of 3 m/s and pressure of gas in a receiver $p \geq 2$ atm an ignition and burning of the propane-air mixture is not stable, that speaks about change of weight rations between propane and air in the system of the gas mixture preparation of the complex installation.

3. At the air stream speed in the chamber of 3 m/s and pressure of the gas in the receiver P=1.1 atm an ignition and burning of the propane-air mixture is stable on the whole time interval at which the gas valve of the gas delivery system is opened.

The carried out cycle of experiments has allowed to determine an optimal value of propane pressure in the receiver of the gas delivery system and the air stream speed necessary for stable burning in the experimental chamber.

It is revealed that pressure in the receiver should be no greater than p=1.1 atm and the air stream speed in the experimental chamber not smaller than 3 m/s. At these parameters and the geometrical sizes of the installation created by us there is a stable flame at burning of the propane-air mixture occupying the space of no greater volume than the internal volume of the experimental chamber.

It is necessary to mark that at various levels of the storing capacitor charging of the the ignition system and a duration of the power supply switching on of this system not smaller, than the values providing an occurrence of the spark discharge, the burning is stable at the chosen optimum parameters of the gas pressure and the air stream speed.

For optimization of an energy level in the spark of the ignition system discharger necessary for stable ignition of the propane - air mixture, a special experiment is made.

The experiment was carried out as follows. A voltage of the power supply of the storing capacitor and duration of the switching on of this source gradually decreased. Occurrence of the spark discharge in the ignition system was fixed by means of the visual observation. It is revealed, that at the voltage of a source of storing capacitor charging $U \leq 4$ kV and duration of the given source staying in the switched on condition of $t \leq 0.05$ seconds the spark does not appear.

Stably the spark of the ignition system appeared at U=5 kV and a duration of t =0.07 second.

At these parameters of the ignition system the gas into the experimental chamber delivered and the air stream in optimum proportions described above was created. It is revealed that the spark arising in the ignition system stably ignited such a gas mixture. In Fig.21 is presented the waveform of the voltage pulse signal on the discharge gap of the spark discharger of the gas mixture ignition system.

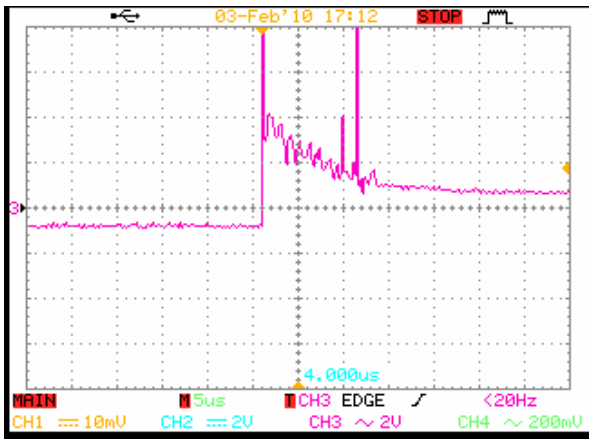

Fig. 21. The waveform of the voltage pulse signal on the spark discharger discharge of the gas mixture ignition system.

Considering the waveform, it is possible to determine a duration of the spark in the discharge gap. Having measured absolute value of a voltage and a current in the discharger, it is possible to estimate a level of energy released in the spark.

In our case the duration of the voltage pulse was t=17 μs.

By the estimated data the level of energy released in the spark gap of the discharger is E = 100÷200 mJ. The parameters defining the work of the ignition system and providing a stable ignition of the propane - air mixture in all subsequent experiments were considered as optimal and were used for ignition of a gas mixture.

2.1.2. Experiments on adjustment of the accelerated electron beam parameters

Parameters of the electron beam taking part in the experiments under the project are limited by possibilities of the applied accelerator. The adjustment of the system scanning system of the accelerator EOL-400M and measurement of relative value of the beam current which has gotten on plates of currents measurement in the experimental chamber was the problem of the experiments present cycle.

In Fig. 22 a and b the scheme of the adjusting experiment on determination of parameters of an electron beam participating in experiments under the project is presented.

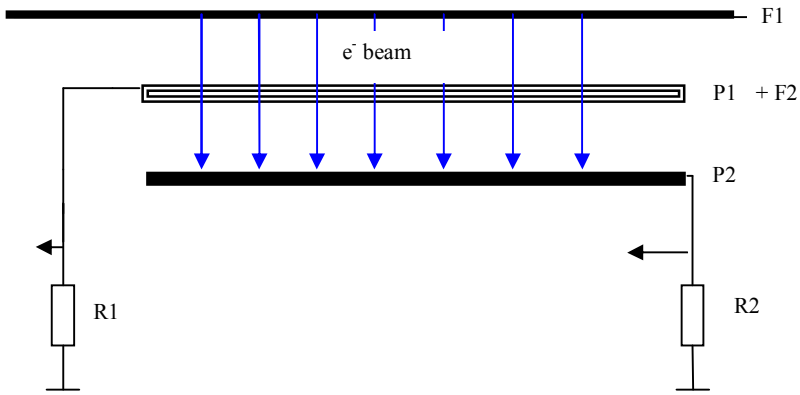

Fig. 22a. A scheme of the experiment on the adjustment of a beam of the accelerated electrons. Appearance from a side.

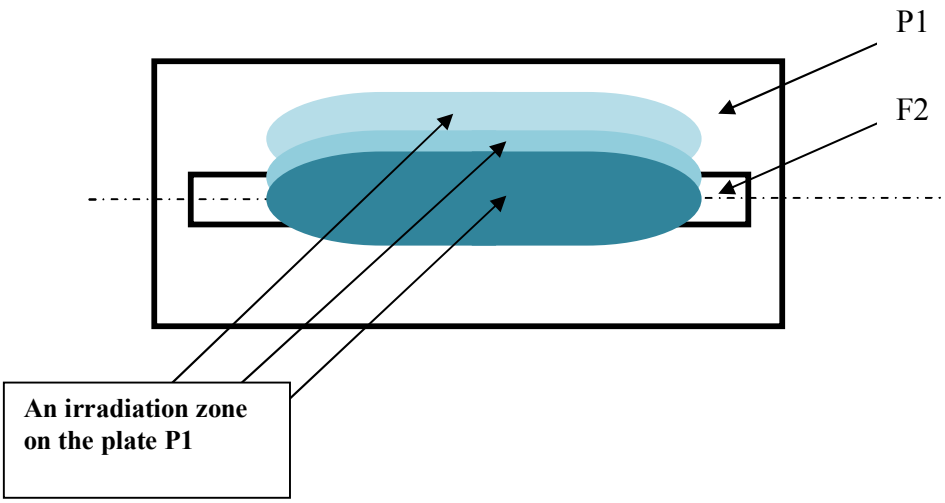

Fig. 22b ***A scheme of the experiment on the adjustment of a beam of the accelerated electrons. Appearance from above.***

The experiment was carried out in the following sequence. The accelerator was switched on and by means of the scanning system the obtained electron beam flux was lead to a collector the accepting the beam lead into the atmosphere. Then by means of the complex installation control system the beam was moved to the vacuum window of the accelerator aimed for its delivering into the experimental chamber. A duration of the beam presence at this window usually did not exceed 7 seconds.

Further the experiment course corresponded to the scheme represented in Fig.22 a and b.

The accelerated electron beam from the accelerator passed through the foil F1, got to the plate P1 of the experimental chamber in which center there was a slit of 2 cm in width closed by the foil F2. A part of the beam through the foil F2 got into the experimental chamber. By signals from resistors R1 and R2 it is possible to estimate a value of a current to the corresponding plates.

The system of the accelerator scanning is adjusted in such a manner that the zone of an irradiation of the experimental volume had the sizes of 30 cm along the slit with the foil F2 and 8 cm across.

The irradiation zone has been measured by means of the dosimetry films darkening at hitting it by the accelerated electrons flux. Thus, the part of the beam passed through the foil F2 and getting to an area of the experimental chamber where there should be an interaction of the electron flux with the gas-air mixture- does not exceed 25 % of a current of an electron beam gotten to the plate P1. The irradiation zone on the plate P1 differs from the sizes of the beam at the outlet window of the accelerator because of a divergence of an electronic flux in the atmosphere. The plate P1 was at the distance of 3 cm from the foil F1 of the accelerator.
Characteristic waveforms of the current gotten to the bottom plate P2 of the experimental chamber and the plate P1 are represented in Fig. 23.

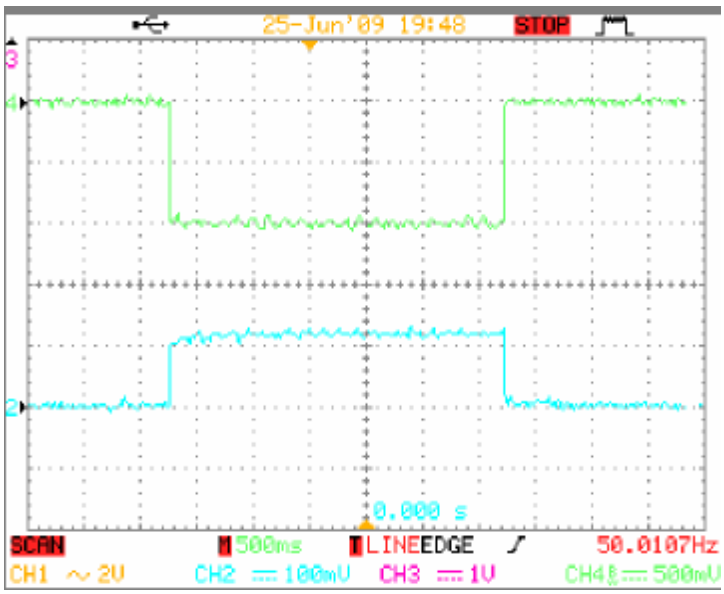

Fig. 23. **Typical waveforms of the beam current gotten to the plate *P2 (beam 2) and P1 (beam 4)***

In Fig. 22b the picture of getting of the electron flux from the accelerator to the plate P1 with respect to a value of a current in the magnetic coil of the scanning system responsible for moving of a beam from a window to a window is shown.

In a course of an adjusting experiment a value of this current has been in a manner to provide the maximum passage of an electron beam to the experimental chamber. It was determined both with the help of current measurements, and by means of the visual observation.

In Fig.24 photos of a luminescence of air under the influence of the electron beam in the volume of the experimental chamber are represented at various values of a current in the magnetic coil of the scanning system.

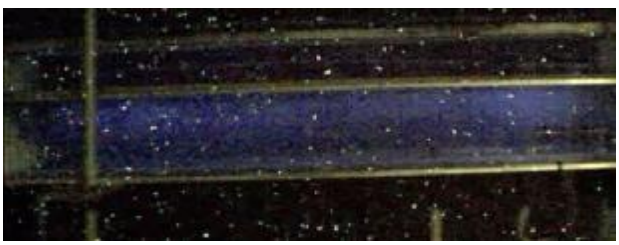

Photo 1

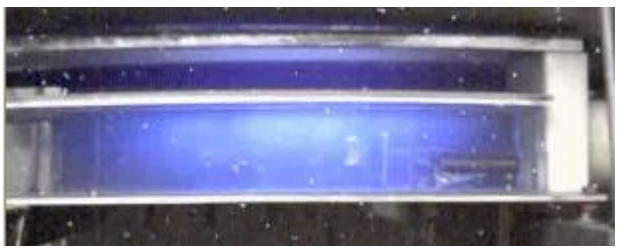

Photo 2

Fig.24 Photos of a luminescence of air under the influence of the electron beam in the volume of the experimental chamber, at various values of a current in the magnetic coil of the scanning system . (The current I_1 the the photo (1) is << than the current I_2 at the photo (2)).

The analysis of current measurements results shows that the current of the beam which has reached the plate P2 of the experimental chamber does not exceed 9 % of the full current which has reached the experimental chamber (see Fig. 23).

2.1.3. Experiments on determination of a working capacity of the temperature sensor

As the basic diagnostic device at carrying out of research works the temperature sensor with thermocouple TCA is used. The design of the given sensor is in detail described in the Chapter 1, part 1.5.3.

A determination of working capacity of the created temperature sensor in the conditions of real experiment in the presence of all external factors capable to affect its indications was a problem of the given experiments cycle.

At tests the time estimation of the temperature sensor indications coming to the stationary value also has been carried out at burning constancy of the propane-air mixture. By the value of this time the opening duration of the gas valve further was determined further .

The experiment scheme on determination of the working capacity of the temperature sensor is represented in Fig.25.

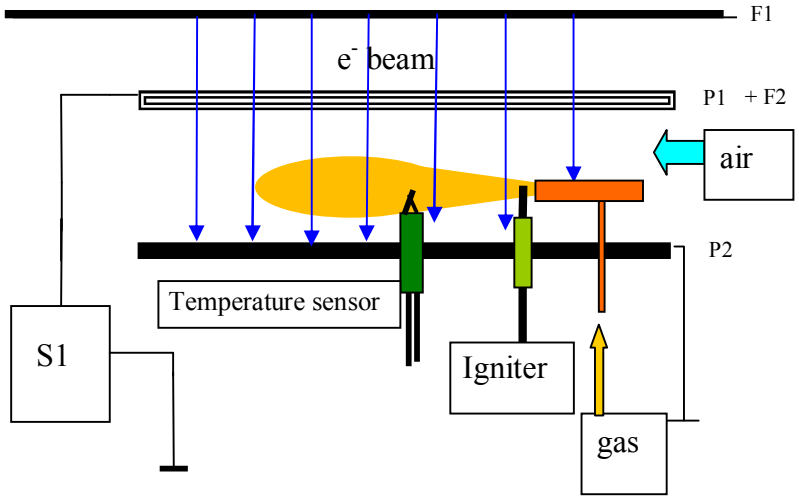

Fig.25. A scheme of the experiment on determination of the temperature sensor working capacity.

The experiment was carried out in the following sequence.
The temperature sensor was located in holes of the bottom plate (P2) the experimental chamber according to the recommendations stated in the part 1.5.3.of Chapter 1.

Measuring withdrawals of the sensor were connected with the oscillograph fixing the form and amplitude of a signal. Then, according to recommendations of the present report part 2.1 of the Chapter 2, in the experimental chamber the stable flame of the propane-air mixture was created.

At the following stage of the experiment measurements of a signal from the temperature sensor were carried out at the various external factors influencing the burning process of the propane-air mixture.

A source of HV creating the electric field in the chamber, or the accelerator EOL -400M, which provides presence of a flux of the accelerated electrons in the experimental volume was switch on.

In Fig.26 and 27 characteristic signals from the temperature sensor are represented under various conditions of the experiment.

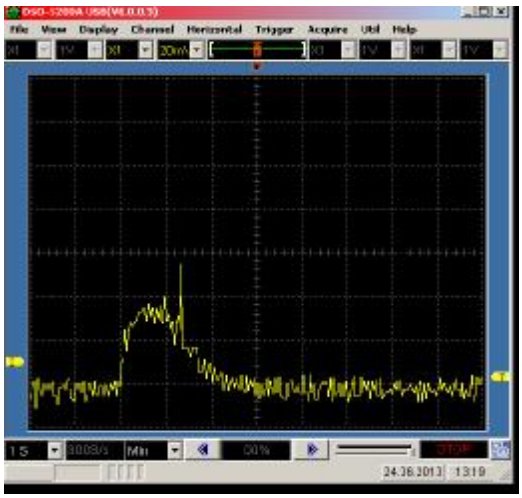

Fig.26. A typical waveform of the signal from the temperature sensor at measurements of a flame temperature without external influences.

Readings sensitivity in the waveform -
1 sec/ div – over the horizontal axis,
20 mV/div – over the vertical axis

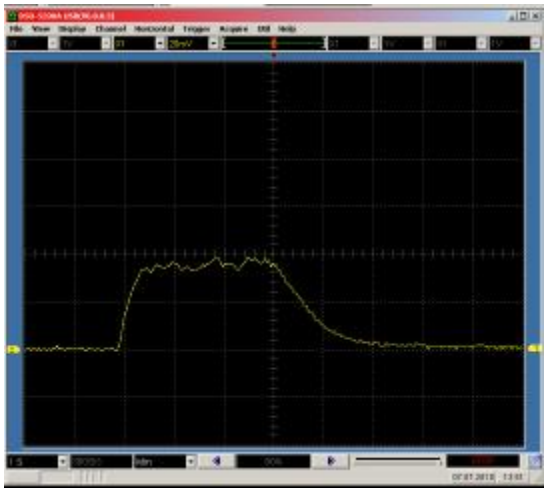

Fig.27. A typical waveform of the signal from the temperature sensor at measurements of a flame temperature at presence of theexternal influences.

In Fig. 26 the waveform of the signal from the temperature sensor is represented at measurement of the flame characteristics, not experienced to the external influences. In the waveform it is clearly seen that the sensor indications are free from a noise, and a duration of the temperature sensor readings coming to the stationary value at the constancy of the propane-air mixture burning does not exceed 1 second. On the basis of the obtained result it is possible to conclude, that

- the chosen system of temperature estimation allows to carry out direct measurements of EMF on contacts of the thermocouple without application of intensifying devices since a level of the noise is small;
- a duration of staying of the gas valve of the complex installation in the open condition, i.e. the duration of a flame, can be no longer than t = 1.5 seconds during the experiments (indications of the temperature sensor at longer duration are practically invariable).

In Fig. 27 the characteristic waveform of a signal from the temperature sensor is represented at measurements of a flame in the presence of external influences. The given kind of the waveform is typical for any type of the external influence, whether it is the electric field in the experimental chamber, an electron beam or complex influence of these factors.

Studying the waveform it is possible to mark, that the level of the noise has increased, but even at such a noise it is possible to carry out the estimated measurements of temperature with a sufficient degree of accuracy. It is necessary to pay attention that a duration of the signal from the temperature sensor here and in all the subsequent experiments was no longer than t = 1.5 seconds. Thus recommendations developed at carrying out of experiments with a flame without external influences have been accounted for.

With the purpose of the installation readiness check to the beginning of the basis cycle researches, has been carried out a trial experiment on measurement of a flame temperature of the gas mixture in various sections of the experimental chamber.

The experiment scheme corresponds to the scheme represented in Fig. 25, but under a condition that the accelerator and a source providing an electric field in the chamber were not switched on.

The temperature sensor was located in holes of the plate P2 at different distances from a place of the propane-air mixture ignition.

A dependence of the flame temperature on a place of the propane-air mixture ignition at removal of the temperature sensor from the place of the propane-air mixture ignition is represented in Fig.28.

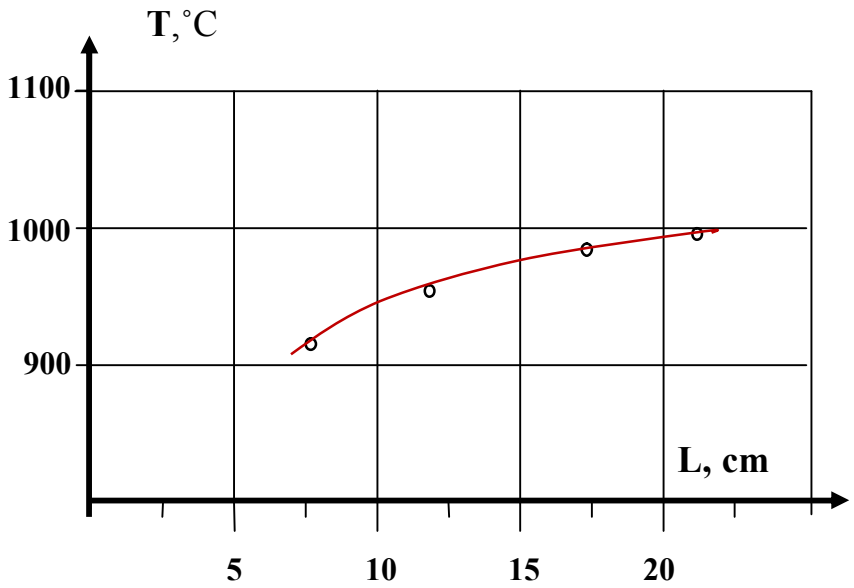

Fig.28. Propane-air mixture temperature dependence on a distance to a place of ignition.

In the given measurements it is shown, that at the propane - air mixture ignition by the spark discharge of the power of 10 kW during $15 \cdot 10^{-6}$ seconds, in the volume the burning of the gas with the flame temperature in the range 920 - 1000 C is realized at a distance from a place of ignition to a place of measurements of 7 ÷ 21 cm.

At this stage the preliminary experiments cycle has been finished.

2.2. **Research experiments (Tasks 5 and 6 of the project)**

At the given stage of researches all the complex of the experiments devoted to studying of influence of various factors on the burning processes of the propane - air mixture has been carried out.

2.2.1. Research of influence of electric field presence on burning process of the propane-air mixture (Task 5 of the project)

The given researches assumed the measurements of a flame temperature of the propane - air mixture at presence of specially created electric field in the experimental chamber .

Also it was supposed to measure values of the currents getting to the plates P1 and P2 of the experimental chamber in the course of burning.

The basic scheme of the experiment is represented in Fig.29.

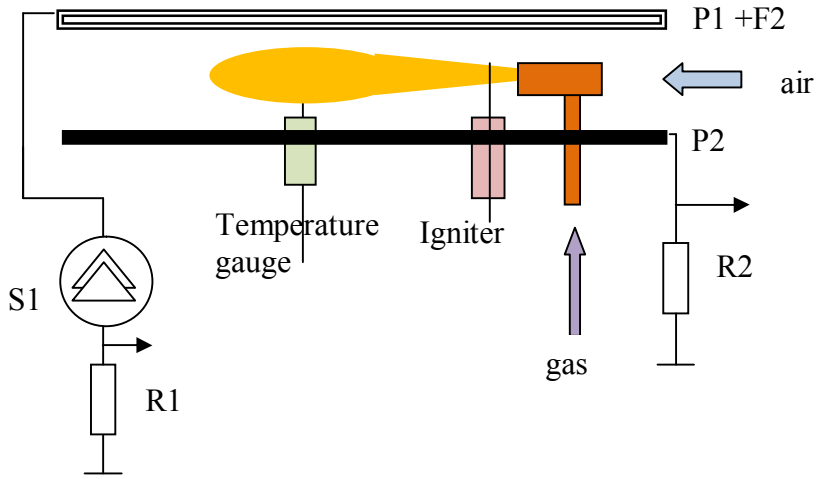

Fig. 29. The principle scheme of the experiment on investigation of the electric field influence on the propane-air mixture ignition process.

The experiment was carried out in the following sequence.

At the initial moment of the experiment, according to the time diagram of sequence of switching on of the equipment of the complex installation (Fig. 15) and recommendations developed in the part 2.1.1 of the Chapter 2, in the chamber was created a stable flame at burning of the propane-air mixture . (In the given cycle of experiments the accelerator was not switch on). Then measurements of a flame temperature and values of currents to the plates P1 and P2 were carried out at various values of voltage of the source S1.

The value of the electric field in the experimental volume, at switching on of the source S1, was estimated as the ratio of the voltage value of the source to those between the plates P1 and P2 of the chamber. Thus at change of the voltage of the source from 0 to10 kV the electric field strength in the chamber changed from 0 to 2 kV/cm.

The flame temperature was measured by the temperature sensor placed in the area of burning at a distance of 12 cm from a place of the gas mixture ignition.

The characteristic form of a signal from the temperature sensor at electric field strength of E = 0.6 kV/cm in the chamber is represented in Fig. 30.

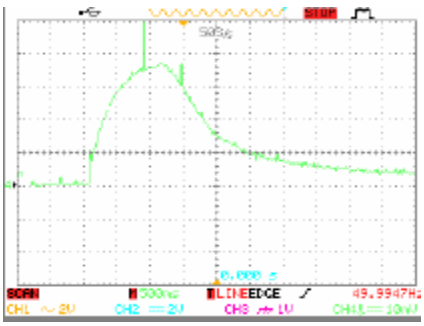

Fig. 30 A waveform of the signal from the temperature sensor at the electric field strength of E = 0.6 kV/cm in the chamber.

In Fig. 31 a dependence of a flame temperature on a value of the electric field strength in the experimental chamber is represented.

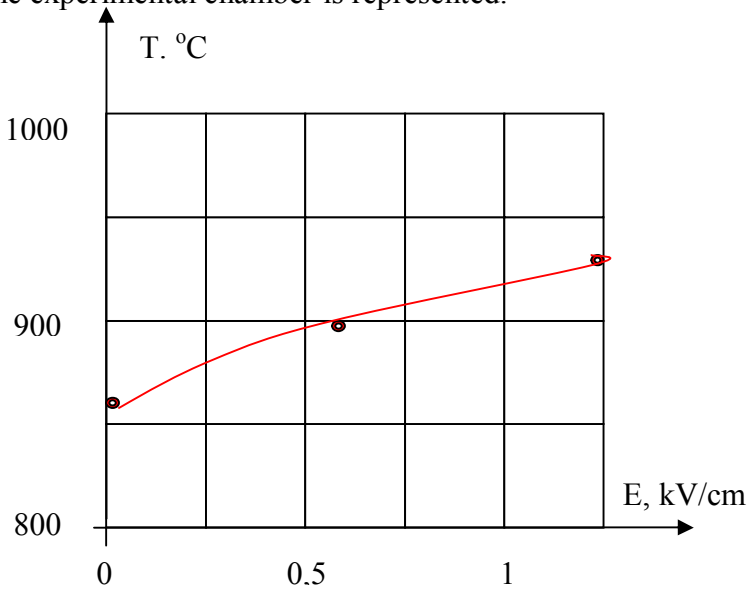

Fig. 31. A d***ependence of the flame temperature on a value of the electric field strength in the experimental chamber***.

As a result of the carried out researches it is revealed that, at increase of a value of the electric field strength in the area of the propane-air mixture burning, the temperature of the flame measured in the same point of the experimental chamber rises.

The relative increase in temperature is 8 ÷ 10 % in comparison with the temperature of a flame without an electric field presence.

Values measurement of currents getting to the plates P1 and P2 in the presence of the electric field and a flame in the experimental chamber was the following step in estimations of the electric field influence on process of propane-air mixture burning.

It is necessary to mark that the forms and amplitudes of the signals to the plates P1 and P2 are absolutely identical and differs only by the polarity. Since from the source S1 to the plate P1 the signal of the positive polarity was given, then the current to this plate had the negative polarity, and a current to the plate P2 - the negative polarity.

In Fig. 32 the typical form of a signal of the current, measured on the plate P2 is shown at presence of the electric field and a flame of propane-air mixture burning in the experimental chamber. It is necessary to pay attention, that in the absence of the flame in the chamber and at any value of the electric field the currents to the plates P1 and P2 were equal to zero.

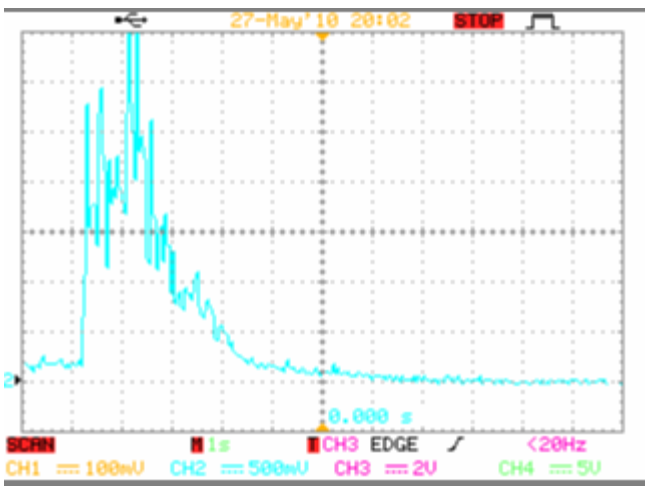

Fig. 32. A typical signal of the current to the plate P2 in the presence of the electric field in the chamber.

At stable burning of the propane-air mixture in the chamber a measurement of the current to the plate P2 dependence on a value of the electric field strength in the experimental volume has been carried out. The graph of this dependence is represented in Fig. 33.

Considering the obtained dependence, it is possible to conclude that the current to the plate P2 increases by 18-20 % at increase of the electric field strength in the experimental chamber by1.5 times in the experimental chamber .

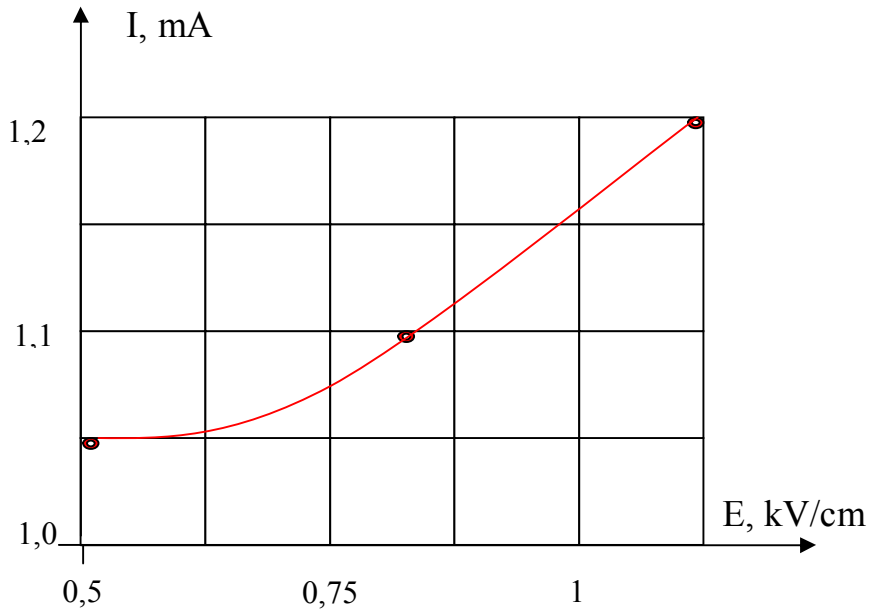

Fig.33 A dependence of the current to the plate P2 on a value of the electric field strength in the experimental chamber .

It means that in the chamber conditions for additional ionization in the electric field were realized at the rise of the temperature and a local decrease of a gas density.

On the basis of the carried out experiments it is possible to conclude that the electric field presence influences a dynamics of the propane-air mixture burning processes.

In particular, in the presence of the electric field the flame temperature increases by 8÷10 % at the electric field increase in the experimental chamber by 1.5 times, and also a value of the ion current increases by 18÷20 % under the same conditions.

2.2.2 Research of influence of the accelerated electron flux on the propane-air mixture burning process (Task 5 of the project)

The given researches assumed the propane-air mixture flame temperature measurement at presence in the experimental chamber of the accelerated electron flux. Also it was supposed to measure values of the currents getting to the plates P1 and P2 of the experimental chamber in the course of burning.

The basic scheme of experiment is represented in Fig. 34.

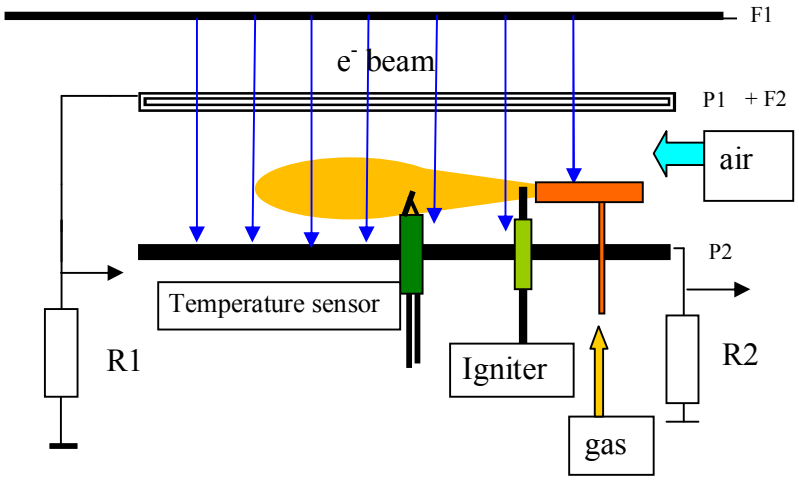

Fig. 34. The principle scheme of the experiment on research of accelerated electrons influence on the propane-air burning process.

The experiment was carried out in the following sequence.

At the initial moment of the experiment, according to the time diagram of the switching on of the complex installation equipment sequence (Fig. 15) and. recommendations developed in the part 2.1.1of the Chapter 2 , in the chamber was created a stable flame of the propane-air mixture burning. (In the given cycle of experiments the source S1 providing presence of the electric field in the experimental chamber was not switched on). Then measurements of temperature of the flame temperature and values of currents to the plates P1 and P2 in the presence of the accelerated electron flux in the chamber were carried out. The total current of the accelerated electrons was measured by the diagnostic system of the accelerator. The beam current in the chamber could be estimated under the recommendations to data given in the part 2.1.2 of the chapter 2 of the present report.

The flame temperature was measured by the temperature sensor located in the area of burning at a distance of 12 cm from the place of the gas mixture ignition.

In Fig.35 signals waveforms of the currents measured on plates P1 and P2 at presence in the chamber of the electron beam and a flame at burning of the propane-air mixture in the chamber are represented.

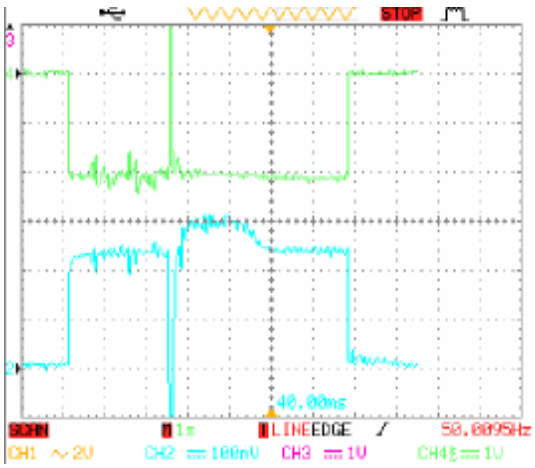

Fig. 35. Waveforms of the currents measured on plates P1 (the upper beam) and P2 (the lower beam) at presence in the chamber of the electron beam and a flame at burning of the propane-air mixture.

In the waveform it is clearly seen that the current to the plate P2 slightly increases at burning of the propane air mixture in the experimental chamber. The sharp failure on the lower beam (Fig. 35) is caused by a capacitor current arising at ignition of the gas mixture, and the further insignificant increase of the current arises at the flame burning. This increase is no greater than of 10÷12 % from the total current which has gotten to the plate.

It is necessary to mark that the value of this increase of the current practically did not change at increase of the beam current from the minimum to the maximum value.

The current getting to the plate P1 is essentially greater than the current getting to the plate P2, therefore its changes at burning of the propane- air mixture is difficult to detect as this change in absolute values is rather insignificant.

The typical form of signals from the temperature sensor at researches of influence of the accelerated electron beam on of the propane- air mixture burning process are represented in Fig.36 and Fig.37.

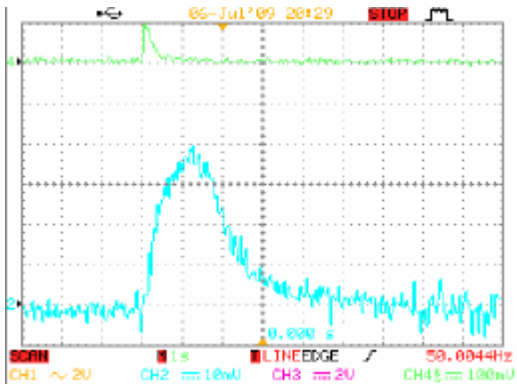

Fig. 36. The waveform of the signal from the temperature sensor at absence of the electron beam in the experimental chamber

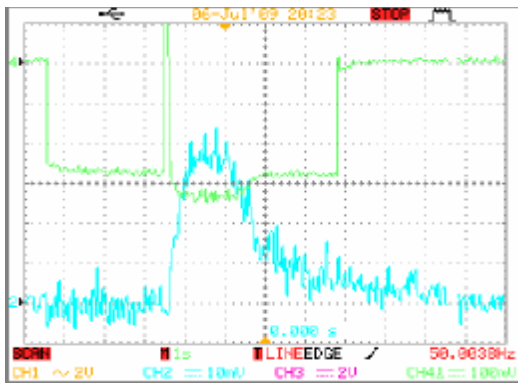

Fig. 37. The waveform of the signal from the temperature sensor at presence of the electron beam in the experimental chamber (The upper beam- the current signal from the plate P2, the lower beam – the signal from the temperature sensor)

Comparing the obtained signal values from the temperature sensor at presence and absence of the electronic beam, it is revealed that the flame temperature varies quite insignificantly. At increase of the current of the beam from maximum to the minimum value the flame temperature has increased no greater than by 2 ÷ 4 % from the temperature of a flame without the beam.

In Fig.38 and Fig.39 typical photos of processes in the experimental chamber are represented at carrying out of the given cycle of experiments.

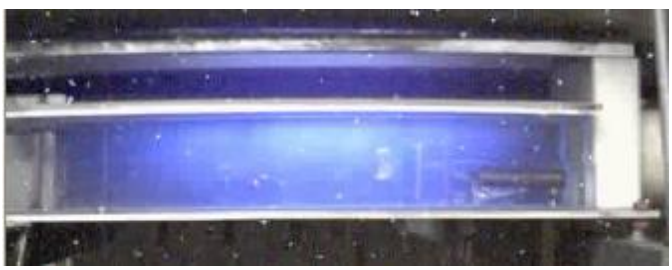

Fig.38. ***Photos of the air luminescence under the influence of the electron beam bunch in the volume of the experimental chamber.***

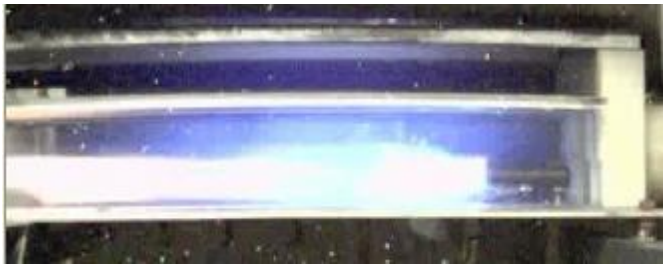

Fig. 39. Flame photos at burning of the propane-air mixture and a luminescence of air under the influence of the electron beam in the volume to the experimental chamber

It is necessary to mark that at influence of the electron beam on a flame the burning process of the propane-air mixture is very stable from the point of view of repeatability of results.

So, on the basis of the carried out experiments it is possible to conclude, that the beam of the accelerated electrons influences the burning process of the propane-air mixture essentially only from the point of view of results repeatability.

Increase of a flame temperature and of the value of the ion currents in the presence of an electron beam is insignificant.

2.2.3. Research of the complex influence of the accelerated electron flux and of the electric field on the propane-air mixture burning process . (Task 5 of the project)

The given researches assumed temperature measurements of a flame the propane-air mixture at presence of the accelerated electron flux and specially created electric field in the experimental chamber.

Also it was supposed to measure values of the currents getting to the plates P1 and P2 of the experimental chamber in the course of burning at complex influence on a flame of the field and the beam.

The basic scheme of the experiment is represented in Fig. 40.

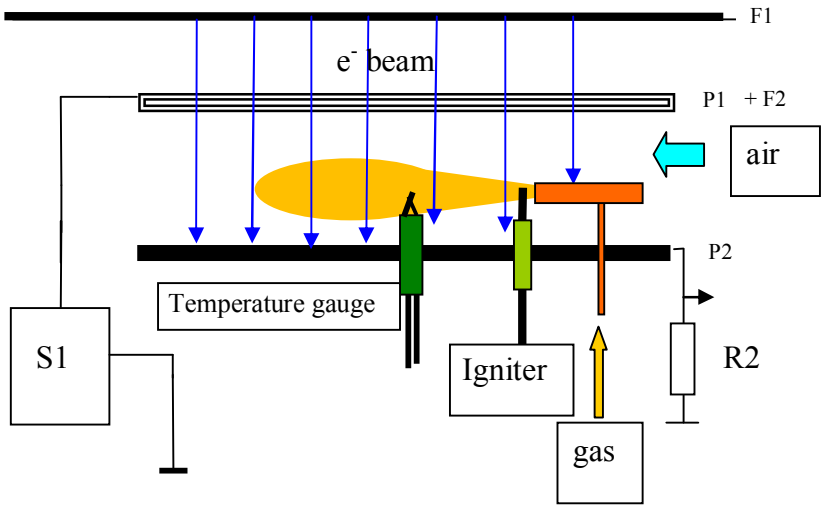

Fig.40. The principle scheme of the experiment on research of complex influence of the electron beam and electric field on the propane-air mixture burning process .

The experiment was carried out in the following sequence.

The initial moment of experiment, according to the time diagram of switching on sequence of the complex installation equipment (Fig. 15) all the equipment involved in experiments was switched on.

Then measurements of a flame temperature and a value of currents to the plates P2 in the presence of electric field and a flux of the accelerated electrons in the chamber were carried out.

Burning process was studied also by means of the visual observation.

The flame temperature was measured by the temperature sensor located in the area of burning at a distance of 12 cm from the place of the gas mixture ignition. Values of the ion current in the course of the experiment were determined by the signal level from the resistance R2.

Typical waveforms of the ion current measured on the plate P2, at complex influence on the propane-air mixture of the electron beam and the electric field in the course of burning are represented in Fig.41÷45.

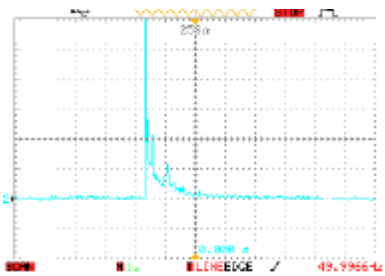

Fig. 41. The waveform of the ion current, measured on the plate P2, at the beam current of I_b=0 and the field strength of E = 1.4 κV/cm

Fig. 42. The waveform of the ion current, Measured on the plate P2, at the beam current of I_b=0.1 mA and the field strength of E = 1.4 κV/cm

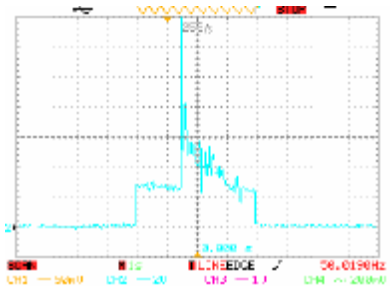

Fig. 43. The waveform of the ion current, Measured on the plate P2, at the beam current of I_b=0.5 mA and the field strength of E = 1.4 κV/cm.

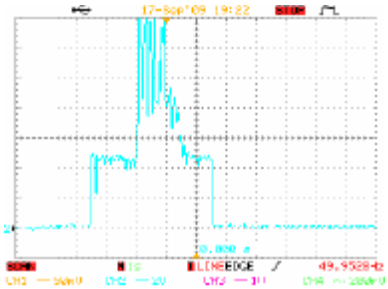

Fig. 44. The waveform of the ion current, Measured on the plate P2, at the beam current of I_b=1.3 mA and the field strength of E = 1.4 κV/cm.

Fig. 45. The waveform of the ion current, Measured on the plate P2, at the beam current of I_b=2 mA and the field strength of E = 1.4 κV/cm.

On the basis of the obtained data it is possible to construct a dependence of values of the ion current in the chamber on the beam current at complex influence of the electron beam and

the external electric field on process of preliminary ionization of a gas mixture and on burning process.

In Fig. 46 graphs of values of the ion current in the chamber are represented at ionization of the gas mixture by the electron beam (curve $\mathbf{I_i}$) and a current in the course of burning of the gas mixture (curve $\mathbf{I_p}$) on the value of the total current the electron beam.

The value of the ion current in the course of burning is determined as a difference of the maximum value of the ion current to the plate P2 and the value of the ion current at ionization of the gas mixture by by the electron beam.

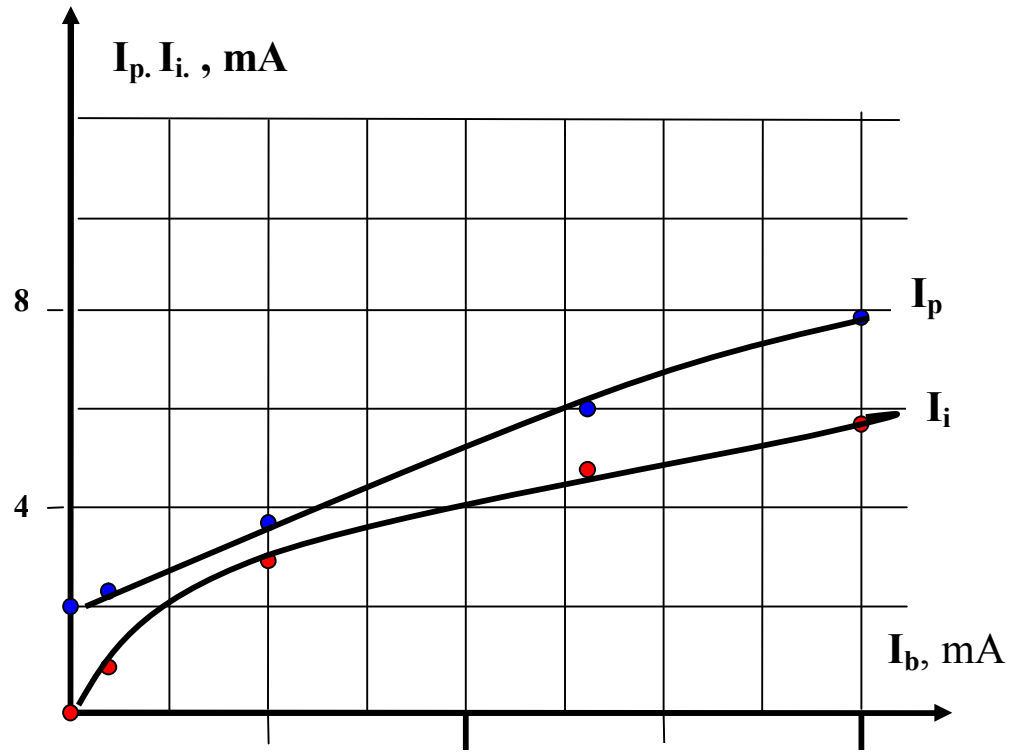

Fig. 46 ***Graphs of the ion current value in the chamber at ionization of the gas mixture by the electron beam (curve I_i) and a current in the course of burning of the gas mixture (curve I_p) on a value of a total current of the electron beam.***

At the analysis of the obtained dependences it is possible to mark that at increase of a current of the electron beam getting to the experimental chamber, increase both the ion current at the ionization of the gas mixture before the ignition moment and the current in the course of burning of the gas mixture. The increase of the ion current in the course of burning at complex influence of the electron beam and the external electric field says that the dynamics of processes proceeding in a flame changes.

Also it is revealed that, at complex influence of the electron beam and the external electric field on burning process of the propane-air mixture, the flame temperature, essentially rises. Typical waveforms of signals from the temperature sensor and the current plates P2, at the electric field strength in the chamber E= 1 κV /cm are represented in Fig.47.

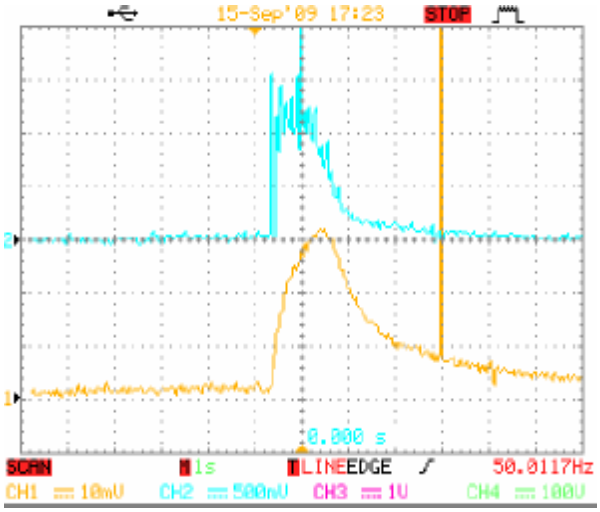

Fig.47. Waveforms of signals from the temperature sensor and the current plates P2, at the electric field strength E = 1 κV/cm in the chamber.

Over results of the carried out experiments the graph of a dependence of the propane-air mixture burning temperature on a current of the electron beam is constructed at the fixed value of the electric field (E = 1 κV/cm). The corresponding graph is presented in Fig.48.

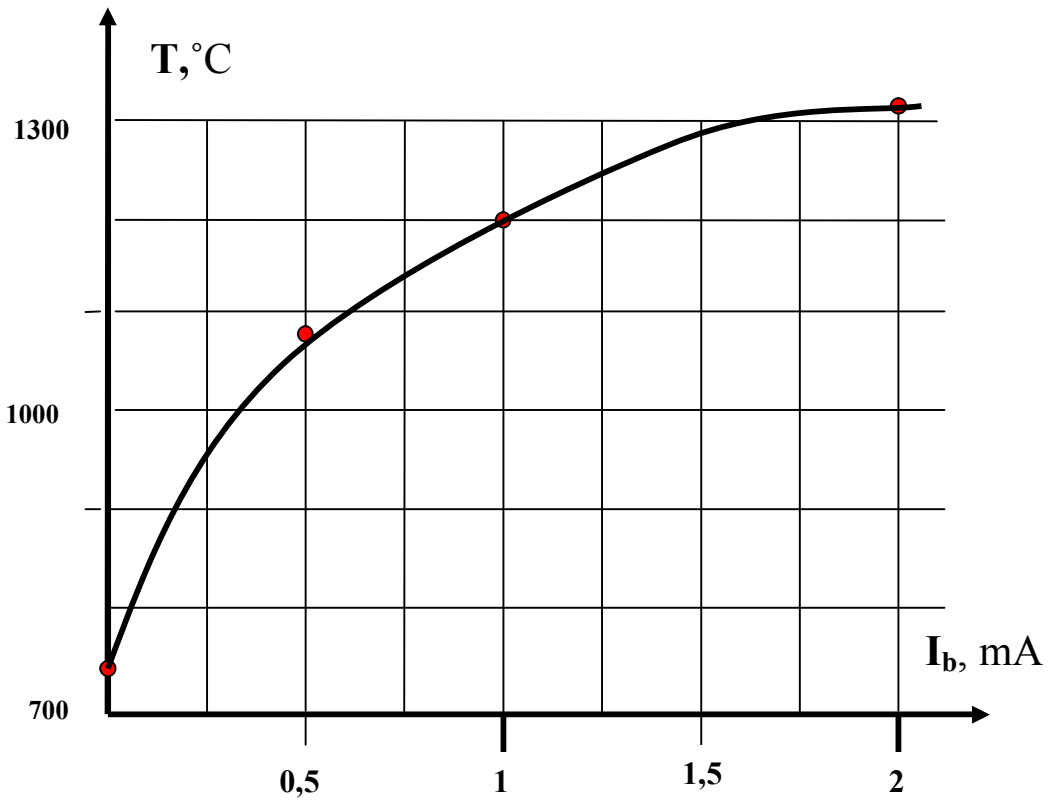

Fig. 48. A graph of dependence of the propane-air mixture burning temperature on the current of the electron beam at the fixed value of the electric field (E = 1 κV/cm).

The obtained results show that at complex influence of the electric field and the electron beam on burning process of the propane-air mixture, the flame temperature essentially increases, that speaks about the increase of the fuel burning efficiency.

The visual observations carried out in the course of experiments, confirm the fact of sharp increase in the temperature of a flame at complex influence of the electric field and an the electron beam process on the burning process.

Photos of the visual observation are resulted in Fig.49 and Fig.50.

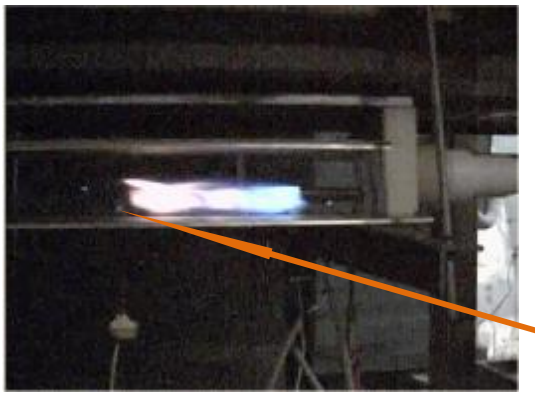

A joint of the thermocouple in the experimental volume.

Fig. 49. A photo of the termination of the propane-air mixture burning process at the value of the electric field strength of E = 1 kV/cm and the beam current I=0.

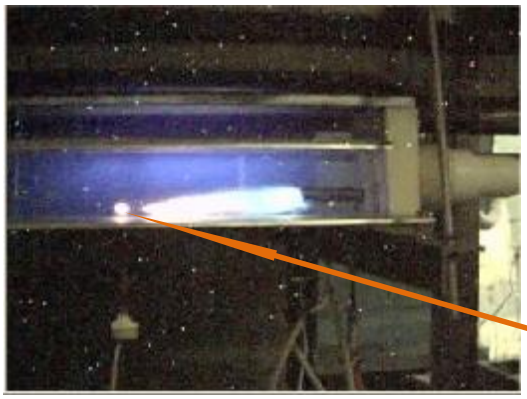

A joint of the thermocouple in the experimental volume.

Fig. 50. A photo of the termination of the propane-air mixture burning process at the value of the electric field strength of E = 1 kV/cm and the beam current I=1 mA.

And at the analysis of photos in Fig.49 and Fig.50 where the gas-mixture burning termination moments are detected at identical values of the electric field in absence and in the presence of the electron beam in the experimental chamber.

It is possible to mark that brightness of a luminescence of the temperature sensor joint at the termination of the mixture burning is essentially greater at experiments with the beam.

The given observations confirm the fact of sharp increase in the flame temperature at complex influence on burning process of the external electric field and the electron beam.

On the basis of the carried out experiments it is possible to draw a conclusion that the complex influence of the external electric field and the electron flux essentially influences the dynamics of the gas-air mixture burning process.

The flame temperature at the complex influence increases more than by 40 %, in comparison with the temperature without the influence. And currents to the plate P2 increase almost by 5 times in the process of the accelerated electrons flux intensity increase.

2.2.4. Research of the complex influence of the accelerated electron flux and of the electric field on the burning process of lean propane - air mixture. (Task 6 of the project)

At this stage of researches experiments on the complex influence of the electric field and the electron beam on lean gas mixture have been made.

The experiment was carried out in the same sequence, as in the researches described in the part 2.2.3. of the present report. The principle scheme of the experiment corresponds to the scheme represented in Fig.40.

The only difference in works was in use of the fan providing an air stream with the speed up to 25 m/s the experimental chamber.

Following the recommendations stated in the of the part 1.3.4, Chapter 1, it is possible to change weight proportions of the propane - air mixture so, that the ratio of the propane and air is below the value 1:16. Such mixture is called as the lean one.

At the speed of the air stream (i.e. increasing of air volume in the chamber in unit of time) greater than 15 m/s, and preservation of the arriving gas volume, have been provided unstable burning of the gas mixture, or obtained full absence of the ignition.

This speaks about change of weight proportions of the propane and air, and obtaining of the lean gas mixture. (At carrying out of the experiments on formation of the lean mixture the accelerator was not switched on).

At this stage of researches the value of the ion current on the plate P2 depending on the air stream speed was measured. In Fig.51 a dependence of the current to the plate P2 on the air stream speed is represented.

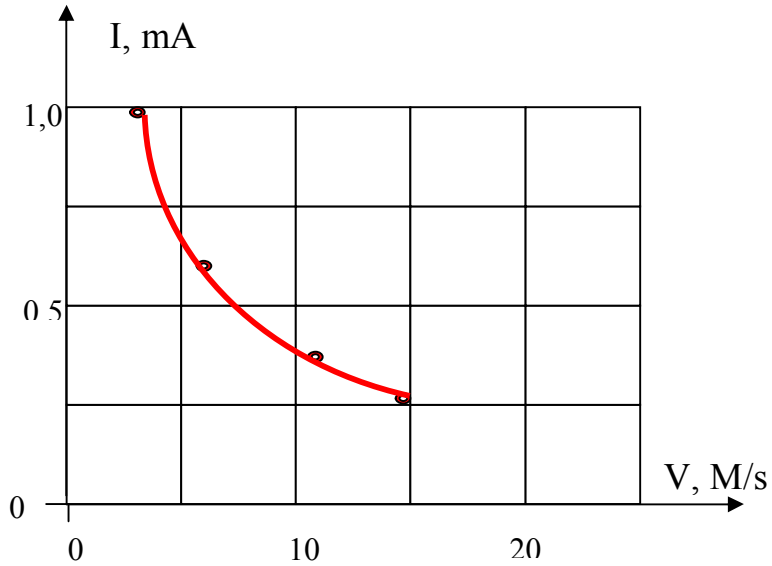

Fig.51. A dependence of the current to the plate P2 depending on the air stream speed.

The analysis of the obtained dependence has shown that the increase of the air stream speed by five times (up to 15 m/s) reduces value of a current by plate P2 more than three times. At the further increase of the air stream speed the burning becomes unstable or completely stops there is no a current to the plate P2.

On the basis of the carried out experiments it has been revealed that at the air stream speed of V> 15 m/s the burning of the propane -air mixture is unstable, and the current on plate P2 is absent. We have obtained the lean propane - air mixture; and at the air stream speed V ≥ 15 m/s it is possible to carry out researches on the complex influence on the burning process of the electron beam and the electric field.

As the basic source of the information at carrying out of researches on ignition and burning of the lean propane -air mixture were the visual observations.

In Fig.52 the photo of one of burning phases of the lean gas mixture in the absence of influence on flame of the electron beam and the electric field is presented.

In Fig. 53 the photo of one of burning phases of the lean gas mixture is presented at the complex influence on flame of the electron beam and the electric field is presented.

Fig. 52. Photos of a burning phase of the lean gas mixture in the absence the electron beam and the electric field influence on flame.

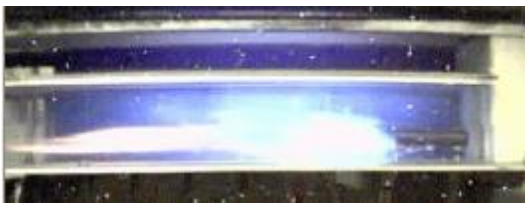

Fig. 53. Photos of a burning phase of the lean gas mixture at presence the electron beam and the electric field influence on flame

From the carried out observations it is revealed that at complex influence of the electron bunch and the electric field on the flame of the lean propane-air mixture burning process is stabilized.

In Fig. 54a and 54b the typical waveforms of the signal from the temperature sensor are represented at the speed of the air stream greater than 15 m/s and in the absence of influence of the electron beam and the electric field on a flame.

Fig. 54a. The Signal from the temperature sensor at the air stream speed greater than 15 m/s.
The maximum value of the flame temperature T = 400˚C.

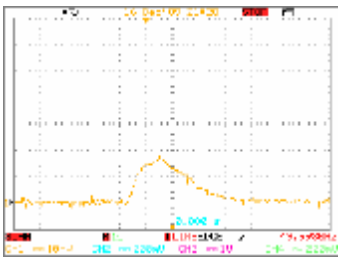

Fig. 54b. The Signal from the temperature sensor at the air stream speed greater than 15 m/s.
The maximum value of the flame temperature T = 400˚C.

In Fig.55 the typical waveforms of a signal from the temperature sensor is represented at the speed of the air stream greater than 15 m/s and at the influence of influence of the electron beam and the electric field on a flame.

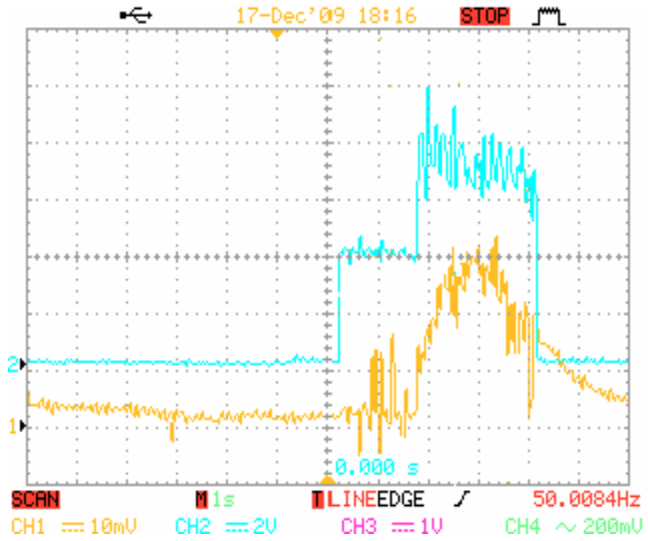

Fig. 55. ***Waveforms of the signal from the temperature sensor (a beam 1) and the signal of the ion current which has gotten to the plate P2 (a beam 2) at the complex influence on the flame of the lean propane-air mixture.***

By consideration of waveforms in Fig. 54a, in itone can see that at the speed of the air stream greater than 15 m/s burning is unstable, and the temperature of the flame no greater T = 400˚C

In Fig.55 the waveform of the signal from the temperature sensor and the current signal which has gotten to the plate P2, measured at researches on complex influence of the electric field and the electron beam on process of burning of the lean propane-air mixture. The temperature sensor in this case was placed in the same place, as at researches without the electron flux and the electric field.

Considering of the obtained waveforms, it is possible to mark that the flame temperature has sharply increased (T = 700˚C) in comparison with the temperature of the flame measured in experiments without of the electron beam (T=400˚C).

Also it is necessary to mark that in experiments with the beam good repeatability of the obtained results was observed. This fact speaks about of the burning stability of the lean propane - air mixture.

The carried out cycle of the experimental researches shows, that at complex influence of the electric field and the beam of the accelerated electrons on the burning process of the propane - air mixture essentially increases the temperature of a flame and the stability of proceeding processes improves. Given results are typical as for optimum weight rations of the propane and air in the gas mixture and in the lean gas mixture.

Chapter 3. Theoretical investigations

Chapter 3.1. Глава 3.1. Influence of electron beams and external electric field on chemically active gas mixtures (Problems 7-9))

3.1.1. Approach

Last decade a new direction of electron-beam application for activation of gases in which composition active organic and inorganic are included has been formed [1-3]. Also works on electron-beam combustion activation and fuel conversion have appeared [4-6]. For example, in reference [4] the application of the electron beam for a ball flow around parameter variations at the electron-beam penetration through Laval nozzle has been considered, at that an electric discharge simultaneously impacted the propane-air mixture. In reference [6] authors considered electron-beam application has been considered for creation of effective conditions of air activation and its following application at propane-air mixture combustion. In [6] were obtained results showing that increase of atomic oxygen in the flammable mixture by 0.1 -1 % allows to decrease an ignition time by 1,5 -6 times. At that in calculations was not accounted that appearance of vibrationally and electronically excited particles also improves the combustion processes and decreases an ignition time [7]. So the goal of our investigations is to determine plasma impact on flammable mixture ignition and combustion under electron-beam action without and with action of external electric field.

During works on the Project we have modernized a program of plasma parameters calculations in air excited by the electron beam [8] and applied in [6]. For this purpose we added to it rate constants of some ion-molecular processes that we did not use earlier and checked rate constants of electron- molecule reactions. Rate constants with participation of complex ions have been included additionally.

The corresponding rate constants and energy costs of processes are represented in Tables 3.1.1. -3.1.2.

During these works we have undertaken numerical calculations for typical parameters of electron-beams.

We have estimated parameters of electron beams at propagation of the electron flux through the outlet foils.

During the works on the Project we have collected rate constants of chemical reactions in propane-air mixture that allowed to use a relatively small reaction scheme that showed itself satisfactory at description of propane-air mixture ignition (see below). The corresponding rate constants of reactions are represented in Table 3.1.3.

We have also undertaken works on collection, choice, estimate and interpolation of lacking rate constants of plasma chemical reactions in propane-air mixture which allow to model ignition and combustion processes in the plasma conditions. The corresponding plasma chemical reaction rate constants are represented in Tables 3.1.1-3.1.3.

Table 3.1.1. Kinetics of Particles in Electron - beam Plasmas in Electric Field, T in-°K

Number	Reaction	Rate (cm^6/s, cm^3/s) /Cost (eV)(C)	Comments	Energy release	Energy defect, eV
1a	$\hat{e} + O_2 \rightarrow O_2^+ + \hat{e} + e$	V_e= 141	Konovalov		
1b	$\hat{e} + O_2(v) \rightarrow O_2^+ + \hat{e} + e$	V_e= 141	Konovalov		
1c	$\hat{e} + O_2(\Delta_{effec}) \rightarrow O_2^+ + \hat{e} + e$	V_e= 141	Konovalov		
1d1	$\hat{e} + N_2 \rightarrow N_2^+ + \hat{e} + e$	V_e= 43.1	Konovalov		
1d2	$\hat{e} + N_2(v) \rightarrow N_2^+ + \hat{e} + e$	V_e= 43.1	Konovalov		
1d3	$\hat{e} + N_2(A^3\Sigma_u^+) \rightarrow N_2^+ + \hat{e} + e$	V_e= 43.1	Konovalov		
1d4	$\hat{e} + N_2(B^3\Pi_g) \rightarrow N_2^+ + \hat{e} + e$	V_e= 43.1	Konovalov		
2a1	$\hat{e} + N_2 \rightarrow N + N + \hat{e}$	V_N =33.6	Konovalov N_2, Rydberg states, with threshold 12.25		
2a2	$\hat{e} + N_2(A^3\Sigma_u^+) \rightarrow N + N + \hat{e}$	V_{N^*} =33.6	Konovalov N_2, Rydberg states, with threshold 12.25 eV		
2a3	$\hat{e} + N_2(B^3\Pi_g) \rightarrow N + N + \hat{e}$	V_{N^*} =33.6	Konovalov N_2, Rydberg , with 12.25 eV threshold		
2a4	$\hat{e} + N_2(v) \rightarrow N + N + \hat{e}$	V_{N^*} =33.6	Konovalov		
3a	$\hat{e} + O_2 \rightarrow O + O + \hat{e}$	V_o =44.4	Konovalov O_2 all from $O_2(A^3\Sigma_u^+$		
3b	$\hat{e} + O_2(v) \rightarrow O + O + \hat{e}$	V_o =44.4	Konovalov O_2 all from $O_2(A^3\Sigma_u^+$		
3c	$\hat{e}+O_2(\Delta_{effective}) \rightarrow O+O+\hat{e}$	V_o =44.4	Konovalov O_2 all from $O_2(A^3\Sigma_u^+$		
3d	$\hat{e}+O_2(b) \rightarrow O+O+\hat{e}$	V_o =44.4	Konovalov O_2 all from		

			$O_2(A^3\Sigma_u^+$		
4a1	$\widehat{e}+O_2 \rightarrow O_2(\Delta_{effective})+\widehat{e}$	V $_{O2(\Delta)}$=93.3	Konovalov $O_2(a^1\Delta)$,		
4a2	$\widehat{e}+O_2(v) \rightarrow O_2(\Delta_{effective})+\widehat{e}$	V $_{O2(\Delta)}$=93.3	Konovalov $O_2(a^1\Delta)$,		
4a3	$\widehat{e}+O_2 \rightarrow O_2(b)+\widehat{e}$	V $_{O2(b}$=386	Konovalov $O_2(b^1\Sigma)$		
4a4	$\widehat{e}+O_2(v) \rightarrow O_2(b)+\widehat{e}$	V $_{O2(\Delta)}$=386	Konovalov $O_2(b^1\Sigma)$		
4a5	$\widehat{e}+O_2 \rightarrow O_2(A)+\widehat{e}$	V $_{O2(b}$=170	Konovalov $O_2(A^3\Sigma_u^+$		
4a6	$\widehat{e}+O_2(v) \rightarrow O_2(A)+\widehat{e}$	V $_{O2(\Delta)}$=170	Konovalov $O_2(A^3\Sigma_u^+)$		
5a1	$e+O_2^+ \rightarrow O+O$	$2\cdot10^{-7}\cdot(300/T_e)^{0.7}$	Smirnov	gas	+7.1
5a2	$O+O \rightarrow O_2^+ +e$	$1.18\cdot10^{-21}\cdot(T)^{2.7}$ exp(-80600/T)	Zamyshlyaev Gupta	gas	-7.1
5b1	$O+M \rightarrow O^+ +M+e$	$2.0\cdot10^{-20}\cdot(T)^{1.5}\cdot\exp(-158000/T)$	Zamyshlyaev M=N_2, O_2, N, O, NO	gas	-16
5b2	$O^+ +M+e \rightarrow O+M$	$6\ 10^{-27}\cdot(300/T_e)^{1.5}$	Kossyi M=N_2, O_2, N, O, NO	gas	+16
5c1	$O+e \rightarrow O^+ +e+e$	$2.0\cdot10^{-20}\cdot(T)^{1.5}\cdot\exp(-158000/T)$	Zamyshlyaev Maikapar	gas	-16
5c2	$O^+ +e+e \rightarrow O+e$	$9.05\cdot10^{-20}\cdot(300/T_e)^{4.5}$	Smirnov	gas	+16
6a1	$e+NO^+ \rightarrow N+O$	$3.7\cdot10^{-7}\cdot(300/T_e)^{0.65}$	Park	gas	+2.75
6a2	$N+O \rightarrow e+NO^+$	$1.5\cdot10^{-15}\cdot(T)\cdot\exp(-32\ 000/T)$	Park	gas	-2.75
6b1	$e+N_2^+ \rightarrow N+N$	$2.8\cdot10^{-7}\cdot(300/T_e)^{0.5}$	Smirnov	gas	+5.85
6b2	$N+N \rightarrow e+N_2^+$	$2.4\cdot10^{-13}\cdot(T)^{0.5}\cdot\exp(-67\ 300/T)$	Zamyshlyaev	gas	-5.85
6c1	$N+M \rightarrow N^+ +M+e$	$2.0\cdot10^{-20}\cdot(T)^{1.5}\cdot\exp(-158000/T)$	M=N_2, O_2, N, O, NO Zamyshlyaev	gas	-14.53
6c2	$N^+ +M+e \rightarrow N+M$	$6\ 10^{-27}\cdot(300/T_e)^{1.5}$	Kossyi	gas	+14.53
6d1	$N+e \rightarrow N^+ +e+e$	$2.0\cdot10^{-20}\cdot(T)^{1.5}\cdot\exp(-158000/T)$	Zamyshlyaev	gas	-14.53
6d2	$N^+ +e+e \rightarrow N+e$	$9.05\cdot10^{-20}\cdot(300/T_e)^{4.5}$	Smirnov	gas	+14.53

6f1	$N_2 + M \rightarrow N_2^+ + M + e$	$2.0 \cdot 10^{-20} \cdot (T)^{1.5} \cdot \exp(-158000/T)$	$M=N_2, O_2, N, O, NO$ Zamyshlyaev	gas	-15.6
6f2	$N_2^+ + M + e \rightarrow N_2 + M$	$6\ 10^{-27} \cdot (300/T_e)^{1.5}$	$M=N_2, O_2, N, O, NO$ Kossyi	gas	+15.6
6g1	$N_2 + e \rightarrow N_2^+ + e + e$	$2.0 \cdot 10^{-20} \cdot (T)^{1.5} \cdot \exp(-158000/T)$	Zamyshlyaev	gas	-15.6
6g2	$N_2^+ + e + e \rightarrow N_2 + e$	$9.05 \cdot 10^{-20} \cdot (300/T_e)^{4.5}$	Smirnov	gas	+15.6
7a	$e + O_2 + O_2 \rightarrow O_2^- + O_2$	$K_{att} = 1.7 \cdot 10^{-31} \cdot \sum_{j=1}^{8} \frac{\alpha_j \cdot f(\varepsilon_j)}{1 + b_j \cdot (N_{O_2}, cm^{-3})}, \ m^6/s$	Alexandrov	gas	-0.43
7b	$O_2^- + O_2 \rightarrow O_2 + e + O_2$	$8.\ 10^{-10} \cdot \exp(-6035/T)$	Mnatsakanyan, Naidis	gas	+0.43
8	$O_2(\Delta) + O_2^- \rightarrow e + O_2 + O_2$	$2.\ 10^{-10}$	kossyi	gas	+0.55
9	$O_2^+ + NO \rightarrow NO^+ + O_2$	$4.4\ 10^{-10}$	kossyi	gas	+2.95
10	$O + O_2 + O_2 \rightarrow O_3 + O_2$	$8.6\ 10^{-31} \cdot T^{-1.25}$	kossyi	gas	+1.04
11	$O + O_2 + N_2 \rightarrow O_3 + N_2$	$5.6\ 10^{-29} \cdot T^{-2.}$	kossyi	gas	+1.04
12a	$O_2(a^1\Delta) + O_3 \rightarrow O + O_2 + O_2$	$9.7 \cdot 10^{-13} \exp(-1564/T)$	kossyi	gas	-0.06
12b	$O_2(a^1\Delta) + N \rightarrow NO + O$	$2.0\ 10^{-14} \exp(-600/T)$	Kossyi	gas	+1.88
12c	$O_2(a^1\Delta) + N_2 \rightarrow N_2 + O_2$	$3.0\ 10^{-21}$	Kossyi	gas	+0.98
12d	$O_2(a^1\Delta) + O_2 \rightarrow O_2 + O_2$	$2.2\ 10^{-18}\ (T/300)^{0.8}$	Kossyi	gas	+0.98
12f	$O_2(a^1\Delta) + O \rightarrow O_2 + O$	$7.0\ 10^{-16}$	Kossyi	gas	+0.98
12g	$O_2(a^1\Delta) + NO \rightarrow O_2 + NO$	$2.5\ 10^{-11}$	Kossyi	gas	+0.98
13a1	$N_2 + O_2 \rightarrow N + N + O_2$	$5.0 \cdot 10^{-8} \cdot \exp(-113200/T) \cdot [1 - \exp(-3354/T)]$	Krinonosova	gas	-9.76
13a2	$N + N + O_2 \rightarrow N_2 + O_2$	$8.27\ 10^{-34} \cdot \exp(500/T)$, T=100-600 K, $1.9\ 10^{-33}$, T=600-6300 K	Krinonosova	gas	+9.76
13b1	$N_2 + N_2 \rightarrow N + N + N_2$	$5.0 \cdot 10^{-8} \cdot \exp(-113200/T) \cdot [1 - \exp(-3354/T)]$	Krinonosova	gas	-9.76
13b2	$N + N + N_2 \rightarrow N_2 + N_2$	$8.27\ 10^{-34} \cdot \exp(500/T)$, T=100-600 K, $1.9\ 10^{-33}$, T=600-6300 K	Krinonosova	gas	+9.76
13c1	$N_2 + NO \rightarrow N + N + NO$	$5.0 \cdot 10^{-8} \cdot \exp(-113200/T) \cdot [1 - \exp(-3354/T)]$	Krinonosova	gas	-9.76
13c2	$N + N + NO \rightarrow N_2 + NO$	$5.0\ 10^{-33} \cdot \exp(500/T)$, T=100-600 K,	Krinonosova	gas	+9.76

		1.14 10^{-32}, T=600-6300 K			
13d1	$N_2 + O \rightarrow N + N + O$	1.1·10^{-7}· exp(-113200/T) · [1- exp(-3354/T)]	Krinonosova	gas	-9.76
13d2	$N + N + O \rightarrow N_2 + O$	5.0 10^{-33}· exp(500/T) , T=100-600 K, 1.14 10^{-32}, T=600-6300 K	Krinonosova	gas	+9.76
13e1	$N_2 + N \rightarrow N + N + N$	1.8·10^{-8}· exp(-113200/T) · [1- exp(-3354/T)], 300-6000 K, 1.4·10^{-2}· $T^{-2.5}$·exp(-113200/T), 6000-20000 K	Krinonosova	gas	-9.76
13e2	$N + N + N \rightarrow N_2 + N$	1.8·10^{-8}· exp(-113200/T) · [1- exp(-3354/T)], 300-6000 K, 1.4·10^{-2}· $T^{-2.5}$·exp(-113200/T), 6000-20000 K	Krinonosova	gas	+9.76
13f1	$N_2 + O \rightarrow N + NO$	1.3 10^{-10}· exp(-38000/T)	Krinonosova	gas	-3.3
13f2	$N + NO \rightarrow N_2 + O$	1.05·10^{-12}·$(T)^{½}$, 200-4000 K	Krinonosova	gas	+3.3
14	$N + O + M \rightarrow NO + M$	1.8 $10^{-31}\cdot T^{-0.5}$	Krivonosova	gas	+9.25
15	$O_2^- + O + O_2 \rightarrow e + O_3 + O_2$	3.0 10^{-30}	Smirnov	gas	+0.61
15a	$O_2^- + O \rightarrow e + O_3$	1.5 10^{-10}	Kossyi	gas	+0.61
16	$O_2^- + O \rightarrow O_2 + O^-$	3.3 10^{-10}	kossyi	gas	+1.03
17	$O_2^- + O_3 \rightarrow O_3^- + O_2$	4. 10^{-10}	Kossyi	gas	+1.57
18	$O^- + O_2(\Delta) \rightarrow e + O_3$	3. 10^{-10}	Smirnov	gas	+0.5
18a	$O^- + O_2 + O_2 \rightarrow O_3^- + O_2$	1.1 10^{-30} (300/T)	Kossyi	gas	+0.54
18b	$O^- + O_2 \rightarrow O_2^- + O$	8.8 10^{-13} $T^{1/2}$ exp(-111837/T)	Naidis	gas	-1.02
18c	$O^- + O_2 + N_2 \rightarrow O_3^- + N_2$	1.1 10^{-30} (300/T)	Kossyi	gas	+0.54
18d	$O^- + O_2(\Delta) \rightarrow O_2^- + O$	1. 10^{-10}	Kossyi	gas	+2.01
19	$O_3^- + O_2 \rightarrow e + O_3 + O_2$	2.3 10^{-11}	Samoilovich	gas	-2
19a	$O_3^- + O \rightarrow O_2^- + O_2$	3.2 10^{-10}	Kossyi	gas	+0.56
20	$O_2^- + O_2^+ \rightarrow O_2 + O_2$	4.2 10^{-7} $(300/T)^{0.5}$	Smirnov	gas	+11.77
21	$O_2^- + O_2^+ + M \rightarrow O_2 + O_2 + M$	0.5·10^{-25} $(300/T)^{1.5}$	Kossyi	gas	+11.77
21a	$O_2^- + O_2^+ + O_2 \rightarrow O_2 + O_2 + O + O$	0.5·10^{-25} $(300/T)^{1.5}$	Flannery	gas	+6.67
22	$O_2^- + O_2^+ \rightarrow O_2 + O + O$	1· $10^{-7}$$(300/T)^{0.5}$	Smirnov	gas	+6.67

23	$O^- + O_2^+ + M \rightarrow O + O_2 + M$	$1.0 \cdot 10^{-25}\ (300/T)^{1.5}$	Flannery	gas	+10.74
24	$O_3^- + O_2^+ \rightarrow O_3 + O_2$	$2\ 10^{-7}\ (300/T)^{0.5}$	Smirnov	gas	+10.2
25	$O_3^- + O_2^+ + M \rightarrow O_3 + O_2 + M$	$1.0 \cdot 10^{-25}\ (300/T)^{1.5}$	Kossyi	gas	+10.2
26	$O_3^- + O_2^+ \rightarrow O + O + O_3$	$2\ 10^{-7}\ (300/T)^{0.5}$	Smirnov	gas	+5.1
27	$O_3^- + O_2^+ + M \rightarrow O_3 + O + O + M$	$1.0 \cdot 10^{-25}\ (300/T)^{1.5}$	Kossyi	gas	+5.1
27b	$O + O_3 \rightarrow O_2 + O_2(\Delta)$	$2.0 \cdot 10^{-11}$ exp(-2275/T)	Baulch	gas	+3.08
28	$O^- + NO^+ \rightarrow NO + O$	$5 \cdot 10^{-7}(300/T)^{0.5}$	Flannery	gas	+7.79
29	$O^- + NO^+ + M \rightarrow O + NO + M$	$1.0 \cdot 10^{-25}\ (300/T)^{1.5}$	Flannery	gas	+7.79
30	$O_2^- + NO^+ \rightarrow NO + O_2$	$3 \cdot 10^{-7}(300/T)^{0.5}$	Smirnov	gas	+8.82
31	$O_2^- + NO^+ + M \rightarrow O_2 + NO + M$	$1.0 \cdot 10^{-25}\ (300/T)^{1.5}$		gas	+8.82
32	$O_3^- + NO^+ \rightarrow O_3 + NO$	$2 \cdot 10^{-7}(300/T)^{0.5}$		gas	+7. 25
33	$O_3^- + NO^+ + M \rightarrow O_3 + NO + M$	$1.0 \cdot 10^{-25}\ (300/T)^{1.5}$	Flannery	gas	+7. 25
34a	$e + e + O_2^+ \rightarrow O_2 + e$	$9.05 \cdot 10^{-20} \cdot (300/T_e)^{4.5}$	Smirnov	gas	+12.1
34b	$e + e + N_2^+ \rightarrow N_2 + e$	$9.05 \cdot 10^{-20} \cdot (300/T_e)^{4.5}$	Smirnov	gas	+15.6
35	$e + e + NO^+ \rightarrow NO + e$	$9.1 \cdot 10^{-20} \cdot (300/T_e)^{4.5}$	Smirnov	gas	+9.25
36	$e+O_2 \rightarrow O^-+O$	Reaction is approximated	under E-field action below $E/N=10^{-15}$ $V \cdot cm^2$ $Te=8.617 \cdot 10^{-5} * T$; T, K. Kochetov	elect	-1.47
36a	$O^- + O \rightarrow e + O_2$	$5.0 \cdot 10^{-10}$	kossyi	gas	+1.47
37	$e+O_2\ (a\Delta) \rightarrow O^-+O$	Reaction is approximated	under E-field action below $E/N=10^{-15}$ $V \cdot cm^2$ $Te=8.617 \cdot 10^{-5} * T$; T, K. Kochetov	elect	-2.45
38	$e+O_2\ (v=1) \rightarrow O^-+O$	Reaction is approximated	under E-field action below $Te=8.617 \cdot 10^{-5} * T$; T, K. Kochetov	elect	-1.28

39a	$e+O_2 \rightarrow O_2(a\Delta)+e$	Reaction is approximated	below $E/N=10^{-15}$ $V\cdot cm^2$ Kochetov	elect	-0.98
39aa	$e+O_2(a\Delta) \rightarrow O_2+e$	Reaction is approximated	Kochetov	elect	+0.98
39b	$e+O_2(v) \rightarrow O_2(a\Delta)+e$	Reaction is approximated	Kochetov	elect	
40a	$e+O_2 \rightarrow O+O+e$	Reaction is approximated	under E-field action below $E/N=10^{-15}$ $V\cdot cm^2$ $Te=8.617\cdot10^{-5}*T$; T, K. Kochetov	elect	-5.11
40b	$e+O_2(v) \rightarrow O+O+e$	Reaction is approximated	Kochetov	elect	-4.9
40c	$e+O_2(\Delta) \rightarrow O+O+e$	Reaction is approximated	Kochetov	elect	-4.12
41	$e+N_2 \rightarrow N_2(v)+e$	Reaction is approximated	below $E/N=10^{-15}$ $V\cdot cm^2$ $Te=8.617\cdot10^{-5}*T$; T, K. Kochetov	elect	-.292
41a	$e+N_2(v) \rightarrow N_2+e$	Reaction is approximated	Kochetov	elect	+0.292
42	$e+O_2 \rightarrow O_2(v)+e$	Reaction is approximated	below $E/N=10^{-15}$ $V\cdot cm^2$ $Te=8.617\cdot10^{-5}*T$; T, K. Kochetov	elect	-0.196
42a	$e+O_2(v) \rightarrow O_2+e$	Reaction is approximated	Kochetov	elect	+0.196
43	$N_2(v)+M \rightarrow N_2+M$	$7\cdot10^{-10}\cdot\exp(-141/(T, K)^{1/3})$	Naidis (M-molec)	gas	+0.293
44	$N_2(v)+O \rightarrow N_2+O$	$5\cdot10^{-12}\cdot\exp(-128/(T, K)^{1/2})$	Naidis	gas	+0.293
45	$O_2(v)+O_2 \rightarrow O_2+O_2$	$1.41\cdot10^{-12}\cdot$ $\exp(-90/(T, K)^{1/3})$, $T\leq500$, m^3/s $1.31\cdot10^{-12}$ $\exp(-126/(T, K)^{1/3})$, m^3/s $T>500$	Naidis	gas	+0.196
46	$\widehat{e}+N_2 \rightarrow N_2(v)+\widehat{e}$	V_e= 14.5	Konovalov (normalized on pure N2 in air)		
47	$\widehat{e}+O_2 \rightarrow O_2(v)+\widehat{e}$	V_e=3.19 eV	Konovalov (normalized on pure O2 in air)		
48a	$e+O_2 \rightarrow O_2^+ + 2e$	Reaction is approximated	$5\cdot10^{-16}<E/N<2\cdot10^{-15}$ $V\cdot cm^2$ Kochetov	elec	-12.1
48b	$e+O_2(v) \rightarrow O_2^+ + 2e$	Reaction is approximated	Kochetov	elec	-11.9
48c	$e+O_2(\Delta_{effec}) \rightarrow O_2^+ + 2e$	Reaction is approximated	Kochetov	elec	-11.1
48d	$e+N_2 \rightarrow N_2^+ + 2e$	Reaction is approximated	Kochetov	elec	-15.6

48e	$e + N_2(v) \rightarrow N_2^+ + 2e$	Reaction is approximated	Kochetov	elec	-15.3
48f	$e + N_2(A^3\Sigma_u^+) \rightarrow N_2^+ + 2e$	Reaction is approximated	Kochetov	elec	-9.43
48g	$e + N_2(B^3\Pi_g) \rightarrow N_2^+ + 2e$	Reaction is approximated	Kochetov	elec	-8.25
49a	$\widehat{e} + N_2 \rightarrow N_2(A^3\Sigma_u^+) + \widehat{e}$	V_N^* =258.0 eV	Konovalov (normalized on pure N2 in air) Threshold E=6.17 eV		
49b	$\widehat{e} + N_2 \rightarrow N_2(B^3\Pi_g) + \widehat{e}$	V_N^* =249.0 eV	Konovalov (normalized on pure N2 in air) Threshold E=7.35 eV		
50a	$e + N_2 \rightarrow N_2(A^3\Sigma_u^+) + e$	Reaction is approximated	$3\cdot10^{-16}$ <E/N <E/N=$2\cdot10^{-15}$ V·cm^2 Kochetov	elec	-6.17
50aa	$e + N_2(A^3\Sigma_u^+) \rightarrow e + N_2$	Reaction is approximated	Kochetov	elec	6.17
50b	$e + N_2 \rightarrow N_2(B^3\Pi_g) + e$	Reaction is approximated	$3\cdot10^{-16}$ <E/N <E/N=$2\cdot10^{-15}$ V·cm^2 Kochetov	elec	-7.35
50bb	$e + N_2(B^3\Pi_g) \rightarrow N_2 + e$	Reaction is approximated	Kochetov	elec	7.35
51	$N_2(A^3\Sigma_u^+) + N_2(A^3\Sigma_u^+) \rightarrow N_2(X^1\Sigma_g^+) + N_2(B^3\Pi_g)$	$2.6\cdot10^{-10}$	**Kossyi**	gas	+4.99
52	$N_2(A^3\Sigma_u^+) + N_2(A^3\Sigma_u^+) \rightarrow N_2(X^1\Sigma_g^+) + N_2(B^3\Pi_g)$	$1.1\cdot10^{-9}$	$N_2(X^1\Sigma_g^+)$ considered as N_2 Kossyi	gas	+4.99
53a	$N_2(A^3\Sigma_u^+) + N_2(X^1\Sigma_g^+, v) \rightarrow N_2(X^1\Sigma_g^+, w) + N_2(B^3\Pi_g)$	$3.0\cdot10^{-10}$	$N_2(X^1\Sigma_g^+, v, w)$ considered as N_2 Kossyi	gas	-0.9
53b	$N_2(A^3\Sigma_u^+) + O_2 \rightarrow N_2 + O + O$	$2.54\cdot10^{-12}$	Baulch Kossyi	gas	+1.07
53c1	$N_2(B^3\Pi_g) + N_2 \rightarrow N_2(A^3\Sigma_u^+) + N_2$	$5.0\cdot10^{-11}$	Kossyi	gas	+1.18
53c2	$N_2(B^3\Pi_g) \rightarrow N_2(A^3\Sigma_u^+) + h\nu$	$1.5\cdot10^5$ s^{-1}	Kossyi	gas	+1.18
53c3	$N_2(B^3\Pi_g) + NO \rightarrow N_2(A^3\Sigma_u^+) + NO$	$2.4\cdot10^{-10}$	Kossyi	gas	+1.18
53c4	$N_2(B^3\Pi_g) + O_2 \rightarrow N_2 + O + O$	$3.0\cdot10^{-10}$	Kossyi	gas	+2.25
54a	$N_2^+ + O_2 \rightarrow O_2^+ + N_2$	$K_{54}=2.86\cdot10^{-10}$ cm^3/s	Charge exchange	gas	+3.4

			N_2^+ ion averaged over N_2^+ and N_4^+ it appears in $N_2^+ + 2N_2 \rightarrow$ and $N_4^+ + O_2 \rightarrow$		
54b	$N_2^+ + O_2(v) \rightarrow O_2^+ + N_2$	$K_{54}=2.86\cdot10^{-10}$ cm^3/s	McIven	gas	+3.4
54c	$N_2^+ + O_2(\Delta_{effec}) \rightarrow O_2^+ + N_2$	$K_{54}=2.86\cdot10^{-10}$ cm^3/s	estimate	gas	+2.4
55a1	$O_2 + O_2 \rightarrow O + O + O_2$	$3.7\cdot10^{-8}\cdot \exp(-59380/T)\cdot$ [1- exp(-2240/T)] , T=300-4000; $16.0\cdot (T)^{-2..5}\exp(-59380/T)$ T=4000-20000;	Krinonosova	gas	-5.1
55a2	$O + O + O_2 \rightarrow O_2 + O_2$	$2.45\ 10^{-31}\cdot (T)^{-0.63}$ T=300-4000;	Krinonosova	gas	+5.1
55b1	$O_2 + N \rightarrow O + O + N$	$9.3\cdot10^{-9}\cdot \exp(-59380/T)\cdot$ [1- exp(-2240/T)] , T=3000-7000	Krinonosova	gas	-5.1
55b2	$O + O + N \rightarrow O_2 + N$	$6.3\ 10^{-32}\cdot (T)^{-0.63}$ T=300-4000	Krinonosova	gas	+5.1
55b3	$O_2 + N \rightarrow O + NO$	$1.0\cdot 10^{-14}\cdot T\cdot\exp(-3150/T)$	Krinonosova	gas	-1.4
55c1	$O_2 + NO \rightarrow O + O + NO$	$9.3\cdot10^{-9}\cdot \exp(-59380/T)\cdot$ [1- exp(-2240/T)] T=300-4000; $4.0\cdot (T)^{-2..5}\exp(-59380/T)$ T=4000-20000	Krinonosova	gas	-5.1
55c2	$O + O + NO \rightarrow O_2 + NO$	$6.3\ 10^{-32}\cdot (T)^{-0.63}$ T=300-4000	Krinonosova	gas	+5.1
55d1	$O_2 + O \rightarrow O + O + O$	$1.3\cdot10^{-7}\cdot \exp(-59380/T)\cdot$ [1- exp(-2240/T)] T=300-4000; $5.8\ 10^{-2}\ (T)^{-2..5}\exp(-59380/T)$ T=4000-20000	Krinonosova	gas	-5.1
55d2	$O + O + O \rightarrow O_2 + O$	$8.8\ 10^{-31}\cdot (T)^{-0.63}$ T=300-4000	Krinonosova	gas	+5.1
55e1	$O_2 + N_2 \rightarrow O + O + N_2$	$9.3\cdot10^{-9}\cdot \exp(-59380/T)\cdot$ [1- exp(-2240/T)]	Krinonosova	gas	-5.1
55e2	$O + O + N_2 \rightarrow O_2 + N_2$	$2.76\ 10^{-34}\cdot \exp(720/T)$	Krinonosova	gas	+5.1
56a1	$NO + O_2 \rightarrow N + O + O_2$	$8.7\ 10^{-9}\cdot \exp(-76\ 000/T)$	Krinonosova	gas	-6.5
56a2	$N + O + O_2 \rightarrow NO + O_2$	$2.8\ 10^{-28}\cdot (T)^{-0..5}$	Zamyshlyaev	gas	+6.5
56b1	$NO + N_2 \rightarrow N + O + N_2$	$8.7\ 10^{-9}\cdot \exp(-76\ 000/T)$	Krinonosova	gas	-6.5
56b2	$N + O + N_2 \rightarrow NO + N_2$	$1.8\ 10^{-31}\cdot (T)^{-0..5}$	Krinonosova	gas	+6.5
56c1	$NO + O \rightarrow N + O + O$	$1.7\ 10^{-7}\cdot \exp(-76\ 000/T)$	Krinonosova	gas	-6.5

56c2	$N + O + O \rightarrow NO + O$	$5.6\ 10^{-27} \cdot (T)^{-0..5}$	Zamyshlyaev	gas	+6.5
56c3	$NO + O \rightarrow N + O_2$	$2.5\ 10^{-15} \cdot (T) \cdot \exp(-19\ 500/T)$	Krinonosova	gas	+1.4
56d1	$NO + N \rightarrow N + O + N$	$1.3\ 10^{-2} \cdot (T)^{-1..5} \exp(-75530/T)$	Zamyshlyaev	gas	-6.5
56d2	$N + O + N \rightarrow NO + N$	$5.6\ 10^{-27} \cdot (T)^{-0..5}$	Zamyshlyaev	gas	+6.5
56d3	$NO + N \rightarrow O + N_2$	$1.05\ 10^{-12} \cdot (T)^{0..5}$ T=200-4000 K	Krinonosova	gas	+3.26
56e1	$NO + NO \rightarrow N + O + NO$	$1.7\ 10^{-7} \cdot \exp(-76\ 000/T)$	Krinonosova	gas	-6.5
56e2	$N + O + NO \rightarrow NO + NO$	$5.6\ 10^{-27} \cdot (T)^{-0..5}$	Zamyshlyaev	gas	+6.5
58	$N + NO \rightarrow N_2 + O$	$1.0\ 10^{-12} \cdot (T)^{0..5}$	Krinonosova	gas	+3.28
62	$N + O_2 \rightarrow NO + O$	$4.1\ 10^{-12} \cdot \exp(-3200/T)$	Baulch	gas	+1.4
63	$N + O_3 \rightarrow NO + O_2$	$5.5\ 10^{-12}$	Baulch	gas	-3.3
64	$N_2(A^3\Sigma_u^+) + O \rightarrow N_2 + O$	$2.1\ 10^{-11}$	Kossyi	gas	+6.17
65	$N_2(A^3\Sigma_u^+) + O \rightarrow NO + N$	$7.0\ 10^{-12}$	Kossyi	gas	+2.91
66	$N_2 + O_2 \rightarrow O + N_2O$	$2.5\ 10^{-10} \cdot \exp(-50391/T)$	krivonosova	gas	-3.9
67	$O^- + NO \rightarrow e + NO_2$	$2.6\ 10^{-10}$	Kossyi	gas	+1.64
68	$O_2(b) + O_3 \rightarrow O + O_2 + O_2$	$1.8 \cdot 10^{-11}$	kossyi	gas	+0. 6
69	$O_2(b) + N_2 \rightarrow N_2 + O_2(a^1\Delta)$	$4.9\ 10^{-15} \cdot \exp(-253/T)$	Kossyi	gas	+0.66
71	$O_2(b) + O_2 \rightarrow O_2 + O_2(a^1\Delta)$	$4.3\ 10^{-22} \cdot T^{2.4} \exp(-241/T)$	Kossyi	gas	+0.66
72	$O_2(b) + O \rightarrow O_2(a^1\Delta) + O$	$8.0\ 10^{-14}$	Kossyi	gas	+0.66
73	$O_2(b) + NO \rightarrow O_2(a^1\Delta) + NO$	$4.0\ 10^{-14}$	Kossyi	gas	+0.66
74	$O_2(A) + O_2 \rightarrow O_2(b) + O_2(b)$	$2.9\ 10^{-13}$	Kossyi	gas	+1.22
75	$O_2(A) + O \rightarrow O_2(b) + O(D)$	$9.0\ 10^{-12}$	Kossyi	gas	+0.89
76	$O_2(A) + N_2 \rightarrow N_2 + O_2(b)$	$3.0\ 10^{-13} \cdot$	Kossyi	gas	+2.86

Table 3.1.2 Reactions with complex ions

N.	Formulae of reaction	Rate constant (cm^6/s, cm^3/s) /Cost (eV)	Defect of energy	Source
1	$O_2^+ + O_2 + O_2 \rightarrow O_4^+ + O_2$	$2.5 \cdot 10^{-30}(293/T)^{3.2}$	0.44 eV (from gas)	Smirnov
2	$O_4^+ + O_2 \rightarrow O_2^+ + O_2 + O_2$	$3.3 \cdot 10^{-6}(300/T)^4 \exp(-2650/T)$	0.44 eV (to gas)	Smirnov, Kossyi

3	$O_4^+ + O_2(\Delta) \rightarrow O_2^+ + O_2 + O_2$	$3.3\cdot10^{-6}(300/T)^4\exp(-2650/T)$	1.42 eV (to gas)	Smirnov, Kossyi
4	$O_4^+ + O_2(b) \rightarrow O_2^+ + O_2 + O_2$	$3.3\cdot10^{-6}(300/T)^4\exp(-2650/T)$	2.08 eV (to gas)	Smirnov, Kossyi
5	$O_4^+ + O_2 + O_2 \rightarrow O_6^+ + O_2$	$7.0\cdot10^{-32}(293/T)^{5.1}$	0.28 eV (from gas)	Smirnov
6	$O_6^+ + O_2 \rightarrow O_4^+ + O_2 + O_2$	$1.0\cdot10^{-13}(300/T)^4$	0.28 eV (to gas)	Smirnov, Kossyi
7	$O_6^+ + O_2 + O_2 \rightarrow O_8^+ + O_2$	$2.5\cdot10^{-29}(90/T)^{5.0}$	0.13 eV (from gas)	Smirnov
8	$O_8^+ + O_2 \rightarrow O_6^+ + O_2$	$1.0\cdot10^{-13}(300/T)^4$	0.13 eV (to gas)	Smirnov Kossyi
9	$e + O_4^+ \rightarrow O_2 + O_2$	$1.0\cdot10^{-6}\cdot(0.025/T_e)^{0.5}(300/T)^{0.5}$	12.33 eV (to gas)	Smirnov Kossyi
10	$e + O_6^+ \rightarrow O_2 + O_2 + O_2$	$1.0\cdot10^{-6}\cdot(0.025/T_e)^{0.5}(300/T)^{0.5}$	12.05 eV (to gas)	Smirnov Kossyi
11	$e + O_8^+ \rightarrow O_2 + O_2 + O_2 + O_2$	$1.0\cdot10^{-6}\cdot(0.025/T_e)^{0.5}(300/T)^{0.5}$	11.92 eV (to gas)	Smirnov Kossyi

Table 3.1.3. Reactions with complex ions

N.	**Formulae of reaction**	**Rate (cm^6/s, cm^3/s) /Cost (eV)**	**Defect of energy electrons, eV**	**Source**
1	$O_4^+ + O_2^- + M \rightarrow O_2 + O_2 + O_2 + M$	$2.0\cdot10^{-25}(300/T)^{2.5}$	12.75 eV (to gas)	Smirnov Kossyi
2	$O_4^+ + O_2^- \rightarrow O_2 + O_2 + O_2$	$1.0\cdot10^{-7}(300/T)^{0.5}$	12.75 eV (to gas)	Smirnov, Kossyi
3	$O_6^+ + O_2^- \rightarrow O_2 + O_2 + O_2 + O_2$	$1.0\cdot10^{-7}(300/T)^{05}$	12.47 eV (to gas)	Smirnov, Kossyi
4	$O_4^+ + O^- + M \rightarrow O + O_2 + O_2 + M$	$2.0\cdot10^{-25}(300/T)^{2.5}$	13.77 eV (to gas)	Smirnov Kossyi
5	$O_6^+ + O_2^- + M \rightarrow O_2 + O_2 + O_2 + O_2 + M$	$2.0\cdot10^{-25}(300/T)^{2.5}$	12.47 eV (to gas)	Smirnov, Kossyi
6	$O_6^+ + O_2^- \rightarrow O_2 + O_2 + O_2 + O_2$	$1.0\cdot10^{-7}(300/T)^{05}$	12.47 eV (to gas)	Smirnov, Kossyi
7	$O_6^+ + O^- + M \rightarrow O + O_2 + O_2 + M$	$2.0\cdot10^{-25}(300/T)^{2.5}$	13.49 eV (to gas)	Smirnov Kossyi
8	$O_6^+ + O^- \rightarrow O + O_2 + O_2 + O_2$	$1.0\cdot10^{-7}(300/T)^{0.5}$	13.49 eV (to gas)`	Smirnov Kossyi
9	$O_8^+ + O_2^- + M \rightarrow 5O_2 + M$	$2.0\cdot10^{-25}(300/T)^{2.5}$	12.62 eV (to gas)	Smirnov Kossyi
10	$O_8^+ + O_2^- \rightarrow 5O_2$	$1.0\cdot10^{-7}(300/T)^{0.5}$	12.62 eV (to gas)	Smirnov Kossyi

11	$O_8^+ + O^- + M \rightarrow O + O_2 + O_2 + O_2 + O_2 + M$	$2.0 \cdot 10^{-25} (300/T)^{2.5}$	13.36 eV (to gas)	Smirnov Kossyi
12	$O_8^+ + O^- \rightarrow O + O_2 + O_2 + O_2 + O_2$	$1.0 \cdot 10^{-7} (300/T)^{0.5}$	13.36 eV (to gas)	Smirnov Kossyi

Literature to Table 3.1.1.

Baulch: Atkinson R., Baulch D.L., Cox R.A., Hampson R.F.Jr, Kerr J.A., troe J. J. Phys. Chem. Ref. Data. 1989. V.18. N.2. P. 881.
Konovalov: C.194-227. Konovalov V.P. Degradation spectra of electrons in nitrogen, oxygen and air. Zhurnal Tekhnicheskoi Fiziki. 1993. V.63.N.3. P.23-33.; Konovalov V.P., Son E.E. Degradation spectra of electrons in gases. In a book Khimia plazmy Ed. B.M.Smirnov Energoatomizdat. 1987.Vol.14.P.194-227. also available in Reviews of Plasma Chemistry, B. M. Smirnov, Ed. New York: Consultants Bureau, 1991.
Kossyi: Kostinsky A.Y., Matveev A.A., Silakov V.P., и др. Plasma Sources. Sci. Tech. 1992. V.1. N.3. P.207.
Kochetov : Akishev Yu.S., Deryugin A.A., Karalchik V.B., Kochetov I.V. Experimental and numerical modeling of atmospheric pressure constant current glow discharge. Fizika Plazmy. 1994. V. 20. N.6. P. 571-584.
Krivonosova : Krivonosova O.E., Losev S.A., Nalivaiko V.P., Mukoseev Yu.K., Shatalov O.P. Recommended data about chemical reactions rate constants between molecules consisting of atoms N and O. In a book Khimia plasmy. V.14. Ed. Prof B.M. Smirnov. Moscow.Energoatomizdat. 1986. P.3-31, also available in Reviews of Plasma Chemistry, B. M. Smirnov, Ed. New York: Consultants Bureau, 1991.
Smirnov: Smirnov B.M. Complex ions. Moscow. Nauka. 1983. 151 p.
Smirnov B.M. Negative ions. Moscow. Atomizdat 1978. 176 p.
Maikapar: Non equilibrium physical and chemical processes in aerodynamics. Ed. G.I. Maikapar. Moscow. Mashinostroenie. 1972. 344 p.
Zamyshlyaev: Zamyshlyaev B.V., Stupitskii E.L., Guz A.G., Zhukov V.N. Composition and thermodynamic functions of plasmas. Moscow. Energoatomizdat. 1984.
Naidis: Mnatsakanyan A. Kh. and Naidis, G. V. "Charged particle production and loss processes in nitrogen-oxygen plasmas," in Reviews of Plasma Chemistry, B. M. Smirnov, Ed. New York: Consultants Bureau, 1991, pp. 259-292.
Also data from the following references have been used:
Eliasson B., Kogelschatz U., J. de Chimie Physique. 1986. V.83. P.279.
Maetzing H. Chemical Kinetics of Flue Gas Cleaning by Irradiation with Electrons. Adv. in Chemical Physics. V. LXXX/Ed. by I. Prigogine and S.A. Rice. ISBN 0-471-53281-9 © John Wiley & Sons, Inc. 1991.
McIven M., Phillips L. Atmospheric Chemistry (Mir. Moscow 1978. Russian Edition. Mir. Moscow 1978. 375 p.
Mukkavilli S., Lee C.K., Tavlarides L.L., IEEE Trans Plasma Sci. 1988. V.16. N. 6. P. 652.
Slovetsky D.I. Mechanisms of chemical reactions in non-equilibrium plasmas. Moscow. Nauka.1980. 310 p.
Person J.C., Ham D.O. Radiat. Phys. Chem. 1988. V. 31. N.1-3. P.
Eliasson B., Kogelschatz U., J. de Chimie Physique. 1986. V.83. P.279.
Mukkavilli S., Lee C.K., Tavlarides L.L., IEEE Trans Plasma Sci. 1988. V.16. N. 6. P. 652.
Person J.C., Ham D.O. Radiat. Phys. Chem. 1988. V. 31. N.1-3. P.1.
Eliasson B., Kogelschatz U., "Basic Data for Modelling of Electrical Discharge in Gases: Oxygen". Asea brown bovert Forschungszentrum CH-5405, Baden KLR 86-11C, June 1986. P.1.
Aleksandrov N.L. Uspekhi Fiz. Nauk. 1988.V.154. N.2. P.147.
Samoilovich V.G., Gibalov V.I., Kozlov K.V. Physical chemistry of barrier discharge. Moscow. MSU publishers. 1989.
Steinfeld J.I., Adler-Golden S.M., Gallagher J.W. J.Phys. Chem. Ref. Data. 1987. V.16. N.4. P.911.
Flannery M.R. Ion-ion recombination in high-pressure discharges. In a book: Gas lasers. ED I.Mc Daniel and W. Nighan. Moscow. Mir .1986. P.177-215.

3.1.2 Electron heating due to fast electrons

For this Project we specially reanalyzed electron energy equation obtained in our previous works.

Nowadays there is no absolutely correct method of electron temperature calculations in the molecular gas at small ionization intensity by the electron beam, when the electron temperature is close to the temperature of the gas. The analogous case for the atomic gas was considered in [8,9]. According to it in case of weak excitation by the electron beam the electron

distribution function over energies is formed in the result of complicated sequence of elementary processes. The electron of a beam and the secondary electrons, which energy is higher than the first excitation potential of atoms, loose their energy mainly in the inelastic processes of excitation of atoms and their ionization. The typical time of the energy loss for such electrons is

$\tau_{inelastic} \sim (v_e \cdot \sigma_{inelastic} \cdot N)^{-1}$

and for atmospheric pressure gas it is in the range 10^{-12}-10^{-10} s (v_e~10^8-10^9 cm/s-the electron velocity, $\sigma_{inelastic}$ ~10^{-18}-10^{-16} cm^2 –typical value of inelastic processes cross section). For electrons with the energy lower the first excitation potential of the atom *I*, the mechanism of the energy loss is connected with the process of the elastic scattering on atoms. The typical time of this process

$$\tau_{elastic} \sim \left(\frac{2m}{M} v_e \cdot \sigma_{elastic} \cdot N \right)^{-1}$$

is about M/m ~ 10^{-8}-10^{-6} s ((M-mass of the atom, m-mass of the electron) times greater than the time of fast electrons cooling ($\sigma_{elastic}$ ~10^{-16}-10^{-15} cm^2 elastic cross section of the electron scattering on the atom).

The typical time of electron recombination

$\tau_{recomb} \sim (N_e \cdot k_{rec})^{-1}$

is about 10^{-7}-10^{-5} s (at N_e~10^{14}-10^{12} cm^{-3}).

So one considers that the electron distribution function over energies consists of two parts. The fast electrons, which energy is higher than that of the excitation potential of the atom *I,* are characterized by rather wide spread over the energy axis. These electrons practically can not recombine, so this part of the electron distribution function plays the role of the source providing electrons to the "slow" section. Due to the difference in thermalization times the number of electrons in the "fast" region is approximately by M/m times less than in the "slow". In other words the electrons with the energy below the lowest excitation potential of the atom *I* represents the main part of electrons in the plasma.

In this case the energy put of these "slow" electrons could be estimated by the equation for electron temperature T_e [8,9]:

$$\frac{\partial T_e}{\partial t} = \frac{Q}{N_e}(U_i \eta - T_e) \qquad (3.1.1)$$

Here *Q*-is the rate of excitation of the gas by the electron beam, N_e –the concentration of the plasma electrons, N is the concentration of the neutrals, T_e is the electron temperature, $U_i\eta$ - energy coming below the lowest excitation potential of the molecule. In case of Air it is the part of energy coming to rotational and elastic levels of freedom of molecules, which were obtained in works [10]

$$\eta = \eta_{O2} \frac{N_{O2} + N_{O2(v)} + N_{O2(\Delta)} + N_{O2(b)}}{M} + \eta_{N2} \frac{N_{N2} + N_{N2(v)} + N_{N2(A)} + N_{N2(B)}}{M} \qquad (3.1.2)$$

where $M = N_{O2} + N_{O2(v)} + N_{O2(\Delta)} + N_{O2(b)} + N_{N2} + N_{N2(v)} + N_{N2(A)} + N_{N2(B)}$

η_{O2}=1.03 ·10^{-3}, η_{N2}=4.68 ·10^{-3}, N_{O2}, $N_{O2(v)}$, $N_{O2(\Delta)}$, $N_{O2(b)}$, and N_{N2}, $N_{N2(v)}$, $N_{N2(A)}$, $N_{N2(B)}$ are concentrations of O_2 and N_2 molecules in ground, vibrational and lower electronically excited states respectively. We specially indicate this states because at high excitation level the combination of these neutral components can be changed.

We remind that power putted to a gas W (we often use it in eV/(cm^3 s)) and excitation of molecules *Q* are connected by the equation

Q=W/(*Ui*),

Where *Ui* is the cost of ionization, in air *Ui* = 31.6 eV.

3.1.3. Electron energy equation

Electron energy equation in the present approach has a form based on [11-13] :

$$\partial T_e/\partial t = W\cdot\eta \ \{1\} + \Sigma K_i [M_i^+]T_e/2 \ \{2\} + \Sigma K_j (2/3\, I_j + 3T_e)[M_j^+][e] \ \{3\} + \\ + I_{aff}\, k_{det} [O_2^-][O_2+N_2] \ \{4\} - K_{at1} [O_2]^2 T_e^2\, d K_{at1}(T_e)/d T_e \ \{5\} - \\ - K_{el1} [O_2+N_2](T_e - T) \ \{6\} \\ - \qquad (3.1.3)$$

where: {1} -heating due to injection of fast electrons into energy region below the threshold of vibrational excitation, see (2); {2}, {3} - heating due to processes of electron-ion recombination [12-13], {4} -heating due to electron detachment; {5}, - Cooling due to attachment processes to O_2 molecules [12-13] , {6} - Cooling due to elastic and inelastic collisions of slow electrons with O_2, and N_2 molecules.

3.1.4. Results of air plasma calculations

We have undertaken preliminary calculations at different rates of excitation of the gas medium by the electron beam and electron beam in external electric field showing appearance of dissociated and electronically excited molecules of air.

In Fig. 3.1.1- 3.1.4 one can see results of corresponding calculations for air pressure of 200 Torr and in Fig. 3.1.5- 3.1.12 at atmospheric pressure.

They have shown high level of molecules excitation in wide parameters range of electron-beam plasmas.

At that the application of under breakdown electric field substantially increases the excitation level (the breakdown field corresponds to E/N=90-100 Td, 1 Td= 10^{-17} V·cm^2; E is an electric field strength, N is the density of neutral molecules)).

The calculated level on high non-equilibrium has a duration of about 2-3 ms. This enables to realize this state in our experiments.

One can show [14] that the excitation velocity W is connected with parameters of relativistic electron-beam (200-500 keV-and even up to1 MeV) by the relation

$$W = 10^{22} J_b \cdot P, \qquad (3.1.4)$$

Here the current density J is expressed in A/cm^2, an pressure P in atm, and in case of non-relativistic beam [15] (E_b = 150keV) $W = 4\cdot 10^{22} J_b \cdot P$.

Inserting calculated parameters one can get the following range of the current density (at pressure 200 Torr) J=1,2·10^{-4} -1,2·10^{-2} A/cm^2 for relativistic beam and J=3,0·10^{-5} -3,0·10^{-3} A/cm^2 for non-relativistic one.

Data on gas discharge air plasma [16] indicate the following effective range of E/N parameter with respect to vibrational and electronic excitation E/N=30-60 Td (or 2-4 kV/cm).

From the formula (3.1.4) follows that the excitation velocity rises proportionally to the gas pressure, so one has to expect increase of the activation effect for the electron source realizing the current density J=1,2·10^{-4}-1,5·10^{-2} A/cm^2 (for relativistic) and J=3,0·10^{-5}-5·10^{-3} A/cm^2 (for non relativistic) which can be realized in our installations with relativistic electron beam (REB) with energy of electrons E_b = 350 keV at gasdynamic rise of pressure in the chamber during our experiments.

However for obtaining more reliable data we have to undertake additional investigations.

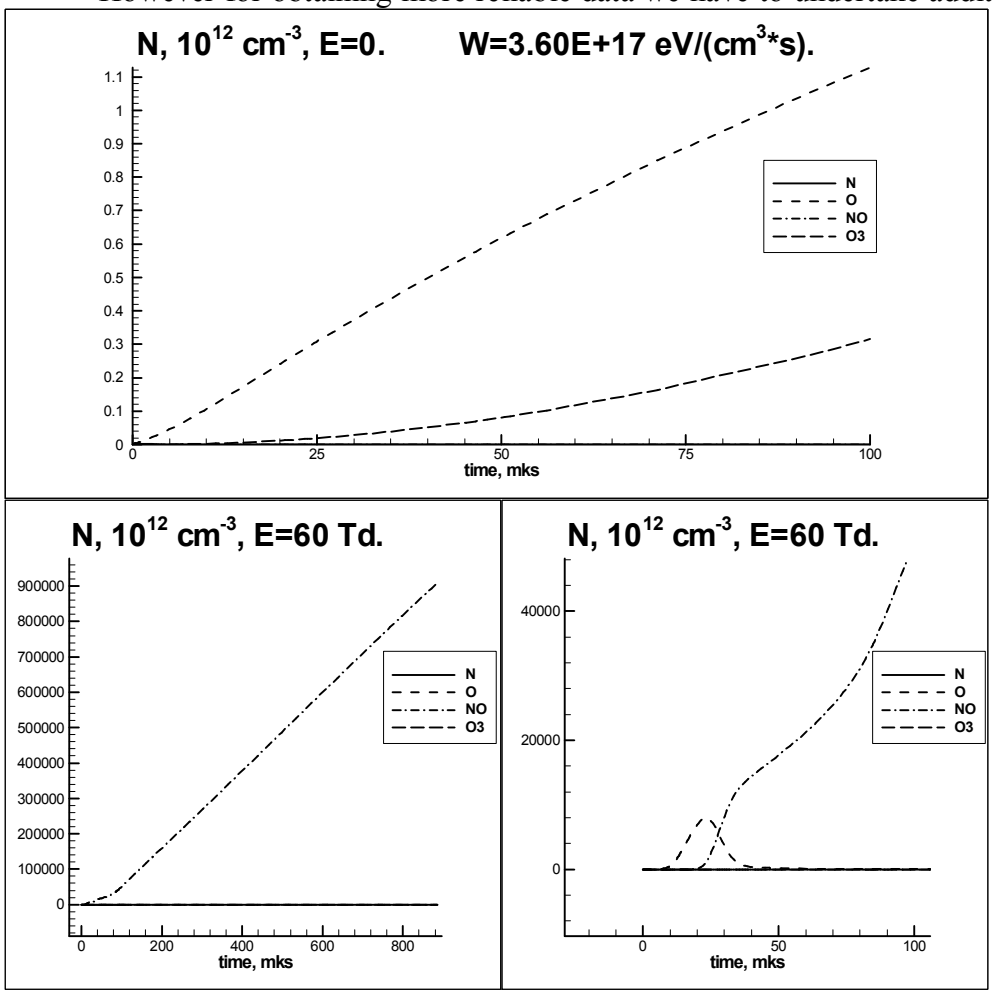

Fig.3.1.1. Neutral particles in beam plasmas at pressure P=200 Torr, at air excitation velocity W= 3,6·10^{17}eV/(cm^{3}s).

The upper figure corresponds to excitation by only the electron beam, the below figure corresponds to excitation by the electron beam in electric field at E/N=60 Td.

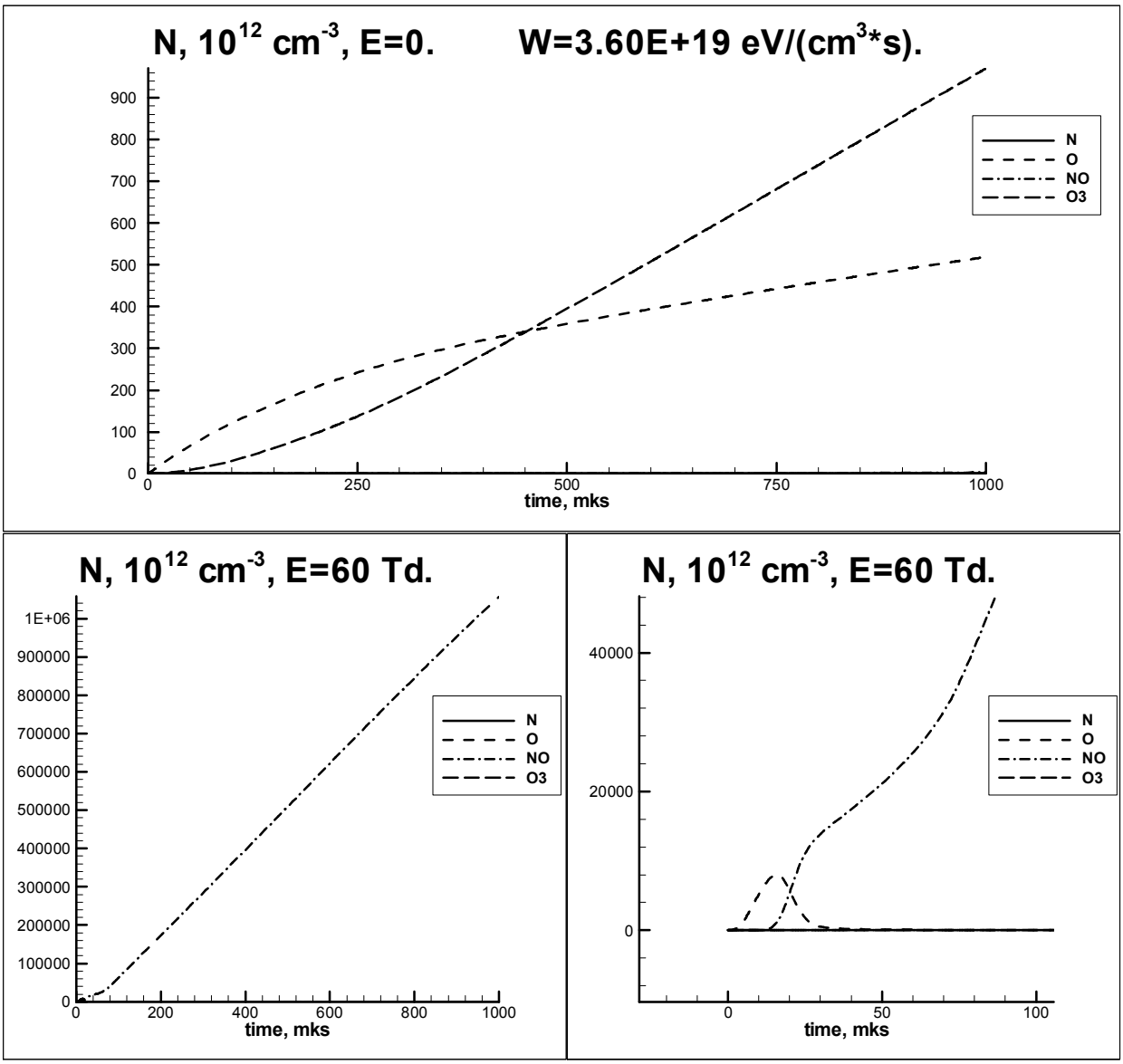

Fig.3.1.2. Neutral particles in beam plasmas at pressure P=200 Torr, at air excitation velocity $W= 3.6 \cdot 10^{19} eV/(cm^3 s)$.

The upper figure corresponds to excitation by only the electron beam, the below figure corresponds to excitation by the electron beam in electric field at E/N=60 Td.

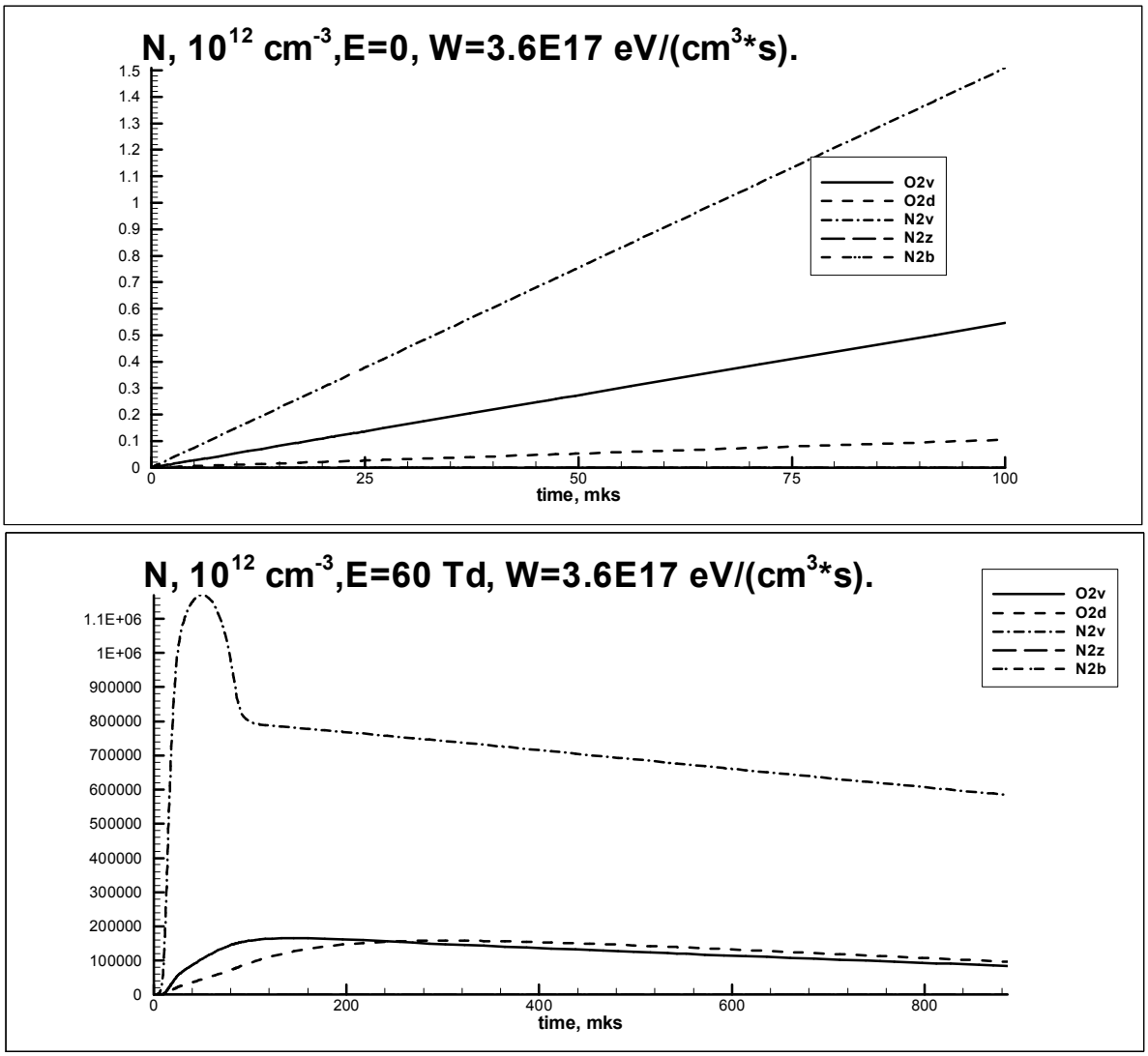

Fig.3.1.3. Excited particles in beam plasmas at pressure P=200 Torr, at air excitation velocity $W= 3.6 \cdot 10^{16} eV/(cm^3 s)$.

The upper figure corresponds to excitation by only the electron beam, the below figure corresponds to excitation by the electron beam in electric field at E/N=60 Td. (Index v- vibrational excitation (v=1), indexes b,d, z- corresponds to electronic excitation of lower electronic states of molecules O_2 and N_2).

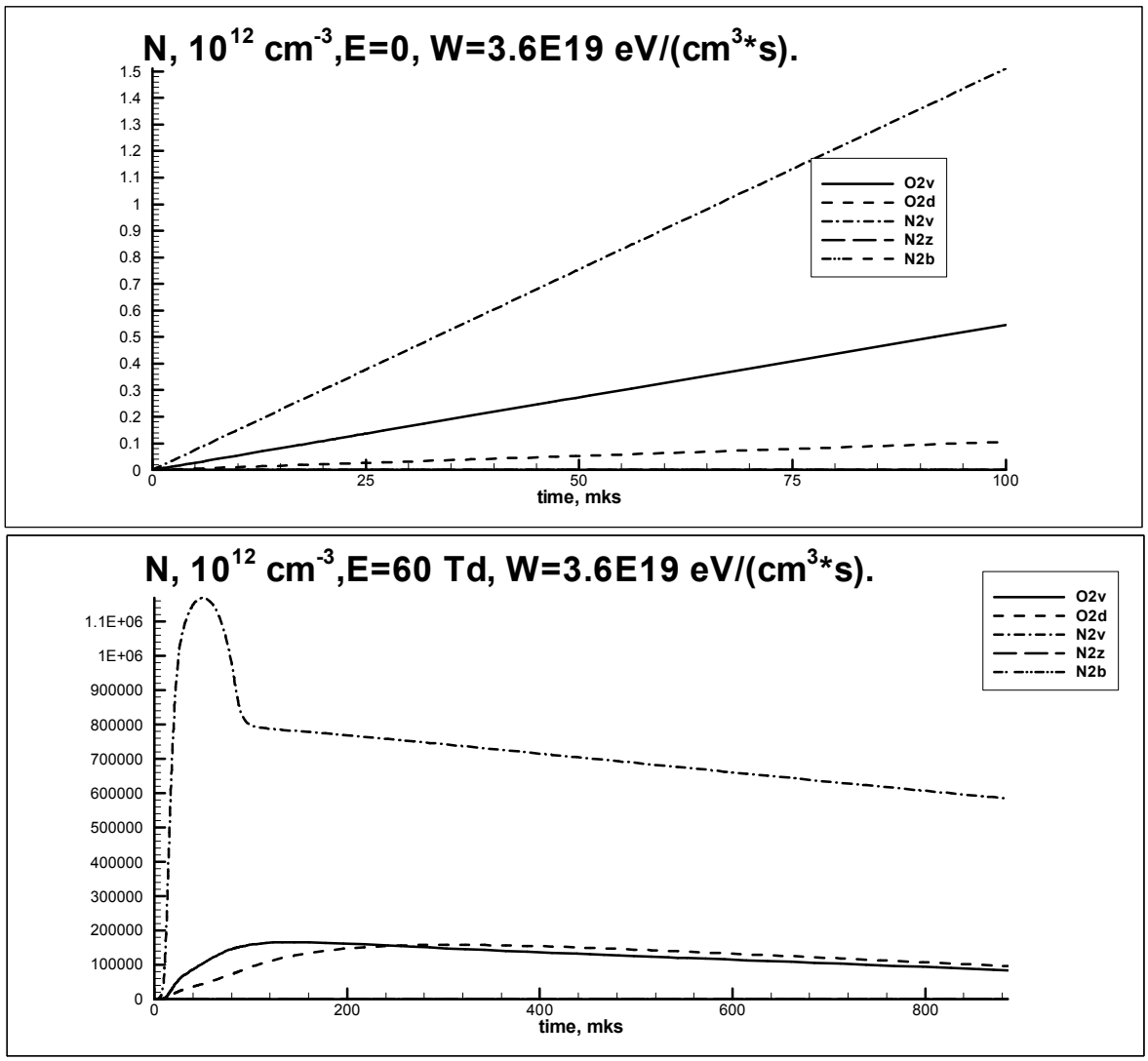

Fig.3.1.4. Excited particles in beam plasmas at pressure P=200 Torr, at air excitation velocity $W= 3.6 \cdot 10^{19} eV/(cm^3 s)$.

The upper figure corresponds to excitation by only the electron beam, the below figure corresponds to excitation by the electron beam in electric field at E/N=60 Td. (Index v- vibrational excitation (v=1), indexes b,d, z- corresponds to electronic excitation of molecules.

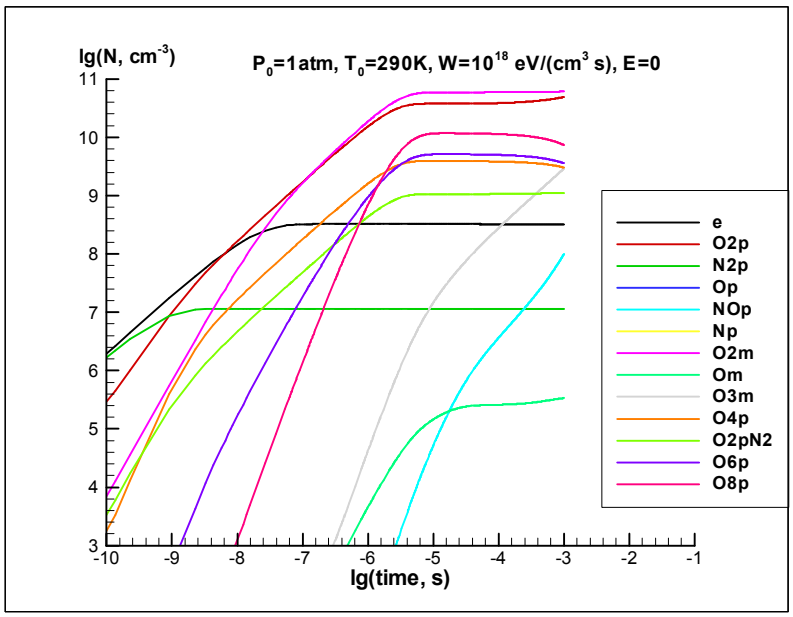

Fig.3.1.5. Charged particles in beam plasmas at pressure P=1 atm, at air excitation velocity W= 10^{18}eV/(cm^{3}s). E/N=0 Td.

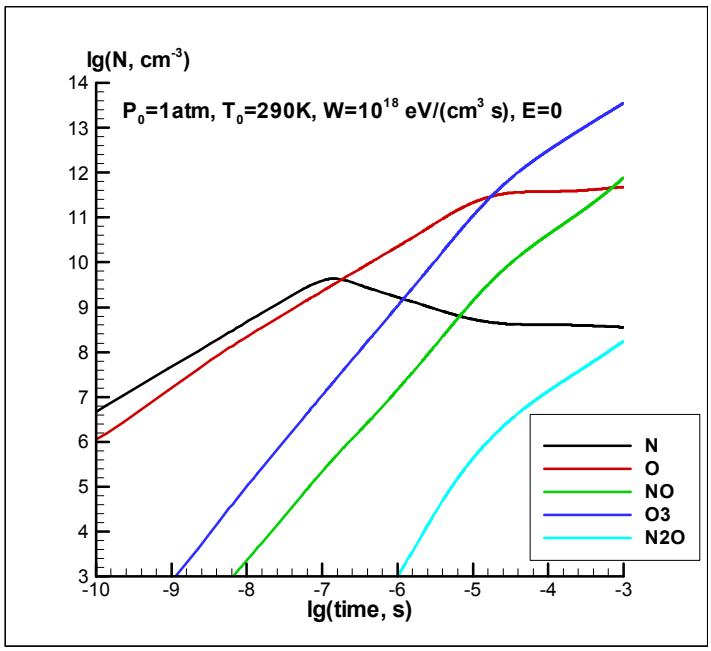

Fig.3.1.6. Neutral particles in beam plasmas at pressure P=1 atm, at air excitation velocity W= 10^{18}eV/(cm^{3}s). E/N=0 Td.

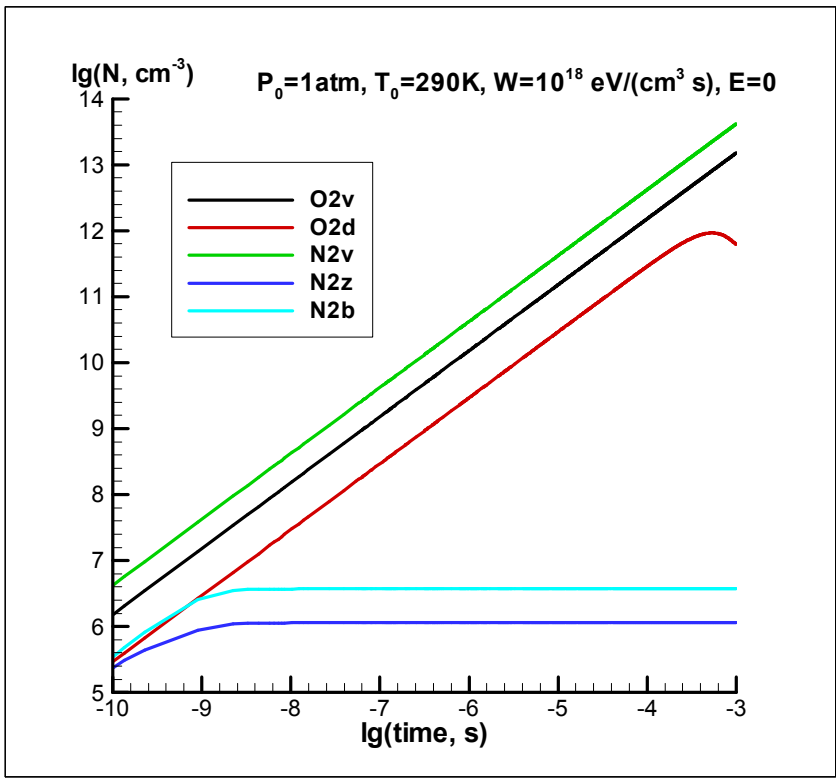

Fig.3.7. Excited particles in beam plasmas at pressure P=1 atm, at air excitation velocity W= 10^{18}eV/(cm^{3}s). E/N=0 Td. (Index v- vibrational excitation (v=1), indexes b,d, z- corresponds to electronic excitation of molecules.

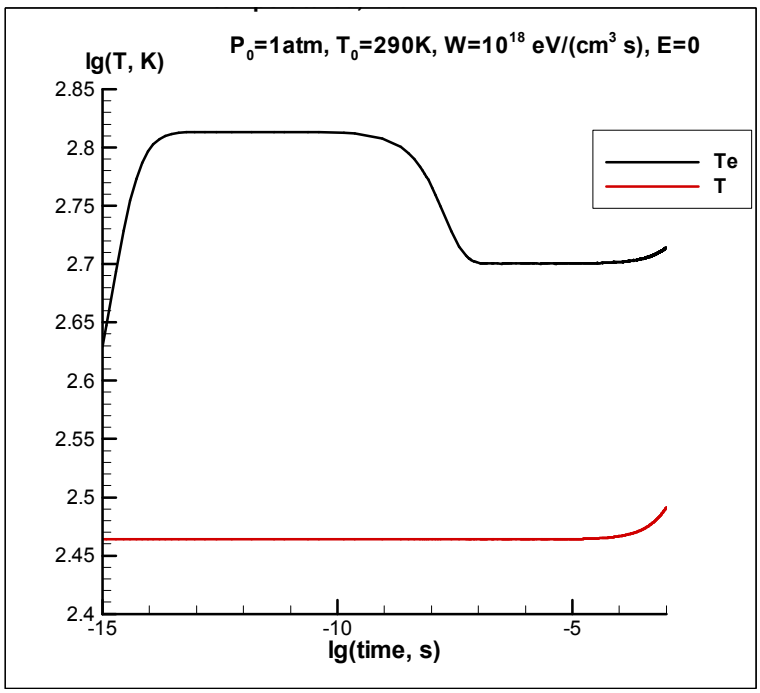

Fig.3.1.8. Electron and gas temperatures in beam plasmas at pressure P=1 atm, at air excitation velocity W= 10^{18}eV/(cm^{3}s). E/N=0 Td.

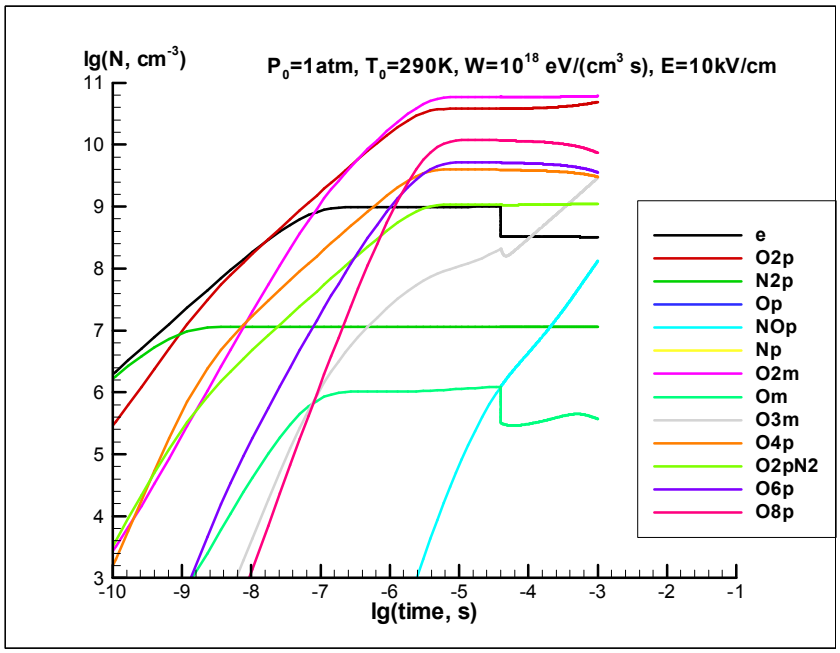

Fig.3.1.9. Charged particles in beam plasmas at pressure P=1 atm, at air excitation velocity W= 10^{18} eV/(cm^{3}s). E/N=30 Td. Duration of the field is 40μs.

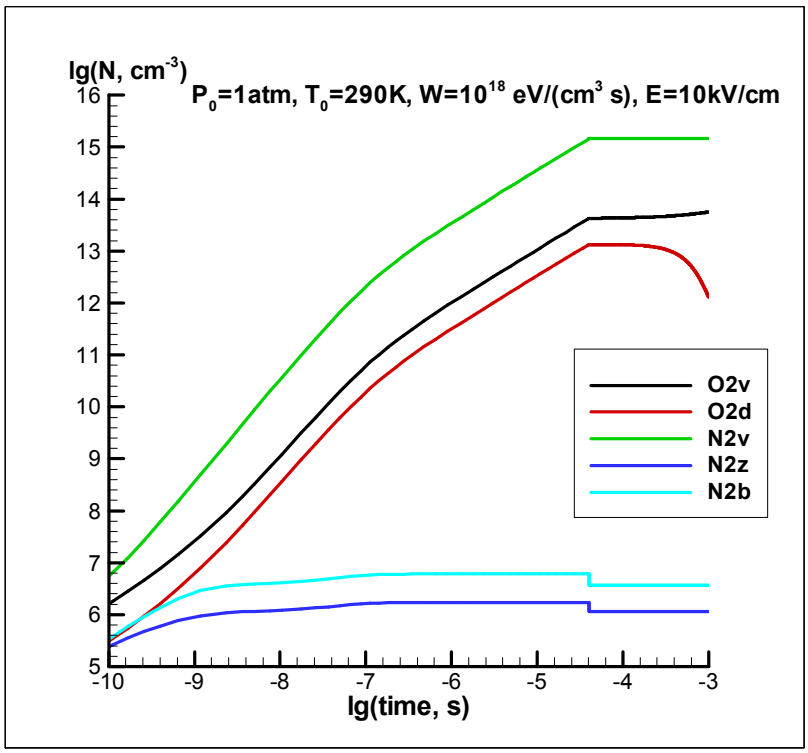

Fig.3.10. Excited particles in beam plasmas at pressure P=1 atm, at air excitation velocity W= 10^{18}eV/(cm^{3}s). E/N=30 Td. Duration of the field is 40μs.

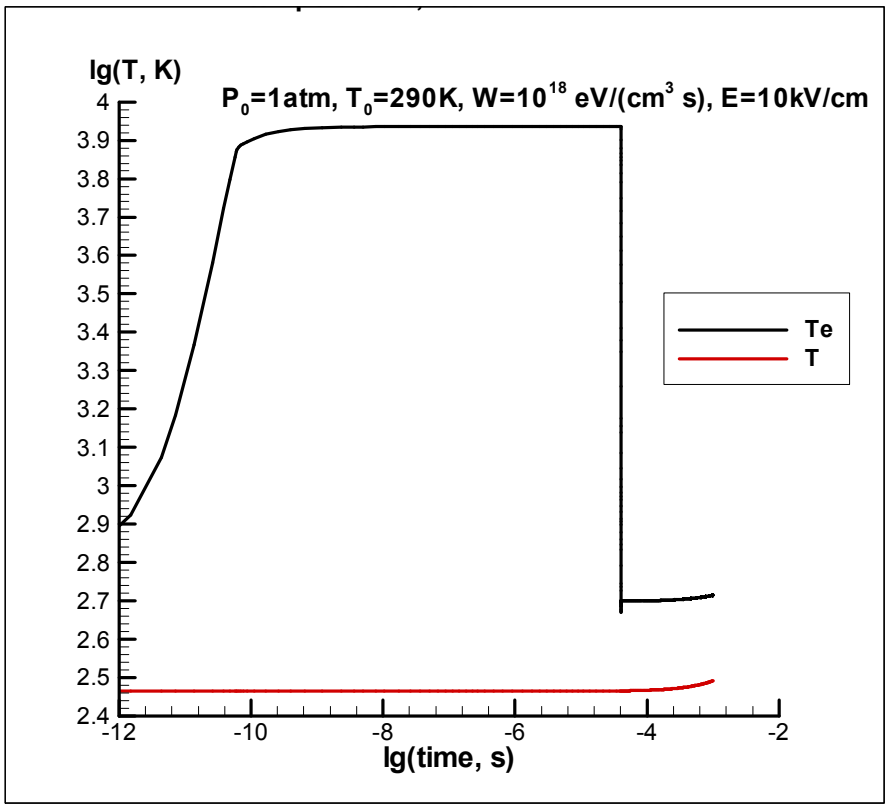

Fig. 3.1.11. Electron and gas temperatures in beam plasmas at pressure P=1 atm, at air excitation velocity W= 10^{18}eV/(cm^{3}s). E/N=30 Td. Field duration is 40μs.

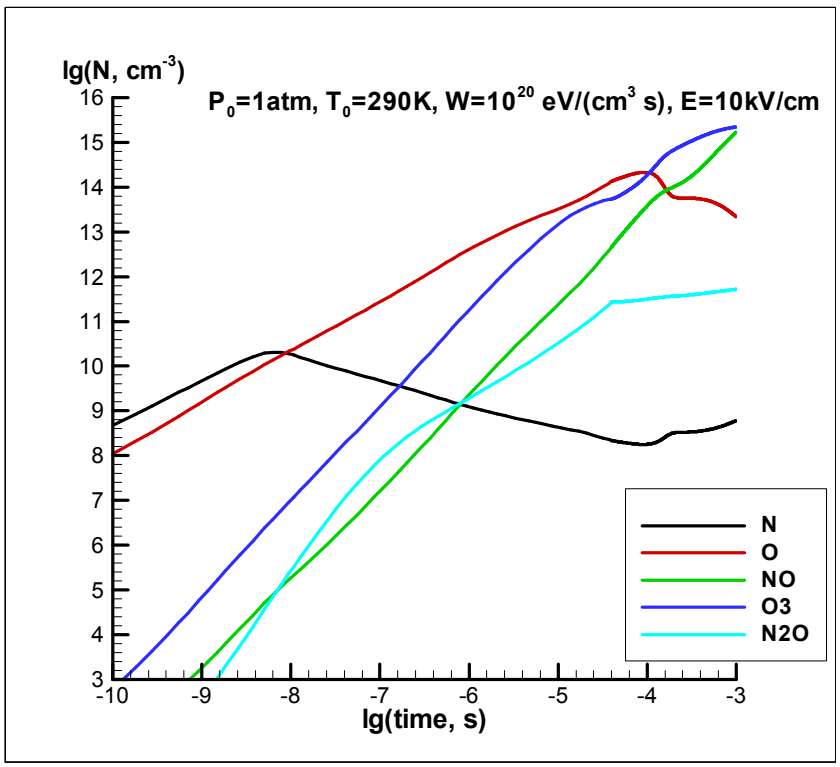

Fig.3.1.12. Neutral particles in beam plasmas at pressure P=1 atm, at air excitation velocity W= 10^{20}eV/(cm^{3}s). E/N=30 Td. Field duration is 40μs.

3.1.5. Chemical reactions in propane-air mixture

Analysis of works devoted to combustion kinetics of propane-air mixture brought us to a choice of relatively simple system of chemical reactions in propane-air mixture [18,19], which satisfactorily describe processes of combustion at atmospheric pressure and temperatures higher than 1500 K. Rate constants of these reactions are represented in the Table.3.1.4 for the short mechanism of C_3H_8 ignition, they will be the first step in joint model of propane-air plasmas.

Table.3.1.4 Rate constants in the form $k = AT^n exp(-E/RT)$**, units mol, cm^3, s, K. kJ/mol**

N	Reactions	A	n	E	
	Hydrogen-Oxygen chain				
1	$H + O_2 \rightarrow OH + O$	$3.52 \cdot 10^{16}$	-0.7	71.4	
	Hydroperoxyl and Hydrogen Peroxide reactions				
2	$H + O_2 + M \rightarrow HO_2 + M$	$2.6 \cdot 10^{19}$	-1.2	0.0	
3	$HO_2 + HO_2 \rightarrow H_2O_2 + O_2$	$3.02 \cdot 10^{12}$	0.0	5.8	
4	$H_2O_2 + M \rightarrow OH + OH + M$	k_0 $7.94 \cdot 10^{24}$	-2.2	212.0	
		k_∞ $2.55 \cdot 10^{20}$	-1.7	219.1	
	Propane reactions				
5	$C_3H_8 \rightarrow CH_3 + C_2H_5$	k_0 $7.83 \cdot 10^{18}$	0.0	271.9	
		k_∞ $1.1 \cdot 10^{17}$	0.0	353.1	
6	$C_3H_8 + H \rightarrow I - C_3H_7 + H_2$	$1.3 \cdot 10^{06}$	2.4	18.7	
7	$C_3H_8 + H \rightarrow N - C_3H_7 + H_2$	$1.88 \cdot 10^{05}$	2.8	26.3	
8	$C_3H_8 + O \rightarrow I - C_3H_7 + OH$	$2.81 \cdot 10^{13}$	0.0	21.8	
9	$C_3H_8 + O \rightarrow N - C_3H_7 + OH$	$1.13 \cdot 10^{14}$	0.0	32.8	
10	$C_3H_8 + OH \rightarrow I - C_3H_7 + H_2O$	$4.67 \cdot 10^{07}$	1.6	-0.1	
11	$C_3H_8 + OH \rightarrow N - C_3H_7 + H_2O$	$1.05 \cdot 10^{10}$	1.0	6.6	
12	$C_3H_8 + HO_2 \rightarrow I - C_3H_7 + H_2O_2$	$5.6 \cdot 10^{12}$	0.0	74.1	
13	$C_3H_8 + HO_2 \rightarrow N - C_3H_7 + H_2O_2$	$1.68 \cdot 10^{13}$	0.0	85.5	
	I-Propyl, N-Propyl and Propene reactions				
14	$I - C_3H_7 \rightarrow C_3H_6 + H$	$8.57 \cdot 10^{18}$	-1.6	168.8	
15	$N - C_3H_7 \rightarrow CH_3 + C_2H_4$	$9.6 \cdot 10^{13}$	0.0	129.8	
16	$N - C_3H_7 \rightarrow C_3H_6 + H$	$1.25 \cdot 10^{14}$	0.0	154.9	
17	$C_3H_6 + O \rightarrow C_2H_4 + CH_2O$	$5.9 \cdot 10^{13}$	0.0	21.0	
18	$C_3H_6 + OH \rightarrow C_2H_5 + CH_2O$	$7.9 \cdot 10^{12}$	0.0	0.0	
	Ethylene, Ethyl, Vinyl, Vinoxy and Ketene reactions				
19	$C_2H_4 + OH \rightarrow C_2H_3 + H_2O$	$5.53 \cdot 10^{05}$	2.3	12.4	
20	$C_2H_4 + O \rightarrow CH_2CHO + H$	$1.21 \cdot 10^{06}$	2.1	0.0	
21	$C_2H_5 + O \rightarrow CH_3 + CH_2O$	$4.24 \cdot 10^{13}$	0.0	0.0	
22	$C_2H_5 + \rightarrow C_2H_4 + H$	k_0 $3.99 \cdot 10^{33}$	-5.0	167.4	
		k_∞ $1.11 \cdot 10^{10}$	1.0	153.8	
23	$C_2H_3 + O_2 \rightarrow CH_2CHO + O$	$7.00 \cdot 10^{14}$	-0.6	22.0	

24	$CH_2CHO \rightarrow CH_2CO + H$	$1.05 \cdot 10^{37}$	-7.2	185.5	
25	$CH_2CO + H \rightarrow CH_3 + CO$	$1.11 \cdot 10^{07}$	2.0	8.4	

	Methyl, Methoxy, Formaldehyde, Formyl reactions				
26	$CH_3 + O \rightarrow CH_2O + H$	$8.43 \cdot 10^{13}$	0.0	0.0	
27	$CH_3 + HO_2 \rightarrow CH_3O + OH$	$2.0 \cdot 10^{13}$	0.0	0.0	
28	$CH_3 + O_2 \rightarrow CH_2O + OH$	$3.3 \cdot 10^{11}$	0.0	37.4	
29	$CH_3 + CH_3 \rightarrow C_2H_6$	k_0 $1.27 \cdot 10^{41}$	-7.0	11.6	
		k_∞ $1.81 \cdot 10^{13}$	0.0	0.0	
30	$CH_3O + O_2 \rightarrow CH_2O + HO_2$	$4.28 \cdot 10^{13}$	7.6	-14.8	
31	$CH_3O + M \rightarrow CH_2O + H + M$	$1.00 \cdot 10^{13}$	0.0	56.5	
32	$CH_2O + OH \rightarrow CHO + H_2O$	$3.9 \cdot 10^{10}$	0.9	1.7	
33	$CHO + M \rightarrow CO + H + M$	$1.86 \cdot 10^{17}$	-1.0	71.1	
34	$CHO + O_2 \rightarrow CO + HO_2$	$3.0 \cdot 10^{12}$	0.0	0.0	

In the total system of equations we also include an equation for the gas temperature as in [11] in which we use standard enthalpies for analysis of gas heating.

3.1. 5. Plasma-chemical reactions in propane-air mixture

Analysis of literature has shown that it is necessary account electron-molecule, electron-ion and ion-ion processes and also the products of fast electrons impact on propane molecules. In spite of the fact that the mass propane proportion in air is 1/16 but presence of the plasma particles can change concentrations of active radicals and velocities of main processes.

So during the Project we have collected, verified, estimated and interpolated rate constants of plasma particles electrons, positive and negative ions including fast electrons of electron beam interaction with neutral particle of propane-air mixture composition and between themselves. In the Table 3.1.5 one can see costs of main reactions with participants of fast electrons taken from [20]. There is no new information on the fast electron impact on propane C_3H_8 molecules. The table data shows appearance of large number of fragments.

Table 3.1.5. Destruction and ionization of C_3H_8 molecule by fast electrons

N	Reaction	Cost
1	$e' + C_3H_8 \rightarrow C_2H_4^+ + CH_4 + e + e'$	294 eV
2	$e' + C_3H_8 \rightarrow C_2H_5^+ + CH_3 + e + e'$	77 eV
3	$e' + C_3H_8 \rightarrow C_3H_5^+ + H_2 + H + e + e'$	357 eV
4	$e' + C_3H_8 \rightarrow C_2H_3^+ + CH_3 + H_2 + e + e'$	357 eV
5	$e' + C_3H_8 \rightarrow C_3H_6 + H_2 + e'$	167 eV
6	$e' + C_3H_8 \rightarrow C_2H_4 + CH_4 + e'$	625 eV
7	$e' + C_3H_8 \rightarrow C_2H_4 + CH_3 + H + e'$	222 eV

We paid special attention to reactions with participation of ions since in these reactions take place simplification of hydrocarbon molecules composition and these reactions can lead to improvement of combustion properties of flammable mixtures. Besides, namely these reactions make specific plasma chemical impact on molecules in the ionized gas [21]. So undertaking of calculations with these reactions

will allow to select namely plasma impact of the fuel activation. All reactions for which there was not experimental information have been estimated and interpolated on a basis of works [22-26]. Channels of reactions with participation of positive ions were chosen on a basis of reference [27]. Rate constants of reactions with positive ions have been chosen of the basis of works [28, 29, 31] at their temperature interpolation according to works [23,24]. Rate constants of dissociative recombination have been chosen on a basis of works [29, 31] at their temperature interpolation according to works [23,24]. Rate constants with participation of negative ions have been chosen on a basis of works [24,25,30].

We included into our model channels of N_2^+ ion reactions with C_3H_8 , CH_4 , C_2H_4 , C_2H_6 ; and O_2^+ reactions with neutrals CH_6, C_2H_2, C_2H_4, C_2H_6, C_3H_8 ; channels of reactions of C^+ ion with O_2, H_2O, CH_4, NO, N_2O; channels of reactions of CH^+ with H , H_2, CH_4, O, H_2O, O_2, CO, NO; and channels of reactions of CH_2^+ with H_2, CH_4, H_2O, O_2, CO_2, NO; reactions of CH_3^+ with CH_4, O, H_2O, O_2, NO; and CH_4^+ with H_2, H_2O, O_2, CO, CO_2, N_2O; reactions of CH_5^+ with H, O, H_2O, CO, CO_2, N_2O; reactions of $C_2H_2^+$ with H_2, CH_4, O, H_2O; reactions of $C_2H_3^+$ with H, H_2O , CH_4; reactions of $C_2H_4^+$ with H; reactions of $C_2H_5^+$ with H H_2O , CH_4; reactions of $C_2H_6^+$ with H, H_2O; reactions of HCO^+ with H_2O ; reactions of H_2CO^+ with H_2O, O_2; reactions of HCO_2^+ with H_2O , CH_4, NO; reactions of HNO^+ with H_2O , CH_4, N_2, CO_2, CO, NO; HN_2O^+ with H_2O, CH_4, CO; reactions of O^- with C_3H_8n, CH_4.

We included electron-ion reactions of dissociative recombination [23,29.31], because it directly leads to dissociation of participating molecule ion : $e + MN^+ \rightarrow M + N^*$ (e –electron, MN^+-molecular ion, N^* -excited particle).

Channels ion-ion recombination were also considered in details, because they determine time of negative ions existence [23, 26]: three- body O^- ion-ion recombination; channels of two body O^- ion-ion recombination; channels of three body O_2^- ion-ion recombination ; channels of two-body O_2^- ion-ion recombination; channels of three body H^- ion-ion recombination; channels of two-body H^- ion-ion recombination; channels of three body OH^- ion-ion recombination; and channels of two body OH^- ion-ion recombination .

Table 3.1.6. Channels of N_2^+ with C_3H_8 , CH_4 , C_2H_4 , C_2H_6 , and O_2^+ reactions with neutrals CH_6, C_2H_2, C_2H_4, C_2H_6, C_3H_8 .

N	Reaction	Rate constant	Source
1	$N_2^+ + C_3H_8 \rightarrow C_2H_4^+ + CH_4 + N_2$	10^{-11} cm^3/s	Estimate
2	$N_2^+ + C_3H_8 \rightarrow C_2H_3^+ + CH_3 + H_2 + N_2$	$3.5 \cdot 10^{-11}$	Estimate
3	$N_2^+ + C_3H_8 \rightarrow C_2H_2^+ + CH_4 + H_2 + N_2$	$0.35 \cdot 10^{-11}$ cm^3/s	Estimate
4	$N_2^+ + CH_4 \rightarrow CH_4^+ + N_2$	$2.0 \cdot 10^{-10}$ cm^3/s	Estimate
5	$N_2^+ + CH_4 \rightarrow CH_3^+ + H + N_2$	$1.0 \cdot 10^{-9}$ cm^3/s	Estimate
6	$N_2^+ + CH_4 \rightarrow CH_2^+ + H_2 + N_2$	$1.5 \cdot 10^{-10}$ cm^3/s	Estimate
7	$N_2^+ + C_2H_4 \rightarrow C_2H_3^+ + H + N_2$	$0.7 \cdot 10^{-10}$ cm^3/s	Estimate
8	$N_2^+ + C_2H_4 \rightarrow C_2H_2^+ + H_2 + N_2$	$0.3 \cdot 0^{-10}$ cm^3/s	Estimate
9	$N_2^+ + C_2H_6 \rightarrow C_2H_6^+ + N_2$	$3.0 \cdot 10^{-11}$ cm^3/s	Estimate
10	$N_2^+ + C_2H_6 \rightarrow C_2H_5^+ + H + N_2$	$1.0 \cdot 0^{-10}$ cm^3/s	Estimate
11	$N_2^+ + C_2H_6 \rightarrow C_2H_4^+ + H_2 + N_2$	$3.0 \cdot 10^{-10}$ cm^3/s	Estimate
12	$N_2^+ + C_2H_6 \rightarrow C_2H_3^+ + H_2 + H + N_2$	$3.0 \cdot 10^{-10}$ cm^3/s	Estimate

13	$N_2^+ + C_2H_6 \rightarrow C_2H_2^+ + H_2 + H_2 + N_2$	1.5 ·0^{-10} cm^3/s	Estimate
14	$N_2^+ + C_2H_6 \rightarrow CH_3^+ + CH_3 + N_2$	6.0 ·10^{-11} cm^3/s	Estimate
15	$N_2^+ + C_3H_8 \rightarrow C_2H_2^+ + CH_4 + H_2 + N_2$	10^{-9} cm^3/s	Estimate
16	$O_2^+ + CH_6 \rightarrow CH_3^+O_2 + H$	10^{-9} cm^3/s	Estimate
17	$O_2^+ + C_2H_2 \rightarrow C_2H_2^+ + O_2$	4 10^{-9} cm^3/s	Estimate
18	$O_2^+ + C_2H_4 \rightarrow C_2H_4^+ + O_2$	5 10^{-9} cm^3/s	Estimate
19	$O_2^+ + C_2H_6 \rightarrow C_2H_6^+ + O_2$	10^{-9} cm^3/s	Estimate
20	$O_2^+ + C_2H_6 \rightarrow C_2H_5^+ + H + O_2$	10^{-9} cm^3/s	Estimate
21	$O_2^+ + C_2H_6 \rightarrow C_2H_4^+ + H_2 + O_2$	10^{-9} cm^3/s	Estimate
22	$O_2^+ + C_2H_6 \rightarrow C_2H_3^+ + H_2 + H + O_2$	10^{-9} cm^3/s	Estimate
23	$O_2^+ + C_2H_6 \rightarrow C_2H_2^+ + 2 \cdot H_2 + O_2$	10^{-9} cm^3/s	Estimate
24	$O_2^+ + C_2H_6 \rightarrow C_2H^+ + 2 \cdot H_2 + H + O_2$	10^{-9} cm^3/s	Estimate
25	$O_2^+ + C_2H_6 \rightarrow CH_3^+ + CH_3 + O_2$	10^{-9} cm^3/s	Estimate
26	$O_2^+ + C_2H_6 \rightarrow CH_2^+ + CH_3 + H + O_2$	10^{-9} cm^3/s	Estimate
27	$O_2^+ + C_2H_6 \rightarrow CH^+ + CH_3 + H_2 + O_2$	10^{-9} cm^3/s	Estimate
28	$O_2^+ + C_3H_8 \rightarrow C_3H_8^+ + O_2$	2.8 10^{-10} cm^3/s	Estimate
29	$O_2^+ + C_3H_8 \rightarrow C_3H_7^+ + H + O_2$	1.6 10^{-10} cm^3/s	Estimate
30	$O_2^+ + C_3H_8 \rightarrow C_3H_6^+ + H_2 + O_2$	1.7 10^{-11} cm^3/s	Estimate
31	$O_2^+ + C_3H_8 \rightarrow C_3H_5^+ + H_2 + H + O_2$	3.0 10^{-11} cm^3/s	Estimate
32	$O_2^+ + C_3H_8 \rightarrow C_2H_6^+ + CH_2 + O_2$	7.0 10^{-12} cm^3/s	Estimate
33	$O_2^+ + C_3H_8 \rightarrow C_2H_4^+ + CH_3 + H + O_2$	2.3 10^{-10} cm^3/s	Estimate
34	$O_2^+ + C_3H_8 \rightarrow C_2H_3^+ + CH_3 + H_2 + O_2$	6.0 10^{-11} cm^3/s	Estimate
35	$O_2^+ + C_3H_8 \rightarrow C_2H_2^+ + CH_3 + H_2 + O_2 + H$	6.0 10^{-12} cm^3/s	estimate
36	$O_2^+ + C_3H_8 \rightarrow C_2H_2^+ + CH_3 + H_2 + O_2 + H$	3.0 10^{-12} cm^3/s	Estimate
37	$O_2^+ + C_3H_8 \rightarrow CH_2^+ + C_2H_5 + H + O_2$	2.0 10^{-12} cm^3/s	Estimate

Table 3.1.7. Channels of reactions of C^+ with O_2, H_2O, CH_4, NO, N_2O

N	Reaction	Rate constant	**Source**
1	$C^+ + O_2 \rightarrow O^+ + CO$	5.2 10^{-10} cm^3/s	Anicich
2	$C^+ + O_2 \rightarrow CO^+ + O$	3.5 10^{-10} cm^3/s	Anicich
3	$C^+ + H_2O \rightarrow H_2O^+ + C$	2.4 10^{-10} cm^3/s	Anicich

4	$C^+ + H_2O \rightarrow HOC^+ + O$	2.2 10^{-9} cm^3/s	Anicich
5	$C^+ + CH_4 \rightarrow C_2H_2^+ + H_2$	3.6 10^{-10} cm^3/s	Anicich
6	$C^+ + CH_4 \rightarrow C_2H_3^+ + H$	9.4 10^{-10} cm^3/s	Anicich
7	$C^+ + NO \rightarrow N^+ + CO$	6 10^{-11} cm^3/s	Anicich
8	$C^+ + NO \rightarrow NO^+ + C$	7.5 10^{-10} cm^3/s	Anicich
9	$C^+ + N_2O \rightarrow NO^+ + CN$	9.1 10^{-10} cm^3/s	Anicich

Table 3.1.8. CH^+ **with** H , H_2 , CH_4 **, O,** H_2O **,** O_2**, CO, NO, and** CH_2^+ **with** CO_2

N	Reaction	Rate constant	Source
1	$CH^+ + H \rightarrow C^+ + H_2$	7.5 10^{-10} cm^3/s	Anicich
2	$CH^+ + H_2 \rightarrow CH_2^+ + H$	1.2 10^{-9} cm^3/s	Anicich
3	$CH^+ + CH_4 \rightarrow C_2H_2^+ + H_2 + H$	1.4 10^{-10} cm^3/s	Anicich
4	$CH^+ + CH_4 \rightarrow C_2H_3^+ + H_2$	1.1 10^{-9} cm^3/s	Anicich
5	$CH^+ + CH_4 \rightarrow C_2H_4^+ + H$	6.5 10^{-11} cm^3/s	Anicich
6	$CH^+ + O \rightarrow H^+ + CO$	3.5 10^{-10} cm^3/s	Anicich
7	$CH^+ + O \rightarrow CO^+ + H$	3.5 10^{-10} cm^3/s	Anicich
8	$CH^+ + H_2O \rightarrow H_3O^+ + C$	10^{-9} cm^3/s	Anicich
9	$CH^+ + H_2O \rightarrow HCO^+ + H_2$	10^{-9} cm^3/s	Anicich
10	$CH^+ + H_2O \rightarrow H_2CO^+ + H$	10^{-9} cm^3/s	Anicich
11	$CH^+ + O_2 \rightarrow HCO^+ + O$	3.2 10^{-10} cm^3/s	Anicich
12	$CH^+ + O_2 \rightarrow CO^+ + OH$	3.2 10^{-10} cm^3/s	Anicich
13	$CH^+ + O_2 \rightarrow O^+ + HCO$	3.2 10^{-10} cm^3/s	Anicich
14	$CH^+ + CO \rightarrow HCO^+ + C$	7.0 10^{-12} cm^3/s	Anicich
15	$CH^+ + CO_2 \rightarrow HCO^+ + CO$	1.6 10^{-9} cm^3/s	Anicich
16	$CH^+ + NO \rightarrow NO^+ + CH$	7.6 10^{-10} cm^3/s	Anicich
17	$CH_2^+ + CO_2 \rightarrow H_2CO^+ + CO$	1.6 10^{-9} cm^3/s	Anicich

Table 3.1.9. CH_2^+ **with** H_2 **,** CH_4 **,** H_2O **,** O_2**,** CO_2**, NO**

N	Reaction	Rate constant	Source
1	$CH_2^+ + H_2 \rightarrow CH_3^+ + H$	1.2 10^{-9} cm^3/s	Estimate
2	$CH_2^+ + CH_4 \rightarrow C_2H_5^+ + H$	4.0 10^{-10} cm^3/s	Anicich
3	$CH_2^+ + CH_4 \rightarrow C_2H_4^+ + H_2$	9.0 10^{-10} cm^3/s	Anicich
4	$CH_2^+ + H_2O \rightarrow CH_3O^+ + H$	2.0 10^{-9} cm^3/s	Anicich
5	$CH_2^+ + O_2 \rightarrow HCO^+ + OH$	6.0 10^{-10} cm^3/s	Anicich
6	$CH_2^+ + O_2 \rightarrow H_2CO^+ + O$	3.0 10^{-10} cm^3/s	Anicich
7	$CH_2^+ + CO_2 \rightarrow H_2CO^+ + CO$	1.6 10^{-9} cm^3/s	Anicich

8	$CH_2^+ + NO \rightarrow NO^+ + CH_2$	4.2 10^{-10} cm^3/s	Anicich

Table 3.1.10. Reactions of CH_3^+ with CH_4, O, H_2O, O_2, NO and CH_4^+ with H_2, H_2O, O_2, CO, CO_2, N_2O

N	Reaction	Rate constant	Source
1	$CH_3^+ + CH_4 \rightarrow C_2H_5^+ + H_2$	1.1 10^{-9} cm^3/s	Anicich
2	$CH_3^+ + O \rightarrow H_3^+ + CO$	4.4 10^{-10} cm^3/s	Anicich
3	$CH_3^+ + O \rightarrow H_2CO^+ + H$	10^{-10} cm^3/s	Anicich
4	$CH_3^+ + O \rightarrow HCO^+ + H_2$	10^{-10} cm^3/s	Anicich
5	$CH_3^+ + O_2 \rightarrow HCO^+ + H_2O$	4.3 10^{-11} cm^3/s	Anicich
6	$CH_3^+ + NO \rightarrow NO^+ + CH_3$	9.7 10^{-10} cm^3/s	Anicich
7	$CH_4^+ + H_2 \rightarrow CH_5^+ + H$	3.5 10^{-11} cm^3/s	Anicich
8	$CH_4^+ + H_2O \rightarrow H_3O^+ + CH_3$	2.5 10^{-9} cm^3/s	Anicich
9	$CH_4^+ + O_2 \rightarrow O_2^+ + CH_4$	3.9 10^{-10} cm^3/s	Anicich
10	$CH_4^+ + CO \rightarrow HCO^+ + CH_3$	10^{-9} cm^3/s	Anicich
11	$CH_4^+ + CO_2 \rightarrow HCO_2^+ + CH_3$	10^{-9} cm^3/s	Anicich
12	$CH_4^+ + N_2O \rightarrow HN_2O^+ + CH_3$	1.3 10^{-9} cm^3/s	Anicich

Table 3.1.11. Reactions of CH_5^+ with *H*, O, H_2O, CO, CO_2, N_2O

N	Reaction	Rate constant	Source
1	$CH_5^+ + H \rightarrow CH_4^+ + H_2$	1.5 10^{-10} cm^3/s	Anicich
2	$CH_5^+ + O \rightarrow H_3O^+ + CH_2$	2.4 10^{-10} cm^3/s	Anicich
3	$CH_5^+ + H_2O \rightarrow H_3O^+ + CH_4$	3.7 10^{-9} cm^3/s	Anicich
4	$CH_5^+ + CO \rightarrow HCO^+ + CH_4$	10^{-9} cm^3/s	Anicich
5	$CH_5^+ + CO_2 \rightarrow HCO_2^+ + CH_4$	3.2 10^{-11} cm^3/s	Anicich
6	$CH_5^+ + N_2O \rightarrow HN_2O^+ + CH_4$	10^{-9} cm^3/s	Anicich

Table 3.1.12. Reactions of $C_2H_2^+$ with H_2, CH_4, O, H_2O.

N	Reaction	Rate constant	Source
1	$C_2H_2^+ + H_2 \rightarrow C_2H_3^+ + H$	1.0 10^{-11} cm^3/s	Anicich
2	$C_2H_2^+ + CH_4 \rightarrow C_3H_4^+ + H_2$	1.9 10^{-10} cm^3/s	Anicich
3	$C_2H_2^+ + CH_4 \rightarrow C_3H_5^+ + H$	7.0 10^{-10} cm^3/s	Anicich
4	$C_2H_2^+ + O \rightarrow HCO^+ + CH$	8.0 10^{-11} cm^3/s	Anicich
5	$C_2H_2^+ + O \rightarrow HC_2O^+ + H$	8.0 10^{-11} cm^3/s	Anicich
6	$C_2H_2^+ + H_2O \rightarrow H_3O^+ + C_2H$	2.2 10^{-10} cm^3/s	Anicich

Table 3.1.13. Reactions of $C_2H_3^+$ with H, H_2O , CH_4 ; $C_2H_4^+$ with H; $C_2H_5^+$ with H H_2O , CH_4 ; $C_2H_6^+$ with H, H_2O ; HCO^+ with H_2O ; H_2CO^+ with H_2O, O_2; HCO_2^+ with H_2O , CH_4 , NO

N	Reaction	Rate constant	Source
1	$C_2H_3^+ + H \rightarrow C_2H_2^+ + H_2$	1.0 10^{-10} cm^3/s	Anicich
2	$C_2H_3^+ + CH_4 \rightarrow C_3H_5^+ + H_2$	1.9 10^{-10} cm^3/s	Anicich
3	$C_2H_3^+ + H_2O \rightarrow H_3O^+ + C_2H_2$	1.1 10^{-9} cm^3/s	Anicich
4	$C_2H_4^+ + H \rightarrow C_2H_3^+ + H_2$	3.0 10^{-10} cm^3/s	Anicich
5	$C_2H_5^+ + H \rightarrow C_2H_4^+ + H_2$	1.0 10^{-11} cm^3/s	Anicich
6	$C_2H_5^+ + CH_4 \rightarrow C_3H_7^+ + H_2$	9.0 10^{-14} cm^3/s	Anicich
7	$C_2H_5^+ + H_2O \rightarrow H_3O^+ + C_2H_4$	1.9 10^{-9} cm^3/s	Anicich
8	$C_2H_6^+ + H \rightarrow C_2H_5^+ + H_2$	1.0 10^{-10} cm^3/s	Anicich
9	$C_2H_6^+ + H_2O \rightarrow H_3O^+ + C_2H_5$	3.0 10^{-9} cm^3/s	Anicich
10	$HCO^+ + H_2O \rightarrow H_3O^+ + CO$	2.6 10^{-9} cm^3/s	Anicich
11	$H_2CO^+ + H_2O \rightarrow H_3O^+ + HCO$	2.1 10^{-9} cm^3/s	Anicich
12	$H_2CO^+ + O_2 \rightarrow H_2O_2^+ + CO$	3.3 10^{-11} cm^3/s	Anicich
13	$H_2CO^+ + O_2 \rightarrow HCO^+ + HO_2$	7.7 10^{-11} cm^3/s	Anicich
14	$HCO_2^+ + CH_4 \rightarrow CH_5^+ + HO_2$	7.2 10^{-10} cm^3/s	Anicich
15	$HCO_2^+ + H_2O \rightarrow H_3O^+ + CO_2$	2.7 10^{-9} cm^3/s	Anicich
16	$HCO_2^+ + NO \rightarrow HNO^+ + CO_2$	5.0 10^{-11} cm^3/s	Anicich

Table 3.1.14. Reactions of HNO^+ with H_2O , CH_4 , N_2, CO_2, CO, NO; HN_2O^+ with H_2O, CH_4 , CO

N	Reaction	Rate constant	Source
1	$HNO^+ + CH_4 \rightarrow CH_5^+ + NO$	1.9 10^{-10} cm^3/s	Anicich
2	$HNO^+ + H_2O \rightarrow H_3O^+ + NO$	2.3 10^{-9} cm^3/s	Anicich
3	$HNO^+ + N_2 \rightarrow N_2H^+ + NO$	5.0 10^{-11} cm^3/s	Anicich
4	$HNO^+ + CO \rightarrow HCO^+ + NO$	1.9 10^{-10} cm^3/s	Anicich
5	$HNO^+ + CO_2 \rightarrow HCO_2^+ + NO$	1.9 10^{-10} cm^3/s	Anicich
6	$HNO^+ + NO \rightarrow NO^+ + HNO$	7.0 10^{-10} cm^3/s	Anicich
7	$HN_2O^+ + H_2O \rightarrow H_3O^+ + N_2O$	2.8 10^{-9} cm^3/s	Anicich
8	$HN_2O^+ + CO \rightarrow HCO^+ + N_2O$	5.3 10^{-10} cm^3/s	Anicich
9	$HN_2O^+ + CH_4 \rightarrow CH_5^+ + N_2O$	10^{-11} cm^3/s	Anicich

Table 3.1.15. Reactions of O^- with C_3H_8n, CH_4 .

N	Reaction	Rate constant	Source
1	$O^- + C_3H_8n \rightarrow OH^- + C_3H_7$	6.0 10^{-10} cm^3/s	Arnold

2	$O^- + C_3H_8n \rightarrow H_2O + C_3H_6 + e$	4.0 10^{-10} cm^3/s	Arnold
3	$O^- + CH_4 \rightarrow OH^- + CH_3$	8.0 10^{-11} cm^3/s	Arnold

Table 3.1.16. Electron-ion reactions of dissociative recombination.

N	Reaction	Rate constant	Source
1	$e + C_3H_8^+ \rightarrow CH_3 + C_2H_5$	5.6 10^{-6} (300/T) $(300/T_e)^{0.5}$ cm^3/s	Mitchel
2	$e + C_3H_7^+ \rightarrow CH_3 + C_2H_4$	10^{-6} (300/T) $(300/T_e)^{0.5}$ cm^3/s	estimate
3	$e + C_3H_6^+ \rightarrow CH_3 + C_2H_3$	10^{-6} (300/T) $(300/T_e)^{0.5}$ cm^3/s	estimate
4	$e + C_3H_5^+ \rightarrow CH_3 + C_2H_2$	3.5 10^{-7} (300/T) $(300/T_e)^{0.5}$ cm	Mitchel
5	$e + C_3H_4^+ \rightarrow CH_3 + C_2H$	10^{-6} (300/T) $(300/T_e)^{0.5}$ cm^3/s	estimate
6	$e + C_3H_3^+ \rightarrow CH + C_2H_2$	1.0 10^{-7} (300/T) $(300/T_e)^{0.5}$ cm^3/s	Mitchel
7	$e + C_2H_6^+ \rightarrow C\ H_3 + CH$	10^{-6} (300/T) $(300/T_e)^{0.5}$ cm^3/s	Estimate
8	$e + C_2H_5^+ \rightarrow C\ H_3 + CH_2$	7.4 10^{-7} (300/T) $(300/T_e)^{0.5}$ cm^3/s	Mitchel
9	$e + C_2H_4^+ \rightarrow C\ H_3 + CH$	10^{-6} (300/T) $(300/T_e)^{0.5}$ cm^3/s	Estimate
10	$e + C_2H_3^+ \rightarrow C\ H_2 + CH$	10^{-6} (300/T) $(300/T_e)^{0.5}$ cm^3/s	Estimate
11	$e + C_2H_2^+ \rightarrow C\ H + CH$	2.7 10^{-7} $(300/T)^{0.5}$ $(300/T_e)^{0.5}$ cm^3/s	Mitchel
12	$e + CH_5^+ \rightarrow H + CH_4$	7 10^{-7} (300/T) $(300/T_e)^{0.5}$ cm^3/s	Mitchel
13	$e + CH_4^+ \rightarrow H + CH_3$	3.5 10^{-7} $(300/T)^{0.42}$ $(300/T_e)^{0.5}$ cm^3/s	Mitchel
14	$e + CH_3^+ \rightarrow H + CH_2$	3.5 10^{-7} $(300/T)^{0.42}$ $(300/T_e)^{0.5}$ cm^3/s	Mitchel
15	$e + CH_2^+ \rightarrow H + CH$	2.5 10^{-7} $(300/T)^{0.42}$ $(300/T_e)^{0.5}$ cm^3/s	Mitchel
16	$e + CH^+ \rightarrow H + C$	1.5 10^{-7} $(300/T)^{0.42}$ $(300/T_e)^{0.5}$ cm^3/s	Mitchel
17	$e + CH_3O_2^+ \rightarrow CH_3 + O_2$	10^{-6} (300/T) $(300/T_e)^{0.5}$ cm^3/s	Estimate
18	$e + HCO^+ \rightarrow CH + O$	2.4 10^{-7} $(300/T)^{0.69}$ $(300/T_e)^{0.5}$ cm^3/s	Mitchel
19	$e + H_2CO^+ \rightarrow CH + OH$	2.4 10^{-7} (300/T) $(300/T_e)^{0.5}$ cm^3/s	Estimate
20	$e + HC_2O^+ \rightarrow CH + CO$	2.4 10^{-7} (300/T) $(300/T_e)^{0.5}$ cm^3/s	Estimate
21	$e + HCO_2^+ \rightarrow CH + O_2$	2.4 10^{-7} $(300/T)^{0.69}$ $(300/T_e)^{0.5}$ cm^3/s	Estimate

22	$e + NO^+ \rightarrow N + O$	4.3 10^{-7} $(300/T)^{0.37}$ $(300/T_e)^{0.5}$ cm^3/s	Mitchel
23	$e + HNO^+ \rightarrow H + NO$	4.2 10^{-7} $(300/T)$ $(300/T_e)^{0.5}$ cm^3/s	Mitchel
24	$e + HN_2O^+ \rightarrow H + N_2O$	4.2 10^{-7} $(300/T)$ $(300/T_e)^{0.5}$ cm^3/s	Mitchel

Table 3.1.17. Additional reactions with neutrals

N	Reaction	Rate constant	Source
1	$O + CH \rightarrow CO + H$	6.6 10^{-11} cm^3/s	baulch
2	$O + CH_2 \rightarrow CO + H + H$	$2.0 \cdot 10^{-11}$ exp (-850/T)	baulch
3	$O + CH_2 \rightarrow CO + H_2$	$1.2 \cdot 10^{-11}$ exp (-850/T)	baulch
4	$O + C_2H \rightarrow CO + CH$	$9.9 \cdot 10^{-11}$	baulch
5	$H + CH \rightarrow C + H_2$	$2.0 \cdot 10^{-10}$	baulch
6	$H + CH_2 \rightarrow CH + H_2$	$2.0 \cdot 10^{-10}$	baulch
7	$C + N_2 \rightarrow CN + N$	$8.72 \cdot 10^{-11}$ exp (-22600/T)	baulch
8	$C + O_2 \rightarrow CO + O$	$1.1 \cdot 10^{-10}$ exp (-320/T)	baulch

Table 3.1.18. Channels of three body O^- ion-ion recombination

N	reaction	Rate constant, cm^3/s, cm^6/s
		Flannery, Kossyi
1	$O^- + C^+ + M \rightarrow CO + M$	$2.0 \cdot 10^{-25}(300/T)^{2.5}$
2	$O^- + CH^+ + M \rightarrow CH + O + M$	$2.0 \cdot 10^{-25}(300/T)^{2.5}$
3	$O^- + HCO^+ + M \rightarrow CHO + O + M$	$2.0 \cdot 10^{-25}(300/T)^{2.5}$
4	$O^- + H_2CO^+ + M \rightarrow H_2 + CO + O + M$	$2.0 \cdot 10^{-25}(300/T)^{2.5}$
5	$O^- + H_2CO^+ + M \rightarrow H_2 + CO + O + M$	$2.0 \cdot 10^{-25}(300/T)^{2.5}$
6	$O^- + HCO_2^+ + M \rightarrow H + CO_2 + O + M$	$2.0 \cdot 10^{-25}(300/T)^{2.5}$
7	$O^- + HC_2O^+ + M \rightarrow CH + CO + O + M$	$2.0 \cdot 10^{-25}(300/T)^{2.5}$
8	$O^- + HNO^+ + M \rightarrow OH + NO + M$	$2.0 \cdot 10^{-25}(300/T)^{2.5}$
9	$O^- + HN_2O^+ + M \rightarrow OH + N_2O + M$	$2.0 \cdot 10^{-25}(300/T)^{2.5}$
10	$O^- + H_2CO^+ + M \rightarrow O + H_2 + CO + M$	$2.0 \cdot 10^{-25}(300/T)^{2.5}$

11	$O^- + CH_2^+ + M \rightarrow O + CH_2 + M$	$2.0 \cdot 10^{-25}(300/T)^{2.5}$
12	$O^- + CH_3O_2^+ + M \rightarrow O + CH_3 + O_2$	$2.0 \cdot 10^{-25}(300/T)^{2.5}$
13	$O^- + CH_3^+ + M \rightarrow O + CH_3 + M$	$2.0 \cdot 10^{-25}(300/T)^{2.5}$
14	$O^- + CH_4^+ + M \rightarrow O + CH_4 + M$	$2.0 \cdot 10^{-25}(300/T)^{2.5}$
15	$O^- + CH_5^+ + M \rightarrow O + CH_5 + M$	$2.0 \cdot 10^{-25}(300/T)^{2.5}$
16	$O^- + C_2H_2^+ + M \rightarrow O + C_2H_2 + M$	$2.0 \cdot 10^{-25}(300/T)^{2.5}$
17	$O^- + C_2H_3^+ + M \rightarrow O + C_2H_3 + M$	$2.0 \cdot 10^{-25}(300/T)^{2.5}$
18	$O^- + C_2H_4^+ + M \rightarrow O + C_2H_4 + M$	$2.0 \cdot 10^{-25}(300/T)^{2.5}$
19	$O^- + C_2H_5^+ + M \rightarrow O + C_2H_5 + M$	$2.0 \cdot 10^{-25}(300/T)^{2.5}$
20	$O^- + C_2H_6^+ + M \rightarrow O + CH_3 + CH_3 + M$	$2.0 \cdot 10^{-25}(300/T)^{2.5}$
21	$O^- + C_3H_3^+ + M \rightarrow CO + C_2H_3 + M$	$2.0 \cdot 10^{-25}(300/T)^{2.5}$
22	$O^- + C_3H_4^+ + M \rightarrow CO + C_2H_4 + M$	$2.0 \cdot 10^{-25}(300/T)^{2.5}$
23	$O^- + C_3H_5^+ + M \rightarrow CO + C_2H_5 + M$	$2.0 \cdot 10^{-25}(300/T)^{2.5}$
24	$O^- + C_3H_6^+ + M \rightarrow CO + CH_3 + CH_3 + M$	$2.0 \cdot 10^{-25}(300/T)^{2.5}$
25	$O^- + C_3H_7^+ + M \rightarrow CO + CH_3 + CH_4 + M$	$2.0 \cdot 10^{-25}(300/T)^{2.5}$
26	$O^- + C_3H_8^+ + M \rightarrow O + C_3H_8 + M$	$2.0 \cdot 10^{-25}(300/T)^{2.5}$

Table 3.1.19 Channels of two body O^- ion-ion recombination

N	**reaction**	**Rate constant, cm^3/s, cm^6/s estimate**
1	$O^- + C^+ \rightarrow CO$	$1.0 \cdot 10^{-7}(300/T)^{0.5}$
2	$O^- + CH^+ \rightarrow CH + O$	$1.0 \cdot 10^{-7}(300/T)^{0.5}$
3	$O^- + HCO^+ \rightarrow CHO + O$	$1.0 \cdot 10^{-7}(300/T)^{0.5}$
4	$O^- + H_2CO^+ \rightarrow H_2 + CO + O$	$1.0 \cdot 10^{-7}(300/T)^{0.5}$
5	$O^- + H_2CO^+ \rightarrow H_2 + CO + O$	$1.0 \cdot 10^{-7}(300/T)^{0.5}$
6	$O^- + HCO_2^+ \rightarrow H + CO_2 + O$	$1.0 \cdot 10^{-7}(300/T)^{0.5}$

7	$O^- + HC_2O^+ \rightarrow CH + CO + O$	$1.0 \cdot 10^{-7} (300/T)^{0.5}$
8	$O^- + HNO^+ \rightarrow OH + NO$	$1.0 \cdot 10^{-7} (300/T)^{0.5}$
9	$O^- + HN_2O^+ \rightarrow OH + N_2O$	$1.0 \cdot 10^{-7} (300/T)^{0.5}$
10	$O^- + H_2CO^+ \rightarrow O + H_2 + CO$	$1.0 \cdot 10^{-7} (300/T)^{0.5}$
11	$O^- + CH_2^+ \rightarrow O + CH_2$	$1.0 \cdot 10^{-7} (300/T)^{0.5}$
12	$O^- + CH_3O_2^+ \rightarrow O + CH_3 + O_2$	$1.0 \cdot 10^{-7} (300/T)^{0.5}$
13	$O^- + CH_3^+ \rightarrow O + CH_3$	$1.0 \cdot 10^{-7} (300/T)^{0.5}$
14	$O^- + CH_4^+ \rightarrow O + CH_4$	$1.0 \cdot 10^{-7} (300/T)^{0.5}$
15	$O^- + CH_5^+ \rightarrow O + CH_5$	$1.0 \cdot 10^{-7} (300/T)^{0.5}$
16	$O^- + C_2H_2^+ \rightarrow O + C_2H_2$	$1.0 \cdot 10^{-7} (300/T)^{0.5}$
17	$O^- + C_2H_3^+ \rightarrow O + C_2H_3$	$1.0 \cdot 10^{-7} (300/T)^{0.5}$
18	$O^- + C_2H_4^+ \rightarrow O + C_2H_4$	$1.0 \cdot 10^{-7} (300/T)^{0.5}$
19	$O^- + C_2H_5^+ \rightarrow O + C_2H_5$	$1.0 \cdot 10^{-7} (300/T)^{0.5}$
20	$O^- + C_2H_6^+ \rightarrow O + CH_3 + CH_3$	$1.0 \cdot 10^{-7} (300/T)^{0.5}$
21	$O^- + C_3H_3^+ \rightarrow CO + C_2H_3$	$1.0 \cdot 10^{-7} (300/T)^{0.5}$
22	$O^- + C_3H_4^+ \rightarrow CO + C_2H_4$	$1.0 \cdot 10^{-7} (300/T)^{0.5}$
23	$O^- + C_3H_5^+ \rightarrow CO + C_2H_5$	$1.0 \cdot 10^{-7} (300/T)^{0.5}$
24	$O^- + C_3H_6^+ \rightarrow CO + CH_3 + CH_3$	$1.0 \cdot 10^{-7} (300/T)^{0.5}$
25	$O^- + C_3H_7^+ \rightarrow CO + CH_3 + CH_4$	$1.0 \cdot 10^{-7} (300/T)^{0.5}$
26	$O^- + C_3H_8^+ \rightarrow O + C_3H_8$	$1.0 \cdot 10^{-7} (300/T)^{0.5}$

Table 3.1.20. Channels of three body O_2^- ion-ion recombination

N	**reaction**	**Rate constant, cm^3/s, cm^6/s estimate**
1	$O_2^- + C^+ + M \rightarrow CO_2 + M$	$2.0 \cdot 10^{-25} (300/T)^{2.5}$
2	$O_2^- + CH^+ + M \rightarrow CH + O_2 + M$	$2.0 \cdot 10^{-25} (300/T)^{2.5}$

3	$O_2^- + HCO^+ + M \rightarrow H + CO + O_2 + M$	$2.0 \cdot 10^{-25}(300/T)^{2.5}$
4	$O_2^- + H_2CO^+ + M \rightarrow H_2 + CO + O_2 + M$	$2.0 \cdot 10^{-25}(300/T)^{2.5}$
5	$O_2^- + HCO_2^+ + M \rightarrow H + CO_2 + O_2 + M$	$2.0 \cdot 10^{-25}(300/T)^{2.5}$
6	$O_2^- + HC_2O^+ + M \rightarrow HC + CO + O_2 + M$	$2.0 \cdot 10^{-25}(300/T)^{2.5}$
7	$O_2^- + HNO^+ + M \rightarrow O_2 + HNO + M$	$2.0 \cdot 10^{-25}(300/T)^{2.5}$
8	$O_2^- + HN_2O^+ + M \rightarrow O_2 + H + N_2O + M$	$2.0 \cdot 10^{-25}(300/T)^{2.5}$
9	$O_2^- + H_2CO^+ + M \rightarrow O_2 + H_2 + C_2O + M$	$2.0 \cdot 10^{-25}(300/T)^{2.5}$
10	$O_2^- + CH_2^+ + M \rightarrow O_2 + CH_2 + M$	$2.0 \cdot 10^{-25}(300/T)^{2.5}$
11	$O_2^- + CH_3O_2^+ + M \rightarrow O_2 + CH_3 + O_2 + M$	$2.0 \cdot 10^{-25}(300/T)^{2.5}$
12	$O_2^- + CH_3^+ + M \rightarrow O_2 + CH_3 + M$	$2.0 \cdot 10^{-25}(300/T)^{2.5}$
13	$O_2^- + CH_4^+ + M \rightarrow O_2 + CH_4 + M$	$2.0 \cdot 10^{-25}(300/T)^{2.5}$
14	$O_2^- + CH_5^+ + M \rightarrow O_2 + CH_5 + M$	$2.0 \cdot 10^{-25}(300/T)^{2.5}$
15	$O_2^- + C_2H_2^+ + M \rightarrow O_2 + C_2H_2 + M$	$2.0 \cdot 10^{-25}(300/T)^{2.5}$
16	$O_2^- + C_2H_3^+ + M \rightarrow O_2 + C_2H_3 + M$	$2.0 \cdot 10^{-25}(300/T)^{2.5}$
17	$O_2^- + C_2H_4^+ + M \rightarrow O_2 + C_2H_4 + M$	$2.0 \cdot 10^{-25}(300/T)^{2.5}$
18	$O_2^- + C_2H_5^+ + M \rightarrow O_2 + C_2H_5 + M$	$2.0 \cdot 10^{-25}(300/T)^{2.5}$
19	$O_2^- + C_2H_6^+ + M \rightarrow O_4 + CH_3 + CH_3 + M$	$2.0 \cdot 10^{-25}(300/T)^{2.5}$
20	$O_2^- + C_3H_3^+ + M \rightarrow CO_2 + C_2H_3 + M$	$2.0 \cdot 10^{-25}(300/T)^{2.5}$
21	$O_2^- + C_3H_4^+ + M \rightarrow CO_2 + C_2H_4 + M$	$2.0 \cdot 10^{-25}(300/T)^{2.5}$
22	$O_2^- + C_3H_5^+ + M \rightarrow CO_2 + C_2H_5 + M$	$2.0 \cdot 10^{-25}(300/T)^{2.5}$
23	$O_2^- + C_3H_6^+ + M \rightarrow CO_2 + CH_3 + CH_3 +$	$2.0 \cdot 10^{-25}(300/T)^{2.5}$
24	$O_2^- + C_3H_7^+ + M \rightarrow CO_2 + CH_3 + CH_4 +$	$2.0 \cdot 10^{-25}(300/T)^{2.5}$
25	$O_2^- + C_3H_8^+ + M \rightarrow O_2 + C_3H_8 + M$	$2.0 \cdot 10^{-25}(300/T)^{2.5}$

Table 3.1.21 Channels of two-body O_2^- ion-ion recombination

N	reaction	Rate constant, cm^3/s, cm^6/s estimate
1	$O_2^- + C^+ \rightarrow CO_2$	$1.0 \cdot 10^{-7} (300/T)^{0.5}$
2	$O_2^- + CH^+ \rightarrow CH + O_2$	$1.0 \cdot 10^{-7} (300/T)^{0.5}$
3	$O_2^- + HCO^+ \rightarrow H + CO + O_2$	$1.0 \cdot 10^{-7} (300/T)^{0.5}$
4	$O_2^- + H_2CO^+ \rightarrow H_2 + CO + O_2$	$1.0 \cdot 10^{-7} (300/T)^{0.5}$
5	$O_2^- + HCO_2^+ \rightarrow H + CO_2 + O_2$	$1.0 \cdot 10^{-7} (300/T)^{0.5}$
6	$O_2^- + HC_2O^+ \rightarrow HC + CO + O_2$	$1.0 \cdot 10^{-7} (300/T)^{0.5}$
7	$O_2^- + HNO^+ \rightarrow O_2 + HNO$	$1.0 \cdot 10^{-7} (300/T)^{0.5}$
8	$O_2^- + HN_2O^+ \rightarrow O_2 + H + N_2O$	$1.0 \cdot 10^{-7} (300/T)^{0.5}$
9	$O_2^- + H_2CO^+ \rightarrow O_2 + H_2 + C_2O$	$1.0 \cdot 10^{-7} (300/T)^{0.5}$
10	$O_2^- + CH_2^+ \rightarrow O_2 + CH_2$	$1.0 \cdot 10^{-7} (300/T)^{0.5}$
11	$O_2^- + CH_3O_2^+ \rightarrow O_2 + CH_3 + O_2$	$1.0 \cdot 10^{-7} (300/T)^{0.5}$
12	$O_2^- + CH_3^+ + M \rightarrow O_2 + CH_3 + M$	$1.0 \cdot 10^{-7} (300/T)^{0.5}$
13	$O_2^- + CH_4^+ \rightarrow O_2 + CH_4$	$1.0 \cdot 10^{-7} (300/T)^{0.5}$
14	$O_2^- + CH_5^+ \rightarrow O_2 + CH_5$	$1.0 \cdot 10^{-7} (300/T)^{0.5}$
15	$O_2^- + C_2H_2^+ \rightarrow O_2 + C_2H_2$	$1.0 \cdot 10^{-7} (300/T)^{0.5}$
16	$O_2^- + C_2H_3^+ \rightarrow O_2 + C_2H_3$	$1.0 \cdot 10^{-7} (300/T)^{0.5}$
17	$O_2^- + C_2H_4^+ \rightarrow O_2 + C_2H_4$	$1.0 \cdot 10^{-7} (300/T)^{0.5}$
18	$O_2^- + C_2H_5^+ \rightarrow O_2 + C_2H_5$	$1.0 \cdot 10^{-7} (300/T)^{0.5}$
19	$O_2^- + C_2H_6^+ \rightarrow O_4 + CH_3 + CH_3$	$1.0 \cdot 10^{-7} (300/T)^{0.5}$
20	$O_2^- + C_3H_3^+ \rightarrow CO_2 + C_2H_3$	$1.0 \cdot 10^{-7} (300/T)^{0.5}$
21	$O_2^- + C_3H_4^+ \rightarrow CO_2 + C_2H_4$	$1.0 \cdot 10^{-7} (300/T)^{0.5}$
22	$O_2^- + C_3H_5^+ \rightarrow CO_2 + C_2H_5$	$1.0 \cdot 10^{-7} (300/T)^{0.5}$

23	$O_2^- + C_3H_6^+ \rightarrow CO_2 + CH_3 + CH_3$	$1.0 \cdot 10^{-7} (300/T)^{0.5}$
24	$O_2^- + C_3H_7^+ \rightarrow CO_2 + CH_3 + CH_4$	$1.0 \cdot 10^{-7} (300/T)^{0.5}$
25	$O_2^- + C_3H_8^+ \rightarrow O_2 + C_3H_8$	$1.0 \cdot 10^{-7} (300/T)^{0.5}$

Table 3.1.22. Channels of three body H^- ion-ion recombination

N	reaction	Rate constant, cm^3/s, cm^6/s estimate
1	$H^- + C^+ + M \rightarrow OH + M$	$2.0 \cdot 10^{-25} (300/T)^{2.5}$
2	$H^- + CH^+ + M \rightarrow CH + H + M$	$2.0 \cdot 10^{-25} (300/T)^{2.5}$
3	$H^- + HCO^+ + M \rightarrow CH_2 + O + M$	$2.0 \cdot 10^{-25} (300/T)^{2.5}$
4	$H^- + H_2CO^+ + M \rightarrow H_2 + CH + O + M$	$2.0 \cdot 10^{-25} (300/T)^{2.5}$
5	$H^- + H_2CO^+ + M \rightarrow H_2 + CO + H + M$	$2.0 \cdot 10^{-25} (300/T)^{2.5}$
6	$HO^- + HCO_2^+ + M \rightarrow H + CO_2 + H + M$	$2.0 \cdot 10^{-25} (300/T)^{2.5}$
7	$H^- + HC_2O^+ + M \rightarrow CH + CH + O + M$	$2.0 \cdot 10^{-25} (300/T)^{2.5}$
8	$H^- + HNO^+ + M \rightarrow H + H + NO + M$	$2.0 \cdot 10^{-25} (300/T)^{2.5}$
9	$H^- + HN_2O^+ + M \rightarrow H + H + N_2O + M$	$2.0 \cdot 10^{-25} (300/T)^{2.5}$
10	$H^- + H_2CO^+ + M \rightarrow H + H_2 + CO + M$	$2.0 \cdot 10^{-25} (300/T)^{2.5}$
11	$H^- + CH_2^+ + M \rightarrow H + CH_2 + M$	$2.0 \cdot 10^{-25} (300/T)^{2.5}$
12	$H^- + CH_3O_2^+ + M \rightarrow H + CH_3 + O_2 + M$	$2.0 \cdot 10^{-25} (300/T)^{2.5}$
13	$H^- + CH_3^+ + M \rightarrow H + CH_3 + M$	$2.0 \cdot 10^{-25} (300/T)^{2.5}$
14	$H^- + CH_4^+ + M \rightarrow H + CH_4 + M$	$2.0 \cdot 10^{-25} (300/T)^{2.5}$
15	$H^- + CH_5^+ + M \rightarrow H + CH_5 + M$	$2.0 \cdot 10^{-25} (300/T)^{2.5}$
16	$H^- + C_2H_2^+ + M \rightarrow H + C_2H_2 + M$	$2.0 \cdot 10^{-25} (300/T)^{2.5}$
17	$H^- + C_2H_3^+ + M \rightarrow H + C_2H_3 + M$	$2.0 \cdot 10^{-25} (300/T)^{2.5}$
18	$H^- + C_2H_4^+ + M \rightarrow H + C_2H_4 + M$	$2.0 \cdot 10^{-25} (300/T)^{2.5}$
19	$H^- + C_2H_5^+ + M \rightarrow H + C_2H_5 + M$	$2.0 \cdot 10^{-25} (300/T)^{2.5}$
20	$H^- + C_2H_6^+ + M \rightarrow H + CH_3 + CH_3 + M$	$2.0 \cdot 10^{-25} (300/T)^{2.5}$

21	$H^- + C_3H_3^+ + M \rightarrow CH + C_2H_3 + M$	$2.0 \cdot 10^{-25}(300/T)^{2.5}$
22	$H^- + C_3H_4^+ + M \rightarrow CH + C_2H_4 + M$	$2.0 \cdot 10^{-25}(300/T)^{2.5}$
23	$H^- + C_3H_5^+ + M \rightarrow CH + C_2H_5 + M$	$2.0 \cdot 10^{-25}(300/T)^{2.5}$
25	$H^- + C_3H_6^+ + M \rightarrow CH + CH_3 + CH_3 + M$	$2.0 \cdot 10^{-25}(300/T)^{2.5}$
26	$H^- + C_3H_7^+ + M \rightarrow CH + CH_3 + CH_4 + M$	$2.0 \cdot 10^{-25}(300/T)^{2.5}$
27	$H^- + C_3H_8^+ + M \rightarrow H + C_3H_8 + M$	$2.0 \cdot 10^{-25}(300/T)^{2.5}$

Table 3.1.23. Channels of two-body H^- ion-ion recombination

N	reaction	Rate constant, cm^3/s, cm^6/s estimate
1	$H^- + C^+ \rightarrow OH$	$1.0 \cdot 10^{-7}(300/T)^{0.5}$
2	$H^- + CH^+ \rightarrow CH + H$	$1.0 \cdot 10^{-7}(300/T)^{0.5}$
3	$H^- + HCO^+ \rightarrow CH_2 + O$	$1.0 \cdot 10^{-7}(300/T)^{0.5}$
4	$H^- + H_2CO^+ \rightarrow H_2 + CH + O$	$1.0 \cdot 10^{-7}(300/T)^{0.5}$
5	$H^- + H_2CO^+ \rightarrow H_2 + CO + H$	$1.0 \cdot 10^{-7}(300/T)^{0.5}$
6	$HO^- + HCO_2^+ \rightarrow H + CO_2 + H$	$1.0 \cdot 10^{-7}(300/T)^{0.5}$
7	$H^- + HC_2O^+ \rightarrow CH + CH + O$	$1.0 \cdot 10^{-7}(300/T)^{0.5}$
8	$H^- + HNO^+ \rightarrow H + H + NO$	$1.0 \cdot 10^{-7}(300/T)^{0.5}$
9	$H^- + HN_2O^+ \rightarrow H + H + N_2O$	$1.0 \cdot 10^{-7}(300/T)^{0.5}$
10	$H^- + H_2CO^+ \rightarrow H + H_2 + CO$	$1.0 \cdot 10^{-7}(300/T)^{0.5}$
11	$H^- + CH_2^+ \rightarrow H + CH_2$	$1.0 \cdot 10^{-7}(300/T)^{0.5}$
12	$H^- + CH_3O_2^+ \rightarrow H + CH_3 + O_2$	$1.0 \cdot 10^{-7}(300/T)^{0.5}$
13	$H^- + CH_3^+ \rightarrow H + CH_3$	$1.0 \cdot 10^{-7}(300/T)^{0.5}$
14	$H^- + CH_4^+ \rightarrow H + CH_4$	$1.0 \cdot 10^{-7}(300/T)^{0.5}$
15	$H^- + CH_5^+ \rightarrow H + CH_5$	$1.0 \cdot 10^{-7}(300/T)^{0.5}$
16	$H^- + C_2H_2^+ \rightarrow H + C_2H_2$	$1.0 \cdot 10^{-7}(300/T)^{0.5}$
17	$H^- + C_2H_3^+ \rightarrow H + C_2H_3$	$1.0 \cdot 10^{-7}(300/T)^{0.5}$

18	$H^- + C_2H_4^+ \rightarrow H + C_2H_4$	$1.0 \cdot 10^{-7} (300/T)^{0.5}$
19	$H^- + C_2H_5^+ \rightarrow H + C_2H_5$	$1.0 \cdot 10^{-7} (300/T)^{0.5}$
20	$H^- + C_2H_6^+ \rightarrow H + CH_3 + CH_3$	$1.0 \cdot 10^{-7} (300/T)^{0.5}$
21	$H^- + C_3H_3^+ \rightarrow CH + C_2H_3$	$1.0 \cdot 10^{-7} (300/T)^{0.5}$
22	$H^- + C_3H_4^+ \rightarrow CH + C_2H_4$	$1.0 \cdot 10^{-7} (300/T)^{0.5}$
23	$H^- + C_3H_5^+ \rightarrow CH + C_2H_5$	$1.0 \cdot 10^{-7} (300/T)^{0.5}$
25	$H^- + C_3H_6^+ \rightarrow CH + CH_3 + CH_3$	$1.0 \cdot 10^{-7} (300/T)^{0.5}$
26	$H^- + C_3H_7^+ \rightarrow CH + CH_3 + CH_4$	$1.0 \cdot 10^{-7} (300/T)^{0.5}$
27	$H^- + C_3H_8^+ \rightarrow H + C_3H_8$	$1.0 \cdot 10^{-7} (300/T)^{0.5}$

Table 3.1.24. Channels of three body OH^- ion-ion recombination

N	reaction	Rate constant, cm^3/s, cm^6/s estimate
1	$OH^- + C^+ + M \rightarrow OH + C + M$	$2.0 \cdot 10^{-25} (300/T)^{2.5}$
2	$OH^- + CH^+ + M \rightarrow CH + OH + M$	$2.0 \cdot 10^{-25} (300/T)^{2.5}$
3	$OH^- + HCO^+ + M \rightarrow HCO + OH + M$	$2.0 \cdot 10^{-25} (300/T)^{2.5}$
4	$OH^- + H_2CO^+ + M \rightarrow H_2 + OH + CO + M$	$2.0 \cdot 10^{-25} (300/T)^{2.5}$
5	$OH^- + H_2CO^+ + M \rightarrow H_2 + CO + OH + M$	$2.0 \cdot 10^{-25} (300/T)^{2.5}$
6	$OH^- + HCO_2^+ + M \rightarrow H + CO_2 + H + M$	$2.0 \cdot 10^{-25} (300/T)^{2.5}$
7	$OH^- + HC_2O^+ + M \rightarrow CH + CH + OH + M$	$2.0 \cdot 10^{-25} (300/T)^{2.5}$
8	$OH^- + HNO^+ + M \rightarrow OH + NO + H + M$	$2.0 \cdot 10^{-25} (300/T)^{2.5}$
9	$OH^- + HN_2O^+ + M \rightarrow OH + H + N_2O + M$	$2.0 \cdot 10^{-25} (300/T)^{2.5}$
10	$OH^- + H_2CO^+ + M \rightarrow OH + H_2 + CO + M$	$2.0 \cdot 10^{-25} (300/T)^{2.5}$
11	$OH^- + CH_2^+ + M \rightarrow OH + CH_2 + M$	$2.0 \cdot 10^{-25} (300/T)^{2.5}$
12	$OH^- + CH_3O_2^+ + M \rightarrow OH + CH_3 + O_2 + M$	$2.0 \cdot 10^{-25} (300/T)^{2.5}$
13	$OH^- + CH_3^+ + M \rightarrow OH + CH_3 + M$	$2.0 \cdot 10^{-25} (300/T)^{2.5}$
14	$OH^- + CH_4^+ + M \rightarrow OH + CH_4 + M$	$2.0 \cdot 10^{-25} (300/T)^{2.5}$

15	$OH^- + CH_5^+ + M \rightarrow OH + CH_5 + M$	$2.0 \cdot 10^{-25}(300/T)^{2.5}$
16	$OH^- + C_2H_2^+ + M \rightarrow OH + C_2H_2 + M$	$2.0 \cdot 10^{-25}(300/T)^{2.5}$
17	$OH^- + C_2H_3^+ + M \rightarrow OH + C_2H_3 + M$	$2.0 \cdot 10^{-25}(300/T)^{2.5}$
18	$OH^- + C_2H_4^+ + M \rightarrow OH + C_2H_4 + M$	$2.0 \cdot 10^{-25}(300/T)^{2.5}$
19	$OH^- + C_2H_5^+ + M \rightarrow OH + C_2H_5 + M$	$2.0 \cdot 10^{-25}(300/T)^{2.5}$
20	$OH^- + C_2H_6^+ + M \rightarrow OH + CH_3 + CH_3 + M$	$2.0 \cdot 10^{-25}(300/T)^{2.5}$
21	$OH^- + C_3H_3^+ + M \rightarrow OH + CH + C_2H_2 + M$	$2.0 \cdot 10^{-25}(300/T)^{2.5}$
22	$OH^- + C_3H_4^+ + M \rightarrow OH + CH_3 + C_2H + M$	$2.0 \cdot 10^{-25}(300/T)^{2.5}$
23	$OH^- + C_3H_5^+ + M \rightarrow OH + CH_2 + C_2H_3 + M$	$2.0 \cdot 10^{-25}(300/T)^{2.5}$
24	$OH^- + C_3H_6^+ + M \rightarrow OH + C_2H_3 + CH_3 + M$	$2.0 \cdot 10^{-25}(300/T)^{2.5}$
25	$OH^- + C_3H_7^+ + M \rightarrow OH + CH_2 + C_2H_5 + M$	$2.0 \cdot 10^{-25}(300/T)^{2.5}$
26	$OH^- + C_3H_8^+ + M \rightarrow OH + C_3H_8 + M$	$2.0 \cdot 10^{-25}(300/T)^{2.5}$

Table 3.1.25. Channels of two body OH^- ion-ion recombination

N	**reaction**	**Rate constant, cm^3/s, cm^6/s estimate**
1	$OH^- + C^+ \rightarrow OH + C$	$1.0 \cdot 10^{-7}(300/T)^{0.5}$
2	$OH^- + CH^+ \rightarrow CH + OH$	$1.0 \cdot 10^{-7}(300/T)^{0.5}$
3	$OH^- + HCO^+ \rightarrow HCO + OH$	$1.0 \cdot 10^{-7}(300/T)^{0.5}$
4	$OH^- + H_2CO^+ \rightarrow H_2 + OH + CO$	$1.0 \cdot 10^{-7}(300/T)^{0.5}$
5	$OH^- + H_2CO^+ \rightarrow H_2 + CO + OH$	$1.0 \cdot 10^{-7}(300/T)^{0.5}$
6	$OH^- + HCO_2^+ \rightarrow H + CO_2 + H$	$1.0 \cdot 10^{-7}(300/T)^{0.5}$
7	$OH^- + HC_2O^+ \rightarrow CH + CH + OH$	$1.0 \cdot 10^{-7}(300/T)^{0.5}$
8	$OH^- + HNO^+ \rightarrow OH + NO + H$	$1.0 \cdot 10^{-7}(300/T)^{0.5}$
9	$OH^- + HN_2O^+ \rightarrow OH + H + N_2O$	$1.0 \cdot 10^{-7}(300/T)^{0.5}$
10	$OH^- + H_2CO^+ \rightarrow OH + H_2 + CO$	$1.0 \cdot 10^{-7}(300/T)^{0.5}$

11	$OH^- + CH_2^+ \rightarrow OH + CH_2$	$1.0 \cdot 10^{-7} (300/T)^{0.5}$
12	$OH^- + CH_3O_2^+ \rightarrow OH + CH_3 + O_2$	$1.0 \cdot 10^{-7} (300/T)^{0.5}$
13	$OH^- + CH_3^+ \rightarrow OH + CH_3$	$1.0 \cdot 10^{-7} (300/T)^{0.5}$
14	$OH^- + CH_4^+ \rightarrow OH + CH_4$	$1.0 \cdot 10^{-7} (300/T)^{0.5}$
15	$OH^- + CH_5^+ \rightarrow OH + CH_5$	$1.0 \cdot 10^{-7} (300/T)^{0.5}$
16	$OH^- + C_2H_2^+ \rightarrow OH + C_2H_2$	$1.0 \cdot 10^{-7} (300/T)^{0.5}$
17	$OH^- + C_2H_3^+ \rightarrow OH + C_2H_3$	$1.0 \cdot 10^{-7} (300/T)^{0.5}$
18	$OH^- + C_2H_4^+ \rightarrow OH + C_2H_4$	$1.0 \cdot 10^{-7} (300/T)^{0.5}$
19	$OH^- + C_2H_5^+ \rightarrow OH + C_2H_5$	$1.0 \cdot 10^{-7} (300/T)^{0.5}$
20	$OH^- + C_2H_6^+ \rightarrow OH + CH_3 + CH_3$	$1.0 \cdot 10^{-7} (300/T)^{0.5}$
21	$OH^- + C_3H_3^+ \rightarrow OH + CH + C_2H_2$	$1.0 \cdot 10^{-7} (300/T)^{0.5}$
22	$OH^- + C_3H_4^+ \rightarrow OH + CH_3 + C_2H$	$1.0 \cdot 10^{-7} (300/T)^{0.5}$
23	$OH^- + C_3H_5^+ \rightarrow OH + CH_2 + C_2H_3$	$1.0 \cdot 10^{-7} (300/T)^{0.5}$
24	$OH^- + C_3H_6^+ \rightarrow OH + C_2H_3 + CH_3$	$1.0 \cdot 10^{-7} (300/T)^{0.5}$
25	$OH^- + C_3H_7^+ \rightarrow OH + CH_2 + C_2H_5$	$1.0 \cdot 10^{-7} (300/T)^{0.5}$
26	$OH^- + C_3H_8^+ \rightarrow OH + C_3H_8$	$1.0 \cdot 10^{-7} (300/T)^{0.5}$

References to section 3.1.

1. Works of Seminar Application of electron beams and pulse discharges for flue gas cleaning. Moscow IVTAN. November. 1992
2. Physical principles of plasma-reactor devices with an application of Relativistic electron beams. MRTI AS USSR. M. 1989.
3. Gerasimov G.Ya, Gerasimova T.S., Makarov V.N., Fadeev S.A. Modeling of physical and chemical processes of nitric and sulfur oxides at electron-beam cleaning of heat plants waste. Khimiya Vysokikh Energyi. 1996.V.30. №1. P.34-38.
4. Klimov A., Bityurin V., Kuznetsov A., Tolkunov B., et al. External and internal plasma-assisted combustion. AIAA-2004-1014. Proc. 42-nd AIAA Aerospace Science Meeting and Exhibit 5-8 January 2004, Reno, Nevada.
5. Sharafutdinov R.G., Zavrin A.E., Madirbaev V., Zh., et al. Generation of Hydrogen from methane in electron-beam plasmas. Pisma v Zhurnal Tekhnicheskoi Fiziki. 2005. V.31. N.15. P.23-28.
6. Ardelyan N., Bychkov V., Gromov V., Kosmachevskii K. Application of two plasma Ignition enhancement methods of Propane-Air mixture. AIAA-2006-0612. Proc. 44-th AIAA Aerospace Science Meeting and Exhibit 9-12 January 2006, Reno, Nevada.

7. Zhukov V.N., Sechenov V.A., Khorunzhenko V.I., A.Yu.Starikovskii, Hydrogcarbon-air mixture ignition kinetics. 3 –d Workshop Thermochemical and plasma processes in aerodynamics. Saint – Petersburg. 28-31 July. 2003. P.296.
8. Eletsky A.V., Kulagin V.D. Kinetics of processes in the plasma createdby the electron beam in dense inert gas. Fizika Plazmy. 1979. V.5. # 1. P. 98-105.
9. Bychkov V.L., Eletsky A.V. High pressure electron-beam plasmas. Khimia Plazmy. Ed. B.M. Smirnov. Moscow. Energoatomizdat. 1985. N.12, P. 119-158.
10. Konovalov V.P. Degradation spectra of electrons in nitrogen, oxygen and air. Zhurnal Tekhnicheskoi Fiziki. 1993. V.63.N.3. P.23-33.; Konovalov V.P., Son E.E. Degradation spectra of electrons in gases. In a book Khimia plazmy Ed. B.M.Smirnov Energoatomizdat. 1987.Vol.14.P.194-227.
11. Ardelyan N., Bychkov V., Kosmachevskii K., Chuvashev S., Malmuth N. Modeling of Plasmas in Electron Beams and Plasma Jets . AIAA 2001-3101 Proc. 32-nd AIAA Plasmadynamics and Lasers Conference and 4 th Weakly Ionized gases Workshop 11-14 June 2001, Anaheim, CA.(15 P).
12. Bychkov V.L., Vasiliev M.N., Koroteev A.S. Electron - Beam Plasma. Generation, Properties, Application. Moscow. MGOU (Moscow State Open University) Publishers. A/O "Rosvuznauka". 1993. 168 P.
13. Bychkov V.L., Eletskyi A.V. In a book Plasma Chemistry V.12. Ed. Prof. B.M. Smirnov Energoatomizdat. 1985. P. 119-158.
14. Andreev S.I., Bychkov V.L., Gordeev O.A., Klepando I.L. Studies of non equilibrium conductivity of air ionized by short pulse of fast electrons. Fizika Plazmy.(Sov.Phys.-Plasma Phys.) 1985. V.11. P. 1134-1139.
15. The nuclear handbook. Editor O.R.Frish. George Newnes Limited. London. 1958.
16. Raizer Yu.P. Gas discharge physics. Moscow. Nauka. 1992.
17. Chernyaev A.P. Interaction of ionizing radiation with matter. Fizmatlit. Moscow. 2004.
18. Abramyan . Electron beam. Atomizdat. 1974.
19. Varatharajan B., Williams F.A. Reduced Chemistry Descriptions for Ignition and Detonation of Higher Hydrocarbons. 40-th AIAA Aerospace Sciences Meeting and Exhibit. 14-17 January, 2002, Reno, NV.
20. Westbrook C.K., Chase L.L. Chemical Kinetics and Thermochemical Data for Combustion Applications. Lawrence Livermore Laboratory UCID-17833. Rev.1, April, 1981.
21. Cserep C., Gyorgy I., Roder M. et. al. Radiation Chemistry of Hydrocarbons Ed.G. Foldiak. Budapest: Akad. Kiado. 1981. 476 p.
22. Williams S., Miller T.M., Khighton W.B., Midey A.J., Arnold S.T., Viggiano A.A. Reactions and Thermochemistry of Alkyl Ions $C_nH_{2n+1}^+$ in the Gas Phase. 41st Aerospace Sciences Meeting & Exhibit. 6-9 Jan.2003, Reno, Nevada.
23. Kostinsky A.Y., Matveev A.A., Silakov V.P., и др. Plasma Sources. Sci. Tech. 1992. V.1. N.3. P.207.
24. Smirnov B.M. Complex ions. Moscow. Nauka. 1983. 151 p.
25. Smirnov B.M. Negative ions. Moscow. Atomizdat 1978. 176 p.
26. Mnatsakanyan A. Kh. and Naidis, G. V. "Charged particle production and loss processes in nitrogen-oxygen plasmas," in Reviews of Plasma Chemistry, B. M. Smirnov, Ed. New York: Consultants Bureau, 1991, pp. 259-292.
27. Flannery M.R. Ion-ion recombination in high-pressure discharges. In a book: Gas lasers. ED I.Mc Daniel and W. Nighan. Moscow. Mir .1986. P.177-215.
28. Virin L.I., Dzhatspanyan R.V., Karachevtsev G.V., Potapov V.K., Tal'rose V.L. Ion-molecule reactions in gases. Moscow. Nauka. 1979. P.548.
29. Anicich V.G. Evaluated Bimolecular Ion-Molecule Gas Phase Kinetics of Positive Ions for Use in Modeling Planetary Atmospheres, Cometary Comae, and Intersteller Clouds. J. Phys. Chem. Ref. Data. Vol. 1993. V.22.N.6. P.1469-1567.

30. Mitchell J.B.A. The Dissociative Recombination of Molecular Ions. Phys. Reports. 1990. V.186. N.5. P. 215-248.
31. Arnold S.T., Morris R.A., Viggiano A.A. Reactions of O^- with Various Alkanes: Competitionbetween Hydrogen Abstraction and Reactive Detachment. J.Phys. Chem. A. 1998. V.102. P.1345-1348.
32. Rebrion-Rowe C., Lehfaoui L., Rowe B.R., Mitchell J.B.A. The dissociative recombination of hydrocarbon ions. J. Chem. Phys. 1998. V.108. N.17. P.7185-7189.

Chapter 3.2. Physical models and their numerical realization for a non-self-maintained discharge in the propane-air mixture in different physical conditions (Tasks 7-9)

At the given stage of non-selfmaintained discharge plasma investigations in propane-air flammable mixture we have considered the following problems.

The first one consisted in calculations of discharge parameters in propane-air mixture at solution of the Boltzmann equation for determination of electron-molecule collision characteristics in this discharge.

The second one consisted in calculations of hot propane-air mixture components chemical kinetics.

The third and fourth problems consisted in combining of the first two so that it would be possible to analyze in the first approximation the plasma influence on the ignition – at limited accounting of propane combustion kinetics and plasma chemistry of air in "dry" propane-air mixture, and also in propane-air mixture with water vapors, the necessity of the last one followed from the calculations of the "dry" propane-air mixture, where appeared noticeable amount of water molecules.

An additional problem consisted in estimations of possible plasma velocity at the outlet from the section of the plasma excitation (in experiments undertaken above).

3.2.1. Calculations of electron-molecular collision parameters of the electric discharge plasma in dry propane-air mixture.

On the first problem we have undertaken a calculation of the Boltzmann equation with application of electron molecule collision cross sections for propane, oxygen and air taken from references [3.2.1-3.2.3].

In Fig.2.1 one can see a set of electron-molecule cross sections in propane. The task consisted in check up of kinetic coefficients description possibility with a help of the cross section set equation set [3.2.1] with a help of the code described in [3.2.4].

In Fig.3.2.2 we represent a comparison of our calculations of a drift velocity with experimental value on E/N dependence[3.2.5, 3.2.6]. One can see a reasonable agreement of a theory and experiment.

In Fig.3.2.3 one can see a comparison of α/N- Townsend ionization coefficient with the experimental values [3.2.7] with respect to E/N parameter in pure propane. One can also see a reasonable agreement of a theory and experiment.

In Fig.3.2.4 one can see ionization and attachment rate constants dependences via E/N in propane-air mixture at percentages of propane concentrations 1, 2, 4, 6 and 10% that are of interest in plasma combustion problems. It can be seen that ionization rate constants become more effective with increase of propane concentrations (due to lower ionization threshold in propane), however, in lean and the stoichiometric mixtures propane weakly impact values of the kinetic coefficients. This allows to use the calculation data on rate constants of electron-molecule collisions obtained for pure air in such mixtures in calculation of chemical kinetics.

Represented results are of interest themselves because they show how propane-air mixture parameters change with propane concentrations in air and allow to analyze and model many practically important situations.

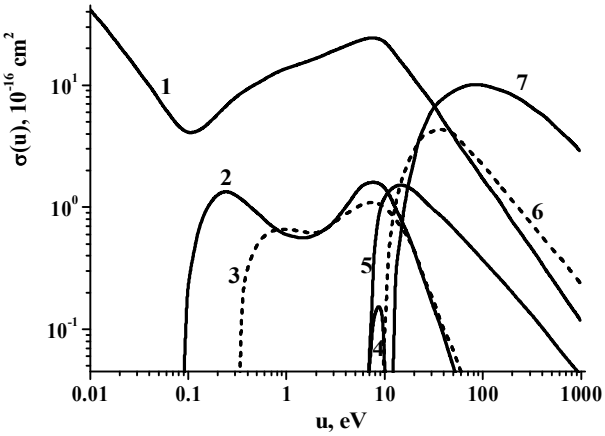

Fig.3.2.1 Electron molecule cross sections via energy in propane [2.1]. 1- elastic cross section, 2,3- vibrational excitation, 4,5,6- electronically excited levels of propane molecule, 7 – ionization cross section.

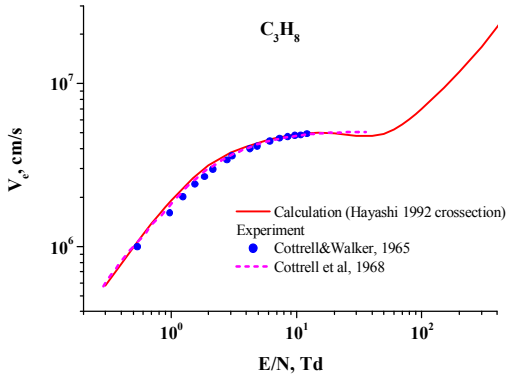

Fig.3.2.2. Drift velocity dependence via E/N in pure propane. A comparison of our calculations with experiments [2.5,2.6].

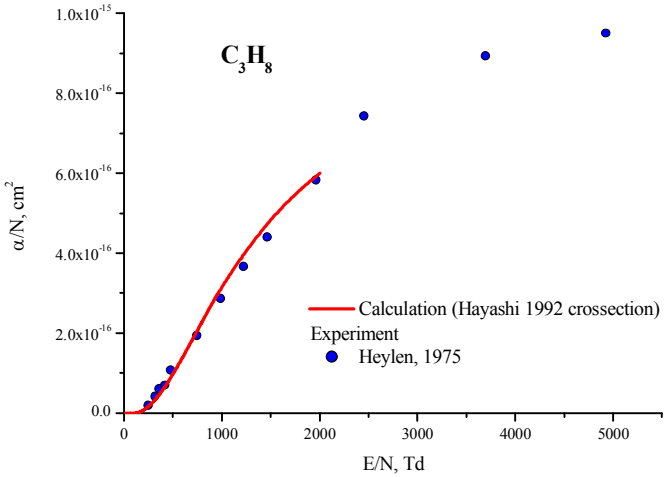

Fig.3.2.3. α/N with respect to reduced electric field in propane (1 Td =10^{-12} V·cm^2) a comparison with experiment [2.7].

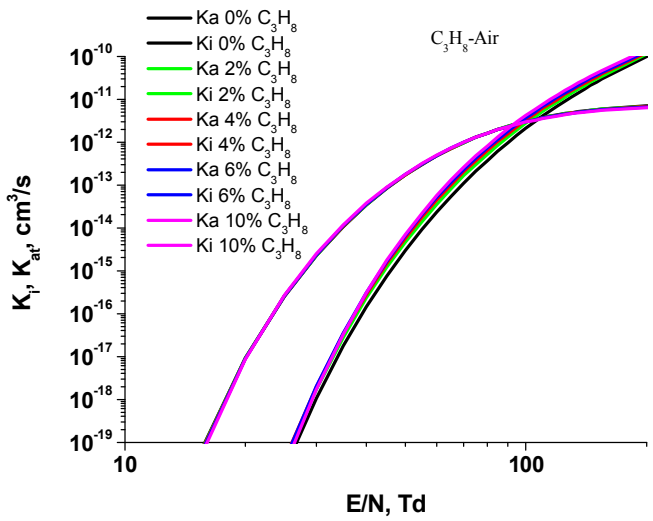

Fig3.2.4. Ionization and attachment rate constants dependences via E/N in propane-air mixture at different percentage of propane

3.2.2. The problem of combustion kinetics calculations in propane-air mixture

For solution of this problem we have created a simplified model of chemical reactions in propane-air mixture. Computations of propane-air stoichiometric mixture components at its inflammation due to its heating have been made. At the basic we have chosen a simplified system of chemical reactions [3.2.8] with added reverse reactions (at first stage we considered stoichiometric mixture 74 reactions: Hydrogen-Oxygen chain , Hydroperoxyl and Hydrogen Peroxide reactions , Propane reactions, I-Propyl, N-Propyl and Propene reactions, Ethylene, Ethyl, Vinyl, Vinoxy and Ketene reactions , Methyl, Methoxy, Formaldehyde, Formyl reactions), standard energy equation with enthalpies computed on the basis of [3.2.9] .

Air chemistry and rate constants for air plasmas were taken from our detailed code for air plasmas [3.2.10] . This model includes 20 components (neutrals, positive and negative ions) and 120 plasma chemical reactions. In details the system of reactions in propane and air plasmas and the corresponding analysis are represented in the Chaper 3.1. of the Present Report and in [3.2.11].

In Fig.3.2.5 one can see results of computations at initial temperature in the stoichiometric propane-air mixture T=1500 K (at small level of ionization by background electrons, W). They show quick ignition and establishing of the front temperature T=2700 K which is close to experimental results, see [3.2.8].

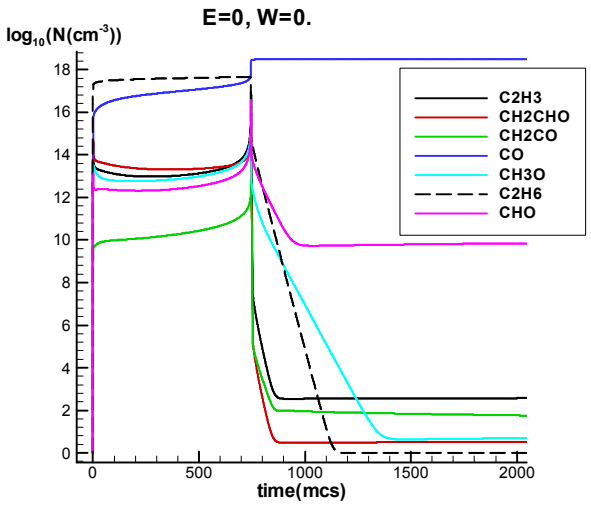

Fig.3.2.5.a

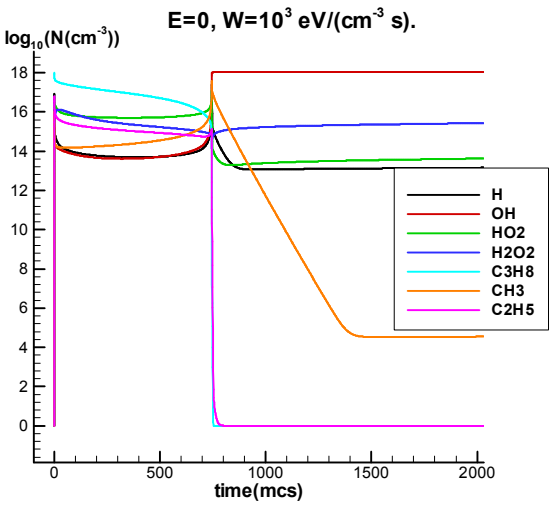

Fig.3.2.5.b

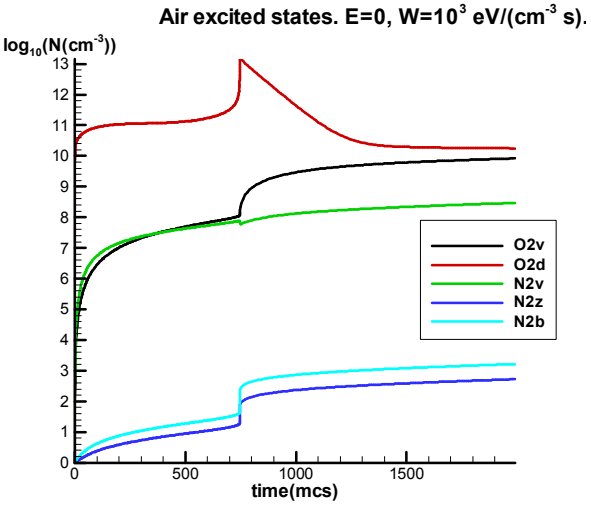

Fig.3.2.5. c

Fig.3.2.5. Propane-air stoichiometric mixture component composition evolution at gas temperature T= 1500 K.

3.2.3. Calculations of the plasma impact on dry propane-air mixture

On the third problem we connected the kinetic scheme of the propane-air mixture with the kinetic scheme for air excited by the electron beam in the external electric field. As in the #3.2.2 as the basic we have chosen a simplified system of chemical reactions [3.2.8] with added reverse reactions (at first stage we considered stoichiometric mixture 74 reactions: Hydrogen-Oxygen chain , Hydroperoxyl and Hydrogen Peroxide reactions , Propane reactions, I-Propyl, N-Propyl and Propene reactions, Ethylene, Ethyl, Vinyl, Vinoxy and Ketene reactions , Methyl, Methoxy, Formaldehyde, Formyl reactions), standard energy equation with enthalpies computed on the basis of [3.2.9] . Air chemistry and rate constants for air plasmas were taken from our detailed code for air plasmas [3.2.10] . This model includes 20 components (neutrals, positive and negative ions) and 120 plasma chemical reactions. It was complete with reactions with participation of CO_2. In detail the system of reactions in propane and air plasmas and the

corresponding analysis are represented in Report for 2008 –the first year of investigations [3.2.11].

At that in the mixture excited by the electron beam electron distribution function of plasma electrons considered to be close to the Maxwell one [3.2.12], [and costs of inelastic processes were taken from [3.2.13]. So the equation for electron temperature was taken in the form

$$\partial Te/\partial t = W\cdot\eta \ \{1\} + \Sigma K_i [M_i^+]Te/2 \ \{2\} + \Sigma K_j (2/3\ Ij + 3Te)\ [M_j^+][e] \ \{3\} + \\ + Iaff\ k_{det}\ [O2-][\ O2+N2]\ \{4\} - K_{at1}\ [O2]^2\ Te^2\ d\ K_{at1}\ (Te)/d\ Te\ \{5\} - \\ - K_{el1}\ [O2+N2](Te - T)\ \{6\} \qquad (3.2.3.1)$$

Here T_e is electron temperature, $[e]$ is their concentration ; η- part of electron beam power W going to rotational and elastic excitation of molecule; K_i, K_j – rate constants of recombination of electrons and ions M_i^+, M_j^+; I_j-ionization energy of molecules; I_{aff} – affinity energy of negative ion, K_{at1} – rate constant of electron three-body attachment to oxygen molecules да; K_{el1}- rate constant of effective elastic and inelastic processes at electron collisions with molecules of air. Figure brackets indicate the following mechanisms: {1} heating of electrons due to injection of fast electrons below the threshold of the vibrational excitation [3.2.12]; {2}, {3} –heating in processes of electron-ion recombination [3.2.12], {4} heating in the process of electron detachment from negative ions; {5}- cooling in the process of electron attachment to the molecule O_2, {6} – heating in elastic and inelastic processes of electron collisions with molecules O_2 and N_2, at that data for rate constants we took from calculations in weak electric fields [3.2.13].

In the case of external electric field existence we included a term of electron heating in external electric field, constants of electron-molecule collisions were also taken from the calculations [3.2.14]. In the equation for gas temperature we have included terms corresponding to vibrational and electronic relaxation of molecules, heating and cooling of the gas in chemical and plasma-chemical reactions.

Let us indicate that the power put in the gas by the electron beam W (we usually use it in eV/(cm^3 s) units) and a velocity of the molecule excitation Q are connected by the equation [3.2.10, 2.12] $Q=W/(U_i)$, where U_i is the ionization cost, for example in air it is U_i = 31.6 eV. An excitation velocity of other molecular states is determined similarly. One can show [3.2.11], that the excitation velocity W in air is connected with parameters of the relativistic electron beam (with electron's energy E_b = 200-500 keV) by the relation $W = 10^{22} J_b \cdot P$, where the current density J is expressed in A/cm^2, and pressure in atm., and in case of the non-relativistic electron beam (at E_b <150 кэВ) $W = 4\cdot 10^{22} J_b \cdot P$. For conditions of our experiments W=10^{17}-10^{19} eV/(cm^3 s) (at the corresponding electron beam current density 10^{-5} -10^{-3} A/cm^2).

In Fig.3.2.6 one can see calculation results of propane-air stoichiometric mixture component composition evolution in the external electric field of 3 kV/cm at gas temperature T= 1500 K.

In Fig.3.2.7 one can see calculation results of Propane-air stoichiometric mixture component composition evolution under electron beam action with intensity $W=10^{18}$ eV/(cm^3 s) at gas temperature T= 1500 K. According to [3.2.12-3.2.13] the excitation velocity W is connected with parameters of relativistic electron beam by a relation $W= U_i \cdot 2.8 \cdot 10^{20} \cdot J_b \cdot P$, here J_b is a current density expressed in A/cm^2, pressure is in atm, U_i is electron-ion pair energy cost (for air it is 36 eV), so $J_b \approx 0.3$ mA/cm^2.

In Fig.3.2.8 one can see calculation results of propane-air stoichiometric mixture component composition evolution under electron beam action with intensity $W=10^{18}$ eV/(cm^3 s) and electric field of 3 kV/cm at gas temperature T= 1500 K.

In Fig.3.2.6-3.2.8 one can see a variation of the composition with respect to impact of energy source. Evidently the composition is is richer in case of external plasma impact than in the hot gas mixture.

In Fig.3.2.9 one can see calculation results of gas temperature evolution for stoichiometric propane-air mixture at initial gas temperature 1000, 1300, 1500 and 2000K. At T= 1000K there is no inflammation and there is only decrease of gas and electron temperatures.

In Fig.3.2.10 one can see calculation results of gas temperature evolution for stoichiometric propane-air mixture excited by the electron beam at initial gas temperature 500 and 1500 K. At that it can be seen temperature difference between electron and gas temperatures.

In Fig.3.2.11. one can see calculation results of gas temperature evolution for stoichiometric propane-air mixture excited by the electron beam in external electric field at initial gas temperature 300, 500 and 1500 K**.**

From Fig.3.2.10-3.2.11 follows that at the excitation of the mixture firstly takes place its heating up to the temperature T~1200K, and then its sharp rise (inflammation) with reaching of the maximal temperature T~2700K. Plasma effect of decrease of inflammation time reaches about a factor of two (the undertaken comparison is made for inflammation computations and auto-ignition at temperature of T=1500 K). Plasma sources work as a heater for some time.

Calculations in the beam plasmas and plasmas of the non-selfmaintained discharge, see Fig.3.2.7,3.2.8, show that water vapor is generated already at heating of the “dry” propane-air mixture up to its inflammation, at that their concentration reaches 1-2 %, that is in principle to take into account for at modeling of propane-air mixture plasma. Presence of water vapor can influence kinetics of ion formation reactions and a velocity of mixture heating. The nest section is devoted to these questions.

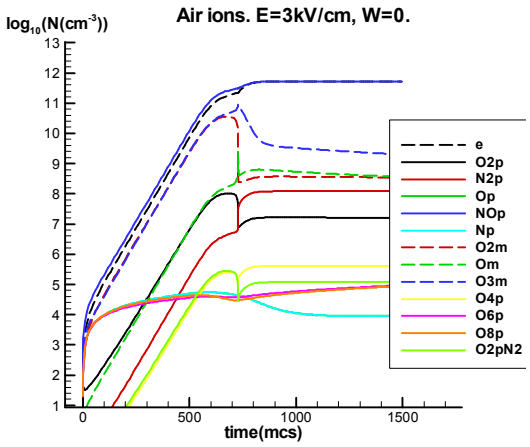

Fig.3.2.6a

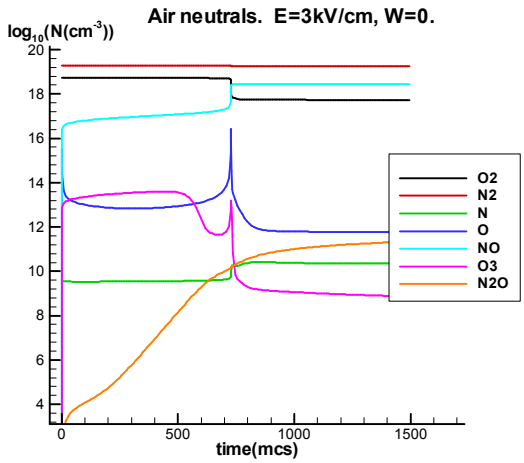

Fig.3.2.6.b

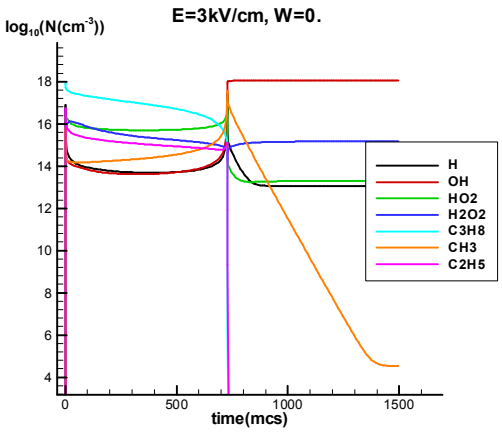

Fig.3.2.6 c

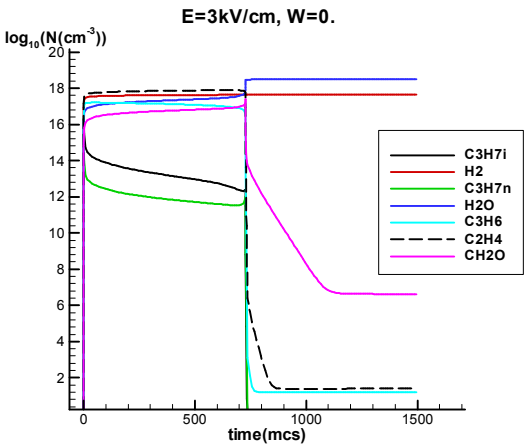

Fig.3.2.6 d.

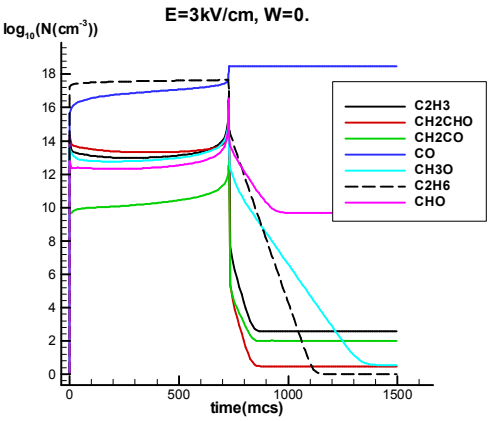

Fig.3.2.6 e.

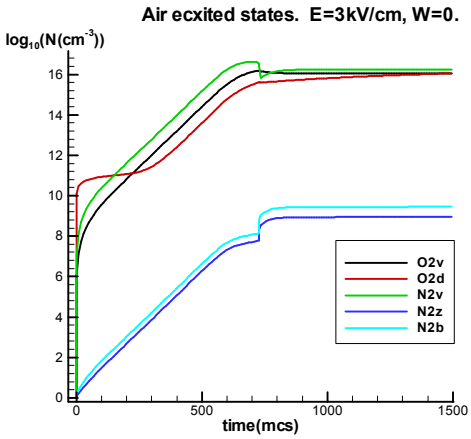

Fig.3.2.6 f.

Fig.3.2.6 Calculation results for stoichiometric propane-air mixture excited in the electric field at gas temperature of 1500 K.

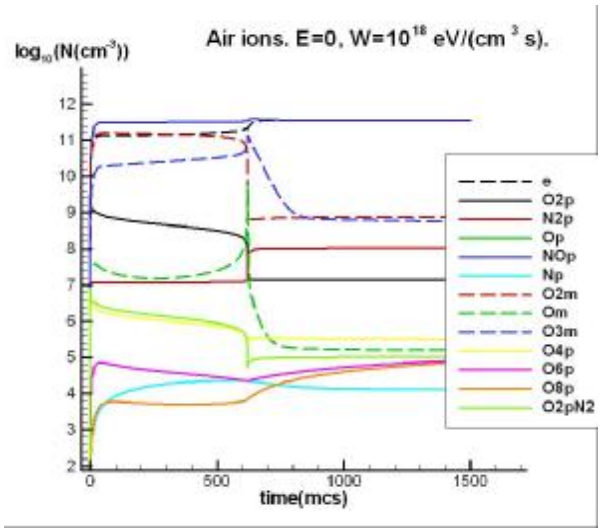

Fig.3.2.7 a.

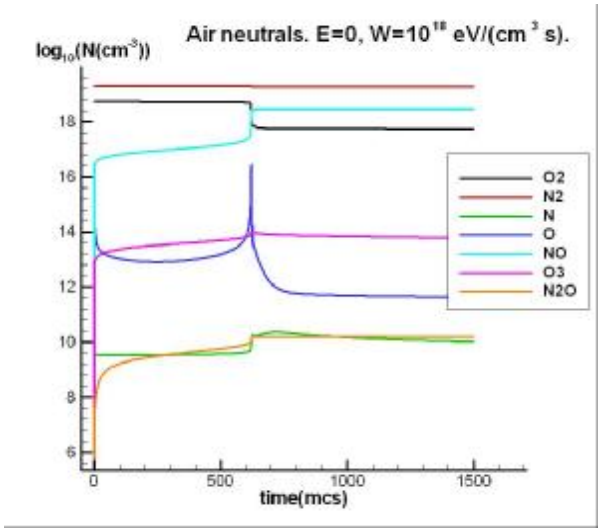

Fig.3.2.7 b.

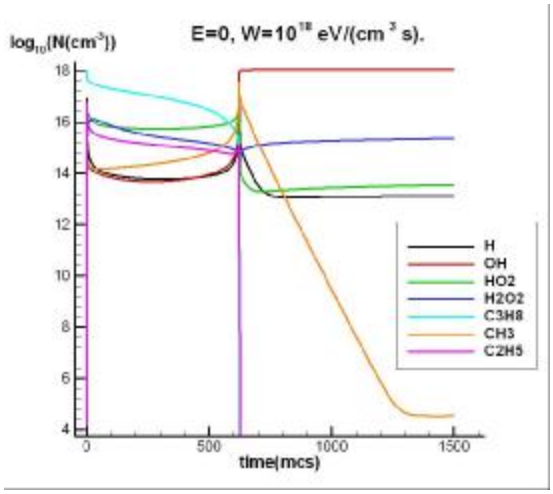

Fig.3.2.7 c.

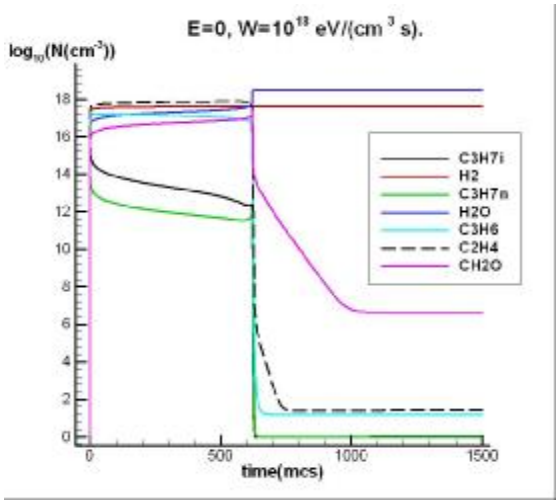

Fig.3.2.7 d.

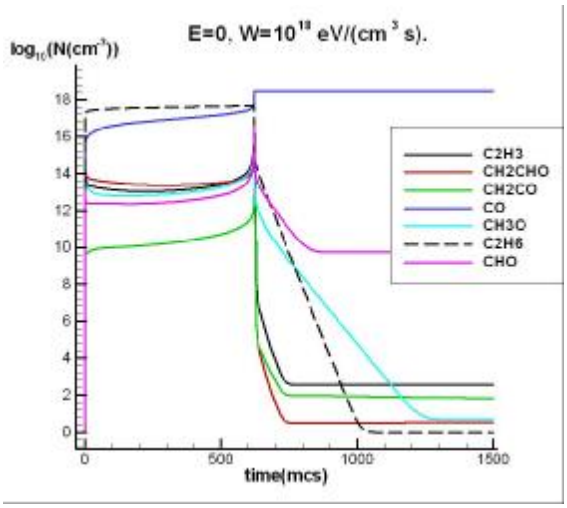

Fig.3.2.7 e.

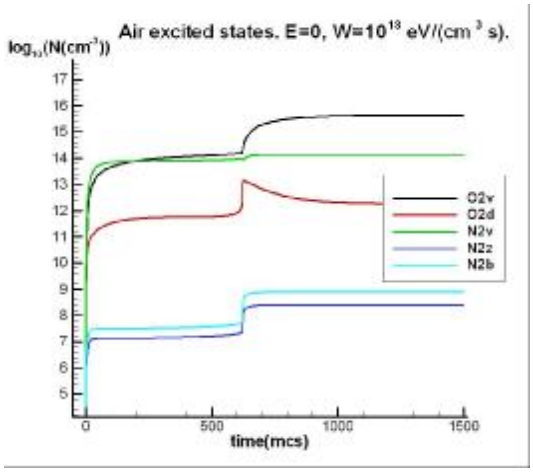

Fig.3.2.7 f

Fig.3.2.7 Calculation results for stoichiometric propane-air mixture excited by the electron beam at gas temperature of 1500 K.

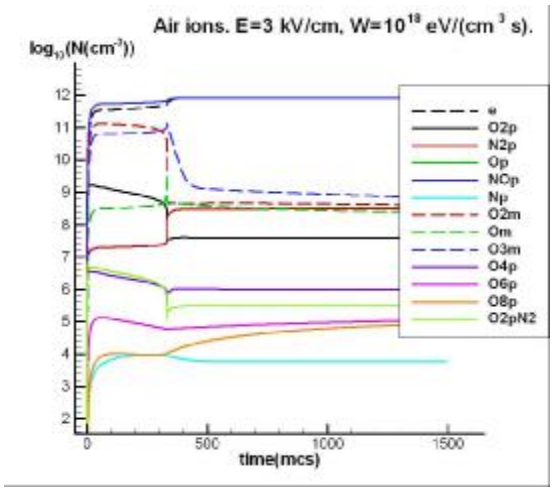

Fig.3.2.8 a.

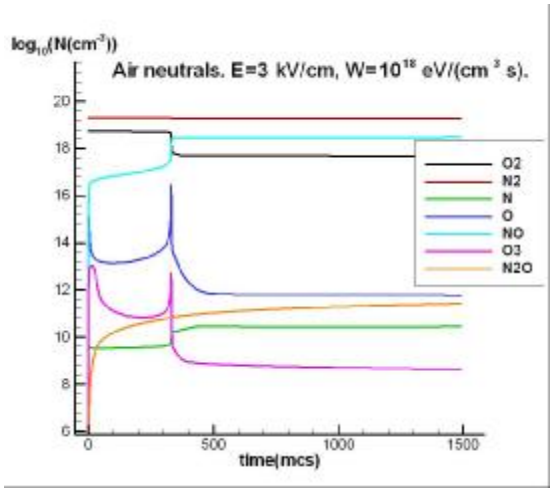

Fig.3.2.8 b.

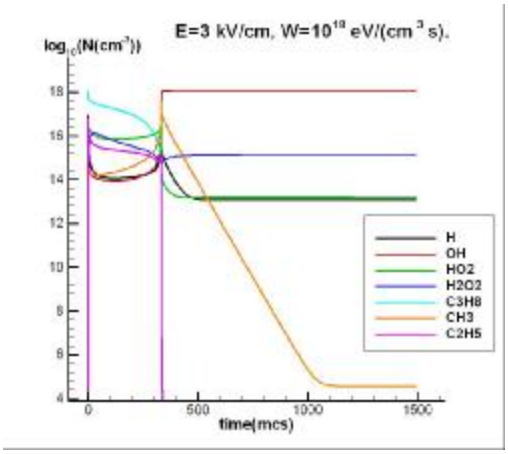

Fig.3.2.8 c.

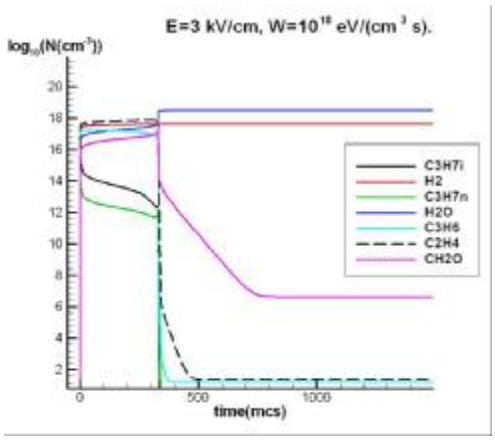

Fig.3.2.8 d.

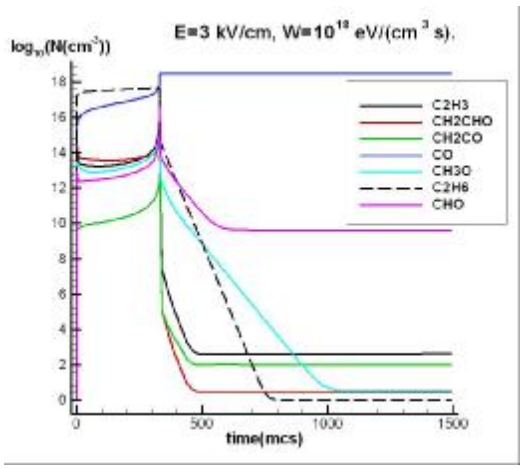

Fig.3.2.8 e.

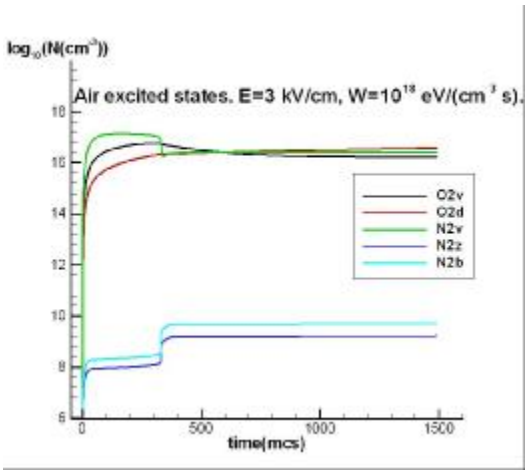

Fig.3.2.8 f.

Fig.3.2.8 Calculation results for stoichiometric propane-air mixture excited by the electron beam in external electric field at gas temperature of 1500 K.

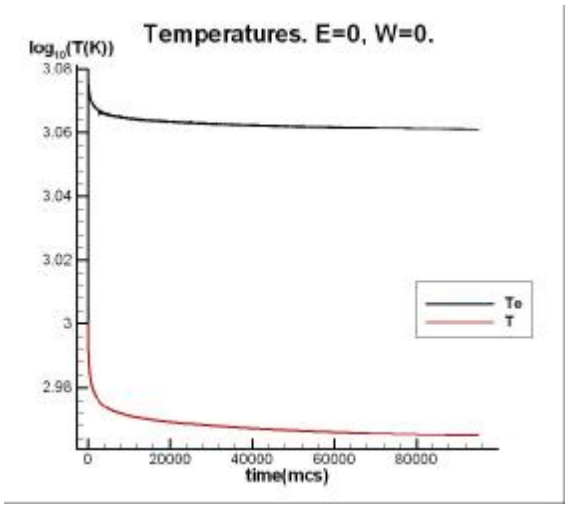

Fig.3.2.9a.

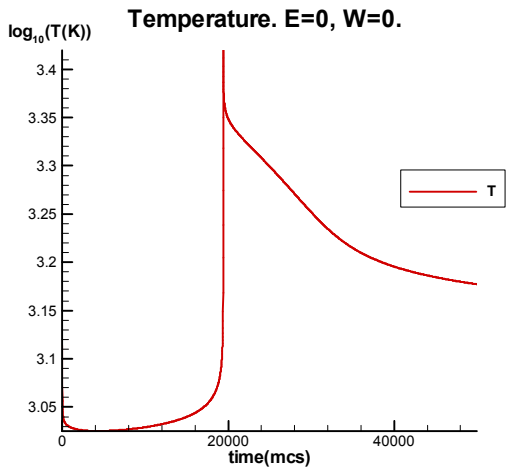

Fig.3.2.9b.

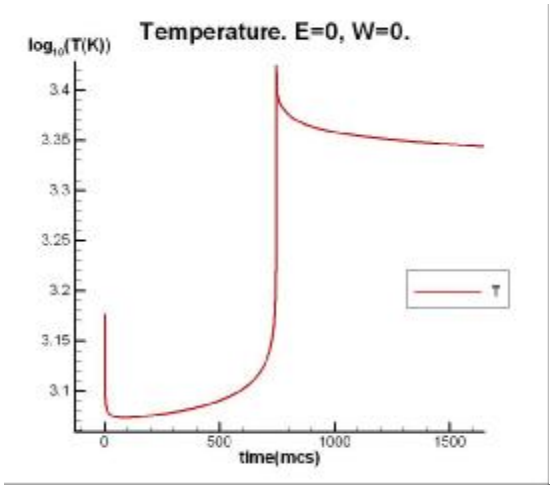

Fig.3.2.9c.

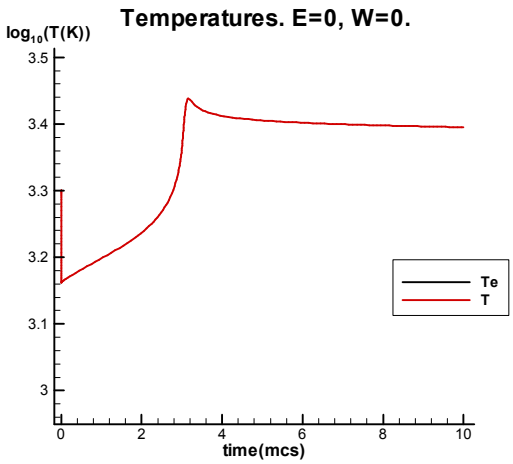

Fig.3.2.9d.

Fig.3.2.9 Calculation results for gas temperature evolution for stoichiometric propane-air mixture at initial gas temperature 1000, 1300, 1500 and 2000 K.

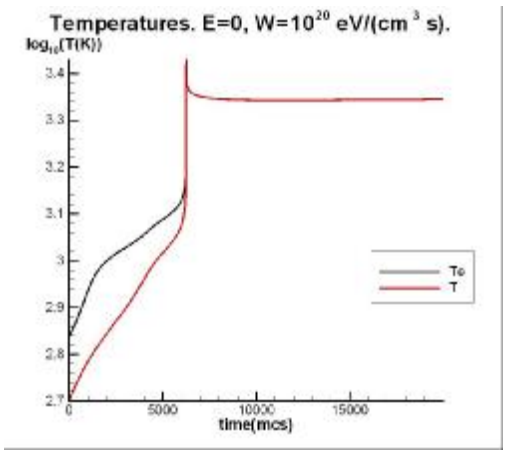

Fig.3.2.10a.

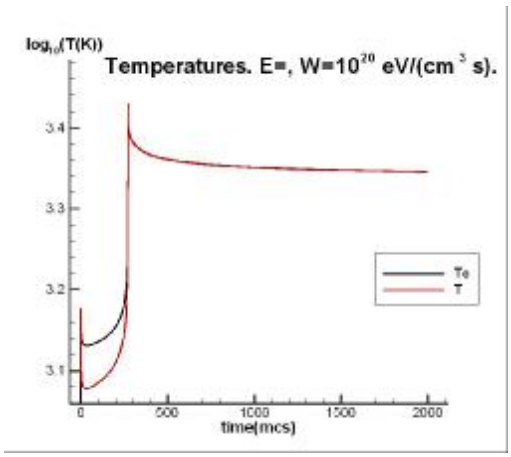

Fig.3.2.10b.

Fig.3.2.10 Calculation results for gas temperature evolution for stoichiometric propane-air mixture excited by the electron beam at initial gas temperature 500 and 1500 K.

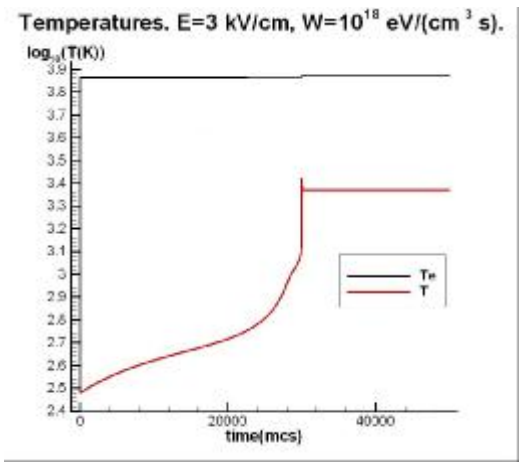

Fig.3.2.11a.

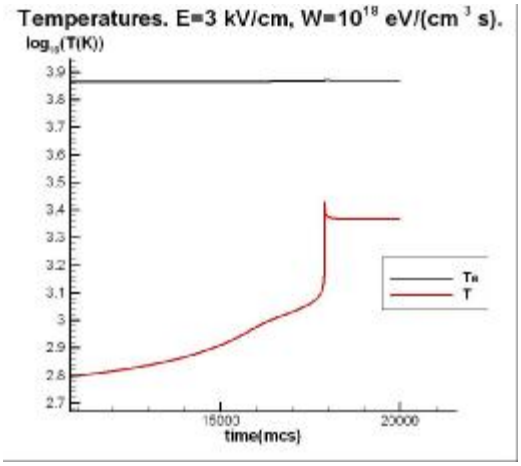

Fig.3.2.11b.

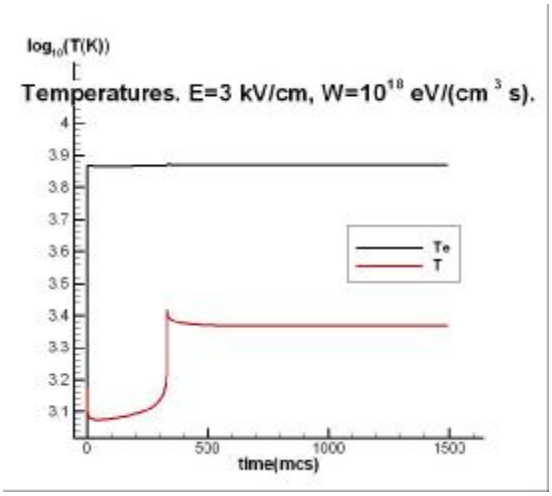

Fig.3.2.11c.

Fig.3.2.11 Calculation results for gas temperature evolution for stoichiometric propane-air mixture excited by the electron beam in external electric field at initial gas temperature 300, 500 and 1500 K.

3.2.4. Calculations of the plasma impact on propane-air mixture containing water vapor ("humid" mixture).

Calculations of "dry" propane-air mixture that does not account water vapor plasma chemistry have shown that visible amount of water vapor –up to 1-2% appears in the process of heating, so it is necessary to account them in modeling of propane-air mixture.

Undertaken analysis of available literature and methods for modeling of reactions has shown that the plasmas in humid air at the first stage of modeling has to include only water molecules in the gas phase without aerosol particles. In this case it is possible to apply previously developed by us air plasmas model [3.2.11]. (Main rate constants for air plasmas used in our calculations are represented in [3.2.11] they are similar to those collected in [3.2.15].)

At the modeling it was necessary [3.2.16] to use reactions with participation of following reagents: positive ions O^+, O_2^+, O_4^+, H^+,H_2^+, OH^+, HO_2^+, H_2O^+, $O_2^+(H_2O)$, H_3O^+, $H_3O^+(H_2O)$,

$H_3O^+(OH)$, $H_3O^+(H_2O)_2$ negative ions O^-, O_2^-, O_3^-, H^-, OH^-, atoms O and H, molecules H_2, O_2, H_2O, O_3, free radicals OH, HO_2, H_2O_2, excited states $O(^1D_1)$, $O(^1S_0)$, $O_2(^1\Delta_g)$ electrons and molecular species including nitrogen from the system of reactions developed by us for dry air, the estimate number of all reactions (including those of dry air) is 280-300, see for example reference [3.2.6, 3.2.11].

Besides reactions with these components it is necessary to consider reactions of ion recombination of each positive ion with each negative ion, and rate constants for these reactions are to be estimated, since these reactions are not investigated yet for all ion combinations. These rate constants are to be determined according to the Flannery method [3.2.17, 3.2.18] with respect to the mixture temperature and pressure. At that their rates are to be normalized by the typical mobility value of these ions 2.5 $cm^2/(V\cdot s)$ and taken from [3.2.19] as it was recommended in [3.2.15].

In the model it is necessary to account the plasma electron cooling due to elastic collisions with water, oxygen and nitrogen molecules, and excitation of their vibrational and rotational levels of freedom [3.2.20]. At that it will be supposed that de-excitation of vibrational and rotational levels takes place mainly during the collisions with molecules. The corresponding heating and cooling terms for the electron energy equations are to be interpolated with respect to electron temperature T_e [3.2.20].

The model has to include reactions of three-body attachment to the molecule O_2 at presence of H_2O as the third body, charge –exchange and ion-ion recombinations with all the positive ions. Rate constants of these reactions are to be estimated also.

Rate constants for electron energy losses at electron collisions with water molecules were taken from the work [3.2.20] for slow electrons and from [3.2.21-3.2.23] for the fast ones where they were obtained on a basis of Boltzmann equation solution. They are represented in Table 3.2.1.

3.2.4.1. Electron energy equation.

Electron energy equation in air mixture with accounting of water molecules we present in the following form based on works [3.2.10, 3.2.12]:

$$\partial T_e/\partial t = eE\,w + W\cdot\eta \;\{1\} + \Sigma K_i\,[M_i^+]T_e/2\;\{2\} + \Sigma K_j\,(2/3\,I_j + 3T_e)\,[M_j^+][e]\;\{3\} +$$
$$+ I_{aff}\,k_{det}\,[O_2^-][\,O_2+N_2+H_2O]\;\{4\} - \;- K_{at1}\,[O_2]^2\,T_e^2\,d\,K_{at1}\,(T_e)/d\,T_e\;\{5\} - K_{at2}\,[O_2]\,[H_2O]\,T_e^2\,d\,K_{at2}\,(T_e)/d\,T_{at2}\;\{6\} - K_{el1}\,[O_2+N_2](T_e - T)\;\{7\} - K_{el2}\,[H_2O](T_e - T)\;\{8\} \qquad (3.2.4.1)$$

where: in the case of external electric field existence we included a term of electron heating in external electric field eEw (E is electric field strength, **w -** electron drift velocity, **e-** electron charge), {1} -heating due to injection of fast electrons into energy region below the threshold of vibrational excitation; {2}, {3} - heating due to processes of electron-ion recombination [3.2.12], {4} -heating due to electron detachment; {5}, {6} - Cooling due to attachment processes to O_2 molecules [3.2.12] , {7}, {8} - Cooling due to elastic and inelastic collisions of slow electrons with O_2, N_2 and H_2O molecules.

3.2.4.2. Excitation and dissociation of water molecules by fast electrons.

In order to account fast electrons of the electron beam we collected from literature G factors included to the Table 3.2.2. G factor is connected with the cost of the Process as $U_i = \frac{100\,eV}{G_i}$.

Costs of processes in water vapor are represented in Table 3.2.3. Costs for excitation of molecules for dry air were taken from [3.2.13].

In Table 3.2.4 we represent rate constants in conditions of water vapor. They were collected on a basis of works cited below the Table 3.2.4. They were verified and enlarged by the new collection of rate constants relevant to water-vapor plasma chemistry presented in [3.2.24].

Ion-ion recombination. Rate constants for ion-ion recombination were obtained basing on works [3.2.17-3.2.18], according to which the rate constant of ion-ion recombination decreases with reduced mass of interacting ions. Available data is also taken from these references. Main channels of neutral particle appearance were taken from [2.25-2.26], where they were obtained from thermochemical analysis. Rate constants for ion-ion recombination between positive and negative ions are represented in Tables 3.2.5-3.2.11.

Table 3.2.1. Rate constant for electron energy losses at electron collisions with water molecules.

T_e, eV	0.026	0.08	1.3	2.1	3.8	6.7
K_{elH2O}, cm^3/s	$7.8\cdot10^{-9}$	$4.4\cdot10^{-8}$	$6.1\cdot10^{-9}$	$6.7\cdot10^{-9}$	$1.5\cdot10^{-8}$	$4.4\cdot10^{-8}$

Table 3.2.2. G factors for e-beam excitation of water molecules

Reaction Formulae	**G factors**	**Ref**
$H_2O + e_b \rightarrow H_2O^+ + e + e_b$	1.68	[2.21]
	1.99	[2.22]
$H_2O + e_b \rightarrow OH^+ + H + e + e_b$	0.373	[2.21]

	0.57	[2.22]
$H_2O + e_b \rightarrow OH + H^+ + e + e_b$	0.461	[2.21]
	0.67	[2.22]
$H_2O + e_b \rightarrow H_2 + O^+ + e + e_b$	0.036	[2.21]
	0.06	[2.22]
$H_2O + e_b \rightarrow H_2^+ + O + e + e_b$	0.0048	[2.21]
	0.01	[2.22]
$H_2O + e_b \rightarrow H + OH + e_b$	4.17	[2.23]
$H_2O + e_b \rightarrow H_2 + O + e_b$	0.45	[2.23]
$H_2O + e_b \rightarrow OH + H^-$	0.356	[2.21]
$H_2O + e_b \rightarrow H_2 + O^-$	0.0175	[2.21]

Table 3.2.3. Energy costs for e-beam excitation of water molecules

N.	Reaction Formulae	Cost, eV	Ref
	$H_2O + e_b \rightarrow H_2O^+ + e + e_b$	59.5 eV	[2.21]
	$H_2O + e_b \rightarrow OH^+ + H + e + e_b$	268.1 eV	[2.21]
	$H_2O + e_b \rightarrow OH + H^+ + e + e_b$	216,9 eV	[2.21]
	$H_2O + e_b \rightarrow H_2 + O^+ + e + e_b$	2777,8 eV	[2.21]
	$H_2O + e_b \rightarrow H_2^+ + O + e + e_b$	20833.3 eV	[2.21]
	$H_2O + e_b \rightarrow H + OH + e_b$	24.0 eV	[2.22]
	$H_2O + e_b \rightarrow H_2 + O + e_b$	222.2 eV	[2.23]
	$H_2O + e_b \rightarrow OH^+ + H^-$	280.9 eV	[2.21]
	$H_2O + e_b \rightarrow H_2^+ + O^-$	5714.3 eV	[2.21]

Table 3.2.4. Rate constants and energy costs relevant to water-vapor plasma chemistry

Gas temperature T is given in K. Electron temperature T_e is given in eV.

*The list of references is represented below the table.

N.	Formulae of reaction	Rate onstant/cost	Defect of energy electrons	referen ce
1	$H_2O + e_b \rightarrow H_2O^+ + e + e_b$	59.5 eV – cost -U		Table 3
2	$H_2O + e_b \rightarrow OH^+ + H + e + e_b$	268.1 eV		Table 3
3	$H_2O + e_b \rightarrow OH + H^+ + e + e_b$	216,9 eV		Table 3
4	$H_2O + e_b \rightarrow H_2 + O^+ + e + e_b$	2777,8 eV		Table 3
5	$H_2O + e_b \rightarrow H_2^+ + O + e + e_b$	20833.3 eV		Table 3
6	$H_2O + e_b \rightarrow H + OH + e_b$	24.0 eV		Table 3
7	$H_2O + e_b \rightarrow H_2 + O + e_b$	222.2 eV		Table 3

8	$H_2O + e_b \rightarrow OH + H^-$	280.9 eV		Table 3
9	$H_2O + e_b \rightarrow H_2 + O^-$	5714.3 eV		Table 3
10	$H_2^+ + e \rightarrow 2H$	$5.\ 10^{-9} \cdot T_e^{-0.5}$	T_e	[1*]
11	$H^+ + 2e \rightarrow H + e$	$4.\ 10^{-27} \cdot T_e^{-9/2}$	$3 \cdot T_e + 13.59$ eV	[1*]
12	$H_2^+ + 2e \rightarrow H_2 + e$	$4.\ 10^{-27} \cdot T_e^{-9/2}$	$3 \cdot T_e + 15.42$ eV	[1*]
13	$H^- + H \rightarrow H_2 + e$	$1.5.\ 10^{-10}$	3.71eV	[13*]
14	$H_2O^+ + H_2O \rightarrow H_3O^+ + OH$	$1.7\ 10^{-9}$		[4*]
15	$H_2O^+ + O_2 \rightarrow O_2^+ + H_2O$	$1.5\ 10^{-10}$		[5*]
16	$H_2O^+ + H_2 \rightarrow H_3O^+ + H$	$1.4\ 10^{-9}$		[13*]
17	$OH^+ + H_2O \rightarrow H_3O^+ + O(D)$	$1.5\ 10^{-9}$		[6*]
18	$OH^+ + H_2O \rightarrow H_2O^+ + OH$	$3.\ 10^{-9}$		[13*]
19	$OH^+ + H \rightarrow O^+ + H_2$	$4.9\ 10^{-10} \cdot \exp(-4177.8/T)$		[1*]
20	$OH^+ + O \rightarrow O^+ + OH$	$1.6\ 10^{-10} \cdot \exp(-5106.2/T)$		[1*]
21	$H^+ + H_2O \rightarrow H_2O^+ + H$	$3.\ 10^{-9}$		[13*]
22	$H^+ + OH \rightarrow OH^+ + H$	$3.\ 10^{-9}$		Typical
23	$H_2^+ + H_2O \rightarrow H_2O^+ + H_2$	$3.6\ 10^{-9}$		[13*]
24	$O^+ + H_2O \rightarrow H_2O^+ + O$	$2.33\ 10^{-9}$		[13*]
25	$O_2^+ + H_2O + M \rightarrow H_2O_3^+ + M$	$2.5\ 10^{-28} \cdot (300/T)^{0.75}$		[7*]
26	$H_2O_3^+ + H_2O \rightarrow H_3O^+ + OH + O_2$	$3.\ 10^{-10}$		[6*]
27	$H_2O_3^+ + H_2O \rightarrow H_4O_2^+ + O_2$	$1.9\ 10^{-9}$		[6*]
28	$H_2O_3^+ + O_2 \rightarrow O_4^+ + H_2O$	$2.\ 10^{-10} \cdot \exp(-300/T)$		[7*]
29	$H_4O_2^+ + H_2O \rightarrow H_5O_2^+ + OH$	$1.\ 10^{-9}$		[4*]
30	$H_2^+ + H_2O \rightarrow H_2 + H_2O^+$	$3.6\ 10^{-9}$		[13*]
31	$H_2^+ + H_2O \rightarrow H + H_3O^+$	$3.4\ 10^{-9}$		[13*]
32	$H_2^+ + O_2 \rightarrow H + HO_2^+$	$1.9\ 10^{-9}$		[13*]
33	$O_2^+ + H_2O \rightarrow H_2O_3^+ + O_2$	$2.2\ 10^{-9}$		[12*]
34	$H_3O^+ + H_2O + M \rightarrow H_5O_2^+ + M$	$3.5\ 10^{-27} \cdot (300/T)^3$		[8*]
35	$H_5O_2^+ + H_2O + M \rightarrow H_7O_3^+ + M$	$2.2\ 10^{-27} \cdot (300/T)^3$		[6*]
36	$H_7O_3^+ + H_2O + M \rightarrow H_9O_4^+ + M$	$2.2\ 10^{-27} \cdot (300/T)^3$		[6*]
37	$e + O_2 + H_2O \rightarrow O_2^- + H_2O$	$2.6\ 10^{-30} T_e^{-1} \cdot \exp(-0.052/T_e)$, eV	$0.5 \cdot T_e + 0.052$ eV	[9*]
38	$H^- + O_2 \rightarrow HO_2 + e$	$1.2\ 10^{-9}$	1.23 eV	[13*]

39	$H^- + H_2O \rightarrow OH^- + H_2$	$3.8\ 10^{-9}$		[13*]
40	$OH^- + O \rightarrow HO_2 + e$	$1.5\ 10^{-9}$	0.89 eV	[13*]
41	$OH^- + H \rightarrow H_2O + e$	$1.\ 10^{-9}$	3.27 eV	[13*]
42	$OH^- + O_3 \rightarrow O_3^- + OH$	$1.\ 10^{-9}$		[13*]
43	$O^- + H_2 \rightarrow H_2O + e$	$6.\ 10^{-10}$	3.56 eV	[13*]
44	$O_2^- + H \rightarrow HO_2 + e$	$1.5\ 10^{-10}$	1.59 eV	[13*]
45	$O_2^- + H_2 \rightarrow OH^- + OH$	$4.\ 10^{-11}$		[13*]
46	$O_2^- + H_2O + M \rightarrow O_2^-H_2O + M$	$19\ 10^{-29}(300/\mathrm{T})^3$		[6*]
47	$O_2^-H_2O + O_2 + H_2O \rightarrow O_2^-(H_2O)_2 + O_2$	$50\ 10^{-29}(300/\mathrm{T})^3$		[6*]
48	$O_3^- + H \rightarrow OH^- + O_2$	$8.4\ 10^{-10}$		[13*]
49	$OH^+ + e \rightarrow O(S) + H$	$6.\ 10^{-9} \cdot T_e^{-0.5}$	T_e	[10*]
50	$H_2O^+ + e \rightarrow H + OH$	$6.6\ 10^{-8} \cdot 0.1 \cdot T_e^{-0.5}$	T_e	[6*]
51	$H_2O^+ + e \rightarrow H_2 + O$	$3.0\ 10^{-8} \cdot 0.1 \cdot T_e^{-0.5}$	T_e	[6*]
52	$H_2O^+ + e \rightarrow 2H + O$	$2.4\ 10^{-8} \cdot 0.1 \cdot T_e^{-0.5}$	T_e	[6*]
53	$H_3O^+ + e \rightarrow H + H_2O$	$1.2\ 10^{-6} \cdot (0.026) \cdot T_e^{-1.}$	T_e	[6*]
54	$H_4O_2^+ + e \rightarrow H + H_2O + OH$	$2.\ 10^{-6}$	$1.5 \cdot T_e$	[10*]
55	$H_5O_2^+ + e \rightarrow H + 2H_2O$	$2.4\ 10^{-6} \cdot (0.026/T_e)^{0.08}$	$1.42 \cdot T_e$	[10*]
56	$H_7O_3^+ + e \rightarrow H + 3H_2O$	$2.4\ 10^{-6} \cdot (0.026/T_e)^{0.08}$	$1.42 \cdot T_e$	[14*]
57	$H_9O_3^+ + e \rightarrow H + 4H_2O$	$2.4\ 10^{-6} \cdot (0.026/T_e)^{0.08}$	$1.42 \cdot T_e$	[14*]
58	$H_2O_3^+ + e \rightarrow 2O + H_2O$	$3.0\ 10^{-6} \cdot (0.026/T_e)^{0.5}$	T_e	[10*]
59	$e + H_2O^+ + H_2O \rightarrow H + OH + H_2$	$2.6\ 10^{-23} \cdot (0.026)^{7/2} \cdot T^{-2} \cdot T_e^{-3/}$		[14*]
60	$e + H_3O^+ + H_2O \rightarrow 2H + OH + H_2$	$2.6\ 10^{-23} \cdot (0.026)^{7/2} \cdot T^{-2} \cdot T_e^{-3}$		[14*]
61	$e + H_5O_2^+ + H_2O \rightarrow H + 3H_2O$	$2.6\ 10^{-23} \cdot (0.026)^{7/2} \cdot T^{-2} \cdot T_e^{-3}$		[14*]
62	$e + H_7O_3^+ + H_2O \rightarrow H + 4H_2O$	$2.6\ 10^{-23} \cdot (0.026)^{7/2} \cdot T^{-2} \cdot T_e^{-3/2}$		[14*]
63	$e + H_9O_4^+ + H_2O \rightarrow H + 5H_2O$	$2.6\ 10^{-23} \cdot (0.026)^{7/2} \cdot T^{-2} \cdot T_e^{-3}$		[14*]

64	$OH^+ + 2e \rightarrow OH + e$	$4.\ 10^{-27} \cdot T_e^{-9/2}$	$3T_e + 13.17$ eV	[1*]
65	$HO_2^+ + 2e \rightarrow HO_2 + e$	$4.\ 10^{-27} \cdot T_e^{-9/2}$	$3T_e + 11.52$ eV	[1*]
66	$H_2O^+ + 2e \rightarrow H_2O + e$	$4.\ 10^{-27} \cdot T_e^{-9/2}$	$3T_e + 12.6$ eV	[1*]
67	$H_3O^+ + 2e \rightarrow H + H_2O + e$	$4.\ 10^{-27} \cdot T_e^{-9/2}$	$3T_e + 6.22$ eV	[1*]
68	$H_4O_2^+ + 2e \rightarrow H + H_2O + OH + e$	$4.\ 10^{-27} \cdot T_e^{-9/2}$	$3T_e + 5.9$ eV	[1*]
69	$H_5O_2^+ + 2e \rightarrow H + 2H_2O + e$	$4.\ 10^{-27} \cdot T_e^{-9/2}$	$3T_e + 4.83$ eV	[1*]
70	$H + H + M \rightarrow H_2 + M$	$4.8\ 10^{-33} \cdot (300/T)^{0.5}$		[13*]
71	$2OH \rightarrow O + H_2O$	$1.8\ 10^{-12}$		[2-3*]
72	$2OH + M \rightarrow M + H_2O_2$	$6.9\ 10^{-31} \cdot (300/T)^{0.8}$		[2-3*]
73	$OH + HO_2 \rightarrow H_2O + O_2$	$4.8\ 10^{-11} \cdot \exp(250/T)$		[2-3*]
74	$OH + O_3 \rightarrow HO_2 + O_2$	$1.9\ 10^{-12} \cdot \exp(-1000/T)$		[2-3*]
75	$OH + H_2O_2 \rightarrow H_2O + HO_2$	$2.9\ 10^{-12} \cdot \exp(-160/T)$		[2-3*]
76	$O + HO_2 \rightarrow OH + O_2$	$3.\ 10^{-11} \cdot \exp(200/T)$		[2-3*]
77	$O + HO \rightarrow H + O_2$	$2.3\ 10^{-11} \cdot \exp(110/T)$		[2-3*]
78	$O(D) + H_2O \rightarrow H_2 + O_2$	$1.4\ 10^{-12}$		[2-3*]
79	$O(D) + H_2O \rightarrow 2OH$	$2.3\ 10^{-10}$		[2-3*]
80	$O(D) + H_2 \rightarrow H + OH$	$1.1\ 10^{-10}$		[2-3*]
81	$O(S) + H_2O \rightarrow O + H_2O$	$3.6\ 10^{-11}$		[9-10*]
82	$O(S) + H_2O \rightarrow O(D) + H_2O$	$1.2\ 10^{-10}$		[9-10*]
83	$O(S) + H_2O \rightarrow 2OH$	$2.5\ 10^{-10}$		[9-10*]
84	$O_2(a^1\Delta) + H_2O \rightarrow O_2 + H_2O$	$4.\ 10^{-18}$		[9-10*]
85	$HO_2 + O_3 \rightarrow OH + 2O_2$	$1.4\ 10^{-14} \cdot \exp(-600/T)$		[2-3*]
86	$H + O_2 \rightarrow HO_2$ $\frac{K_1}{(1+K_1/K_2)} \cdot 0.6^{1/\left[1+lg^2(K_1/K_2)\right]}$	$\frac{K_1}{(1+K_1/K_2)} \cdot 0.6^{1/\left[1+lg^2(K_1/K_2)\right]}$		[2-3*]
		$K_1 = 5.9\ 10^{-32} \cdot (300/T) \cdot M$		[2-3*]
		$K_2 = 7.5\ 10^{-11}$		
87	$H + O_2 + H_2O \rightarrow HO_2 + H_2O$	$6.4\ 10^{-31}(300/T)^3$		[2-3*]
88	$OH + H_2 \rightarrow H + H_2O$	$7.7\ 10^{-12} \cdot \exp(-2100/T)$		[2-3*]
89	$H + O_3 \rightarrow OH + O_2$	$1.4\ 10^{-10} \cdot \exp(-480/T)$		[2-3*]
90	$H + HO_2 \rightarrow H_2 + O_2$	$7.\ 10^{-12}$		[2-3*]

91	$H + HO_2 \rightarrow 2OH$	$8.\ 10^{-11}$		[2-3*]
92	$H + HO_2 \rightarrow H_2O + O$	$2.\ 10^{-12}$		[2-3*]
93	$H + OH \rightarrow H_2 + O$	$1.8\ 10^{-11} \cdot \exp(-4015.3/T)$		[13*]
94	$H_2 + O \rightarrow H + OH$	$1.8\ 10^{-11} \cdot \exp(-4920.5/T)$		[13*]
95	$H + OH + M \rightarrow H_2O + M$	$4.3\ 10^{-31}(300/T)^3$		[13*]
96	$O + H_2O_2 \rightarrow OH + HO_2$	$1.4\ 10^{-12} \cdot \exp(-2000/T)$		[2-3*]
97	$2HO_2 \rightarrow H_2O_2 + O_2$	$2.2\ 10^{-13} \cdot \exp(-600/T)$		[2-3*]
98	$2HO_2 + M \rightarrow H_2O_2 + O_2 + M$	$1.7\ 10^{-33} \cdot \exp(998/T)$		[2-3*]

Literature to the Table 3.2.4.

***-indication of references**

1. Smirnov B.M.Ions and excited states in plasmas. Moscow Atomizdat. 1974.
2. Baulch D.L., Atkinson R., et.al. Evaluated kinetic and photochemical data for atmospheric chemistry. J. Phys. Chem. Ref. Data. 1980. V. 9. N.2. P.295; Atkinson R., Baulch D.L., et.al. Evaluated kinetic and photochemical data for atmospheric chemistry. J. Phys. Chem. Ref. Data. 1989. V. 18. N.2. P.881.
3. Mac-Iven M., Phillips L. Atmospheric chemistry. Moscow. Mir. 1978.
4. Shul R.J. et al. Ion -molecule reactions involving H_3O^+, H_3O^+ and OH^+ reactions at thermal energy. J. Phys. Chem. 1988. V.92. N.17. P.4947.
5. Bruskin L.G. et al. Modeling of neutral gas releases into the Earth ionosphere. Pure Appl. Geophys. 1988. V.127. N.2/3. P.415.
6. Smirnov B.M. Complex ions. Moscow Nauka. 1983.
7. Good A. et al. Mechanisms and rate constants of ion-molecule reactions leading to formation of $H^+(H_2O)_n$ in moist oxygen and air. J. Chem. Phys. 1970. V.52. N.1. P.222.
8. Aleksandrov N.L. Three body attachment of electron to a molecule. Uspekhi Fizicheskikh Nauk. 1988. VT. 154. № 2. P. 177
9. Krivonosova O.E. et al. Recommended data on chemical reaction rates between molecules consisting of atoms O and N. In Collection of works Khimia Plasmy. Ed. B.M. Smirnov. Moscow. Energoatomizdat. 1987. № 14. P.3.
10. Fomin O.K. Elementary processes in air plasmas with participation of electronically excited particles and their kinetic characteristics. Works of Institute of Experimental Meteorology (123). N. 40. Leningrad. Gigrometeoizdat. 1986. P.75.
11. Fehsenfeld F.G., et al. Ion-molecule reactions in $O_2 - H_2O$ system. J. Chem. Phys. 1971. V.55. N.5. P.2115.

12. Kondratiev V.N. Rate constants of gas-phase reactions. Reference book. Moscow. Nauka. 1970.
13. Virin L.I. et al. Ion-molecule reactions in gases. Reference book. Moscow. Nauka. 1979.
14. Bychkov V., Yurovskii V.A. The modeling of water vapor beam plasma. Teplofizika Vysokikh Temperatur (High Temperature in English edition). 1993. V.31. P.8-17.

Table 3.2.5. Channels of ion O^- recombination in humid air.

N	reaction	Rate constant, cm^3/s, cm^6/s
1	$O^- + H_2O^+ \rightarrow O + H_2O$	$9.5\cdot10^{-8}(300/T)^{0.5}$
2	$O^- + H_2O^+ + M \rightarrow O + H_2O + M$	$2.0\cdot10^{-25}(300/T)^{2.5}$
3	$O^- + OH^+ \rightarrow O + OH$	$1.3\cdot10^{-7}(300/T)^{0.5}$
4	$O^- + OH^+ + M \rightarrow O + OH + M$	$2.0\cdot10^{-25}(300/T)^{2.5}$
5	$O^- + H^+ \rightarrow O + H$	$2.8\cdot10^{-7}(300/T)^{0.5}$
6	$O^- + H^+ + M \rightarrow O + H + M$	$2.0\cdot10^{-25}(300/T)^{2.5}$
7	$O^- + H_2^+ \rightarrow O + H_2$	$2.1\cdot10^{-7}(300/T)^{0.5}$
8	$O^- + H_2^+ + M \rightarrow O + H_2 + M$	$2.0\cdot10^{-25}(300/T)^{2.5}$
9	$O^- + HO_2^+ \rightarrow O + H + O_2$	$8.4\cdot10^{-8}(300/T)^{0.5}$
10	$O^- + HO_2^+ + M \rightarrow O + H + O_2 + M$	$2.0\cdot10^{-25}(300/T)^{2.5}$
11	$O^- + H_3O^+ \rightarrow O + H + H_2O$	$9.4\cdot10^{-8}(300/T)^{0.5}$
12	$O^- + H_3O^+ + M \rightarrow O + H + H_2O + M$	$2.0\cdot10^{-25}(300/T)^{2.5}$
13	$O^- + H_2O_3^+ \rightarrow O_2 + O + H_2O$	$7.9\cdot10^{-8}(300/T)^{0.5}$
14	$O^- + H_2O_3^+ + M \rightarrow O_2 + O + H_2O + M$	$2.0\cdot10^{-25}(300/T)^{2.5}$
15	$O^- + H_4O_2^+ \rightarrow O + 2H_2O$	$8.3\cdot10^{-8}(300/T)^{0.5}$
16	$O^- + H_4O_2^+ + M \rightarrow O + 2H_2O + M$	$2.0\cdot10^{-25}(300/T)^{2.5}$
17	$O^- + H_5O_2^+ \rightarrow O + H + 2H_2O$	$8.3\cdot10^{-8}(300/T)^{0.5}$
18	$O^- + H_5O_2^+ + M \rightarrow O + H + 2H_2O + M$	$2.0\cdot10^{-25}(300/T)^{2.5}$
19	$O^- + H_7O_3^+ \rightarrow O + H + 3H_2O$	$7.8\cdot10^{-8}(300/T)^{0.5}$
20	$O^- + H_7O_3^+ + M \rightarrow O + H + 3H_2O + M$	$2.0\cdot10^{-25}(300/T)^{2.5}$
21	$O^- + H_9O_4^+ \rightarrow O + H + 4H_2O$	$8.0\cdot10^{-8}(300/T)^{0.5}$
22	$O^- + H_9O_4^+ + M \rightarrow O + H + 4H_2O + M$	$2.0\cdot10^{-25}(300/T)^{2.5}$

Table 3.2.6. Channels of ion O_2^- recombination in humid air.

N	reaction	Rate constant, cm^3/s, cm^6/s
1	$O_2^- + H_2O^+ \rightarrow O_2 + H_2O$	$8.1\cdot10^{-8}(300/T)^{0.5}$
2	$O_2^- + H_2O^+ + M \rightarrow O_2 + H_2O + M$	$2.0\cdot10^{-25}(300/T)^{2.5}$

3	$O_2^- + OH^+ \rightarrow O_2 + OH$	$8.1 \cdot 10^{-8} (300/T)^{0.5}$
4	$O_2^- + OH^+ + M \rightarrow O_2 + OH + M$	$2.0 \cdot 10^{-25} (300/T)^{2.5}$
5	$O_2^- + H^+ \rightarrow O_2 + H$	$2.8 \cdot 10^{-7} (300/T)^{0.5}$
6	$O_2^- + H^+ + M \rightarrow O_2 + H + M$	$2.0 \cdot 10^{-25} (300/T)^{2.5}$
7	$O_2^- + H_2^+ \rightarrow O_2 + H_2$	$2.0 \cdot 10^{-7} (300/T)^{0.5}$
8	$O_2^- + H_2^+ + M \rightarrow O_2 + H_2 + M$	$2.0 \cdot 10^{-25} (300/T)^{2.5}$
9	$O_2^- + HO_2^+ \rightarrow O_2 + H + O_2$	$6.9 \cdot 10^{-8} (300/T)^{0.5}$
10	$O_2^- + HO_2^+ + M \rightarrow O_2 + H + O_2 + M$	$2.0 \cdot 10^{-25} (300/T)^{2.5}$
11	$O_2^- + H_3O^+ \rightarrow O_2 + H + H_2O$	$8.0 \cdot 10^{-8} (300/T)^{0.5}$
12	$O_2^- + H_3O^+ + M \rightarrow O_2 + H + H_2O + M$	$2.0 \cdot 10^{-25} (300/T)^{2.5}$
13	$O_2^- + H_2O_3^+ \rightarrow 2O_2 + H_2O$	$6.2 \cdot 10^{-8} (300/T)^{0.5}$
14	$O_2^- + H_2O_3^+ + M \rightarrow 2O_2 + H_2O + M$	$2.0 \cdot 10^{-25} (300/T)^{2.5}$
15	$O_2^- + H_4O_2^+ \rightarrow O_2 + 2H_2O$	$6.7 \cdot 10^{-8} (300/T)^{0.5}$
16	$O_2^- + H_4O_2^+ + M \rightarrow O_2 + 2H_2O + M$	$2.0 \cdot 10^{-25} (300/T)^{2.5}$
17	$O_2^- + H_5O_2^+ \rightarrow O_2 + H + 2H_2O$	$6.7 \cdot 10^{-8} (300/T)^{0.5}$
18	$O_2^- + H_5O_2^+ + M \rightarrow O_2 + H + 2H_2O + M$	$2.0 \cdot 10^{-25} (300/T)^{2.5}$
19	$O_2^- + H_7O_3^+ \rightarrow O_2 + H + 3H_2O$	$6.0 \cdot 10^{-8} (300/T)^{0.5}$
20	$O_2^- + H_7O_3^+ + M \rightarrow O_2 + H + 3H_2O + M$	$2.0 \cdot 10^{-25} (300/T)^{2.5}$
21	$O_2^- + H_9O_4^+ \rightarrow O_2 + H + 4H_2O$	$5.8 \cdot 10^{-8} (300/T)^{0.5}$
22	$O_2^- + H_9O_4^+ + M \rightarrow O_2 + H + 4H_2O + M$	$2.0 \cdot 10^{-25} (300/T)^{2.5}$

Table 3.2.7. Channels of ion O_3^- recombination in humid air .

N	reaction	Rate constant, cm^3/s, cm^6/s
1	$O_3^- + H_2O^+ \rightarrow O_3 + H_2O$	$7.6 \cdot 10^{-8} (300/T)^{0.5}$
2	$O_3^- + H_2O^+ + M \rightarrow O_3 + H_2O + M$	$2.0 \cdot 10^{-25} (300/T)^{2.5}$
3	$O_3^- + OH^+ \rightarrow O_3 + OH$	$7.8 \cdot 10^{-8} (300/T)^{0.5}$
4	$O_3^- + OH^+ + M \rightarrow O_3 + OH + M$	$2.0 \cdot 10^{-25} (300/T)^{2.5}$
5	$O_3^- + H^+ \rightarrow O_3 + H$	$2.8 \cdot 10^{-7} (300/T)^{0.5}$
6	$O_3^- + H^+ + M \rightarrow O_3 + H + M$	$2.0 \cdot 10^{-25} (300/T)^{2.5}$
7	$O_3^- + H_2^+ \rightarrow O_3 + H_2$	$2.0 \cdot 10^{-7} (300/T)^{0.5}$
8	$O_3^- + H_2^+ + M \rightarrow O_3 + H_2 + M$	$2.0 \cdot 10^{-25} (300/T)^{2.5}$
9	$O_3^- + HO_2^+ \rightarrow O_3 + H + O_2$	$6.2 \cdot 10^{-8} (300/T)^{0.5}$
10	$O_3^- + HO_2^+ + M \rightarrow O_3 + H + O_2 + M$	$2.0 \cdot 10^{-25} (300/T)^{2.5}$
11	$O_3^- + H_3O^+ \rightarrow O_3 + H + H_2O$	$7.5 \cdot 10^{-8} (300/T)^{0.5}$
12	$O_3^- + H_3O^+ + M \rightarrow O_3 + H + H_2O + M$	$2.0 \cdot 10^{-25} (300/T)^{2.5}$

13	$O_3^- + H_2O_3^+ \rightarrow O_2 + O_3 + H_2O$	$5.6 \cdot 10^{-8} (300/T)^{0.5}$
14	$O_3^- + H_2O_3^+ + M \rightarrow O_2 + O_3 + H_2O + M$	$2.0 \cdot 10^{-25} (300/T)^{2.5}$
15	$O_3^- + H_4O_2^+ \rightarrow O_3 + 2H_2O$	$5.9 \cdot 10^{-8} (300/T)^{0.5}$
16	$O_3^- + H_4O_2^+ + M \rightarrow O_3 + 2H_2O + M$	$2.0 \cdot 10^{-25} (300/T)^{2.5}$
17	$O_3^- + H_5O_2^+ \rightarrow O_3 + H + 2H_2O$	$5.9 \cdot 10^{-8} (300/T)^{0.5}$
18	$O_3^- + H_5O_2^+ + M \rightarrow O_3 + H + 2H_2O + M$	$2.0 \cdot 10^{-25} (300/T)^{2.5}$
19	$O_3^- + H_7O_3^+ \rightarrow O_3 + H + 3H_2O$	$5.2 \cdot 10^{-8} (300/T)^{0.5}$
20	$O_3^- + H_7O_3^+ + M \rightarrow O_3 + H + 3H_2O + M$	$2.0 \cdot 10^{-25} (300/T)^{2.5}$
21	$O_3^- + H_9O_4^+ \rightarrow O_3 + H + 4H_2O$	$5.1 \cdot 10^{-8} (300/T)^{0.5}$
22	$O_3^- + H_9O_4^+ + M \rightarrow O_3 + H + 4H_2O + M$	$2.0 \cdot 10^{-25} (300/T)^{2.5}$

Table 3.2.8. Channels of ion H^- recombination in humid air .

N	**reaction**	**Rate constant, cm^3/s, cm^6/s**
1	$H^- + H_2O^+ \rightarrow H + H_2O$	$2.8 \cdot 10^{-7} (300/T)^{0.5}$
2	$H^- + H_2O^+ + M \rightarrow H + H_2O + M$	$2.0 \cdot 10^{-25} (300/T)^{2.5}$
3	$H^- + OH^+ \rightarrow H + OH$	$2.8 \cdot 10^{-7} (300/T)^{0.5}$
4	$H^- + OH^+ + M \rightarrow H + OH + M$	$2.0 \cdot 10^{-25} (300/T)^{2.5}$
5	$H^- + H^+ \rightarrow H + H$	$3.9 \cdot 10^{-7} (300/T)^{0.5}$
6	$H^- + H^+ + M \rightarrow H + H + M$	$2.0 \cdot 10^{-25} (300/T)^{2.5}$
7	$H^- + H_2^+ \rightarrow H + H_2$	$3.4 \cdot 10^{-7} (300/T)^{0.5}$
8	$H^- + H_2^+ + M \rightarrow H + H_2 + M$	$2.0 \cdot 10^{-25} (300/T)^{2.5}$
9	$H^- + HO_2^+ \rightarrow H + H + O_2$	$2.8 \cdot 10^{-7} (300/T)^{0.5}$
10	$H^- + HO_2^+ + M \rightarrow H + H + O_2 + M$	$2.0 \cdot 10^{-25} (300/T)^{2.5}$
11	$H^- + H_3O^+ \rightarrow H + H + H_2O$	$2.8 \cdot 10^{-7} (300/T)^{0.5}$
12	$H^- + H_3O^+ + M \rightarrow H + H + H_2O + M$	$2.0 \cdot 10^{-25} (300/T)^{2.5}$
13	$H^- + H_2O_3^+ \rightarrow O_2 + H + H_2O$	$2.8 \cdot 10^{-7} (300/T)^{0.5}$
14	$H^- + H_2O_3^+ + M \rightarrow O_2 + H + H_2O + M$	$2.0 \cdot 10^{-25} (300/T)^{2.5}$
15	$H^- + H_4O_2^+ \rightarrow H + 2H_2O$	$2.8 \cdot 10^{-7} (300/T)^{0.5}$
16	$H^- + H_4O_2^+ + M \rightarrow H + 2H_2O + M$	$2.0 \cdot 10^{-25} (300/T)^{2.5}$
17	$H^- + H_5O_2^+ \rightarrow H + H + 2H_2O$	$2.8 \cdot 10^{-7} (300/T)^{0.5}$
18	$H^- + H_5O_2^+ + M \rightarrow H + H + 2H_2O + M$	$2.0 \cdot 10^{-25} (300/T)^{2.5}$
19	$H^- + H_7O_3^+ \rightarrow H + H + 3H_2O$	$2.8 \cdot 10^{-7} (300/T)^{0.5}$
20	$H^- + H_7O_3^+ + M \rightarrow H + H + 3H_2O + M$	$2.0 \cdot 10^{-25} (300/T)^{2.5}$
21	$H^- + H_9O_4^+ \rightarrow H + H + 4H_2O$	

22	$H^- + H_9O_4^+ + M \rightarrow H + H + 4H_2O + M$	$2.0 \cdot 10^{-25}(300/T)^{2.5}$

Table 3.2.9. Channels of ion OH^- recombination in humid air .

N	reaction	Rate constant, cm^3/s, cm^6/s
1	$OH^- + H_2O^+ \rightarrow OH + H_2O$	$9 \cdot 10^{-8}(300/T)^{0.5}$
2	$OH^- + H_2O^+ + M \rightarrow OH + H_2O + M$	$2.0 \cdot 10^{-25}(300/T)^{2.5}$
3	$OH^- + OH^+ \rightarrow OH + OH$	$9.5 \cdot 10^{-8}(300/T)^{0.5}$
4	$OH^- + OH^+ + M \rightarrow OH + OH + M$	$2.0 \cdot 10^{-25}(300/T)^{2.5}$
5	$OH^- + H^+ \rightarrow OH + H$	$2.8 \cdot 10^{-7}(300/T)^{0.5}$
6	$OH^- + H^+ + M \rightarrow OH + H + M$	$2.0 \cdot 10^{-25}(300/T)^{2.5}$
7	$OH^- + H_2^+ \rightarrow OH + H_2$	$2.1 \cdot 10^{-7}(300/T)^{0.5}$
8	$OH^- + H_2^+ + M \rightarrow OH + H_2 + M$	$2.0 \cdot 10^{-25}(300/T)^{2.5}$
9	$OH^- + HO_2^+ \rightarrow OH + H + O_2$	$8.2 \cdot 10^{-8}(300/T)^{0.5}$
10	$OH^- + HO_2^+ + M \rightarrow OH + H + O_2 + M$	$2.0 \cdot 10^{-25}(300/T)^{2.5}$
11	$OH^- + H_3O^+ \rightarrow OH + H + H_2O$	$9.2 \cdot 10^{-8}(300/T)^{0.5}$
12	$OH^- + H_3O^+ + M \rightarrow OH + H + H_2O + M$	$2.0 \cdot 10^{-25}(300/T)^{2.5}$
13	$OH^- + H_2O_3^+ \rightarrow O_2 + OH + H_2O$	$7.7 \cdot 10^{-8}(300/T)^{0.5}$
14	$OH^- + H_2O_3^+ + M \rightarrow O_2 + OH + H_2O +$	$2.0 \cdot 10^{-25}(300/T)^{2.5}$
15	$OH^- + H_4O_2^+ \rightarrow OH + 2H_2O$	$8.1 \cdot 10^{-8}(300/T)^{0.5}$
16	$OH^- + H_4O_2^+ + M \rightarrow OH + 2H_2O + M$	$2.0 \cdot 10^{-25}(300/T)^{2.5}$
17	$OH^- + H_5O_2^+ \rightarrow OH + H + 2H_2O$	$8.1 \cdot 10^{-8}(300/T)^{0.5}$
18	$OH^- + H_5O_2^+ + M \rightarrow OH + H + 2H_2O + M$	$2.0 \cdot 10^{-25}(300/T)^{2.5}$
19	$OH^- + H_7O_3^+ \rightarrow OH + H + 3H_2O$	$7.7 \cdot 10^{-8}(300/T)^{0.5}$
20	$OH^- + H_7O_3^+ + M \rightarrow OH + H + 3H_2O + M$	$2.0 \cdot 10^{-25}(300/T)^{2.5}$
21	$OH^- + H_9O_4^+ \rightarrow OH + H + 4H_2O$	$7.4 \cdot 10^{-8}(300/T)^{0.5}$
22	$OH^- + H_9O_4^+ + M \rightarrow OH + H + 4H_2O + M$	$2.0 \cdot 10^{-25}(300/T)^{2.5}$

Table 3.2.10. Channels of ion O_2^- H_2O recombination in humid air .

N	reaction	Rate constant, cm^3/s, cm^6/s
1	$O_2^- H_2O + H_2O^+ \rightarrow O_2 + 2H_2O$	$7.6 \cdot 10^{-8}(300/T)^{0.5}$
2	$O_2^- H_2O + H_2O^+ + M \rightarrow O_2 + 2H_2O + M$	$2.0 \cdot 10^{-25}(300/T)^{2.5}$

3	$O_2^- H_2O + OH^+ \rightarrow O_2 + H_2O + OH$	$7.6 \cdot 10^{-8} (300/T)^{0.5}$
4	$O_2^- H_2O + OH^+ + M \rightarrow O_2 + H_2O + OH + M$	$2.0 \cdot 10^{-25} (300/T)^{2.5}$
5	$O_2^- H_2O + H^+ \rightarrow O_2 + H_2O + H$	$2.8 \cdot 10^{-7} (300/T)^{0.5}$
6	$O_2^- H_2O + H^+ + M \rightarrow O_2 + H_2O + H + M$	$2.0 \cdot 10^{-25} (300/T)^{2.5}$
7	$O_2^- H_2O + H_2^+ \rightarrow O_2 + H_2O + H_2$	$2.0 \cdot 10^{-7} (300/T)^{0.5}$
8	$O_2^- H_2O + H_2^+ + M \rightarrow O_2 + H_2O + H_2 + M$	$2.0 \cdot 10^{-25} (300/T)^{2.5}$
9	$O_2^- H_2O + HO_2^+ \rightarrow O_2 + H_2O + H + O_2$	$6.2 \cdot 10^{-8} (300/T)^{0.5}$
10	$O_2^- H_2O + HO_2^+ + M \rightarrow O_2 + H_2O + H + O_2 + M$	$2.0 \cdot 10^{-25} (300/T)^{2.5}$
11	$O_2^- H_2O + H_3O^+ \rightarrow O_2 + H + 2H_2O$	$7.4 \cdot 10^{-8} (300/T)^{0.5}$
12	$O_2^- H_2O + H_3O^+ + M \rightarrow O_2 + H_2O + H + H_2O + M$	$2.0 \cdot 10^{-25} (300/T)^{2.5}$
13	$O_2^- H_2O + H_2O_3^+ \rightarrow 2O_2 + 2H_2O$	$5.5 \cdot 10^{-8} (300/T)^{0.5}$
14	$O_2^- H_2O + H_2O_3^+ + M \rightarrow 2O_2 + 2H_2O + M$	$2.0 \cdot 10^{-25} (300/T)^{2.5}$
15	$O_2^- H_2O + H_4O_2^+ \rightarrow O_2 + 3H_2O$	$6.0 \cdot 10^{-8} (300/T)^{0.5}$
16	$O_2^- H_2O + H_4O_2^+ + M \rightarrow O_2 + 3H_2O + M$	$2.0 \cdot 10^{-25} (300/T)^{2.5}$
17	$O_2^- H_2O + H_5O_2^+ \rightarrow O_2 + H + 3H_2O$	$6.0 \cdot 10^{-8} (300/T)^{0.5}$
18	$O_2^- H_2O + H_5O_2^+ + M \rightarrow O_2 + H + 3H_2O + M$	$2.0 \cdot 10^{-25} (300/T)^{2.5}$
19	$O_2^- H_2O + H_7O_3^+ \rightarrow O_2 + H + 4H_2O$	$5.4 \cdot 10^{-8} (300/T)^{0.5}$
20	$O_2^- H_2O + H_7O_3^+ + M \rightarrow O_2 + H + 4H_2O + M$	$2.0 \cdot 10^{-25} (300/T)^{2.5}$
21	$O_2^- H_2O + H_9O_4^+ \rightarrow O_2 + H + 5H_2O$	$5.1 \cdot 10^{-8} (300/T)^{0.5}$
22	$O_2^- H_2O + H_9O_4^+ + M \rightarrow O_2 + H + 5H_2O + M$	$2.0 \cdot 10^{-25} (300/T)^{2.5}$

Table 3.2.11. Channels of ion $O_2^- (H_2O)_2$ recombination in humid air.

N	reaction	Rate constant, cm^3/s, cm^6/s
1	$O_2^- (H_2O)_2 + H_2O^+ \rightarrow O_2 + 3H_2O$	$7.3 \cdot 10^{-8} (300/T)^{0.5}$
2	$O_2^- (H_2O)_2 + H_2O^+ + M \rightarrow O_2 + 3H_2O + M$	$2.0 \cdot 10^{-25} (300/T)^{2.5}$

3	$O_2^-(H_2O)_2 + OH^+ \rightarrow O_2 + 2H_2O + OH$	$7.3\cdot10^{-8}(300/T)^{0.5}$
4	$O_2^-(H_2O)_2 + OH^+ + M \rightarrow O_2 + 2H_2O + OH + M$	$2.0\cdot10^{-25}(300/T)^{2.5}$
5	$O_2^-(H_2O)_2 + H^+ \rightarrow O_2 + 2H_2O + H$	$2.8\cdot10^{-7}(300/T)^{0.5}$
6	$O_2^-(H_2O)_2 + H^+ + M \rightarrow O_2 + 2H_2O + H + M$	$2.0\cdot10^{-25}(300/T)^{2.5}$
7	$O_2^-(H_2O)_2 + H_2^+ \rightarrow O_2 + 2H_2O + H_2$	$2.0\cdot10^{-7}(300/T)^{0.5}$
8	$O_2^-(H_2O)_2 + H_2^+ + M \rightarrow O_2 + 2H_2O + H_2 + M$	$2.0\cdot10^{-25}(300/T)^{2.5}$
9	$O_2^-(H_2O)_2 + HO_2^+ \rightarrow O_2 + 2H_2O + H + O_2$	$5.6\cdot10^{-8}(300/T)^{0.5}$
10	$O_2^-(H_2O)_2 + HO_2^+ + M \rightarrow O_2 + 2H_2O + H + O_2 + M$	$2.0\cdot10^{-25}(300/T)^{2.5}$
11	$O_2^-(H_2O)_2 + H_3O^+ \rightarrow O_2 + H + 3H_2O$	$7.2\cdot10^{-8}(300/T)^{0.5}$
12	$O_2^-(H_2O)_2 + H_3O^+ + M \rightarrow O_2 + H + 3H_2O + M$	$2.0\cdot10^{-25}(300/T)^{2.5}$
13	$O_2^-(H_2O)_2 + H_2O_3^+ \rightarrow 2O_2 + 3H_2O$	$5.5\cdot10^{-8}(300/T)^{0.5}$
14	$O_2^-(H_2O)_2 + H_2O_3^+ + M \rightarrow 2O_2 + 3H_2O + M$	$2.0\cdot10^{-25}(300/T)^{2.5}$
15	$O_2^-(H_2O)_2 + H_4O_2^+ \rightarrow O_2 + 4H_2O$	$5.7\cdot10^{-8}(300/T)^{0.5}$
16	$O_2^-(H_2O)_2 + H_4O_2^+ + M \rightarrow O_2 + 4H_2O + M$	$2.0\cdot10^{-25}(300/T)^{2.5}$
17	$O_2^-(H_2O)_2 + H_5O_2^+ \rightarrow O_2 + H + 4H_2O$	$5.7\cdot10^{-8}(300/T)^{0.5}$
18	$O_2^-(H_2O)_2 + H_5O_2^+ + M \rightarrow O_2 + H + 4H_2O + M$	$2.0\cdot10^{-25}(300/T)^{2.5}$
19	$O_2^-(H_2O)_2 + H_7O_3^+ \rightarrow O_2 + H + 5H_2O$	$5.0\cdot10^{-8}(300/T)^{0.5}$
20	$O_2^-(H_2O)_2 + H_7O_3^+ + M \rightarrow O_2 + H + 5H_2O + M$	$2.0\cdot10^{-25}(300/T)^{2.5}$
21	$O_2^-(H_2O)_2 + H_9O_4^+ \rightarrow O_2 + H + 6H_2O$	$4.6\cdot10^{-8}(300/T)^{0.5}$
22	$O_2^-(H_2O)_2 + H_9O_4^+ + M \rightarrow O_2 + H + 6H_2O + M$	$2.0\cdot10^{-25}(300/T)^{2.5}$

3.2.4.2. Calculation results for propane-air mixture containing water vapor.

Below we represent calculation results for propane-air mixture containing water vapor and reactions in it both by the model accounting for water vapor and reactions in it and by the model in the dry mixture without accounting of reactions with water molecules. We have carried out calculations both for the plasmas created by the electron beam and for those created in the non-selfmaintained discharge. We also represent data on temperature evolution in these mixtures, dry and humid air, since it helps to analyze results of investigations.

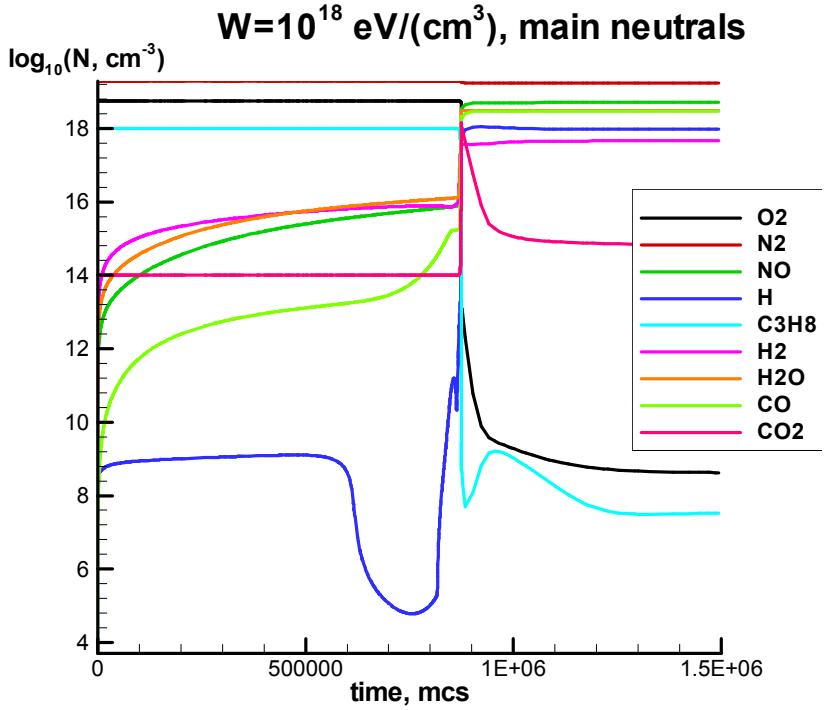

Fig.3.2.12. Main neutral components in the electron-beam plasma of dry propane-air mixture at the excitation velocity by the electron beam $W=10^{18}$ eV/(cm^3·s).

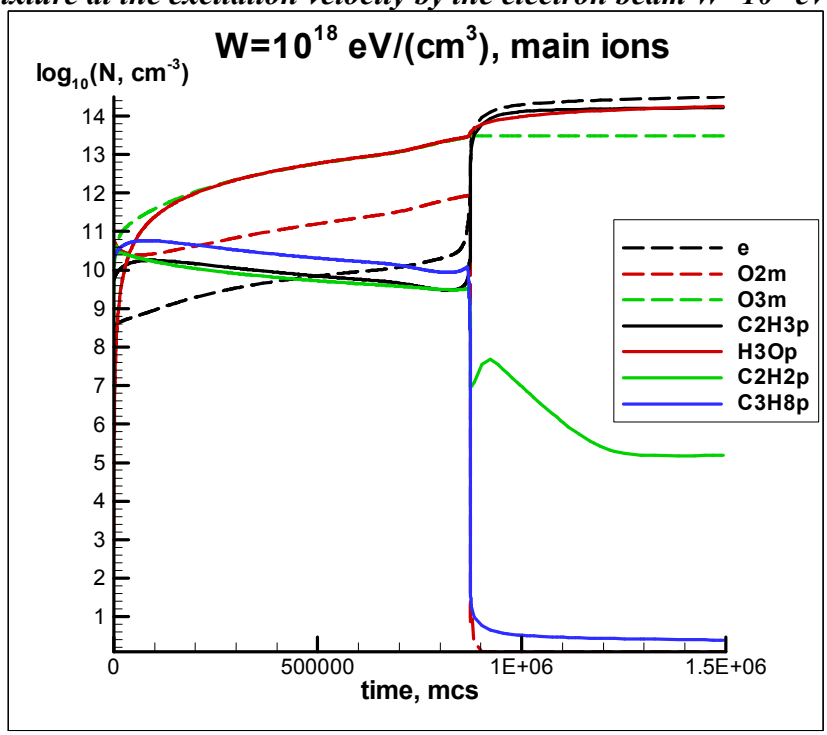

Fig.3.2.13. Main charged components (m-negative, p-positive, e-electrons), in the electron-beam plasma of dry propane-air mixture at the excitation velocity by the electron beam $W=10^{18}$ eV/(cm^3·s).

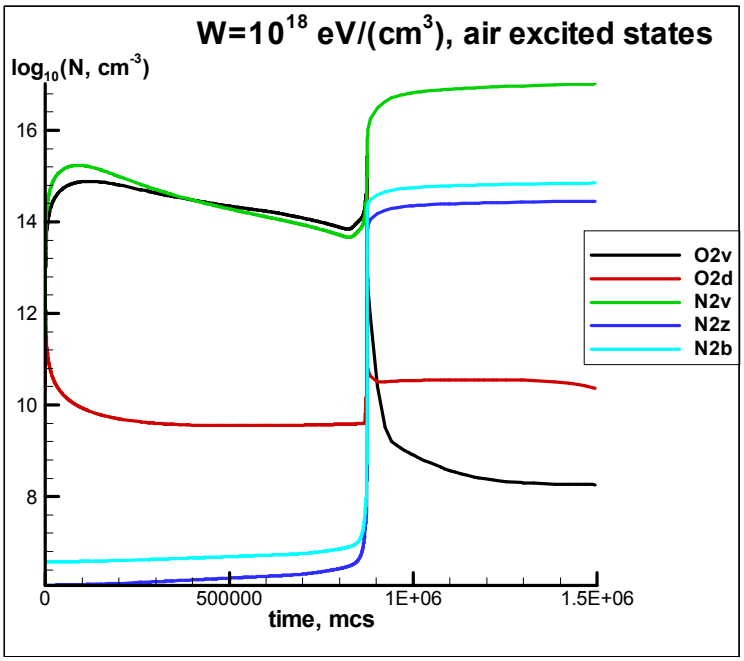

Fig.3.2.14. Main excited particles (v-vibrational, d,b,z-electronic excitation)), in the electron-beam plasma of dry propane-air mixture at the excitation velocity by the electron beam $W=10^{18}eV/(cm^3 \cdot s)$.

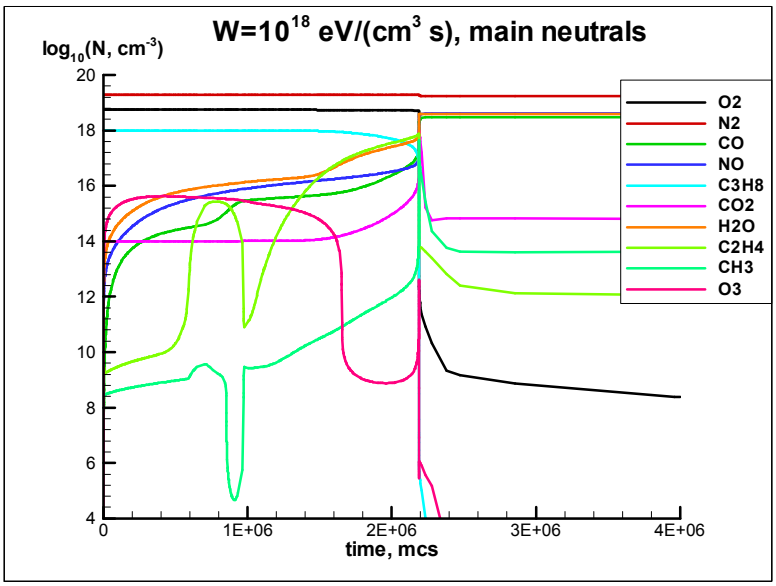

Fig.3.2.15. Main neutral components in the electron-beam plasma of the humid propane-air mixture at the excitation velocity by the electron beam $W=10^{18}eV/(cm^3 \cdot s)$.

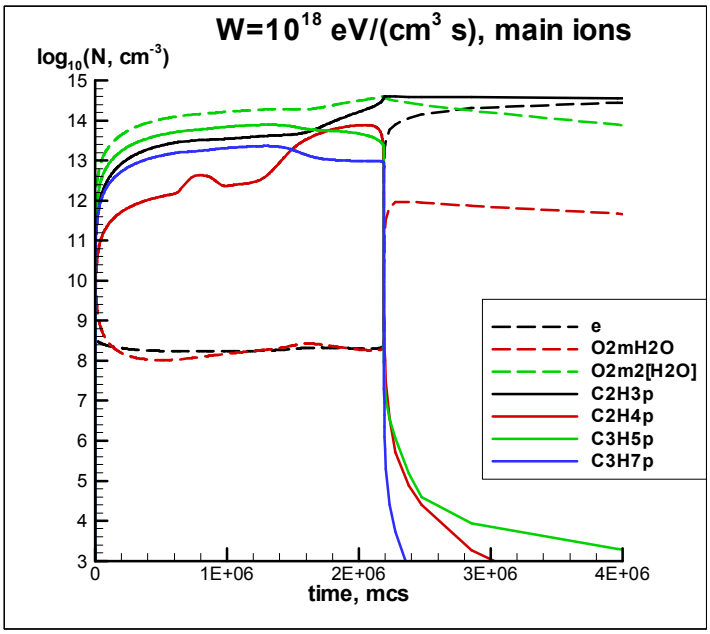

Fig.3.2.16. Main ions in the electron-beam plasma of the humid propane-air mixture at the excitation velocity by the electron beam $W=10^{18}eV/(cm^3 \cdot s)$.

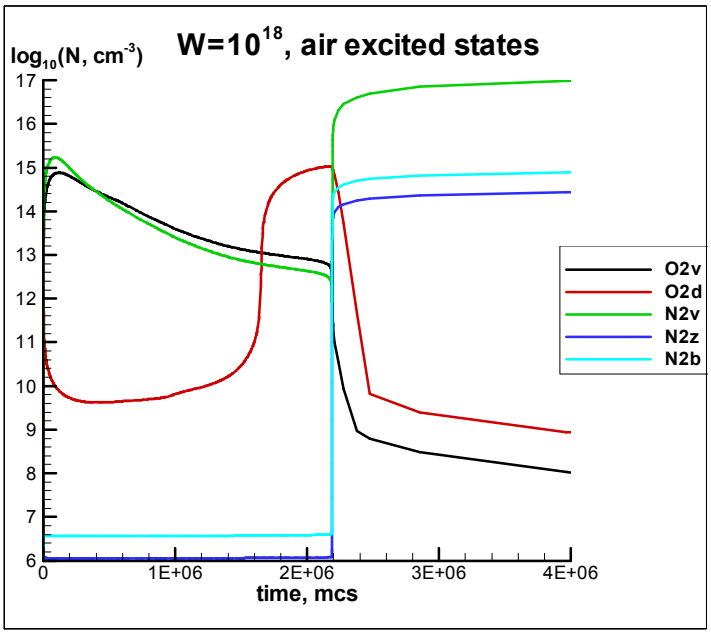

Fig.3.2.17. Main excited particles (v-vibrational, d,b,z-electronic excitation)), in the electron-beam plasma of humid propane-air mixture at the excitation velocity by the electron beam of $W=10^{18}eV/(cm^3 \cdot s)$.

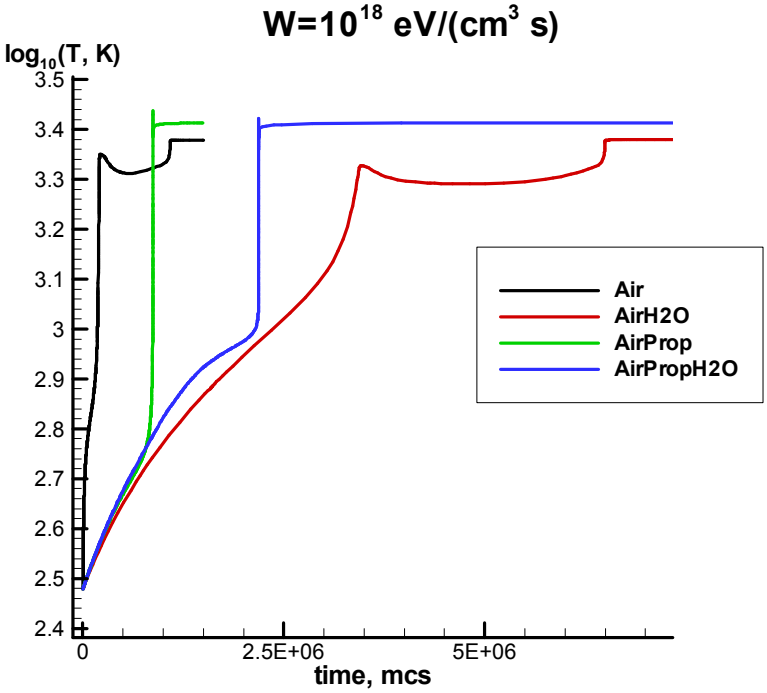

Fig.3.2.18. Temperature evolution in the beam plasma of dry air, humid air, dry propane-air mixture and humid propane-air mixture at the excitation velocity by the electron beam of $W=10^{18}$ eV/(cm^3·s).

In Fig.3.2.12-3.2.18 one can see results electron-beam impact on the propane-air mixture at the excitation velocity by the electron-beam of $W=10^{18}$ eV/(cm^3·s).

It follows from the Fig.3.2.12 that main neutral particles in "dry" mixture after the inflammation are molecules N_2, H_2O, NO and CO. This composition indicates practically complete burning out of molecular oxygen in processes of dissociation into atoms and chemical reactions, leading in particular to creation and accumulation of NO molecules.

One can see in Fig.3.2.13 that main charged particles before the inflammation were negative ions O_3^- and positive ions H_3O^+; but after the inflammation main particles become electrons, e, and positive ions H_3O^+ and $C_2H_3^+$; at that the concentrations of the latter rise that is connected with slower electron-ion recombination in the hot gas (after the inflammation) with respect to the ion – ion recombination in the cold gas (before the inflammation).

It follows from the Fig.3.2.14 that main excited particles that play important role at the ignition are oxygen molecules in the state $O_2(^1\Delta)$.

It follows from the Fig.3.2.15 that main neutral particles in the humid mixture in the beam plasma after the inflammation are N_2, H_2O, NO and CO. This composition indicates practically complete burning out of molecular oxygen in processes of dissociation into atoms and chemical reactions, leading in particular to creation and accumulation of NO molecules, and because of this the generation of CO_2 is decelerated.

One can see in Fig.3.2.16 that main charged particles before the inflammation were negative ions O_3^- and positive ions H_3O^+, and after the inflammation they become electrons e, and positive ions H_3O^+ and $C_2H_3^+$, at that the concentrations of the latter rise that is connected with slower electron-ion recombination in the hot gas (after the inflammation) with respect to the ion – ion recombination in the cold gas (before the inflammation).

It follows from the Fig.3.2.17 that that main excited particles that play important role at the ignition are oxygen molecules in the state $O_2(^1\Delta)$.

Fig.3.2.18 that heating time in the plasma of the humid mixture decelerates approximately for a one order of magnitude with respect to the plasma gas heating in the dry

mixture. At that the inflammation features of the plasma in the dry mixture are close to the plasma of the dry air, but the plasma features in the humid mixture are close to those of the humid air plasma.

In Fig.3.2.19 – 3.2.25 we represent computation results of the non-selfmaintained gaseous discharge impact on the propane air stoichiometric mixture at the velocity of the excitation by the electron beam $W=10^{18}$ eV/(cm^3·s) and the external electric field strength of E=3 kV/cm. (Conditions are close to the experimental ones).

One can see from Fig.3.2.19 that main neutral particles in the dry mixture of non-selfmaintained gaseous discharge after the inflammation become N_2, H_2O, NO и CO. This composition indicates practically complete burning out of molecular oxygen in processes of dissociation into atoms and chemical reactions, leading in particular to creation and accumulation of NO molecules, and because of this the generation of CO_2 is decelerated (this is the nonequilibrium state with respect to CO_2 molecules).

One can see from Fig.3.2.20 that main charged particles before the inflammation were negative ions $O_2^-\cdot 2\cdot H2O$ and positive ions $C_2H_3^+$ and C_3H_5; but after the inflammation electrons, e, and positive ions $C_2H_3^+$ become main particles, and their concentrations rise, that is connected with more slow electron-ion recombination in the hot gas with respect to ion-ion recombination in the cold plasma.

It follows from Fig.3.2.21 that in this case oxygen molecules in the states $O_2(^1\Delta)$ and $O_2(v)$ (effective vibrational state of the oxygen molecule) play important role in inflammation.

One can see from Fig.3.2.22 that main neutral particles in the humid mixture of non-selfmaintained gaseous discharge after the inflammation become N_2, H_2O, NO and CO. This composition again indicates practically complete burning out of molecular oxygen in processes of dissociation into atoms and chemical reactions, leading in particular to creation and accumulation of NO molecules, and because of this the generation of CO_2 is decelerated (this is the nonequilibrium state with respect to CO_2 molecules).

One can see from Fig.3.2.23 that main charged particles before the inflammations were negative ions $O_2^-\cdot 2\cdot H2O$ and positive ions $C_2H_3^+$ and $C_3H_5^+$; and after the inflammationa electrons, e, and positive ions $C_2H_3^+$ become main particles, at that their concentrations rise insignificantly.

It follows from Fig.3.2.24 that molecules of oxygen and nitrogen in states $O_2(^1\Delta)$, $O_2(v)$ and $N_2(v)$ play an important role at inflammation.

Fig.3.2.25 shows that the heating time in the plasma of the non-selfmaintained discharge decelerates approximately for a order of magnitude with respect to the plasma in the dry mixture. At that the inflammation features of the plasma in the dry mixture are close to the plasma of the dry air, but the plasma features in the humid mixture are close to those of the humid air plasma.

For better visual and detailed presentation of obtained results we have created Table 12, in which we represent results and main parameters of the calculations.

In the first line of the Table 3.2.4.12 one can see calculation results of propane-air plasma where we used a system of reactions of propane in air [3.2.8] (shortened reaction scheme reliably describing ignition of propane), and also plasma chemical reactions in the dry air [3.2.11, 3.2.27].

In the second line of the Table3.2.4.12 we represent results of propane-air mixture calculations where we used a system of reactions of propane in air [2.8] (shortened reaction scheme reliably describing ignition of propane), also plasma chemical reactions in the dry air [2.11,2.27] and also reactions typical for propane plasma chemical reactions (excitation, dissociation, charge exchange, ion-ion and electron-ion reactions). No typical reactions for humid air.

In the third line of the Table 3.2.4.12 we represent results of propane-air mixture calculations where we used a system of reactions of propane in air [3.2.8] (shortened reaction scheme reliably describing ignition of propane), plasma chemical reactions in the dry air [3.2.11,

3.2.27] , reactions typical for propane plasma chemical reactions (excitation, dissociation, charge exchange, ion-ion and electron-ion reactions), and typical reactions for humid air represented above.

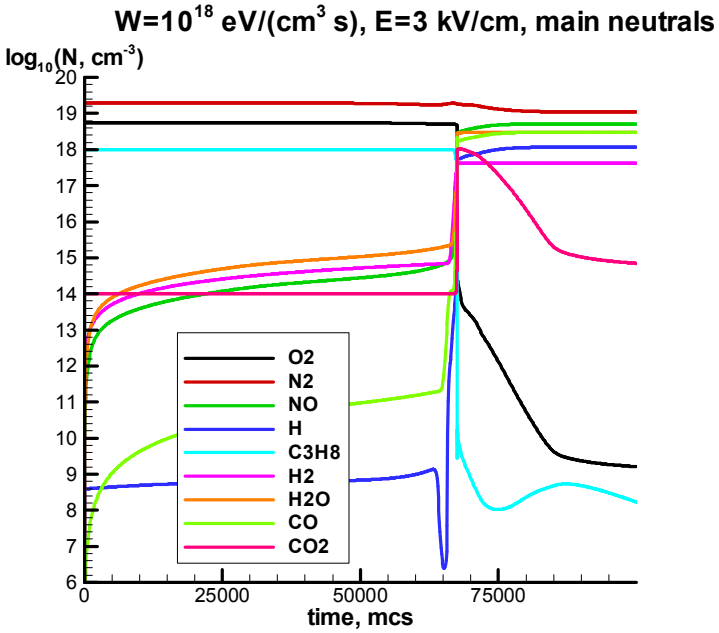

Fig.3.2.19. Main neutral components in the plasma of non-selfmaintained discharge in dry propane-air mixture at the excitation velocity by the electron beam $W=10^{18}eV/(cm^3 \cdot s)$ and external electric field strength E=3 kV/cm.

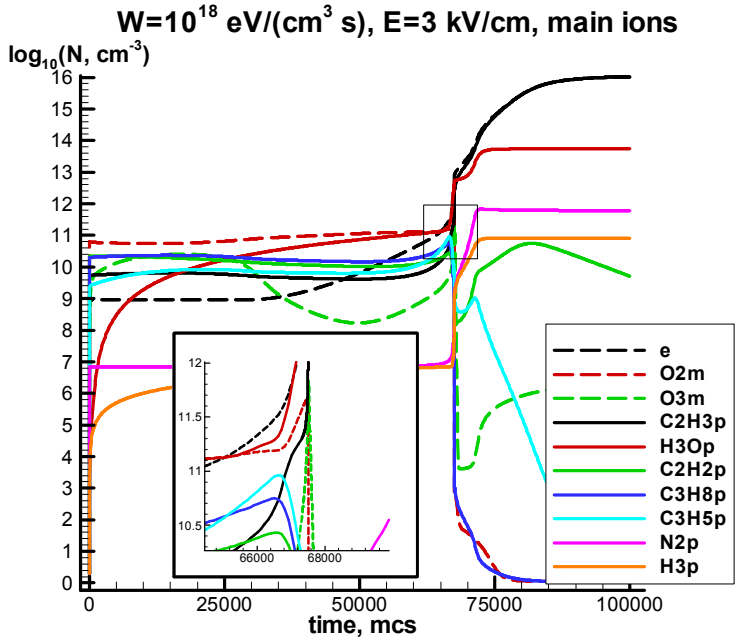

Fig.3.2.20. Main charged components in the plasma of non-selfmaintained discharge in dry propane-air mixture at the excitation velocity by the electron beam $W=10^{18}eV/(cm^3 \cdot s)$ and external electric field strength E=3 kV/cm.

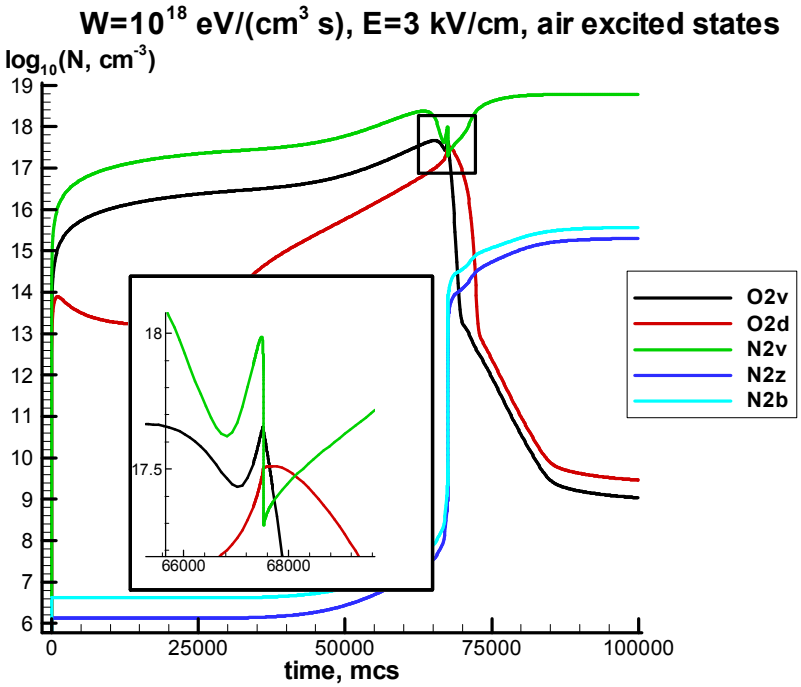

Fig.3.2.21. Main excited molecule components in the plasma of non-selfmaintained discharge in dry propane-air mixture at the excitation velocity by the electron beam $W=10^{18}$ eV/(cm^3·s) and external electric field strength E=3 kV/cm.

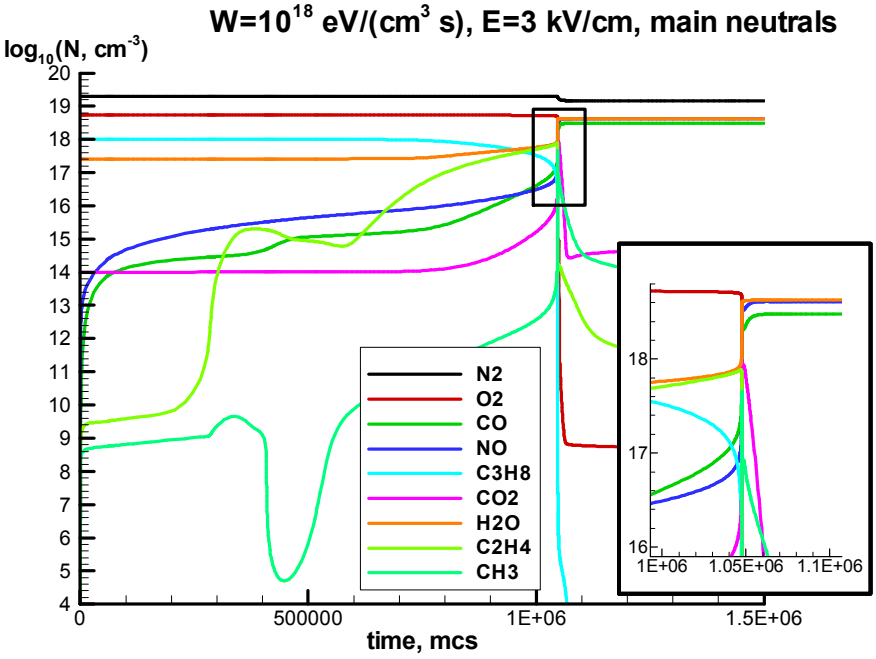

Fig.3.2.22. Main neutral components in the plasma of non-selfmaintained discharge in humid propane-air mixture at the excitation velocity by the electron beam $W=10^{18}$ eV/(cm^3·s) and external electric field strength E=3 kV/cm.

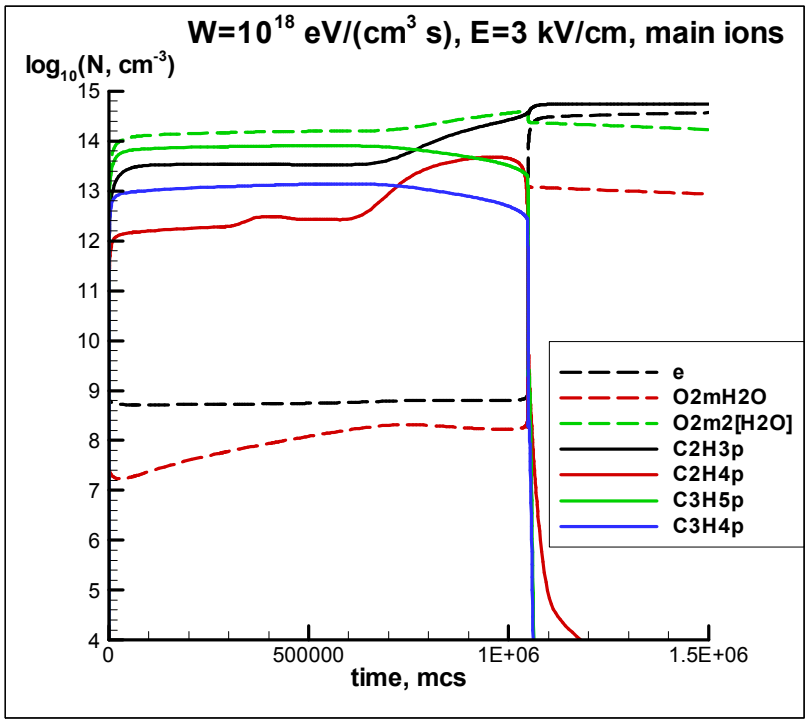

Fig.3.2.23. Main charged components in the plasma of non-selfmaintained discharge in humid propane-air mixture at the excitation velocity by the electron beam $W=10^{18}$ eV/(cm^3·s) and external electric field strength E=3 kV/cm.

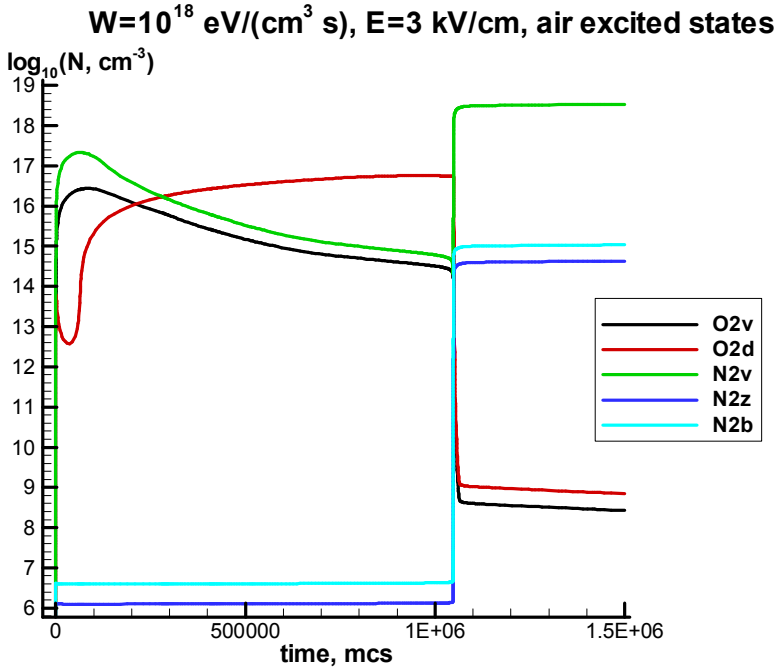

Fig.3.2.24. Main excited molecule components in the plasma of non-selfmaintained discharge in humid propane-air mixture at the excitation velocity by the electron beam $W=10^{18}$ eV/(cm^3·s) and external electric field strength E=3 kV/cm.

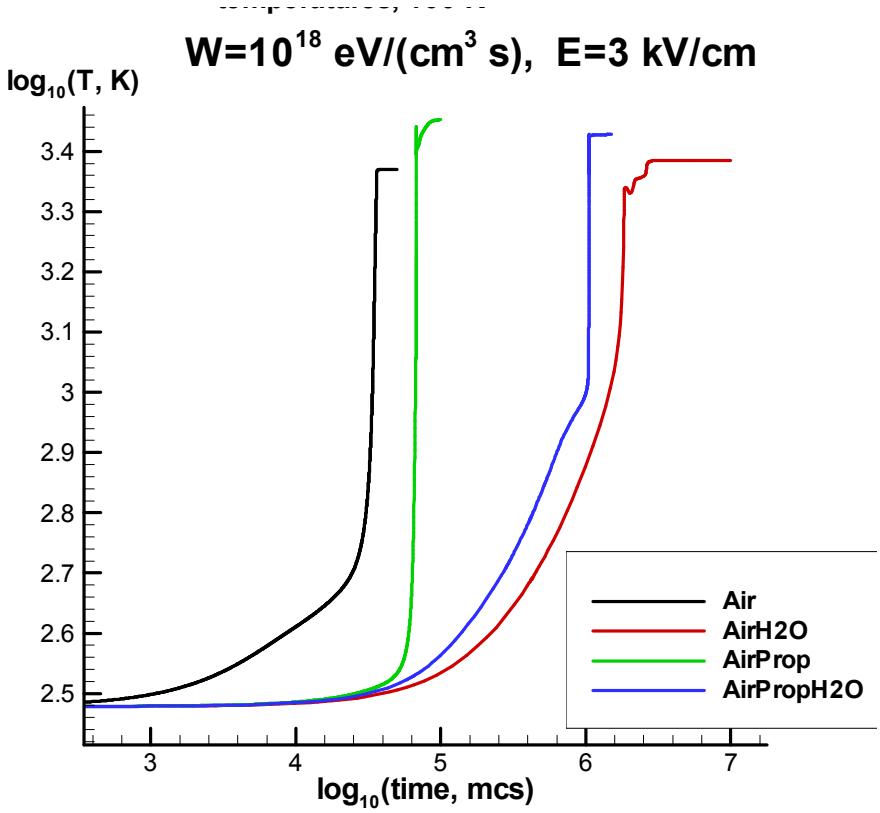

Fig.3.2.25. Temperature evolution in the plasma of non-selfmaintained discharge in dry air, humid air, dry propane-air mixture and humid propane-air mixture at the excitation velocity by the electron beam $W=10^{18}$ eV/(cm^3·s) and external electric field strength E=3 kV/cm.

3.2.4.3. Summed data over the calculations

In connection with great volume of the obtained computation data we have tried to unite them in the foreseeable table of the results presented more low.

Under inflammation in the Table 3.2.4.12 we understand sharp rise of temperature (see for example Fig.3.2.25) .

Under external impact (influence) we understand action of the electron beam or a combination of the electron beam and the external electric field.

Notation Wa means a velocity (rate) of the electron beam excitation equal to a eV/(cm^3·s). Notation Ea means an influence of the electric field of the electric field strength of a kV/cm.

For the concentration of main components we represent an exponent a at the concentration equal to 10^a cm^{-3}.

For the inflammation time AeM means A·10^M μs.

All data are represented for calculations in the propane-air stoichiometric mixture or close to it as in case of the humid mixture.

Table 3.2.4.12. Calculated data of mixtures inflammation characteristics under impact of plasma sources

№	Composition of a mixture, initial conditions	External impact	Inflammation time, μs	Gas Tгаза after inflammation, K°	Main ions before inflammation	Main ions after inflammation	Main neutrals before inflammation	Main neutrals after inflammation
1	Propane-air mixture. Short propane reaction system. Plasma of air without propane-plasma reactions. Initial normal conditions.	W**18**E**3**	3.0e4	2335	$O2^-$(11.21) NO^+(11.23)	e (11.9) NO^+(11.9)	C_2H_4(17.44) H_2(17.24)	NO(18.49) H_2O(18.49) CO(18.48)
		W19E3	8.3 e3	2375	$O2^-$(11.65) NO^+(11.65)	e (12.26) NO^+(12.26)	C_2H_4(17.61) H_2(17.4)	NO(18.48) H_2O(18.49) CO(18.48)
2	Propane-air mixture. Short propane reaction system. Plasma of air with propane-plasma reactions; without accounting of water plasma reactions. Initial normal conditions.	W**18**	8.8 e5	2580	O_3^-(13.42) H_3O^+(13.44)	e (14.48) H_3O^+(14.23) $C_2H_3^+$(14.21)	NO(15.87) H_2O(16.11) H_2(15.87)	NO(18.71) H_2O(18.49) CO(18.48)
		W**19**	1.1e5	2560	O_3^-(13.68) H_3O^+(13.69)	e (14.71) H_3O^+(14.41) $C_2H_3^+$(14.48)	NO(15.97) H_2O(16.15) H_2(16.01)	NO(18.71) H_2O(18.48) CO(18.48)
		W**18**E**3**	6.8 e4	2800	O_2^-(11.10) H_3O^+(11.07)	e (16.02) $C_2H_3^+$(16.01)	NO(14.84) H_2O(15.31) H_2(14.84)	NO(18.71) H_2O(18.48) CO(18.48)
		W**19**E**3**	1.4 e4	2800	O_2^-(11.56) H_3O^+(11.58)	e (16.09) $C_2H_3^+$(16.09)	NO(14.8) H_2O(15.29) H_2(14.83)	NO(18.69) H_2O(18.47) CO(18.44)
3	Propane-air mixture. Short propane	W**18**	2.2 e6	2570	O_2^- 2[H2O](14.25) $C_2H_3^+$(13.57) $C_3H_5^+$(13.87)	e (14.45) $C_2H_3^+$(14.46)	H_2O(16.61) C_2H_4(16.65)	NO(18.62) H_2O(18.60) CO(18.48)

№	Composition of a mixture, initial conditions	External impact	Inflammation time, μs	Gas Tгаза after inflammation, K°	Main ions before inflammation	Main ions after inflammation	Main neutrals before inflammation	Main neutrals after inflammation
	reaction system. Plasma of air with propane-plasma reactions. With accounting of water plasma reactions. Initial normal conditions.	W**19**	2.7e5	2600	O_2^- 2[H2O](14.24) $C_2H_3^+$(13.56) $C_3H_5^+$(13.91)	e (14.50) $C_2H_3^+$(14.60)	H_2O(17.82) C_2H_4(17.81)	NO(18.62) H_2O(18.63) CO(18.48)
		W**18**E**3**	1.05 e6	2680	O_2^- 2[H2O](14.20) $C_2H_3^+$(13.53) $C_3H_5^+$(13.91)	e (14.57) $C_2H_3^+$(14.74)	H_2O(17.79) C_2H_4(17.76)	NO(18.61) H_2O(18.63) CO(18.48)
		W**19**E**3**	1.2 e5	2680	O_2^- 2[H2O](14.20) $C_2H_3^+$(13.53) $C_3H_5^+$(13.91)	e (14.59) $C_2H_3^+$(14.75)	H_2O(17.83) C_2H_4(17.85)	NO(18.61) H_2O(18.63) CO(18.48)

Results of calculations represented in the Table 3.2.4.12 show that calculations without accounting for reactions with participation of ions and plasma reactions of propane give the smallest inflammation time. Comparison of these results with those accounting features of plasma chemical reactions show the decelerating role of the plasma chemical processes. One can suppose that accumulation of initial active radical values (important for starting of the inflammation process) taking place in the result of ion-ion and electron-ion recombination, which at initial plasma impact go very slowly, is the bottle neck of the plasma –chemical reaction system of the plasma impact on the mixture.

Calculations of the inflammation time of initially cold stoichiometric propane-air mixture calculated by the model of dry propane-air mixture proves to give $9\cdot10^5$ -$1.0\cdot10^5$ μs at the electron beam impact with the excitation velocity of $W=10^{18}$ - 10^{19} eV/(cm^3·s). Gas temperature in this case reaches a value of T≈2600 K.

In case of the non-selfmaintained discharge at the external electric field strength of E=3 kV/cm and the excitation velocity of electron beam $W=10^{18}$ - 10^{19} eV/(cm^3·s) the model of dry propane-air mixture gives the inflammation time $7\cdot10^4$ -$1.0\cdot10^4$ μs, i.e. it decreases up to 10 times at application of the external electric field. Gas temperature in this case reaches a value of T ≈2800 K.

Calculations of the inflammation time of initially cold stoichiometric propane-air mixture calculated by the model of humid propane-air mixture proves to give $2.0\cdot10^6$ -$3.0\cdot10^5$ μs at the electron-beam impact with the excitation velocity of $W=10^{18}$ - 10^{19} eV/(cm^3·s). Gas temperature in this case reaches a value of T ≈2600 K.

In case of the non-selfmaintained discharge at the external electric field strength of E=3 kV/cm and the excitation velocity of electron beam $W=10^{18}$ - 10^{19} eV/(cm^3·s) the model of humid propane-air mixture gives the inflammation time $1\cdot10^6$ -$1.0\cdot10^5$ μs, i.e. it decreases from 2 to 3 times. Gas temperature in this case reaches a value of T ≈2700 K.

Undertaken calculations show that in real conditions one can expect that the inflammation time of the mixture at the given parameters of the excitation only by the electron beam will lie in the 10^5 -10^6 μs, and by the non-selfmaintained discharge – in the range 10^4-10^5 μs. The scatter of the calculations data is connected with the decrease of temperature in the humid propane-air plasma since namely high temperature defines a velocity of chemical reactions.

Main neutral particles after the inflammation prove to be N_2, H_2O, NO and CO. This speaks about non-equilibrium of processes in the plasma, when formation of NO molecules takes place, and presence of which prevents transformation of CO to CO_2. It also speaks about the fact that it is necessary to account for principle difference of air and combustion products composition at analysis of the mixture combustion processes, it has to be taken into the account at theoretical modeling and analysis of experimental results.

Main ion compositions of the dry and humid mixtures plasmas of the non-self maintained discharge are essentially different. In the plasma of the humid mixture one can observe ions O_2^- $2{\cdot}H_2O$, $C_2H_3^+$, and $C_3H_5^+$ before the inflammation, at the same time in the dry mixture before the inflammation exist ions O_2^- and H_3O^+. After the inflammation main compositions of charged particles prove to be similar- there are electrons, e, and positive ions $C_2H_3^+$ in them. This speaks about the fact that destruction of negative ions and electron detachment from them takes place at high temperature. Electrons and ions with sufficient high concentrations will continue an excitation and realize Joule heating of the mixture after the inflammation.

3.2.5. Calculations of plasma parameters of in non-stoichiometric propane-air mixture

Our theoretical model described above has been completed by a number of reactions typical for water-air mixtures, we have also included recombination of light ions of water and air. We have also included channels of dissociative recombination of water ions with electrons, these reactions influence amount of electrons in the plasma. This amount decreases with respect to those in computations this process.

In Fig. 3.2.5.1.- 3.2.5.8 are presented results for excited propane - air mixture containing 2 % of the-propane, 1 % of water vapor (C_3H_8: H_2O: N_2: O_2 = 2: 1: 75.7: 21.3) in the initial moment of time.

In Fig. 3.2.5.9. 3.2.5.16 are presented results for excited propane - air mixture containing 4 % of the-propane, 1 % of water vapor (C_3H_8: H_2O: N_2: O_2 = 4: 1: 74.1: 20.9) in the initial moment of time.

In Fig. 3.2.5.17.- 3.2.5.24 are presented results for excited propane - air mixture containing 6 % of the-propane, 1 % of water vapor (C_3H_8: H_2O: N_2: O_2 = 6: 1: 72.5: 20.5) in the initial moment of time.

In a Fig. 3.2.5.25 results of calculations of evolution of the propane-air mixture temperature under the influence of excitation by the non-self-maintained discharge at different composition of the flammable mixture are presented.

3.2.5.1. Discussion of obtained results

Our calculations have been carried out for two modes:: 1) W=10^{18} eV/(cm^{3}s), E=3 kV/cm; 2) W=10^{19} eV/(cm^{3}s), E=3 kV/cm – for propane concentrations 2,4, and 6% from air concentration. In all the cases propane addition increases plasma concentration, what can be caused by increase of ionization rate with propane increase, since propane has lower ionization potential with respect to oxygen and nitrogen.

Curves represented in Fig.3.2.5.1-3.2.5.25 show an evolution of temperature in air and propane air mixtures at 0, 2, 4, and 6% of propane in the mixture. They show that at given parameters the heating of the gas takes place during about 8.5 10^5 μs to 2290K, the ignition delay at 6% of propane takes almost the same time. It can be explained by decrease of the oxygen amount necessary for effective combustion.

In case of 2 and 4 % percents the delay time of ignition takes place during 7.5 10^5 μs and 8.0 10^5 μs, respectively . It means that there is an optimum concentration of propane for ignition of the mixture.

Propane air mixture, propane 2 %

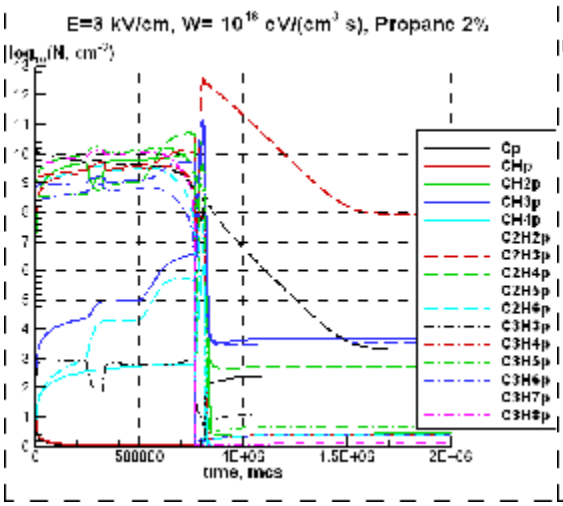

Fig. 3.2.5.1. Propane-air mixture ***propane 2 %. Ions***

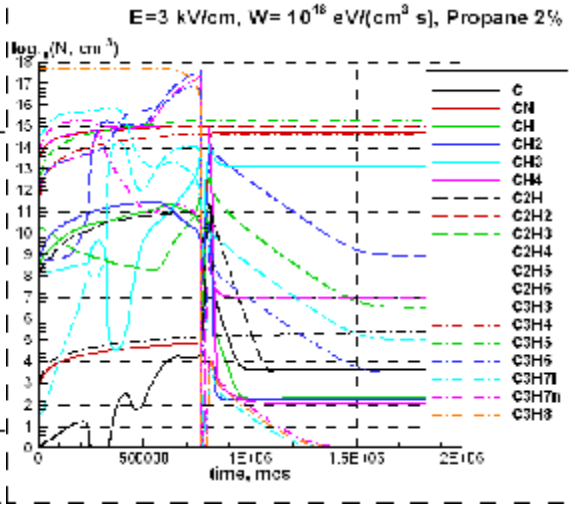

Fig. 3.2.5.2. Propane-air mixture ***propane 2 %. Neutrals***

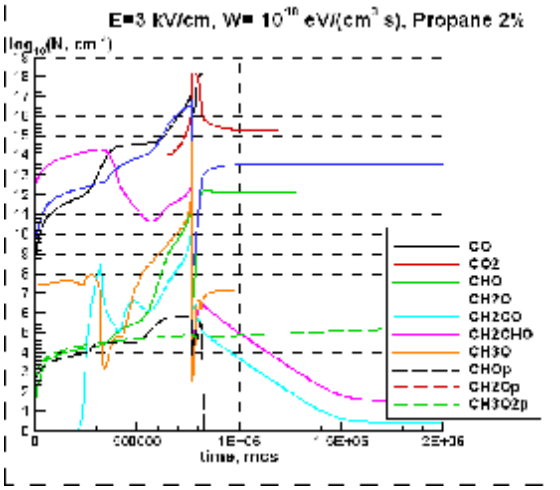

Fig. 3.2.5.3. Propane-air mixture ***propane 2 %. components***

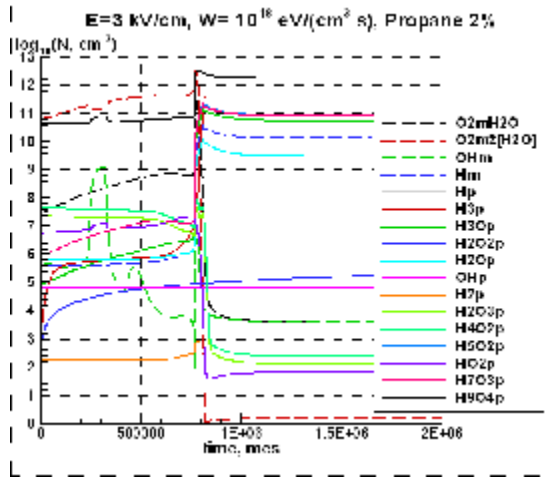

Fig. 3.2.5.4. Propane-air mixture ***propane 2 %. Ions***

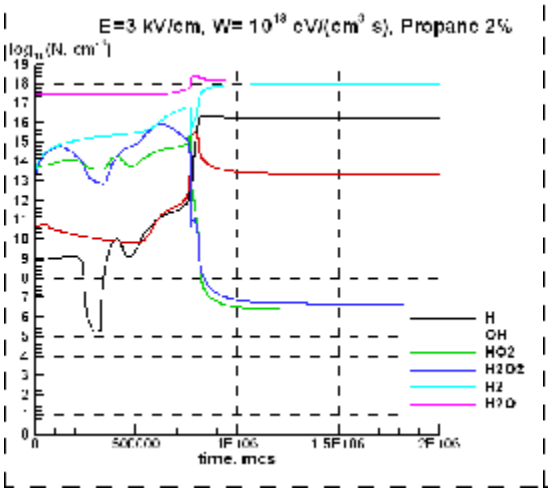

Fig. 3.2.5.5. Propane-air mixture ***propane 2 %. Neutrals***

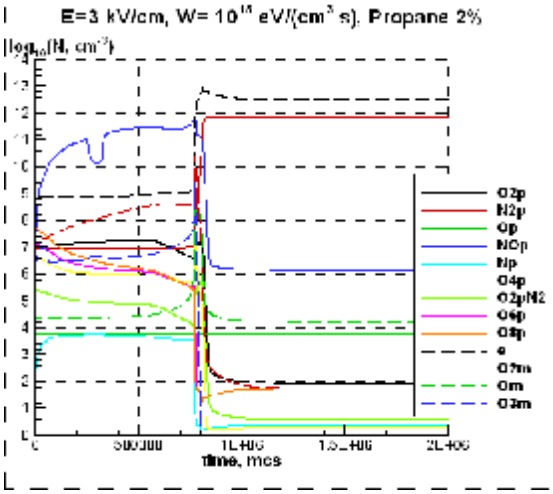

Fig. 3.2.5.6. Propane-air mixture ***propane 2 %. Ions***

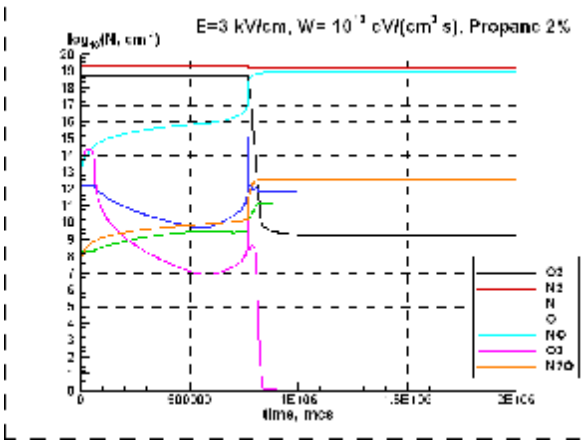

Fig. 3.2.5.7. Propane-air mixture ***propane 2 %. Neutrals***

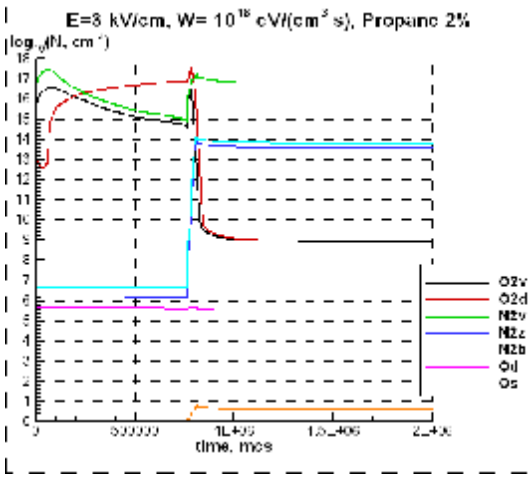

Fig. 3.2.5.8. Propane-air mixture ***propane 2 %. Excited states.***

Propane air mixture, propane 4 %

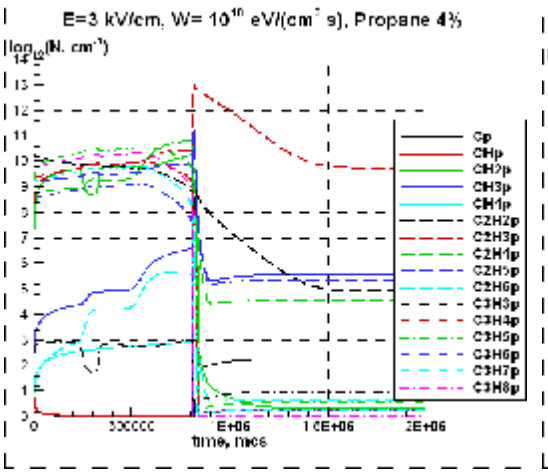

Fig. 3.2.5.9. Propane-air mixture ***propane 4 %. Ions***

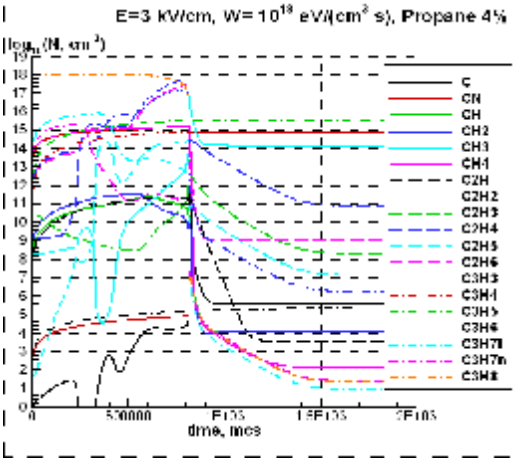

Fig. 3.2.5.10. Propane-air mixture ***propane 4 %. Neutrals***

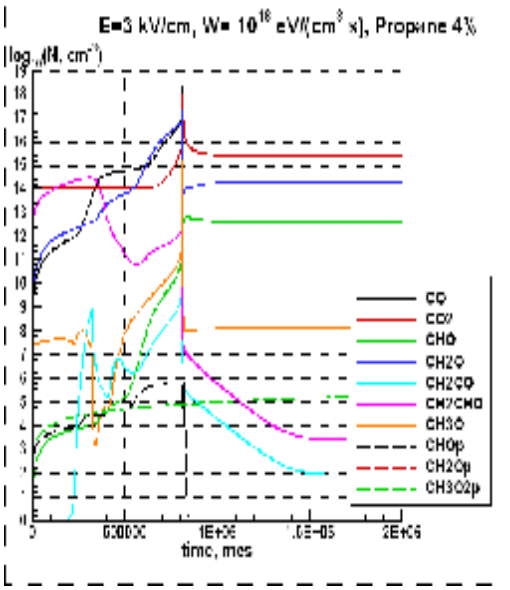

Fig. 3.2.5.11. Propane-air mixture ***propane 4 %. IComponents.***

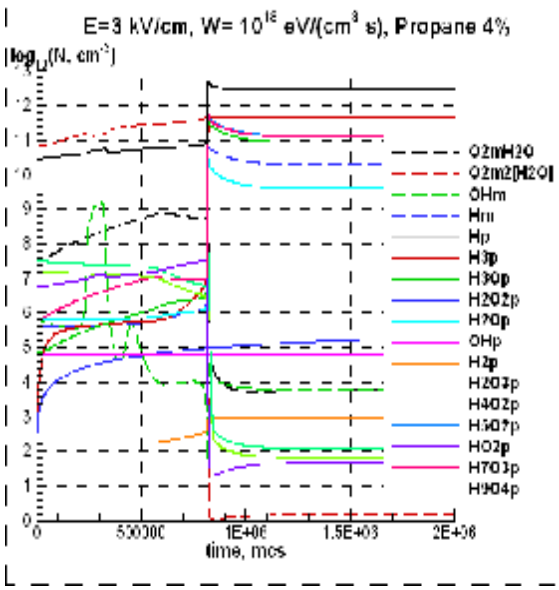

Fig. 3.2.5.12. Propane-air mixture ***propane 4 %. Ions***

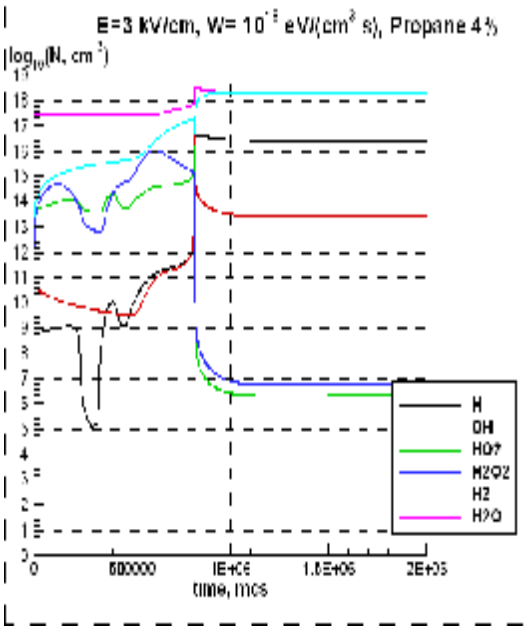

Fig. 3.2.5.13. Propane-air mixture ***propane 4 %. Ions***

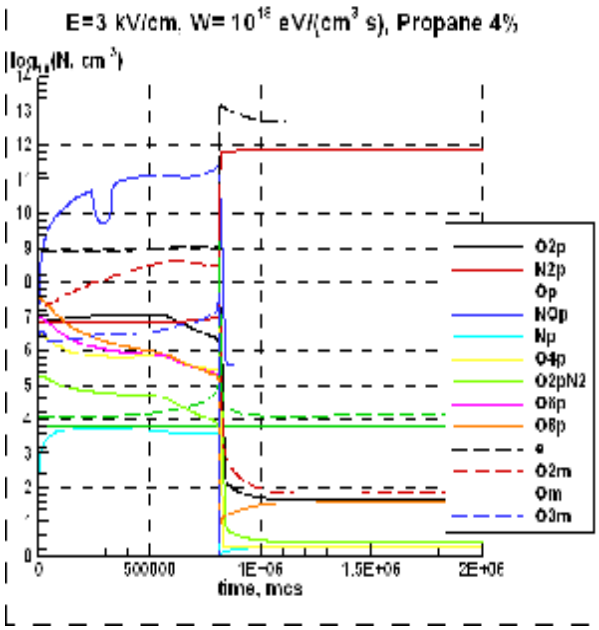

Fig. 3.2.5.14. Propane-air mixture ***propane 4 %. Ions***

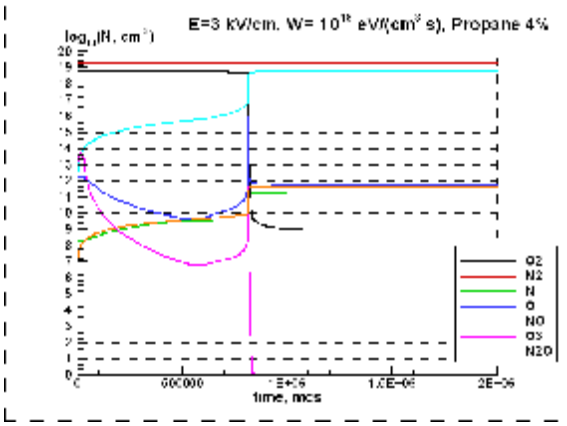

Fig. 3.2.5.15. Propane-air mixture ***propane 4 %. Neutrals***

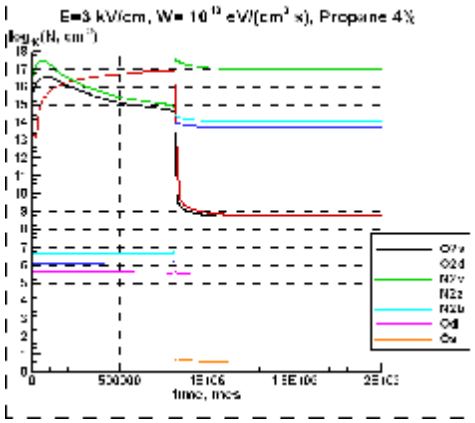

Fig. 3.2.5.16. Propane-air mixture ***propane 4 %. Excited states***

Propane air mixture, propane 6 %

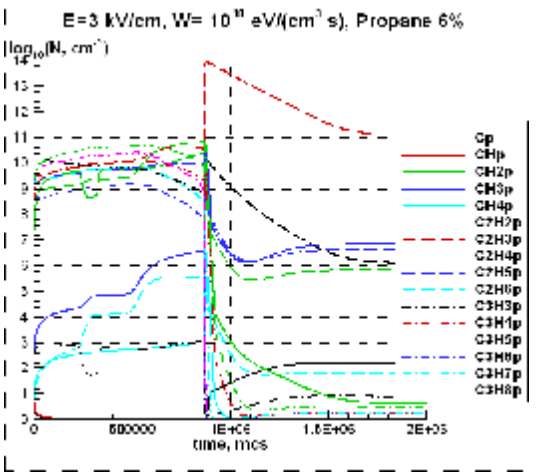

Fig. 3.2.5.17. Propane-air mixture ***propane 6 %. Ions***

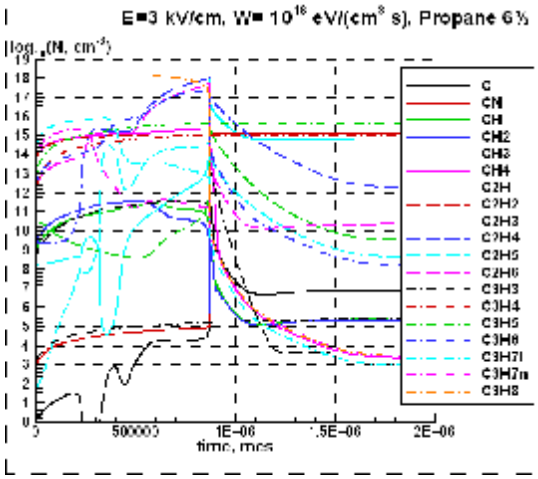

Fig. 3.2.5.18. Propane-air mixture ***propane 6 %. Neutrals***

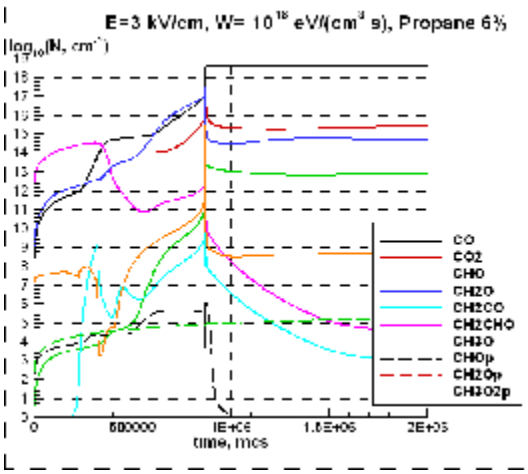

Fig. 3.2.5.19 Propane-air mixture ***propane 6 %. Componentss***

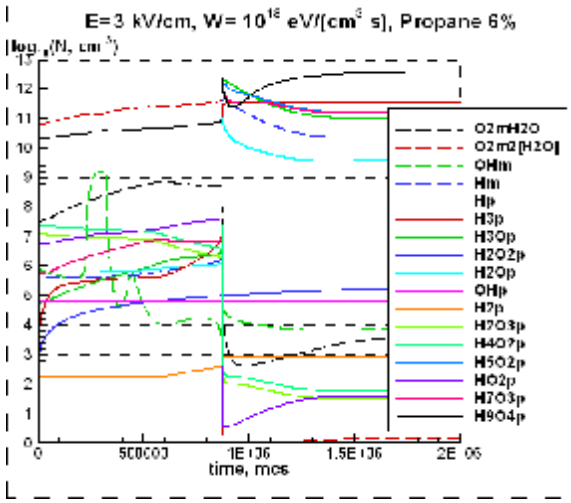

Fig. 3.2.5.20 Propane-air mixture ***propane 6 %. Ions***

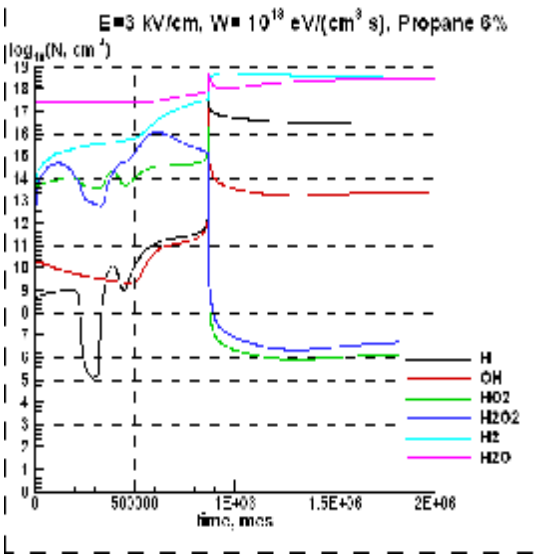

Fig. 3.2.5.21 Propane-air mixture ***propane 6***

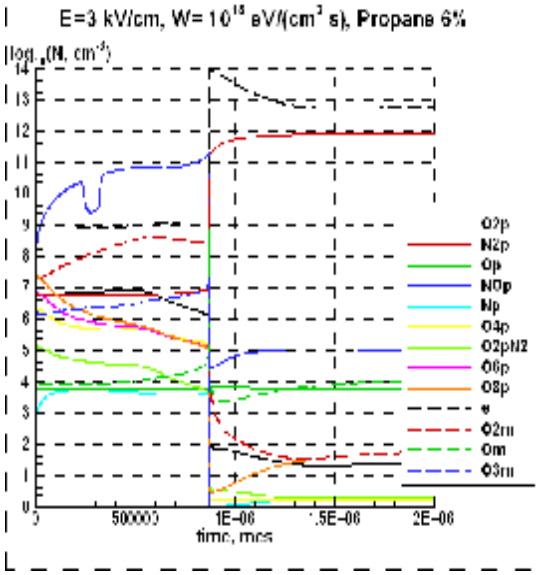

Fig. 3.2.5.22 Propane-air mixture ***propane 6***

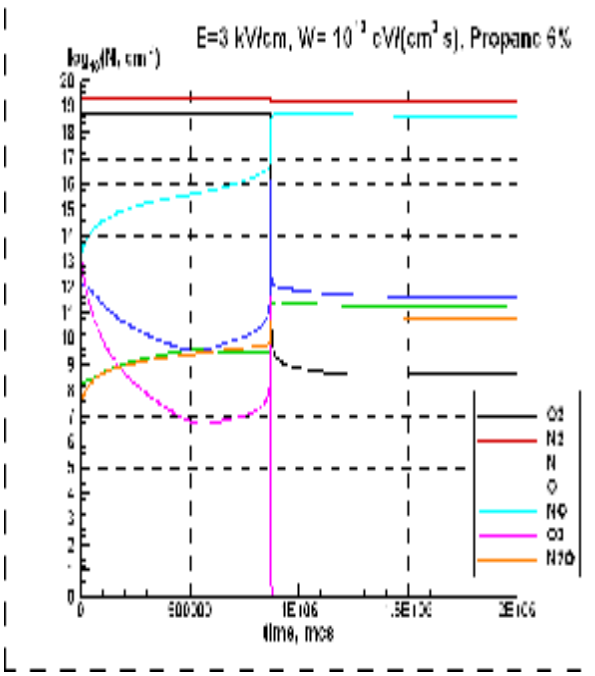

Fig. 3.2.5.23 Propane-air mixture ***propane 6***

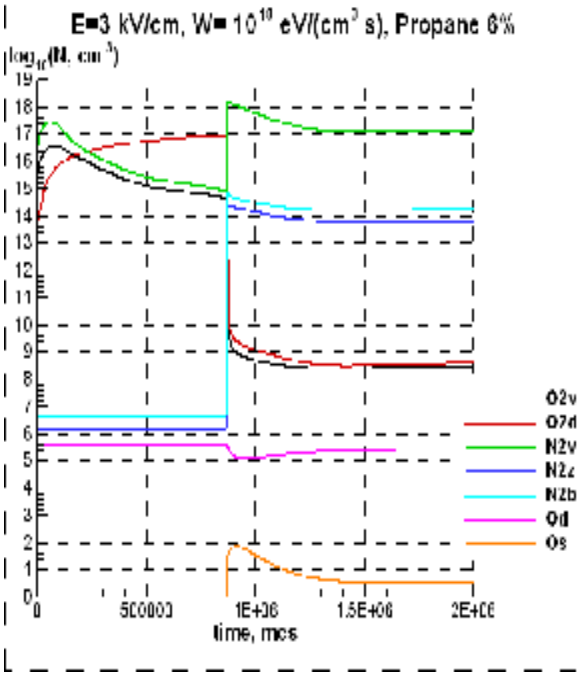

Fig. 3.2.5.24 Propane-air mixture ***propane 6***

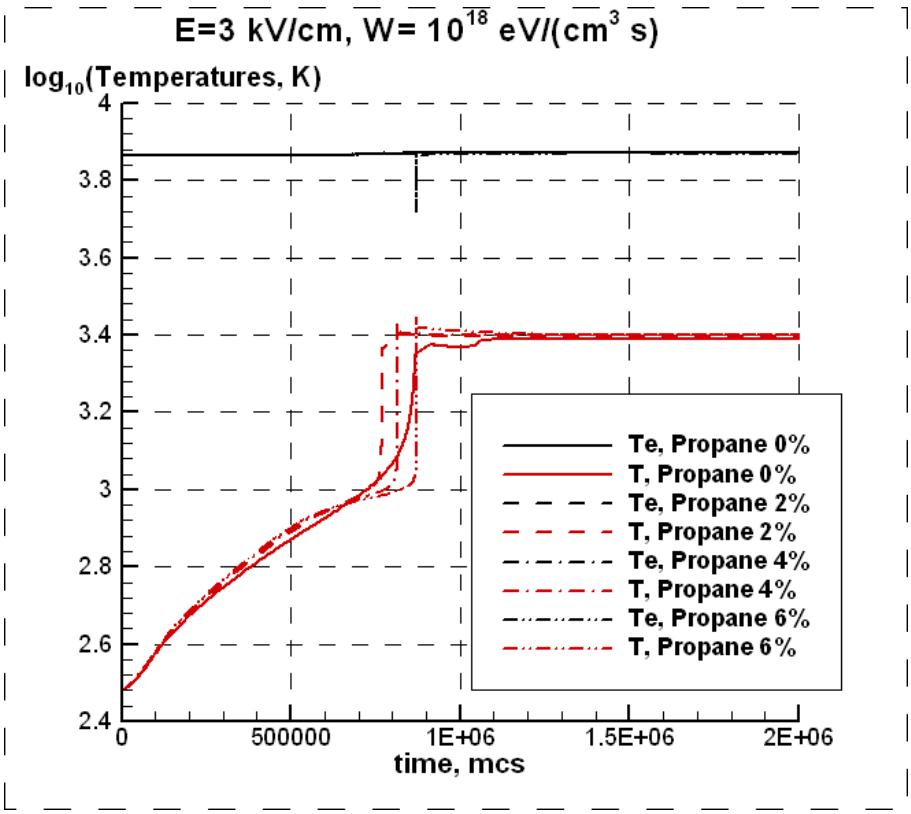

Fig. 3.2.5. 25. Evolution of temperature in air and propane air mixtures at 0, 2, 4, and 6% of propane in the mixture.

References to Chapter 3.2.

3.2.1. Hayashi M. in Proc. 4-th Swarm Seminar and Inelastic Collisions Sympos. Ed. L. Pitchford, 1985.
3.2.2. Itikawa Y., Hayashi M., Ichimura A. et.al. Journ. Phys. Chem. Ref. Data. 1986. V.15. N.3. P.985.
3.2.3. Itikawa Y., Ichimura A., Onda K. et.al. Journ. Phys. Chem. Ref. Data. 1989. V.18. N.1. P.23.
3.2.4. Akishev Yu. S., Deriugin A. A., Kochetov I.V., Napartovich A.P., Trushkin N.I. Effectiveness of chemical active particles generation in self-maintained glow discharge. Fizika Plazmy. V.20, N.6. P. 585-592 .
3.2.5. Cottrell T.L., Walker I.C. Drift velocities of Slow Electrons in Polyatomic Gases. Trans. Faraday Soc.1965. V. 61. P.1585-1593.
3.2.6. Cottrell T.L., Pollock W.J., Walker I.C. Electron Drift Velocities in Quadrupolar and Polar Gases. Trans. Faraday Soc.1968. V. 64. P.2260-2266.
3.2.7. Heylen A.E.D. Ionization coefficients and sparking voltages from methane to butane. Int. J. Electronics. 1975. V.39. N.6. P.653-660.
3.2.8. Varatharajan B., Williams F.A. Reduced Chemistry Descriptions for Ignition and Detonation of Higher Hydrocarbons. 40-th AIAA Aerospace Sciences Meeting and Exhibit. 14-17 January, 2002, Reno, NV.
3.2.9. Westbrook C.K., Chase L.L. Chemical Kinetics and Thermochemical Data for Combustion Applications. Lawrence Livermore Laboratory UCID-17833. Rev.1, April, 1981.
3.2.10. Ardelyan N., Bychkov V., Kosmachevskii K., Chuvashev S., Malmuth N. Modeling of Plasmas in Electron Beams and Plasma Jets . AIAA 2001-3101 Proc. 32-nd AIAA Plasmadynamics and Lasers Conference and 4 th Weakly Ionized gases Workshop 11-14 June 2001, Anaheim, CA.
3.2.11. MRTI Year Technical Report on the Project ISTS №3775p. 31 August 2008.

3.2.12. Bychkov V.L., Eletskii A.V. Electron beam high density plasmas. Khimia Plasmy (Plasma Chemistry in English edition) Ed. prof. Smirnov B.M. Moscow. Energoatomizdat Publishers. 1985. V.12. P.119-158.
3.2.13. Konovalov V.P., Son E.E. Degradation spectra of electrons in gases. In collection of works Plasma Chemistry. Ed. Prof. B.M.Smirnov . V. 14. Moscow. Energoatomizdat. 1987. P. 194-227.
3.2.14. Akishev Yu. S., Deriugin A. A., Kochetov I.V., Napartovich A.P., Trushkin N.I. Effectiveness of chemical active particles generation in self-maintained glow discharge. Fizika Plazmy. V.20, N.6. P. 585-592.
3.2.15. Kossyi I.A., Kostinsky A.Yu., Matveev A.A., Silakov V.P. Plasmochemical processes in non-equilibrium nitrogen-oxygen mixture. Works of General Physics Institute .Physics and chemistry of gaseous discharges in beams of MW-waves. Moscow. Nauka. V.47.P.37-57.
3.2.16. Bychkov V., Yurovskii V.A. The modeling of water vapor beam plasma. Teplofizika Vysokikh Temperatur (High Temperature in English edition). 1993. V.31. P.8-17.
3.2.17. Flannery M.P. Ion-ion recombination in high pressure discharges. In a book Gas Lasers. Eds. I. Mac Daniel, W. Nihgan. Moscow. Mir. 1986.
3.2.18. Smirnov B.M. Complex ions. Moscow. Nauka.1983.
3.2.19. Smith K., Thomson R.M. Computer modeling of gas lasers. Plenum Press. NY-London. 1978.
3.2.20. Ness K.F., Robson R.E. Transport properties of electrons in water vapor. Phys. Rev. A. 1988. V.38, N.3, P.1446-1456.
3.2.21. Konovalov V.P. Formation of ions in air under action of ionizing radiation. Khimia Vysokhikh Energii (High energy Chemistry) . 1993, V.27.N.1. P.3-6.
3.2.22. Willis C., Boyd A.W. Excitation in radiation- chemistry of inorganic gases. Int. J. Rad. Phys. 1976. V.8. N.1/2. P. 71.
3.2.23. Busi F. et al. Radiation treatment of combustion gases formulation and test of a reaction model. Radiat. Phys. Chem. 1985. V.25. N. 1/3. P.47.
3.2.24. Kutepov, A.M., Zakharov A.G., Maksimov A.I. Vacuum-plasma and plasma –solution modification of polymer materials. Moscow. Nauka. 2004.
3.2.25. Kondratiev V.N. Rate constants of gas-phase reactions. Reference book. Moscow. Nauka. 1970.
3.2.26. Virin L.I. et al. Ion-molecule reactions in gases. Reference book. Moscow. Nauka. 1979.
3.2.27. Ardelyan N., Bychkov V., Kosmachevskii K., Denisiuk S., Gudovich V., Bychkov D., Kochetov I. Electron-beams for Plasma Impact on Gas Flammable Mixtures. AIAA-2009-0693. 47th AIAA Aerospace Sciences Meeting. 5-8 January 2009. Orlando World Center Marriott. Orlando. Florida.

.Chapter 3.3. Theoretical analysis of installation specific parameters

3.3.1. Supposed electron-beam parameters in the chamber

We suppose that fast electrons have to pass through two foil layers of titan and aluminum. We estimate an energy E_{out} of electrons with energy 350 keV injected to the foil that is realized at the outlet from the foils and a current velocity of the fast electrons in the chamber.

Literature data [3.3.1- 3.3.3] allows to estimate possible parameters of the electron-beam in supposed experiments. Estimates of these parameters are represented in Table 3.3.1 with respect to metal of the foil and effective electron scattering angle.

Table 3.3.1. **Estimated parameters of the electron-beam in experiments**

Metal	Foil width	Foil with L g/cm^2	ρ, g/cm^3	Θ	E_{out}, MeV
Al	50μm	0,023	4.51	60°	0,268
Ti	50μm	0,013	2.63	60°	0,123
Layer	Ti 50 μm Al 50 μm			60°	0,038
Layer	Al 50 μm Al 50 μm			60°	0,21
Layer	Ti 20 μm Al 50 μm			60°	0,15

Here 60° is effective electron scattering angle.

It follows from the table that electrons become non-relativistic at the outlet from the foil.

Suppose that electrons have to penetrate a volume with height of 70 mm, width 20 mm and length 100 mm (we use parameters of our installation). Accounting that their effective scattering angle is ~ 60°, then it is possible to find out that the current density at the 30 mm from the injection plate is equal to $j_b = I_0 / 70$ A/cm^2, and at a distance of 70 mm is $j_b = I_0 /160$ A/cm^2. This gives the following current densities $j_{b1} = 4.3 \cdot 10^{-5}$ A/cm^2, $j_{b2} = 1.9 \cdot 10^{-5}$ A/cm^2 at the current $I_0 = 3 \cdot 10^{-3}$ A that can be realized in the chamber.

3.3.2. Determination of the excitation rate

Let us indicate that the power put in the gas by the electron beam W (we usually use it in eV/(cm^3 s) units) and a velocity of the molecule excitation Q are connected by the equation [3.3.4-7] $Q=W/(U_i)$, where U_i is the ionization cost, in air it is $U_i = 31.6$ eV.

One can show [3.3.4-7] that the excitation velocity W in air is connected with parameters of the relativistic electron beam (with electron's energy E_b = 200-500 keV) by the relation $W = 10^{22} J_b \cdot P$, where the current density J is expressed in A/cm^2, and pressure in atm., and in case of the non-relativistic electron beam (at E_b <150 keV) $W = 4 \cdot 10^{22} J_b \cdot P$. For conditions of our experiments estimates give W=10^{17}-10^{18} eV/(cm^3·s) (at the corresponding electron beam current density 10^{-5} -10^{-3} A/cm^2).

We have made initial primary analysis of experimental results. It is known, that the current of ions I_i, their mobility K_i, concentration N_i and electric field strength E in the plasma are connected by a relation [3.3.8]::

$$I_i = e \cdot K_i \cdot E \cdot N_i \cdot S ,$$

here e is electron charge. Therefore, at known current, field strength, mobility and area of measuring electrode one can find the concentration of ions in the experiment. Assuming that the mobility of positive ions which current is measured in the experiment in the external electric field E= 1.75 kV/cm, is K_i =2.5 -3 cm^2/(V·s) [3.3.9] one can find that average concentration of ions at I_p= 1 mA (at beam current I_b= 0.1 mA, see Fig.16) and electric field E= 1.75 kV/cm. It proved to be N_i= $1.1 \cdot 10^{11}$ cm^{-3}.

For conditions of the experiment without combustion at external field E= 1.75 kV/cm we made calculations of the ion composition in the range of W=$2 \cdot 10^{17}$-$2 \cdot 10^{18}$ eV/(cm^3 s). An example of obtained results at W=$2 \cdot 10^{18}$eV/(cm^3 s) is represented in Fig., at this rate of E-beam gas excitation ion values of theory and experiment are close. So this value of the excitation can be chosen as the reference one.

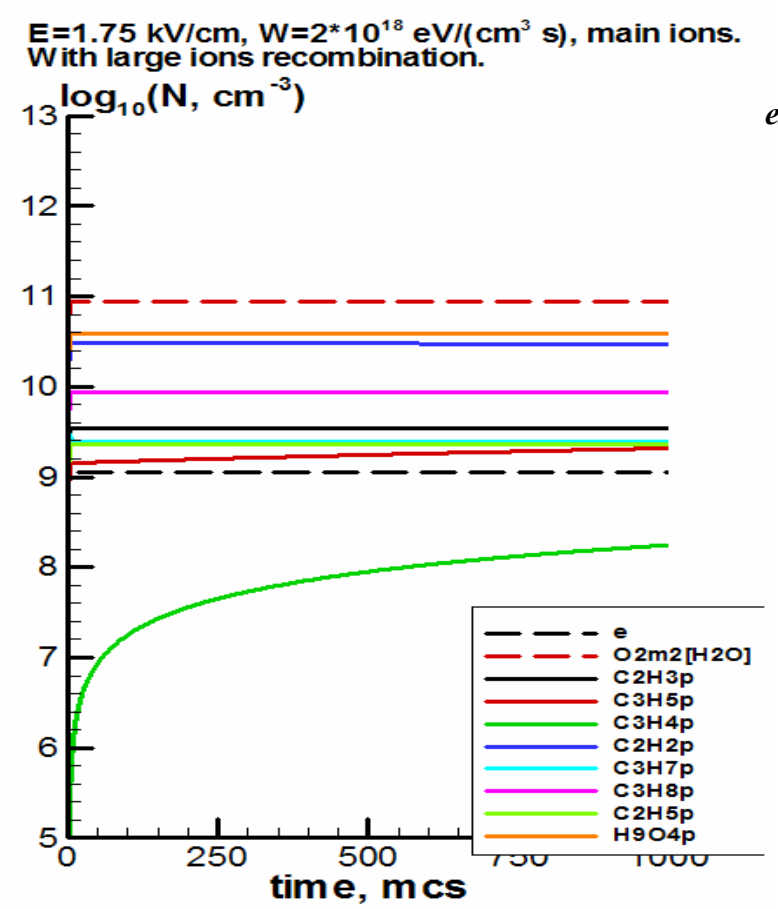

Fig.. Main ions in the experimental conditions

References to Chapter 3.3.

3.3.1. The nuclear handbook. Editor O.R.Frish. George Newnes Limited. London. 1958.

3.3.2. Chernyaev A.P. Interaction of ionizing radiation with matter. Fizmatlit. Moscow. 2004.

3.3.3. Abramyan . Electron beam. Atomizdat. 1974.

3.3.4. Bychkov V.L., Vasilev M.N., Koroteev A.S. Electron- beam plasmas: generation, features, applications. Moskow. MGOU publoishers. “Rosvuznauka”. 1993. 168 pp.

3.3.5. Bychkov V.L., Eletskyi A.V. Beam plasmas of high pressure. In collection Plasma Physics. Ed. B.M. Smirnov N.12 Moscow. Energoatomizdat. 1985. P. 119-158.

3.3.6. Andreev S.I., Bychkov V.L., Gordeev O.A., Klepando I.L. Studies of non equilibrium conductivity of air ionized by short pulse of fast electrons. Fizika Plazmy. (Sov.Phys.-Plasma Phys.) 1985. V.11. P. 1134-1139.

3.3.7. Ardelyan N., Bychkov V., Kosmachevskii K., Chuvashev S., Malmuth N. Modeling of Plasmas in Electron Beams and Plasma Jets . AIAA 2001-3101 Proc. 32-nd AIAA Plasmadynamics and Lasers Conference and 4 th Weakly Ionized gases Workshop 11-14 June 2001, Anaheim, CA.

3.3.8. Raizer Yu.P. Gas discharge physics. Moscow. Nauka. 1992.

3.3.9. Flannery M.P. Ion-ion recombination in high pressure discharges. In a book Gas Lasers. Eds. I. Mac Daniel, W. Nihgan. Moscow. Mir. 1986.

Chapter 3.4. Estimate of airflow velocity at the exit from the excitation area. (Tasks 8, 10, 11)

3.4.1. Physical formulation of the problem.

A simplified scheme of our gasdynamic installation is represented in Fig. 3.4.1. Electrons of the beam come to the area where appear a gas of the mixture. At that an external electric field can be applied to this area.

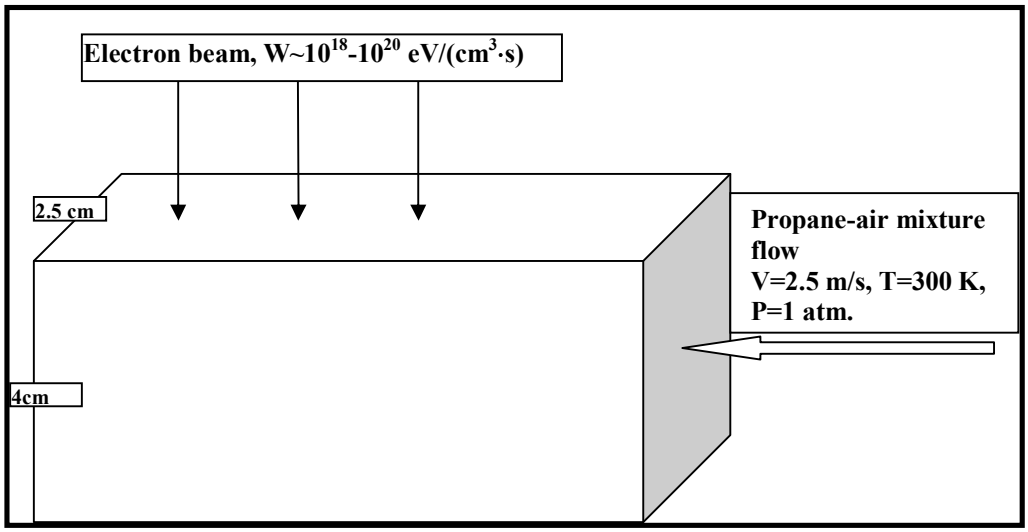

Fig.3.4.1. A simplified scheme of the installation.

Temperature is measured at a distance of ~ 20 cm, a velocity is measured at the exit from the chamber, beam scanning frequency is 150 Hz. External electric field now is 1-3 kV/cm. A flow of propane-air mixture propagates through the chamber, the beam and electric field are switched on in the initial time moment (can be different situations).

Let us make a simple estimate at the flow velocity about of 1 m/s:

P~1 atm $\approx 10^5$ Pa (J/m^3) >> $\rho v^2/2 \sim 10$ J/m^3,

Where P is pressure in the chamber, v is a velocity of the flow, ρ is density of the mixture. From the equation of state follows a comparison of flow energy with the internal energy in the mixture

$$\varepsilon = \frac{P}{(\gamma - 1)\rho} \sim 10^5 \text{J/kg} >> v^2/2 \sim 10 \text{ J/kg},$$

So one can consider the pressure to be constant at our velocity.

So the following relations will be valid

$$P = \rho R T, \qquad (2.5.1)$$

Here T-is gas temperature, R- universal gas constant. It follows from made estimates that

$$P = const, \qquad (2.5.2)$$

Present work is fulfilled under a Contract with International Scientific-Center (ISTC), Moscow, at financial support (Financing Side).European Office of Aerospace Research and Development (EOARD)

And constancy of the flow rate

$$\rho v S = const, \qquad (2.5.3)$$

here S – is the area of the transversal cross section of the channel.
It follows from here

$$\rho_1 v_1 = \rho_2 v_2 , \qquad (2.5.4)$$

Accounting for (2.5.1) and (2.5.2) we obtain:

$$v_2 = \frac{T_2}{T_1} v_1 = k \cdot v_1 , \qquad (2.5.5)$$

Where k is the coefficient of the velocity increase. It follows from here that the flow velocity increase at heating by the plasma source, and it is possible to undertake calculations at any experimental parameter.

However it is unclear what will be in real conditions, when the stream will expand in the volume (in the submerged space), that is observed in the experiment. Here it can be necessary to consider later the problem in two dimension approach.

An approximate solution gives a computation on the time interval defined through the average velocity if the stream is heated not very strongly. Our approximate time is 0.1 s =100 ms.

The flow velocity in the experiment is about 2 ms, the heating by the beam takes place at the distance of 0.2 m, so the duration of heating by the beam is about 0.1 second.

Temperatures for it can be taken from the undertaken calculations, and put into the Table results for different conditions and different plasma sources.

Let us represent a table of temperatures and coefficients of the velocity increase in Table 13 for the average time moment equal to 0.1 s (100 ms). In this approximation considered case we do not account for possible relaxation of temperature after the trajectory covers the area of the beam action.

Table 3.4.1. Coefficients of the velocity increase k ($k = T_2/T_1 = T_2/300$ K).

Air plasma, normal conditions			Air mixture with 1% water vapor plasma, normal conditions		Dry propane-air plasma, normal conditions			Humid propane-air plasma, normal conditions											
W18	W19*	W20*	W18 E3*	W19 E3*	W18	W19	W20*	W18 E3	W19 E3	W18	W19	W20*	W18 E3*	W19 E3*	W18	W19	W20*	W18 E3	W19 E3
676 K	2290 K	2330 K	2345 K	2376 K	323 K	588 K	2280 K	346 K	740 K	335 K	710 K	2600 K	2800 K	2800 K	335 K	630 K	2600 K	365 K	1000 K
k =2.25	k =7.63	k =7.77	k =7.82	k =7.92	k =1.08	k =1.96	k =7.6	k =1.15	k =2.47	k =1.12	k =2.37	k =8.67	k =9.33	k =9.33	k =1.12	k =2.1	k =8.67	k =1.22	k =3.33

A sign * in cells corresponds to a variant where an inflammation took place already for the time 100 ms.

It follows from the Table 3.4.1 that possible stream velocity will not exceed 24 m/s in the experimental conditions of the excitation by the plasma (namely in conditions of the excitation by the non-selfmaintained discharge); even increase of the excitation by 10 times will not disturb the rightfulness of the approach, so undertaken experiments one can consider as correct.

Mark that in real experiment that the complete internal area is heated by the beam and the field. And the propane-air stream is surrounded by flowing. So the inflammation can take place earlier in air surrounding the stream if air is dry. If air is humid then the inflammation then the inflammation will take place earlier in the stream. So it is possible to make choice of time of influence of the beam and the field in order to ignite the stream without inflammation of air area. Also is possible a realization of the ionization wave in opposite sides. It can be a separate specific effect, which represents an interest in case of sufficiently powerful external plasma influence.

We have carried out special computations with the experimental data $W=10^{17}$ $eV/(cm^3 \cdot s)$ and electric field strength E=**1.5** kV/cm the beam is switched off after the trajectory covers the distance 20 cm, with a velocity 2 m/s. The calculation was carried out in most close to real plasma conditions: we considered the model of propane air mixture at 1% water vapor and 4% propane (volumetric). Time of calculations was 500 ms. The calculations without accounting of the beam switching off and without trajectories show that the gas is heated for 4 K degrees during the time of 100 ms..

The dry air at this plasma impact is heated up to 500 K during 100 mc, and sharp rise of temperature takes place after 340 ms.

Our calculations show that the subsonic stream is realized in the channel, and in case of homogeneous flow creation one could use obtained calculation data for comparison with the experimental results. However a stream has spreading form. At that measured temperatures require additional analysis that is caused by complex conditions of the stream formations and requires additional gasdynamic investigations.

3.5. Conclusions to theoretical part

Works on choice of electron-molecule interaction processes rate constants in propane-air mixture with accounting of excitation, ionization, attachment and detachment processes have been made. On a basis of the Boltzmann equation solution accounting cross sections of electron-molecule interaction processes in propane, oxygen and nitrogen rate constants for ionization and attachment processes have been determined. These constants values vary insignificantly at propane concentration below 10% with respect to the constants of these processes in pure air, this allows to use the rate constants of electron-molecule interaction processes obtained for air at calculation of propane-air plasma at propane concentrations of practical interest (i.e lean and stoichiometric ones).

At application of the simplified chemical model for inflammation of propane-air mixture and our model for air plasma we have created a general model and the code of plasma parameter calculations in external electric field, under influence of the electric field and at combined influence of the external electric field and the electron beam.

The plasma effect of decrease of the inflammation time in the model which does not ion-molecule and charge-exchange reactions with participation of propane molecules reaches 2 times (at the gas temperature of T=1500 K). Plasma sources work as heaters for some time.

This model has been developed, plasma chemical reactions inherent to propane plasma were added to it, so we have created, so called, plasma chemical model of dry propane-air mixture, we also added plasma chemical reactions inherent to water plasma to this model, and obtained , so called, plasma chemical model of humid propane-air mixture.

Calculations of the inflammation time of initially cold stoichiometric propane-air mixture calculated by the model of dry propane-air mixture proves to give $9 \cdot 10^5$ -$1.0 \cdot 10^5$ μs at the electron beam impact with the excitation velocity of $W=10^{18}$ - 10^{19} $eV/(cm^3 \cdot s)$. Gas temperature in this case reaches a value of T≈2600 K.

In case of the non-selfmaintained discharge at the external electric field strength of E=3 kV/cm and the excitation velocity of electron beam W=10^{18} - 10^{19} eV/(cm^3·s) the model of dry propane-air mixture gives the inflammation time $7\cdot10^4$ -$1.0\cdot10^4$ μs. Gas temperature in this case reaches a value of T ≈2800 K.

Calculations of the inflammation time of initially cold stoichiometric propane-air mixture calculated by the model of humid propane-air mixture proves to give $2.0\cdot10^6$ -$3.0\cdot10^5$ μs at the electron-beam impact with the excitation velocity of W=10^{18} - 10^{19} eV/(cm^3·s). Gas temperature in this case reaches a value of T ≈2600 K.

In case of the non-selfmaintained discharge at the external electric field strength of E=3 kV/cm and the excitation velocity of electron beam W=10^{18} - 10^{19} eV/(cm^3·s) the model of humid propane-air mixture gives the inflammation time $1\cdot10^6$ -$1.0\cdot10^5$ μs, i.e. it decreases from 2 to 3 times. Gas temperature in this case reaches a value of T ≈2700 K.

Undertaken calculations show that in real conditions the inflammation time of the mixture at the given parameters of the excitation only by the electron beam will lie in the 10^5 - 10^6 μs, and by the non-selfmaintained discharge – in the range 10^4-10^5 μs. The scatter of the calculations data is connected with the decrease of temperature in the humid propane-air plasma since namely high temperature defines a velocity of chemical reactions.

Main neutral particles after the inflammation prove to be N_2, H_2O, NO and CO. This speaks about non-equilibrium of processes in the plasma, when formation of NO molecules takes place, and presence of which prevents transformation of CO to CO_2. It also speaks about the fact that it is necessary to account for principle difference of air and combustion products composition at analysis of the mixture combustion processes, it has to be taken into the account at theoretical modeling and analysis of experimental results.

Our calculations have been carried out for propane air mixtures at 0, 2, 4, and 6% of propane in the mixture. They show that at given parameters the heating of the gas takes place during about 8.5 10^5 μs to 2290K, the ignition delay at 6% of propane takes almost the same time. It can be explained by decrease of the oxygen amount necessary for effective combustion.

In case of 2 and 4 % percents the delay time of ignition takes place during 7.5 10^5 μs and 8.0 10^5 μs, respectively . It means that there is an optimum concentration of propane for ignition of the mixture.

We want to mark that the developed model at this stage of investigations is incomplete from the point of view of propane chemistry. The model can be improved further in this direction. There are much more questions at accounting for the humidity. Appearance of heavy water clusters leads to the slow ion-ion recombination at the initial stage and decelerates the inflammation. For development of the model it is necessary additional investigations of cluster ions destruction with rise of temperature, also are required the data on temperature dependences of rate constant of these clusters conversion. Namely because of this we represent the ranges of the inflammation time, which indicates the inflammation time at absence of heavy water clusters and in their presence (but without definite determination of their existence time in conditions of heating).

Preliminary calculations of the stream that the subsonic stream is realized in the channel, and in case of homogeneous flow creation one could use obtained calculation data for comparison with the experimental results. However a stream has spreading form. At that in different conditions experimentally measured temperatures require additional analysis. Sharp rise of temperature in case of electron beam and external electric field impact that can be caused by complex conditions of the stream formation and requires additional gasdynamic investigations.

Results

In the course of project performance basically the technical in and experimental problems have been solved.

In a current of the first and the beginning of the second stages on works on modernization of existing accelerator EOL-400 which have provided a lead of an electron beam into atmosphere with the set parameters that has given the opportunity to realize the electron beam put into the combustion chamber of with the propane-air mixture.

The combustion chamber with the propane-air mixture for performance of experimental researches on excitation influence of an electron -beam and external electric field on combustion processes in various conditions is developed and designed.

The delivery system of a stream the propane - air mixture is developed, designed and manufactured. Sensors for measurement of the propane-air mixture characteristics are developed, manufactured and tested. The control system is developed and created. The system of burning processes visual observations is assembled and tested. Thus the experimental installation is created, allowing to carry out researches of the propane-air mixture combustion processes at influence of the electron beam and the external electric field.

Starting from the middle of the second stage of the project we have been begun our experimental researches of the propane-air mixture combustions processes of the propane-air mixture .

Results of the carried out researches have shown, that separate influence of an electronic bunch and external electric field do not influence significantly on combustion processes of the propane-air mixture.

Qualitative estimates of results of the carried out researches on complex influence of the electron beam and external electric field on the propane-air mixture burning processes show, that such an influence considerably rises a combustion temperature of the mixture, increases a speed of burning, and also rises a stability of burning. The Stability of combustion under the conditions specified above is insured in the lean propane-air mixture.

The experimental researches in the project were accompanied by theoretical support which have shown good qualitative coincidence of experimental results with physical models of processes of burning.

In a theoretical part of the project the following problems have been solved:

Works on choice of electron-molecule interaction processes rate constants in propane-air mixture with accounting of excitation, ionization, attachment and detachment processes have been made. On a basis of the Boltzmann equation solution accounting cross sections of electron-molecule interaction processes in propane, oxygen and nitrogen rate constants for ionization and attachment processes have been determined. These constants values vary insignificantly at propane concentration below 10% with respect to the constants of these processes in pure air, this allows to use the rate constants of electron-molecule interaction processes obtained for air at calculation of propane-air plasma at propane concentrations of practical interest (i.e lean and stoichiometric ones).

At application of the simplified chemical model for inflammation of propane-air mixture and our model for air plasma we have created a general model and the code of plasma parameter calculations in external electric field, under influence of the electric field and at combined influence of the external electric field and the electron beam.

The plasma effect of decrease of the inflammation time in the model which does not ion-molecule and charge-exchange reactions with participation of propane molecules reaches 2 times (at the gas temperature of T=1500 K). Plasma sources work as heaters for some time.

This model has been developed, plasma chemical reactions inherent to propane plasma were added to it, so we have created, so called, plasma chemical model of dry propane-air

mixture, we also added plasma chemical reactions inherent to water plasma to this model, and obtained , so called, plasma chemical model of humid propane-air mixture.

Calculations of the inflammation time of initially cold stoichiometric propane-air mixture calculated by the model of dry propane-air mixture proves to give $9\cdot10^5$ -$1.0\cdot10^5$ μs at the electron beam impact with the excitation velocity of $W=10^{18}$ - 10^{19} eV/(cm^3·s). Gas temperature in this case reaches a value of T≈2600 K.

In case of the non-selfmaintained discharge at the external electric field strength of *E*=3 kV/cm and the excitation velocity of electron beam $W=10^{18}$ - 10^{19} eV/(cm^3·s) the model of dry propane-air mixture gives the inflammation time $7\cdot10^4$ -$1.0\cdot10^4$ μs. Gas temperature in this case reaches a value of T ≈2800 K.

Calculations of the inflammation time of initially cold stoichiometric propane-air mixture calculated by the model of humid propane-air mixture proves to give $2.0\cdot10^6$ -$3.0\cdot10^5$ μs at the electron-beam impact with the excitation velocity of $W=10^{18}$ - 10^{19} eV/(cm^3·s). Gas temperature in this case reaches a value of T ≈2600 K.

In case of the non-selfmaintained discharge at the external electric field strength of *E*=3 kV/cm and the excitation velocity of electron beam $W=10^{18}$ - 10^{19} eV/(cm^3·s) the model of humid propane-air mixture gives the inflammation time $1\cdot10^6$ -$1.0\cdot10^5$ μs, i.e. it decreases from 2 to 3 times. Gas temperature in this case reaches a value of T ≈2700 K.

Undertaken calculations show that in real conditions the inflammation time of the mixture at the given parameters of the excitation only by the electron beam will lie in the 10^5 - 10^6 μs, and by the non-selfmaintained discharge – in the range 10^4-10^5 μs. The scatter of the calculations data is connected with the decrease of temperature in the humid propane-air plasma since namely high temperature defines a velocity of chemical reactions.

Main neutral particles after the inflammation prove to be N_2, H_2O, NO and CO. This speaks about non-equilibrium of processes in the plasma, when formation of NO molecules takes place, and presence of which prevents transformation of CO to CO_2. It also speaks about the fact that it is necessary to account for principle difference of air and combustion products composition at analysis of the mixture combustion processes, it has to be taken into the account at theoretical modeling and analysis of experimental results.

Our calculations have been carried out for propane air mixtures at 0, 2, 4, and 6% of propane in the mixture. They show that at given parameters the heating of the gas takes place during about 8.5 10^5 μs to 2290K, the ignition delay at 6% of propane takes almost the same time. It can be explained by decrease of the oxygen amount necessary for effective combustion.

In case of 2 and 4 % percents the delay time of ignition takes place during 7.5 10^5 μs and 8.0 10^5 μs, respectively . It means that there is an optimum concentration of propane for ignition of the mixture.

We want to mark that the developed model at this stage of investigations is incomplete from the point of view of propane chemistry. The model can be improved further in this direction. There are much more questions at accounting for the humidity. Appearance of heavy water clusters leads to the slow ion-ion recombination at the initial stage and decelerates the inflammation. For development of the model it is necessary additional investigations of cluster ions destruction with rise of temperature, also are required the data on temperature dependences of rate constant of these clusters conversion. Namely because of this we represent the ranges of the inflammation time, which indicates the inflammation time at absence of heavy water clusters and in their presence (but without definite determination of their existence time in conditions of heating).

Preliminary calculations of the stream that the subsonic stream is realized in the channel, and in case of homogeneous flow creation one could use obtained calculation data

for comparison with the experimental results. However a stream has spreading form. At that in different conditions experimentally measured temperatures require additional analysis. Sharp rise of temperature in case of electron beam and external electric field impact that can be caused by complex conditions of the stream formation and requires additional gasdynamic investigations.

Conclusions

The present project is the first, but considerable step to an area of non-self maintained discharge application for fuel activation.

Realization of problems put forward in the project has given us the opportunity to create a unique experimental installation, allowing to carry out experimental researches of gas mixtures combustion processes at the complex influence of an electron beam and an external electric field.

Experimental researches of the propane-air mixture excitation under the influences of the electronic beam and the external electric field have allowed to determine an impact of these influences on characteristics of burning.

So it has been defined that separate influence as the electron beam and the external electric field weakly influence on combustion processes. An application of the complex influence of the electronic beam and the external electric field on combustion processes realizes a considerable influence on the propane-air mixture combustion processes at subsonic speeds of a stream. Namely, the complex influence of the electron beam and the external electric field leads to the substantial increase of the mixture combustion temperature , rises of the combustion process stability, increases the speed of combustion.

The same influence realizes the complex influence of the electron beam and the external electric field on processes of burning of the lean flammable mixture.

Qualitative coincidence of theoretical calculations and results of the experimental researches give the basis for continuation of works on studying of questions of use of the non-self-maintained discharge for the fuel activation.

The further development of works is considered as expedient for obtaining of combustion and other physical processes numerical results and determination of a chemical composition of combustion products.

For this purpose it is necessary to - improve and add a diagnostic equipment and to continue modernization of the experimental installation for the purpose of insurance of the propane-air mixture delivery with the set weight ratios. It will allow to determine experimentally the optimum experimental characteristics of the electron beam and the external electric field for improvement of combustion characteristics of the propane-air mixture, and also to make closer results of theoretically-computation physical models and those of experiments.

Continuation of theoretical researches requires development a consecutive gasdynamic model of the modernized experimental installation; inclusion in consideration of processes realized at a mixture ignition mix firing by an additional spark source, and also change partial component composition during burning and under the combined action of the electron beam and the external electric field.

Comments

No Comments

Attachment 1: **The list of the published reports and reports (with abstracts)**

1. Ardelyan N.V., Bychkov V.L., Kosmachevskii K.V. Features of Combined Plasmas. IEEE Trans on Plasma Science. 2008. December. V.36. N.6.P.2892-2897.
2. Ardelyan N., Bychkov V., Kosmachevskii K., Denisiuk S., Gudovich V., Bychkov D., Kochetov I. Electron-beams for Plasma Impact on Gas Flammable Mixtures. AIAA-2009-0693. 47th AIAA Aerospace Sciences Meeting. 5-8 January 2009. Orlando World Center Marriott. Orlando. Florida.
3. Ardelyan N.V., Bychkov V.L., Bychkov D.V., Denisiuk S.V., Kosmachevskii K.V., Kochetov I.V. Modeling of Plasma Impact on Propane-Air Mixture. 5-th Intern. Workshop and Exhibit. On Plasma assisted Combustion (IWEPAC) 15-18 September 2009. Hilton Alexandria Mark Center, Alexandria, VA, USA. P.46-48.
4. Bychkov V. L., Kochetov I.V., Bychkov D. V., and Volkov S.A. Air-Propane Mixture Ionization Processes in Gas Discharges . IEEE Trans on Plasma Science. 2009. December. V.37. N.12, P.2280-2285
5. Ardelyan N.V., Bychkov D.V., Bychkov V.L., Gudovich V.A., Denisiuk S.V., Kochetov I.V., Kosmachevskii K., V. Non-Selfmaintained Gas Discharge for Plasma Impact on Gas Flammable Mixtures. AIAA -2010-0269. 48-th AIAA Aerospace Science Meeting, Orlando World Center Marriott, 4-7 January, 2010, Orlando, Florida.(12P)
6. Ardelyan N.V., Bychkov V.L., Kochetov I.V., Kosmachevskii K., V. On Pulsed Discharge in Humid Air. AIAA -2010-1589. 48-th AIAA Aerospace Science Meeting, Orlando World Center Marriott, 4-7 January, 2010, Orlando, Florida. (10P)

Attachment 2: The list of presentations at conferences and meetings (with abstracts)
The published reports 2-3, 5-6 subitems of the Appendix 1 have been presented at corresponding conferences and meetings

Attachment 3: The information on patents and copyrights (to list and describe patents and copyrights which were or can be received as a result of project performance)
Patents and copyrights are not present